Mesoporous Silica/Polymer Nanocomposites

A Dissertation
Presented to
The Academic Faculty

by

Yi Liu

In Partial Fulfillment
of the Requirements for the Degree
PhD in the
School of POLYMER, TEXTILE & FIBER ENGINEERING

Georgia Institute of Technology
DECEMBER 2009

Mesoporous Silica/Polymer Nanocomposites

Approved by:

Dr. Karl Jacob, Advisor
School of Polymer, Textile and Fiber Engineering
Georgia Institute of Technology

Dr. Anselm Griffin
School of Polymer, Textile and Fiber Engineering
Georgia Institute of Technology

Dr. Yonathan S. Thio
School of Polymer, Textile and Fiber Engineering
Georgia Institute of Technology

Dr. Donggang Yao
School of Polymer, Textile and Fiber Engineering
Georgia Institute of Technology

Dr. Rina Tennenbaum
School of Material Science and Engineering
Georgia Institute of Technology

Date Approved: 11/04/2009

To my wife Xiaolin Xu and My son, Kevin Liu

&

My Parents

ACKNOWLEDGEMENTS

I would like to think many people who help me a lot during my previous research to finish my thesis

I am highly indebted to my advisor, Dr. Karl Jacob, for his guidance, advice, encouragement, research support and allowance of freedom during my entire PhD studies. I have learned a lot from him over the years not only in my research but also my personal life. The improvements that he has brought to me will especially help me for my future. I am especially thankful to my committee members, Dr. Anselm Griffin, Dr. Rina Tannenbaum, Dr. Yonathan S. Thio, Dr. Donggang Yao, for their valuable time, constructive suggestions and valuable comments.

I would like to thank to Dr. Malcolm B. Polk, Dr, Philip J. McMullan, and Hongfeng Ren in my synthesis work and constructive suggestions.

I am grateful to Dr. Hohannes Leisen and Bo Xu for solid NMR characterization, Yaodong Liu for XRD characterization, Wei Zhang for TGA training, Sudhakar Jagannath and Neha Bighane for BET characterization, Ryan Kincer for GPC characterization, Chris Hubell for DSC and TGA training, Sunghyun Nam for FT-IR training, Yolanda Berta for SEM training.

Finally, I would like to thank my family. Thank my wife for her long time support, understanding, love and encouragement at any time when I meet difficulties. My lovely son, Kevin Liu, always brings me the most happiness in my life.

TABLE OF CONTENTS

	Page
ACKNOWLEDGEMENTS	iv
LIST OF TABLES	vii
LIST OF FIGURES	ix
LIST OF SYMBOLS AND ABBREVIATIONS	xiv
SUMMARY	xv
CHAPTER	
1 INTRODUCTION	1
1.1Motivation	1
1.2 Objective	5
2 LITERATURE REVIEW	7
2.1 Development of mesoporous silica	7
2.2 Hybrid mesoporous silica/organic nanocomposites	13
2.2.1 Mesoporous silica with organically modified surface	14
2.2.2 Periodic mesoporous organosilicate	16
2.3 Mesoporous silica/polymer nanocomposites 18	18
2.4 Ring polymerization to synthesize nylon 6	22
2.4.1 Cationic polymerization	22
2.4.2 Hydrolytic polymerization	23
2.4.3 Anionic polymerization	24
3 EXPERIMENTAL DETAILS	27
3.1 Chemical and Materials	27
3.2 Measurements and instrumentation	27

3.3 Synthesis 30

3.1.1 Mesoporous Silica/PMMA nanocomposites 30

3.3. 2 Preparation of mesoporous silica/nylon nanocomposites 33

3.3.3 Mesoporous silica/polystyrenesulfonic acid or polyacrylic acid nano comoposites 37

4 MESOPOROUS SILICA/PMMA NANOCOMPOSITES 42

4.1 Synthesis of SBA-15/PMMA composites 4

4.1.1 The initiator ABCC immobilized mesoporous silica SBA-15 44

4.1.2 Synthesized SBA-15/PMMA nanocomposites 49

4.2 Synthesis of BMS/PMMA nanocomposites 52

4.2.1 Surface analysis of BMS and its derivatives 54

4.2.2 Thermal analysis of BMS/PMMA nanocomposites 56

4.3.3 SEM analysis of BMS/PMMA nanocomposites 61

4.2.4 XRD analysis of BMS/PMMA nanocomposites 64

4.3 Spherical PMMA capsule after Silica removed with hydrofluoric acid 67

4.3.1 Thermal behavior of spherical PMMA capsule after silica was removed 67

4.3.2 SEM characterization of spherical PMMA capsule after silica was removed 73

4.4.3 GPC analysis of spherical PMMA capsule after silica was removed 77

4.4 Comparison of bulk polymerization and solution polymerization with and without vacuum steps 80

4.5 Conclusion 85

5 MESOPOROUS SILICA/NYLON 6 NANOCOMPOSITES 87

5.1 Designed procedure 1 to synthesize mesoporous silica/nylon 6 nanocomposites 87

5.1.1 Synthesis and characterization of of Chloro-isophthaloyl-N-ε-caprolactam 90

5.1.2 Immobilizing N-acyllactam onto the surface of SBA-15 93

5.1.3 Solid NMR characterization of mesoporous silica derivatives 98

5.1.4 Thermal analysis and BET analysis of BMS derivatives 102

5.1.5 Synthesized nylon/SBA-15 nanocomposites 104

5.1.4 Nylon-6/BMS nanocomposites 108

5.2 New designed approach to synthesize mesoporous silica/nylon-6 nanocomposites 110

5.2.1 Synthesis of N-3-((N-3-(trimethoxysilanyl)n-propyl)benzamidyl)-benzoyl-epsilon-caprolactam 112

5.2.2 Immobilizing the synthesized long chain N-acyllactam onto the surfaceof bi-modal mesoporous silica 114

5.2.3 Initiating anionic ring-opening polymerization inside the nano - channels and obtained mesoporous silica/nylon-6 nanocomposites 120

5.3 Conclusion 148

6 MESOPOROUS SILICA/POLYELECTROLYTE NANOCOMPOSITES 151

6.1 Synthesis of mesoporous silica with different ethyl acetate 152

6.2 Synthesis of mesoporous silica/PAA or PSSA nanocomposite with different conditions 157

6.3 Synthesis of other mesoporous silica/ polyelectrolyte nanocomposite 163

6.4 Poly-epsilon-caprolatone synthesized with derived mesoporous silica/PSSA nanocomposites 168

6.5 Conclusion 171

7 CONCLUSION AND RECOMMECTADTION 173

7.1 Conclusions 173

7.2 recommendations 176

REFERENCE 180

LIST OF TABLES

Page

Table 4. 1 Adsorption isotherms of nitrogen data for BMS, amine immobilized BMS and ABCA immobilized BMS 56

Table 4. 2 GPC data for PMMA spherical capsule 79

Table 5. 1 Possible molecular formula corresponding to molecular weight obtained from mass spectrometry. 92

Table 5. 2 ^{13}C CP-MAS NMR Chemical Shifts for amine immobilized SBA-15, N-acyllactam immobilized SBA-15 and capping N-acyllactam immobilized SBA-15 99

Table 5. 3 Materials parameters get from nitrogen isotherms 104

Table 5. 4 ^{13}C CP-MAS NMR Chemical Shifts for amine immobilized SBA-15, N-acyllactam immobilized SBA-15 and capping N-acyllactam immobilized SBA-15 118

LIST OF FIGURES

Page

Figure 2. 1 Representative TEM of -41 8

Figure 2. 2 TEM of calcinated hexagonal SBA-15 mesoporous silica with different pore size: (A) 60A, (B) 89A, (C) 200A, (D) 260A. The thickness of the silica wall are estimated to be (A) 53A (B)30A (C)40A (D) 40A 8

Figure 2. 3 Surfactant-directed formation of mesoporous materials from inorganic building blocks. 9

Figure 2. 4 SEM of representative mesoporous silica shapes and sureface pattern: a, rope; b, toroid; c, discoid; d, pinwheel; e, weel; f, gyroid; g, bagel; h, shell; i, knot; j, clock; k, eccentric1; l, eccentric 2. 11

Figure 2. 5 Mesostructured nanofibers with the circular pore architecture. (a) SEM image. The inset is a TEM image. (b) High- magnification TEM image of a 214-nm-diameter nanofiber. (c) TEM image taken on microtomed nanofiber samples. 12

Figure 2. 6 Mesostructured nanofibers with the longitudinal pore architecture. (a) SEM image. The inset is a TEM image. (b) High-magnification TEM image of a 93-nm-diameter nanofiber. (c) TEM image taken on microtomed nanofiber. 12

Figure 2. 7 Conceptual schemes of nanocomposte materials of mesoporous silica with organic components 14

Figure 4. 1 H^1 NMR of ABCA 46

Figure 4. 2 H^1 NMR of ABCC 47

Figure 4. 3 Spectra of (A) SBA-15, (B) immobilized amine and (C) immobilized ABCA 47

Figure 4. 4. D. s. c thermograms of ABCC 48

Figure 4. 5 D. s. c thermograms of ABCC immobilized SBA-15 48

Figure 4. 6 D. s. c thermograms of synthesized PMMA without covalent bonds with mesoporous silica 50

Figure 4. 7 D. s. c thermograms of SBA-15/PMMA composites 50

Figure 4. 8 TGA graph of PMMA free of mesoporous SBA-15 51

Figure 4. 9 TGA graph of PMMA/SBA-15 nanocomposite 52

Figure 4. 10 Scanning electron microscopy(SEM) images of BMS with different magnifications. 53

Figure 4. 11 Adsorption isotherms of nitrogen at 77K on BMS, amine immobilized BMS and ABCA immobilized BMS 55

Figure 4. 12 Pore size distribution of BMS, amine immobilized BMS and ABCA immobilized BMS 55

Figure 4. 13 Scanning electron microscopy(SEM) images of ABCC immobilized BMS with different maginifcations. 56

Figure 4. 14 Thermogravimetic analysis (TGA) graph of amine immobilized BMS (upper) and ABCA immobilized BMS (lower) 57

Figure 4. 15 D.S.C thermograms of BMS/PMMA (upper) and pure commercial PMMA (lower) 58

Figure 4. 16 Thermogravimetic analysis (TGA) graph of BMS/PMMA spheres (upper) and pure commercial PMMA (lower) 59

Figure 4. 17 Scanning electron microscopy(SEM) images of BMS/PMMA spherical composites with different magnification. 62

Figure 4. 18 Scanning electron microscopy (SEM) images of BMS/PMMA sphere after thermal defunctionalization (700°C) with different magnifications. 62

Figure 4. 19 X-ray diffraction pattern of BMS/PMMA sphere composites 65

Figure 4. 20. X-ray diffraction pattern of BMS sphere 65

Figure 4. 21 X-ray diffraction pattern of BMS/PMMA sphere using BMS as background 66

Figure 4. 22 X-ray diffraction pattern of commercial pure PMMA 66

Figure 4. 23. D.S.C thermograms pure commercial PMMA 70

Figure 4. 24 D.S.C thermograms of silica free spherical PMMA 70

Figure 4. 25 Thermogravimetic analysis (TGA) graph of spherical PMMA derived from BMS/PMMA composites 71

Figure 4. 26 Thermogravimetic analysis (TGA) graph of PMMA/BMS composites 71

Figure 4. 27 Thermogravimetic analysis (TGA) graph of synthesized free PMMA 72

Figure 4. 28 Thermogravimetic analysis (TGA) graph of pure commercial PMMA 72

Figure 4. 29 Scanning electron microscopy (SEM) of BMS/PMMA composites synthesized with bulk polymerization (upper graph), PMMA spherical capsules produce from bulk polymerization after silica were removed with hydrofluoric acid (lower graph). 75

Figure 4. 30 Scanning electron microscopy(SEM) of spherical PMMA capsules with different maginifications produced with solution polymerization after silica were removed with hydrofluoric acid 76

Figure 4. 31 Thermogravimetic analysis (TGA) graph of BMS/PMMA composites (sample 1) synthesized with solution polymerization without vacuum steps. 83

Figure 4. 32 Thermogravimetic analysis (TGA) graph of BMS/PMMA composites (sample 2) synthesized with bulk polymerization with vacuum steps. 83

Figure 4. 33 Thermogravimetic analysis (TGA) graph of BMS/PMMA composites (sample 3) synthesized with solution polymerization with vacuum steps. 84

Figure 4. 34 Thermogravimetic analysis (TGA) graph of BMS/PMMA composites (sample 4) synthesized with solution polymerization with vacuum steps. 84

Figure 5. 1 ^{1}H NMR spectrum of Chloro-isophthaloyl-N-ε-caprolactam 91

Figure 5. 2 Mass spectrometry spectrum of Chloro-isophthaloyl-N-ε-caprolactam 91

Figure 5. 3 FT-IR spectra of Chloro-isophthaloyl-N-ε-caprolactam 92

Figure 5. 4 ^{29}Si CP-MAS NMR spectra for sample (1): dried SBA-15; sample (2): amine immobilized SBA-15; sample (3): N-acyllactam immobilized SBA-15; sample (4): capping N-acyllactam SBA-15 97

Figure 5. 5 ^{13}C CP-MAS NMR spectra for sample 2: amine immobilized SBA-15; sample 3: N-acyllactam immobilized SBA-15; sample 4: capping N-acyllactam SBA-15 100

Figure 5. 6 TGA graph of (A) SBA-15; (B) amine immobilized SBA-15; (C) N-acyllactam immobilized SBA-15; 102

Figure 5. 7 Pore volume distribution with pore size of (A) SBA-15; (B) amine immobilized SBA-15; (C) N-acyllactam immobilized SBA-15; (D) capping N-acyllactam immobilized SBA-15 103

Figure 5. 8 TGA graph of synthesized nylon/SBA-15 nanocomposites (upper), D.S.C graph of nylon/SBA-15 nanocomposites(lower) 106

Figure 5. 9 TGA of BMS/nylon 6 composites 109

Figure 5. 10 TGA of pure nylon 6 109

Figure 5. 11 NMR spectrum of N-acyllactam bonding APTMS 113

Figure 5. 12 ^{29}Si CP-MAS NMR spectra for sample (1b): dried bimodal Si; sample (2b): N-acyllactam immobilized bimodal Si; sample (3b): capping N-acyllactam BMS; (4): capping N-acyllactam SBA-15 117

Figure 5. 13 ^{13}C CP-MAS NMR spectra for sample (2b): N-acyllactam immobilized BMS; sample (3b): capping N-acyllactam BMS; (4): capping N-acyllactam SBA-15 119

Figure 5. 14 ^{29}Si CP-MAS NMR spectra for sample (3b) capping N-acyllactam BMS; sample (5) synthesized BMS/nylon 6 nanocomposites 121

Figure 5. 15 ^{13}C CP-MAS NMR spectra for sample (3b) capping N-acyllactam BMS; sample (5)nylon 6/BMS nanocomposites. 122

Figure 5. 16 FT-IR spectra of sample (2b): N-acyllactam immobilized BMS; sample (3b): capping N-acyllactam-immobilized-BMS; 124

Figure 5. 17 FT-IR spectra of sample sample (5) BMS/nylon 6 nanocomposites. 125

Figure 5. 18 Scanning electron microscopy(SEM) images of BMS with different magnifications. 127

Figure 5. 19 Scanning electron microscopy(SEM) images of synthesize nylon 6/BMS nanocomposites after repeated washed with formic acid with different magnifications. 128

Figure 5. 20 Scanning electron microscopy(SEM) images of synthesize nylon 6/BMS nanocomposites film before free nylon was washed out with different magnifications. 129

Figure 5. 21 Scanning electron microscopy (SEM) images of physical blending of nylon 6/BMS composites film 130

Figure 5. 22 Scanning electron microscopy (SEM) images BMS obtained from physical blending of nylon 6/BMS nanocomposites repeatedly washed with formic acid 131

Figure 5. 23 TGA graph of dried bimodal mesoporous silica 134

Figure 5. 24 TGA graph of uncapping N-Acyllactam immobilized BMS 135

Figure 5. 25 TGA graph of capping N-Acyllactam immobilized BMS 135

Figure 5. 26 TGA graph of synthesized nylon 6/BMS nanocomposites 136

Figure 5. 27 TGA graph of synthesized free nylon 6 without covalent bond with BMS136

Figure 5. 28 TGA graph of synthesized nylon 6/BMS nanocomposites 141

Figure 5. 29 DSC of synthesized nylon 6/BMS nanocomposites 142

Figure 5. 30 DSC of synthesized nylon 6 without covalent bonds with BMS 142

Figure 5. 31 X-ray diffraction pattern of synthesized nylon 6 separated from solution 146

Figure 5. 32 X-ray diffraction pattern of synthesized nylon 6/BMS composites 146

Figure 5. 33 X-ray diffraction pattern of nylon 6/BMS composites after spectra subtracted spectra of pure BMS 147

Figure 5. 34 X-ray diffraction pattern of commercial nylon 6 from Aldrich 147

Figure 6. 1 SEM image of MS-1 with different magnifications 154

Figure 6. 2 SEM image of MS-2 with different magnifications 155

Figure 6. 3 SEM image of MS-3 with different magnifications 156

Figure 6. 4 FT-IR spectra of (A) as-synthesized and (B) template free silica/PAA nanocomposite 157

Figure 6. 5 SEM image of (A) AA-MS-1; (B) SSA-MS-1 160

Figure 6. 6 SEM image of (C) AA-MS-2; (D) SSA-MS-2. 161

Figure 6. 7 SEM image of (E) AA-MS-3; (F) SSA-MS-3 162

Figure 6. 8 SEM image of sample 4: mesoporous silica/PAA composites under base environment with different magnification. 164

Figure 6. 9 SEM image of sample 6: mesoporous silica/PSAA composites under acid environment with different magnification. 165

Figure 6. 10 N2 sorption isotherms(upper) and the corresponding BJH pore size distribution curves(lower) for sample 1: AA-MS-1; sample 2: AA-MS-2; sample 3: AA-MS-3; sample 4: AA-MS-4; sample 6: SSA-MS-6 167

Figure 6. 11 ^{1}H NMR spectrum of synthesized poly-epsilon-caprolactone with catalysts of mesoporous silica/PSSA nanocomposites 169

Figure 6. 12 ^{1}H NMR spectrum of synthesized poly-epsilon-caprolactone with catalysts of PSSA-MS-03 170

LIST OF SYMBOLS AND ABBREVIATIONS

DSC	Differential scanning calorimetry
FT-IR	Fourier transform infra red
GPC	Gel permeation chromatography
PDI	Polydispersity index
XRD	X-ray diffraction
WXRD	Wide angle X-ray diffraction
SBA-15	Mesoporous silica SBA-15
BMS	Bimodal mesoporous silica
ABCA	4, 4’-azobis(4-cyanopentanoic acid)
ABCC	4'-azobis(4-cyanopentanoyl chloride)
HMDS	1,1,1,3,3,3-hexamethyldisilazane
APTMS	Aminopropyltrimethoxysilane
CTAB	Hexadecyltrimethylammonium bromide
MMA	Methyl methacrylate
PMMA	Poly(methyl methacrylate)
PSSA	Poly(4-styrenesulfonic acid)
THF	Tetrahydrofuran
FT-IR	Fourier transform infrared spectroscopy
SEM	Scanning electric microscope
DMSO	Dimethyl sulfoxide
PAA	Poly (acrylic acid)

SUMMARY

The primary purpose of this work is to investigate the different methods from the literature to synthesize mesoporous silica/polymer nanocomposites, the possibility of synthesizing highly oriented polymer inside mesoporous silica channels and to use mesoporous silica as reinforcements in composites. Literature contains some methods to synthesize mesoporous silica/polymer composites, but these reported methods only used nano-channels as nano-reactor and the synthesized polymers had no direct connection with silica surface. To address some of the limitations found in the literature, new approaches through grafting initiators onto the surface of inner-wall of mesoporous silica were developed and investigated. Using the newly developed approach, PMMA was successfully synthesized through free radical polymerization and nylon 6 though in situ anionic ring-opening polymerization inside the nano-channels. The synthesized polymer had direct covalent bonds with silica surface and they couldn't be removed by solvent. This research involved two main parts: development of approaches and characterization of properties of newly synthesized composites and polymer.

ABCC, a kind of azo-initiator, was grafted onto silica surface through multiple grafting steps. The resulting ABCC-immobilized-MS could be used to initiate monomers with ethyl groups using free radical polymerization. Monomer of MMA was used as an example to be initiated inside the nano-channels and spherical mesoporous silica/PMMA composites were synthesized. The resulting composites showed a higher glass transition temperature, higher decomposition temperature and narrower decomposition range than

pure commercially available PMMA. Spherical PMMA capsules were obtained after the silica network was dissolved with hydrofluoric acid, these pure PMMA spheres had the same thermal properties and morphology as they had with in the composites.

Most grafting steps based on silica surface involved APTMS grafting which grafted amine groups on silica surface. The existence of amine groups on the surface of mesoporous silica would terminate the anionic ring-opening polymerization of epsilon caprolactam and produced caprolactactam salt with catalysts of magnesium bromide ethyl etherate. N-3-((N-3-(trimethoxysilanyl)n-propyl)benzamidyl)-benzoyl-epsilon-caprolactam was synthesized and directly grafted onto the surface of inner-walls of mesoporous silica, and nylon 6 propagated inside the nano-channels from the initiator center from the walls. The resulting nylon 6/BMS nanocomposites were spheres with the same diameter as pure BMS. About 50 wt% of the composites was newly synthesized nylon 6. The synthesized nylon 6 was proven to contain both α-form crystallite and γ-form crystallites with covalent bonds with the surface of silica inside the nano-channels. The synthesized spherical composites had the same glass transition temperature and melting temperature as pure commercial nylon 6, having the same decomposition temperature as N-acyllactam-immobilized BMS but lower than commercial pure nylon 6.

Traditional surface grafting on the surface of mesoporous silica only produced materials with organic groups occurred mostly near the openings of the channels. To overcome the limitation, one-pot sol-gel synthesis could produce ordered mesoporous silica with organic functional groups homogeneously distributed on the silica surface. Mesoporous silica/polyelectrolyte with high surface and regular morphology was directly synthesized with one-pot sol-gel method. The synthesized mesoporous silica/PSSA could

be used as catalyst to initiate the polymerization of epsilon caprolactone. The resulting polycaprolactone showed very low polydispersity index of 1.2, which was much lower than those produced with catalyst of organometallics.

CHAPTER 1

INTRODUCTION

1.1 Motivation

Since the publication of the first paper of M41S periodic mesoporous silica in 1992, mesoporous materials have attracted so much interest because these materials have regular pore morphologies, controllable pore sizes, and extra large surface area which enable these materials to be widely useful in the area of catalysis, separations, high performance composites etc.

All mesoporous silica with organic compounds on silica surface or penetrating the mesoporous silica framework can be called mesoporous silica/organic nanocomposites. For different purposes, many of the different organic groups, such as thiol, amine, sulfonic acid et al, are directly grafted onto the mesoporous silica surface through R-$Si(OR')_3$ groups or incorporated to mesoporous silica surface through functional silica sources during the formation of mesoporous silica through sol-gel procedure. These nano-channels of the mesoporous silica were also used as nano-reactors for polymerization. It was Aida T who named extrusion polymerization as polymerization which was initiated from the nano-channels of the mesoporous materials. Polystyrene, polyethylene, polyaniline, polyacrylonitrile, PMMA and polyesters were already successfully polymerized in mesoporous nanochannels and formed mesoporous silica/polymer nanocomposites. Polymers synthesized with extrusion polymerization were found with special properties. The reason is that the nano-reactor gives space constraints on polymer chains when they grow inside the nano-channels. For example,

polyethylene made with this method had ultra high molecular weight, high melting temperature, and only extended chain crystals rather than folded chain crystals because of the space constraint which controlled the formation of crystals. For mesoporous silica/organic nanocomposites, organic features introduce flexibility into the framework, and the inorganic silica provides structural, mechanical and thermal stability.

Currently, there are two methods to initiate extrusion polymerization inside nano-channels of mesoporous materials. The first method is to evaporate the mixture of initiator and monomer inside the nano-channels, and polymerization is initiated under certain conditions. The second method is to graft catalysts inside the nano-channels and then polymerization is initiated. However, not all polymers can be initiated from the nano-channels with the two methods currently in use because it is impossible to graft some kind of catalysts onto the surface of mesoporous silica. To overcome the limitations of these two polymerization methods, we investigated a new method, to graft initiator onto the surface of walls of nano-channels, which is a potential third method to initiate the extrusion polymerization inside the nano-channels. Unlike the two currently reported methods by which polymers are initiated and propagated inside the nano-channels without producing covalent bonds with the surface of mesoporous silica, the third method can connect the silica surface and synthesized polymer using covalent bonds because polymers are initiated and propagated from the initiator which is covalent bonded with silica surface through grafting steps. Thus this method introduces one more route to produce mesoporous silica/polymer nanocomposites.

Most composites materials consist of a thermoplastic matrix and particulate fillers with a method of mechanically blending components of the composites above the melting

temperature of the polymer. But the physical blending can't produce a homogeneous mixture of polymer matrix and the filler, and the organic phase and inorganic phases are easily phase separated, the direct connection of the polymer with the surface of the filler is also a potential method to overcome disadvantages of the current methods.

ABCC, an azo-initiator which can initiate free radical polymerization of most monomers with vinyl groups, is proposed to be grafted onto the surface of mesoporous silica through several surface grafting steps. With this ABCC-immobilized mesoporous silica, different monomers with vinyl groups are expected to be initiated and propagated though free radical polymerization under specific conditions. MMA is used as an example to check the feasibility of this method to produce mesoporous silica/polymer nanocomposites through surface initiated free radical polymerization. The thermal properties, mechanical properties and morphologies of the composites can also be investigated and compared with the traditional processing methods.

Some vinyl monomer with strong polar functional groups and cyclic monomer can't be initiated through free radical polymerization and therefore anionic polymerization should be used. The catalysts of anionic polymerization are alkali metals and strong anions, most of which can't be grafted onto silica surface. Initiator grafting onto silica surface also provides a very good method to initiate anionic polymerization inside the nano-channels of mesoporous silica. Nylon 6, a very common engineering plastics with its special properties, such as high toughness, high tensile strength , high elasticity, high resistant to abrasion and chemicals etc, can be polymerized through anionic ring-opening polymerization of epsilon-caprolactam with alkali metal as catalysts. Researchers already synthesized nylon 6/silica composites with physical blending method

and found their excellent mechanical properties, but there are no publications showing nylon 6 was polymerized inside the nano-channels of mesoporous silica through surface initiated anionic ring-opening polymerization. To initiate the anionic ring-opening polymerization inside the nano-channels, a new synthesis route with initiator surface grafting steps should be designed to achieve mesoporous silica/nylon 6 nanocomposites. Through grafting initiator of N-acyllactam onto the surface of mesoporous silica, epsilon-caprolactam is expected to be initiated inside the nano-channels. This initiator surface grafting method also provides a third choice to initiate a kind of polymerization where no catalysts could be grafted onto silica surface. We were encouraged to investigate the anionic ring-opening polymerization with initiator of N-acyllactam from the surface of mesoporous silica.

At present, the common method to graft functional groups onto silica surface is through post-synthesis procedures which can't distribute the functional groups onto silica surface very well. Researchers found most functional groups will gather near the openings of the silica channels with the post-synthesis procedures. If polymer with certain functional groups can be introduced into the mesoporous silica framework in a well distributed manner, this kind of mesoporous silica/polymer nanocomposites will have potential in the fields of catalysts, fuel cell, drug delivery etc. With sol-gel method, polyethylene, polyacrylate and nafion resin were successfully interpenetrated into the mesoporous silica framework. Based on the current development of mesoporous silica, it is also possible to introduce polyelectrolyte like polyacrylic acid (PAA) and poly(4-styrenensulfonic acid) (PSSA) into the mesoporous silica framework. We are planning to find a direct one-step method to quickly synthesize mesoporous silica/polyelectrolyte

nanocomposites with controllable functionalities and morphologies. The well distributed polyelectrolyte cross the mesoporous silica framework will have potential use in self-assembly, fuel cell, drug delivery etc. Thus we are encouraged to synthesize mesoporous silica/poly(4-styrenensulfonic acid) nanocomposites and mesoporous silica/polyacrylic acid nanocomposites using one step of sol-gel method, and to understand whether epsilon-caprolactone can be polymerized using the synthesized mesoporous silica/polyelectrolyte nanocomposites as catalysts are used to check the catalysis of nanocomposites.

1.2 Objective

The objective of this research is to introduce alternative procedures to produce mesoporous silica/polymer nanocomposites with controlled morphologies and special properties. The work involves:

1). Introduce a common procedure to initiate free radical polymerization through surface initiated free radical polymerization inside the nano-channels of mesoporous silica and produce mesoporous silica/polymer nanocomposites. PMMA is used as an example to verify the feasibility of this procedure. The synthesized PMMA and mesoporous silica/PMMA nanocomposites are characterized for mechanical and morphological properties.

2). Introduce a procedure to initiate the anionic ring-opening polymerization of epsilon-caprolactam inside the mesoporous silica to produce mesoporous silica/nylon 6 nanocomposites.

3). Synthesize mesoporous silica/polyelectrolyte nanocomposite with a simple direct sol-gel procedure. Try to find the best reaction condition to get controlled morphologies, uniform channels size, uniformly distributed functional groups etc. Epsilon caprolactone was polymerized by using synthesized mesoporous silica/PSSA nanocomposites as catalysts.

CHAPTER 2

LITERATURE REVIEW

2.1 Development of mesoporous silica

According to IUPAC notation, mesoporous materials are materials containing pore with diameters between 2 and 50 nm; microporous materials have pore diameters of less than 2 nm and macroporous materials have pore diameters of greater than 50 nm. Because of its large surface area and suitable channel size, mesoporous silica and their derivative nanocomposites attracted a lot of interest and researchers already made a noticeable of progress toward synthesis of new mesoporous materials and their derivative materials.

In 1992, a new family of mesoporous inorganic materials named as MCM-41[1,2,3] was originally developed by Mobile scientists through surfactant-templated mechanism which uses the hydrolysis of silica sources in water under the existence of surfactant which is self-assemblied as micelles in water. MCM-41, one of the members of this extensively family of mesoporous sieves, possesses a hexagonal array of uniform mesopores which can vary from 1.5nm to 10nm in size, has surface area above 700m^2/g and hydrocarbon sorption capacities of 0.7cc/g or greater. Because of the excellent properties of MCM-41, it abstracted significant many interests in the fields of catalysts, filtration, separation etc. Figure 2.1 is the representative TEM of MCM-41 which shows the ordered array of hexagonal channels with a diameter of 4nm.

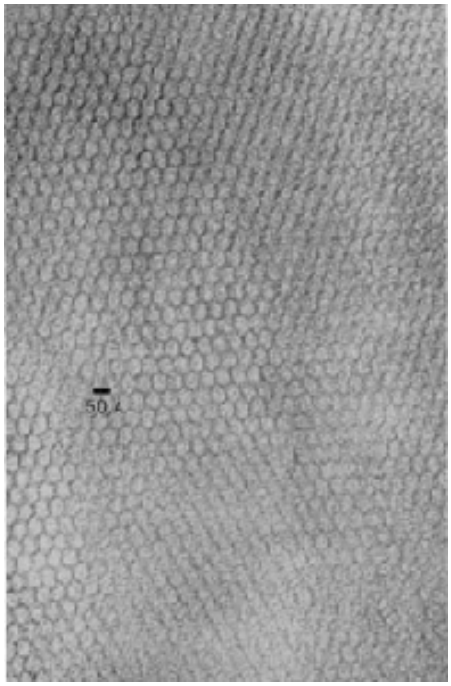

Figure 2. 1 Representative TEM of -41

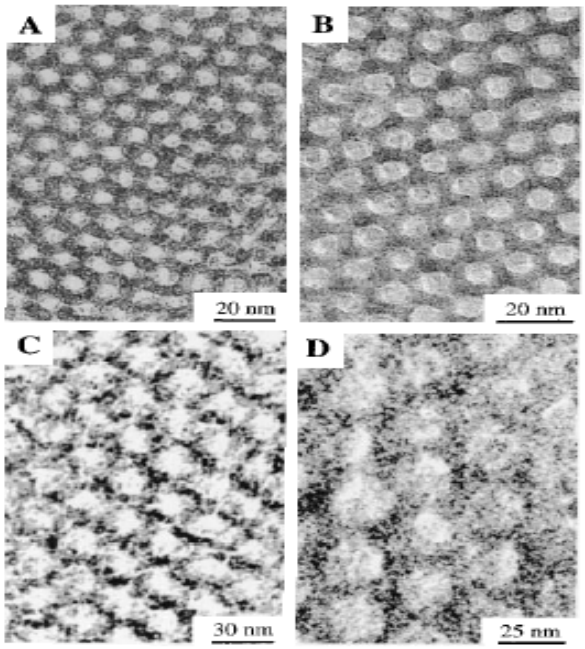

Figure 2. 2 TEM of calcinated hexagonal SBA-15 mesoporous silica with different pore size: (A) 60A, (B) 89A, (C) 200A, (D) 260A. The thickness of the silica wall are estimated to be (A) 53A (B)30A (C)40A (D) 40A

After the development of MCM-41, another milestone in the development of mesoporous inorganic solids was SBA-15[4,5] which was synthesized in 1997 in Stucky's group. Dr Zhao synthesized well-ordered hexagonal mesoporous silica structure named as SBA-15 with use of an amphiphilic block copolymer of PEO-PPO-PEO to direct the organization of polymerizing silica species. Through choosing the length of block copolymer, reaction condition, the pore sizes can vary from 4.6 to 30 nm, pore volume fractions up to 0.85, and silica wall thickness change from 3.1 to 6.4 nm. Figure 2.2 is the representative TEM picture of SBA-15.

Both MCM-41s family and SBA-15s family used surfactant to direct and assemble building blocks into mesoscopically ordered structure. The surfactant-templated mechanism can be clearly shown in Figure 2.3[6]

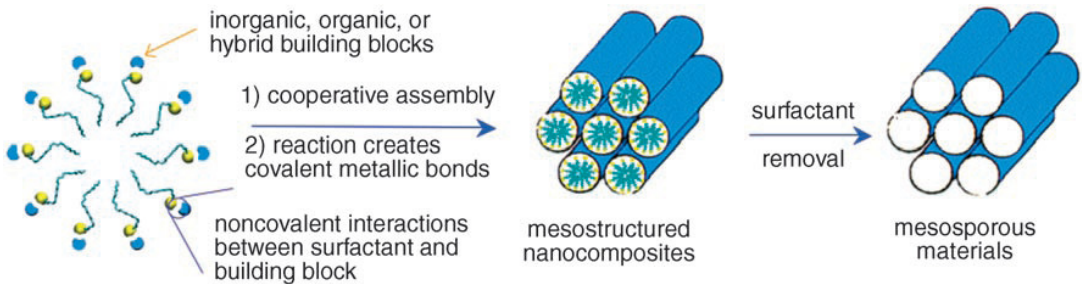

Figure 2. 3 Surfactant-directed formation of mesoporous materials from inorganic building blocks.

According to the surfactant-templated mechanism, the self-assembly of building block is an essential part. In general, self-assembly refers to a spontaneous organization of building blocks driven by non-covalent interactions, such as hydrogen bonding, π-π stacking, and electrostatic interactions. The building blocks can range from predesigned

molecules (for example, organic molecules, oligomers, and polymer), molecular clusters (for example, inorganic and hybrid organic-inorganic clusters), and low-dimensional objects (for example, nanoparticles, nanorods, and nanowires) to more complicated components. The self-assembly of the building blocks in water can produce well-ordered two dimensional systems or three dimensional systems. Then the silica species can hydrolyze and polymerize in water and form the mesostructured nanocomposites, after calcinations of the surfactant under very high temperature, mesoporous materials are derived.

With this surfactant template mechanism, mesoporous silica with different pore sizes, morphologies and pore directions are derived. Yang H and Ozin GA[7] synthesized a series of hexagonal mesoporous silica with curved morphologies. Figure 2.4 shows representative SEM pictures of different kinds of morphologies of the mesoporous silica. Mesoporous silica fiber (MSF) with excellent long range hexagonal order and structure was first synthesized in 1997[8], thereafter many different MSF were synthesized with different methods, Wang JF[9] and his collaborators synthesized ultra-long MSF with controllable pore directions in 2003. Figure 2.5 shows mesostructured nanofibers with the circular pore architecture, and Figure 2.6 shows mesostuctured nanofibers with the longitudinal pore structure.

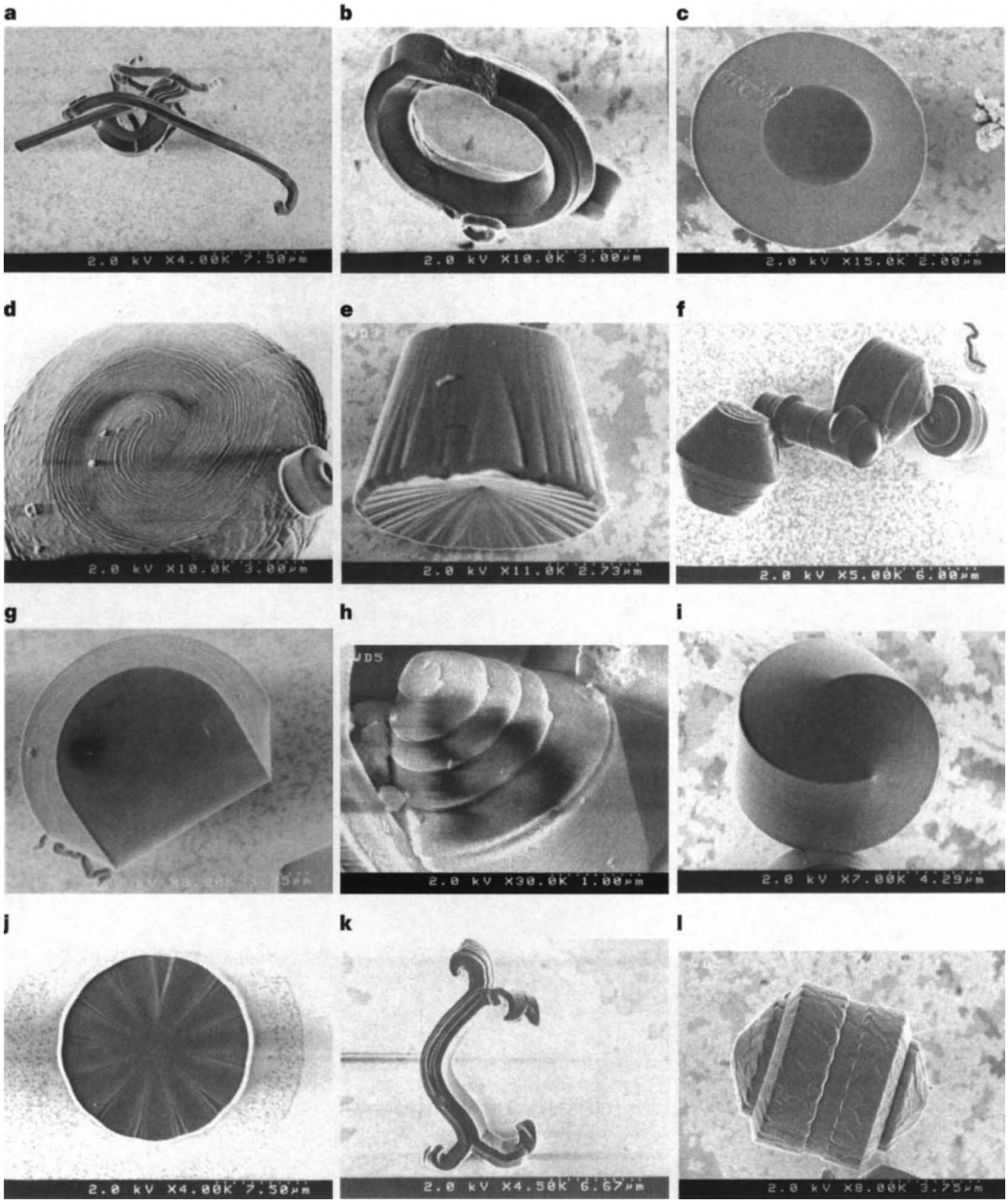

Figure 2. 4 SEM of representative mesoporous silica shapes and sureface pattern: a, rope; b, toroid; c, discoid; d, pinwheel; e, weel; f, gyroid; g, bagel; h, shell; i, knot; j, clock; k, eccentric1; l, eccentric 2.

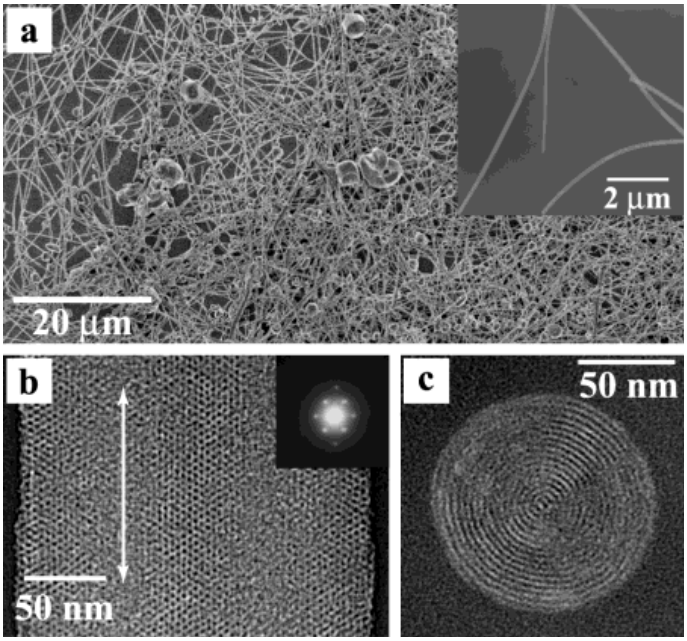

Figure 2. 5 Mesostructured nanofibers with the circular pore architecture. (a) SEM image. The inset is a TEM image. (b) High- magnification TEM image of a 214-nm-diameter nanofiber. (c) TEM image taken on microtomed nanofiber samples.

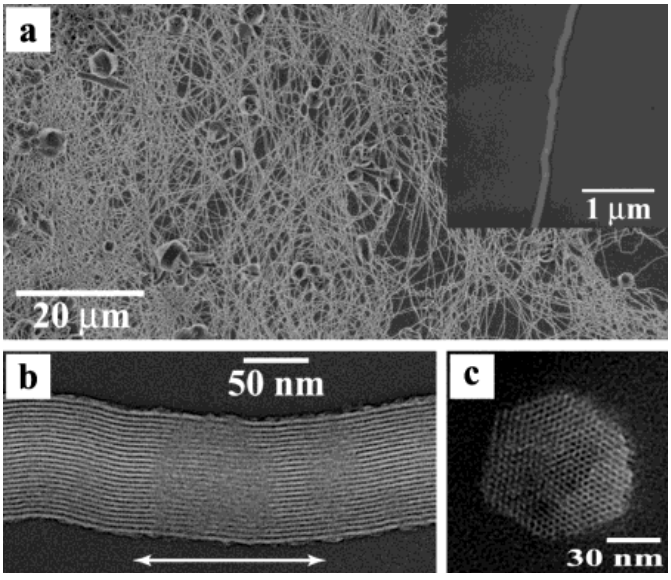

Figure 2. 6 Mesostructured nanofibers with the longitudinal pore architecture. (a) SEM image. The inset is a TEM image. (b) High-magnification TEM image of a 93-nm-diameter nanofiber. (c) TEM image taken on microtomed nanofiber.

2.2 Hybrid mesoporous silica/organic nanocomposites

Nanocomposite materials are widely studied in the past decades, and are found in various places in the earth. Some nanocomposites in our biological system with special properties, for example: the nacre of abalone shell which is composed of 99% of alternating layers of aragonite ($CaCO_3$) and 1% of biopolymer but twice as hard and 1,000 times as tough as its constituent phases[10], encourage our researchers to make all kinds of inorganic/organic nanocomposites to mimic the materials in nature.

Researches on mesoporous silica/organic nanocomposites have become very important fields of recent material science. Mesoporous silica/organic nanocomposite can be categorized as four different groups which are shown in Figure 2.7[11]. The first category is surface modification, where organic components such as R-Si(OR')$_3$ can be used to functionalize the mesoporous silica surface. The second category is framework modification which produces nanocomposites called periodic mesoporous organosilica(PMO), where organic functional group is in the silica species having the form of (OR')$_3$Si-R-Si(OR')$_3$ which is hydrolyzed and polymerized in water and thus organic functional groups are also in the frame of mesoporous structure. Different PMO can be synthesized just changing the structure of R. The third category is polymer composite in pore void, where catalysts or initiators which are grafted onto the inner walls of the mesoporous silica nano-pores can initiate the polymerization and form polymer in the void. The last category is framework polymer composites, which is formed during the formation of mesoporous silica through sol-gel method where polymer is cross the framework of the mesoporous silica.

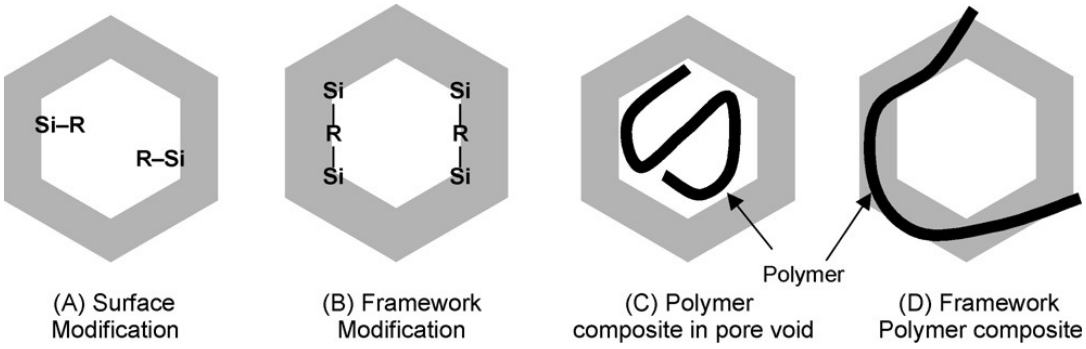

Figure 2. 7 Conceptual schemes of nanocomposite materials of mesoporous silica with organic components

2.2.1 Mesoporous Silica with organically Modified Surface

There are two general strategies to do chemical surface modification of periodic mesoporous silica via covalent bonding of organic molecules. The first method is called as post-synthesis procedure which grafts organic groups onto the surface of mesoporous silica. The second method is co-condensation procedures which introduce organic groups onto the surface of mesoporous silica when mesoporous silica frame is formed from silica sources.

2.2.1.1 Postsynthesis Procedures.

To achieve organic groups on the surface of mesoporous silica, the direct method is grafting organic groups with the silanol group on the surface of mesoporous silica. There are three main approaches for post-synthesis surface modification or derivatization of mesoporous silica. The first surface modification is directly grafting a suitable organosilane reagent with silica surface using an appropriate solvent under reflux

conditions[12]. Grafting with silane coupling agents such as chlorosilanes, alkoxysilanes, and silylamines under anhydrous conditions is more commonly referred to as silylation[13]. The grafting reactions make use of two types of surface silanols which are free single silanol group (-SiOH) and germinal silanol groups ($-Si(OH)_2$)[14]. When the silylation procedure is performed under controlled wet conditions, the grafted organosilane species form a continuous layer on the silica surface. The procedure is also referred to as coating. With this primary modification, amine, thiol group[15] etc, can be directly grafted onto the surface of mesoporous silica. The second surface modification method consists of further reactions of the previous grafted species to create new functionalities. For example, amine group can be used for further surface modification. The third surface modification is transformation of the materials prepared under the first two methods by additional treatments. For example, thiol group[67] which is directly grafted onto the surface of mesoporous silica can be transferred to sulfonic acid through oxidation.

2.2.1.2 One-pot Synthesis of Mesoporous Silica with Organically Modified Surface.

Co-condensation of siloxane and organosiloxane precursors via the sol-gel technique to produce functionalized amorphous xerogels silica has been extensively investigated[16 17]. In these materials, an organic moiety is covalently linked via a nonhydrolyzable Si-C bond to a siloxane species, which hydrolyzes to form silica network. Burkett[18] et al. and Macquarrie[19] were the first to use this approach to produce ordered mesoporous silica based nanocomposites with covalently linked organic functionalities protruding from the inorganic walls into the pores. Burkett prepared phenyl bearing MCM-41, while Macquarrie produced a kind of hexagonal mesoporous

silica via the nonionic amine route modified with cyanoethyl ligands. The researchers also found the ordered structure can be kept well while the percentage of organosiloxane is up to 20%, but the upper limit of its incorporation into the mesoporous hybrid materials is 40%. Stein and coworkers[20] use this one-spot method to synthesize MCM-41 type hybrid materials containing vinyl functions group, and they found that one-pot synthesis can produce ordered mesoporous silica with organic functional groups homogeneously distributed on the silica surface while postsynthesis procedures can only produce materials with organic groups occurred mostly near the openings of the channels. Lu YF[21] and his coworkers synthesized mesoporous silica frame with propyl methacrylate on the surface using (3-trimethoxysilyl) propyl methacrylate with the one-spot method, and the research groups can polymerize the vinyl groups on the surface with other monomers to produce nanocomposites with better thermal and mechanical properties. Some other different mesoporous silicas functionalized with sulfonic acid groups[22], HMS[23], aminopropyl[24] etc.

2.2.2 Periodic Mesoporous Organosilicate

Periodic mesoporous organosilicate(PMOs) are materials where the organic component is built in the walls of the channels instead of on the surface of the silica[25, 26]. To synthesize periodic mesoporous organosilicate, bridged silsesquioxanes $(RO)_3Si\text{-}R'\text{-}Si(OR)_3$ are often used as precursors which hydrolyze in water and form mesoporous silica frame with other silica sources like TEOS via sol-gel technique[27]. In contrast with the previously described hybrid mesophases in which the organic moieties are located on the pore surface, in this class of materials, the organic constituents are fully incorporated

in the pore walls as molecularly dispersed bridging ligands. So the organic groups are an integral part of the mesoporous framework. Furthermore, the use of bridged silsesquioxanes as silica precursors allowed the complete incorporation of organic functionalities of organotrialkoxysilanes leveled off at around 25% because additional silica, usually in the form of TEOS, is required for condensation into rigid walls. In addition, highly ordered surface modified mesoporous silica is difficult to obtain using organotrialkoxysilanes because the surfactant micelle structure is perturbed by the organic groups that share the same confined channels.

Periodic mesoporous organosilicas(PMO) is a very important category for hybrid mesoporous silica/organic nanocomposites. Researchers synthesize a lot of PMO through changing the organic segments among different silica sources. Most of PMO were prepared under basic conditions, using procedures very similar to those of their pure silica counterparts.

Using CTMAC as a surfactant, Inagaki and coworkers[28] and sayari et al[29] made independent discoveries of a cubic ethane silica mesophase. Stein and co-workers[30] developed a synthesis procedure requiring close control of the solution PH. The hydrolysis of the bridged silsesquioxane was performed under acidic conditions, while the precipitation step was performed under basic conditions using either sulfuric acid or sodium hydroxide accordingly. Ozin and coworkers synthesized a series of MCM-41 type hybrid materials using BTEY silica precursor alone or mixed in different ratios with TEOS in the presence of CTMAB surfactant. Brinker and coworkers[31] used an evaporation-induced self-assembly procedure to prepare poly(bridged silsesquioxane) films and spherical nanoparticles under acidic conditions in the presence of ethanol. Kai

Landskron[32] and his colleagues synthesized a periodic mesoporous organosilica composed of interconnected three-ring $[Si(CH_2)]_3$ units built of three $SiO_2(CH_2)_2$ tetrahedral subunits in the form of powder or film. This PMO show low dielectric constant and good mechanic stability which make it very interesting for microelectronic applications. Lu YF[33] and his collaborators synthesized responsive periodic mesoporous polydiacetylene/silica nanocomposites through silica sources of silsesquioxanes containing a bridged diacetylenic group, and these nanocomposites have potential use in the fields of sensors, actuators and other device applications.

2.3 Mesoporous silica/Polymer nanocomposites

Mesoporous silica has a large surface area and a lot of constrained space in the form of nano-channels. Polymers grown within the constrained space of periodic mesoporous silica may exhibit unusual mechanical, electronic, magnetic, and optical properties. The spatial control of the growth process is limited by the channel network of the host allows the fabrication of materials with designed shapes, particularly nanofibers[34], wires[35], and porous particles[36]. Especially, nanofabrication of polymer fibers with the silica nano-channels has attracted much attention. For example, MCM-41 was used as a container for polymerization of ethylene, aniline, acrylonitrile[37], methyl methacrylate[38], and phenol-formaldehyde[39]. The monomers were first adsorbed from the gas phase into the inorganic host and then polymerized inside the channeled networks using initiators such as benzoyl peroxide or anhydrous HCl vapor. The resulting polymer fibers didn't exhibit the same properties as bulk polymers. For example, polystyrene fibers[40] constrained inside the channels of MCM-41 silica didn't exhibit a glass transition

temperature. Using a contactless microwave adsorption technique, Wu and Bein[41] prepared conducting filament of polyaniline up to several hundred aniline rings in the 3 nm wide hexagonal channel system of aluminosilicate of MCM-41. The resulting filaments have significant conductivity while encapsulated in the channels which represent a significant step toward the design of nanometer electronic devices. The microwave conductivity of oxidized polyaniline filaments entrapped inside the channels of MCM-41 was one-fourth that of bulk polyaniline, that is, 0.00014S/cm compared to 0.0057 S/cm. Keisuke Kageyama and Takuzo Aida synthesized linear polyethylene fibers within a mesoporous silica fiber through extrusion polymerization. The resulting polyethylene show unique properties: ultra-high molecular weight of 6,000,000g/mol; melting temperature 10 degree C higher than that of ordinal polyethylene; this PE only form extended chain crystals rather than folded chain crystals because of space constraint when polymers are formed in the nano-channels.

Mesoporous silica/polymer nanocomposites can also be made through entrapping polymers in the nano-channels of mesoporous silica through the hydrogen bonding between the silanol groups on the silica surface and the groups in polymer chain. So groups which can form hydrogen bond with silanol groups are very necessary for a certain polymer if high loading of polymers want to be trapped. The hydrogen donating property of silanol moieties is so strong that organic polymers having hydrogen accepting groups such as amide moieties form hydrogen bonds with silanol groups. Transparent and homogeneous polymer hybrids could be obtained from amide-containing polymers such as poly(2-methyl-2-oxazoline)[42], poly(N-vinylpyrrolidone), and poly(N,N-dimethylacrylamide). For polymers without hydrogen accepting groups, methods should

be used to grafting hydrogen accepting groups onto polymer chain. Oleg Yu[43] made guest-host MEH-PPV/MCM-41 composites by liquid-phase self-assembly via insertion of poly[2-methoxy-5-(29-ethyl-hexyloxy)-1,4-phenylene vinylene] (MEH-PPV) macromolecules inside mesoporous silica. Through choosing suitable solvent, the polymer contents can be up to 12.9 wt%.

One method to synthesize organic polymer/inorganic silica hybrid composites is to form covalent bond between polymer and silica when silica sources (TEOS or TMOS) hydrolyze to form mesoporous silica. During the hydrolysis procedure, alkoxysilane moieties which are used to modify organic polymers as side chain will co-hydrolyze or co-condense with silica source during the sol-gel system. Polymer hybrids with polyacrylate[44], polystyrene[45], polyimide[46], poly(acrylonitrile)[47] were prepared using the alkoxysilane moieties organic polymers. Using similar methods, mesoporous silica/polymer nanocomposites can be synthesized. Surfactants which are used as template to form mesoporous silica contain both polymerizable functional groups which can polymerize with themselves and co-condensable groups which can co-condense with silica sources. Lu YF and his co-workers[48] synthesized mesoscopically ordered chromatic polydiacetylene/silica nanocomposites using oligoethylene glycol functionalized diacetylenic surfactants having a structure of scheme 2.1. The surfactants will self-assemble and template the formation of mesoporous silica, then the diacetylene groups can be initiated and form conjugated polymer inside the nano-channels of mesoporous silica. The use of polymerizable surfactants as both structure-directing agents and monomers in the various evaporation-driven self-assembly schemes developed recently[49,

[50,51] represents a general, efficient route to the formation of robust and functional nanocomposites.

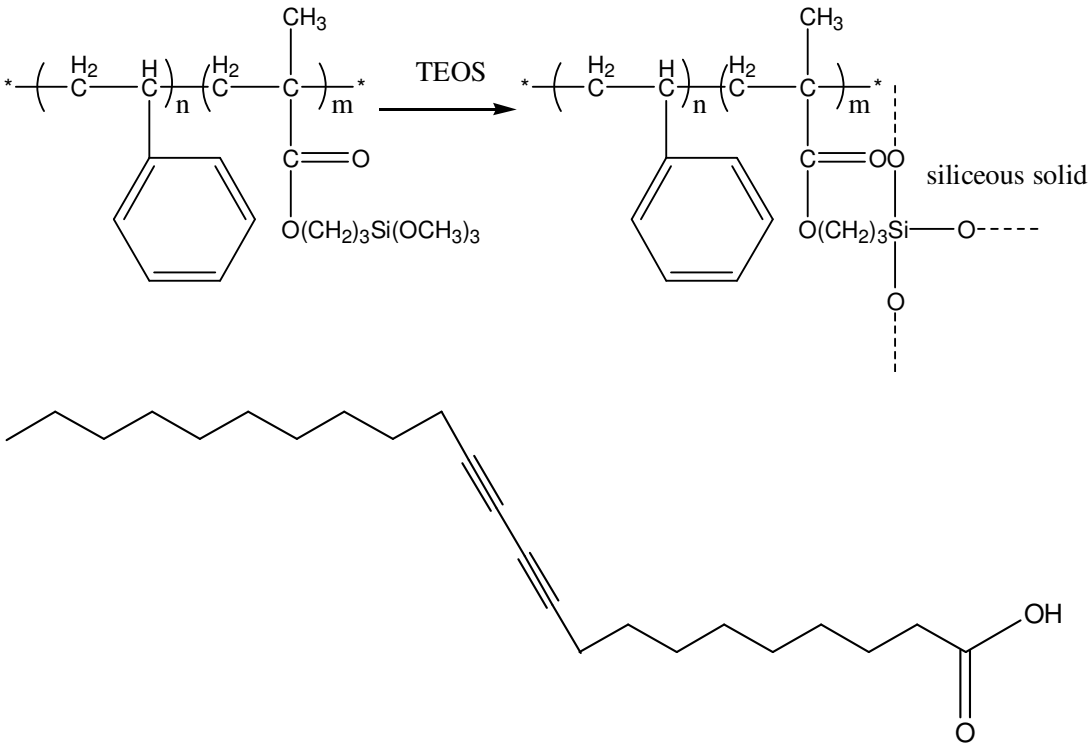

Scheme 2. 1 Surfactant structure and synthesis scheme

Organic-inorganic polymer hybrids show both organic polymer and inorganic properties. The properties of an organic polymer include high flexibility, versatility in design of functional groups, film-forming property, and so on. Inorganic compounds provide the potential for great tensile strength, gas barrier properties, and high thermal and mechanical stability. Bulk properties of polymer hybrids depend on the ratio of organic polymer to inorganic materials.

2.4 Ring-opening Polymerization to Synthesize Nylon

The polymerization of lactams can be initiated by acid, water and bases through cationic polymerization, hydrolytic polymerization and anionic polymerization. The mechanisms of these three polymerizations are as following[52]:

2.4.1 Cationic polymerization

Protonic and Lewis acids initiate the cationic polymerization of lactams, and the reaction follows the mechanism of acid-catalyzed nucleophilic substitution reactions of amides. The initiation and propagation mechanism can be shown in the following Scheme 2.2 :

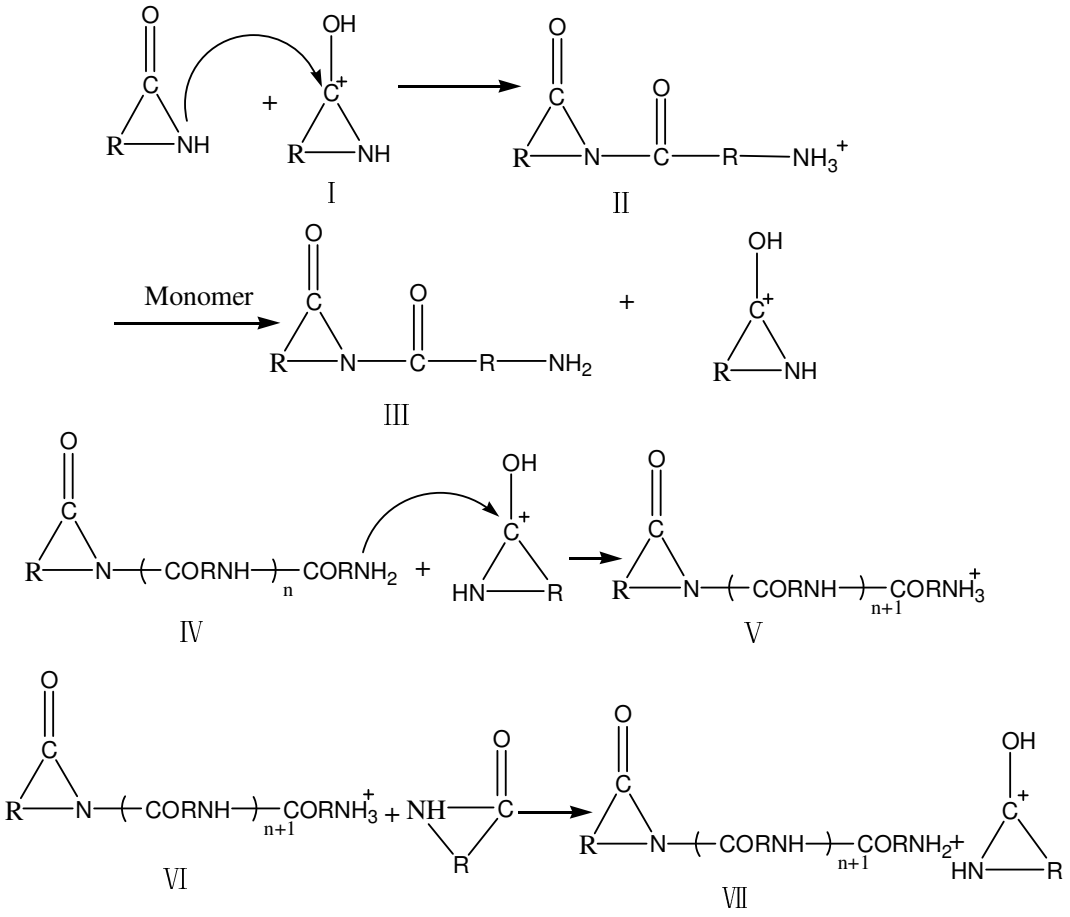

Scheme 2. 2 Mechanism of cationic polymerization of epsilon caprolactam

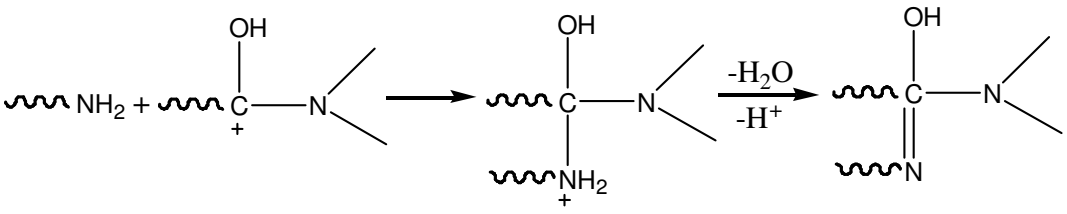

Scheme 2. 3 Side reaction during cationic polymerization of epsilon caprolactam

In the initiation, the acid attack the monomer to form the protonated monomer(Ⅰ) which can react with the monomer to form an ammonium salt(Ⅱ) which can exchange proton with monomer to produce Ⅲ. Propagation follows in a similar manner as a nucleophilic attack by the primary amine end group of a growing polymer chain (Ⅳ) on protonated monomer to yield Ⅴ which exchanges proton with monomer. The side reactions from scheme 2.3 limit the conversions and polymer molecular weights. The highest molecular weights obtained with cationic polymerization are only 10,000-20,000 g/mol. The cationic polymerization to produce nylon 6 is not considered as a good method in industry.

2.4.2 Hydrolytic Polymerization

Hydrolytic polymerization is currently commercially used to produce nylon-6 nowadays. The temperature of the reaction system which includes monomer and 5-10 wt% of water is increased to 250-270 degree C for periods of 12-24 hrs. The reaction mechanism is as following procedure. First lactam is hydrolyzed to epsilon-aminocaproic acid, afterwards the acid reacts with the amine to produce nylon 6 as Scheme 2.4.

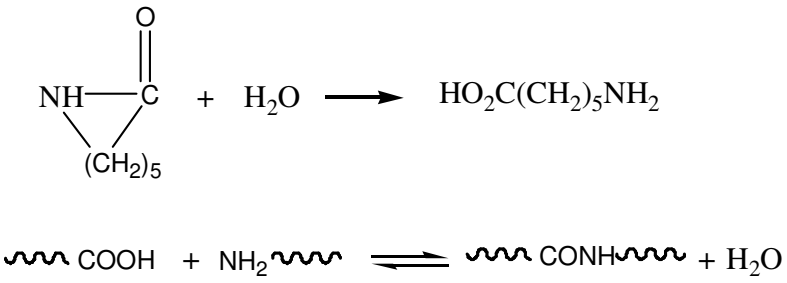

Scheme 2. 4 Mechanism of water initiate epsilon caprolactam

The existence of acid which can attack the monomer results in cationic polymerization, but the major reaction is still step polymerization. Ring-opening polymerization determines the overall conversion of lactam to polymer, however, step polymerization determine the molecular weight of the polymer. The procedure to synthesize nylon 6 using hydrolytic polymerization is simple and easy to control, and the synthesized nylon has very high molecular weight and excellent mechanic properties, therefore, hydrolytic polymerization is often used to produce nylon in industry.

2.4.3 Anionic Polymerization

Strong bases and organometallic compounds can initiate anionic polymerization to produce nylon 6. First, the strong base reacts with the monomer to produce lactam anion which will attack the monomer to form the primary amine anion which can exchange proton with monomer and form the imide dimer, these steps are shown in Scheme 2.6. This imide dimer is the actual initiating species for the anionic polymerization. The imide dimer will react with lactam anion to produce high molecular weight polymer. But the step of forming imide dimer costs more than 20 hours which is very uneconomical and difficulty to control, the actual initiating center N-acyllactam is necessary for anionic polymerization to produce nylon 6 because it can be synthesized

directly using the monomer with acid chloride and then placed into the reaction system. The structure of N-acyllactam and its one step synthesis is shown in Scheme 2.5. The hydrogen from the amide of monomer is easy to react with some reactive functional group, such as acid chloride, isocyanic acid etc. In actual anionic ring-opening polymerization to synthesize nylon 6, a few of chemicals with such kind of reactive functional group can be added to reaction system to form enough N-acyllactam immediately, and the resulting N-acyllactam can immediately initiate the ring-opening polymerization to produce nylon 6 within 10 minutes. Therefore, the actual initiator center of N-acyllactam is very important for ring-opening anionic polymerization. Information on how to synthesize different kinds of useful chemicals with functional group of N-acyllactam is also very useful to promote the development of synthesis of polyamide.

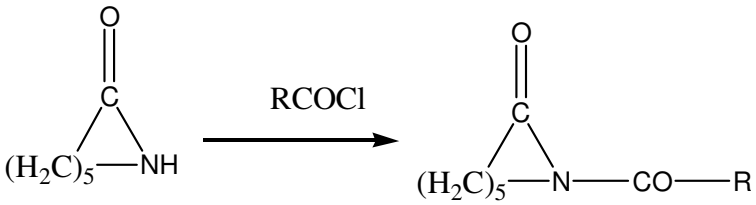

Scheme 2. 5 One step of synthesize N-acyllactam

Although anionic ring-opening polymerization to produce pure nylon 6 is not very often used in industry, it still attracts a lot of interests because of its advantages. Especially it is useful to synthesize in-situ nylon 6/inorganic filler composites. The living polymerization can produce high molecular weight nylon 6 in a very short time, but the reaction condition is much stricter than hydrolytic polymerization because even moisture will affect the polymerization.

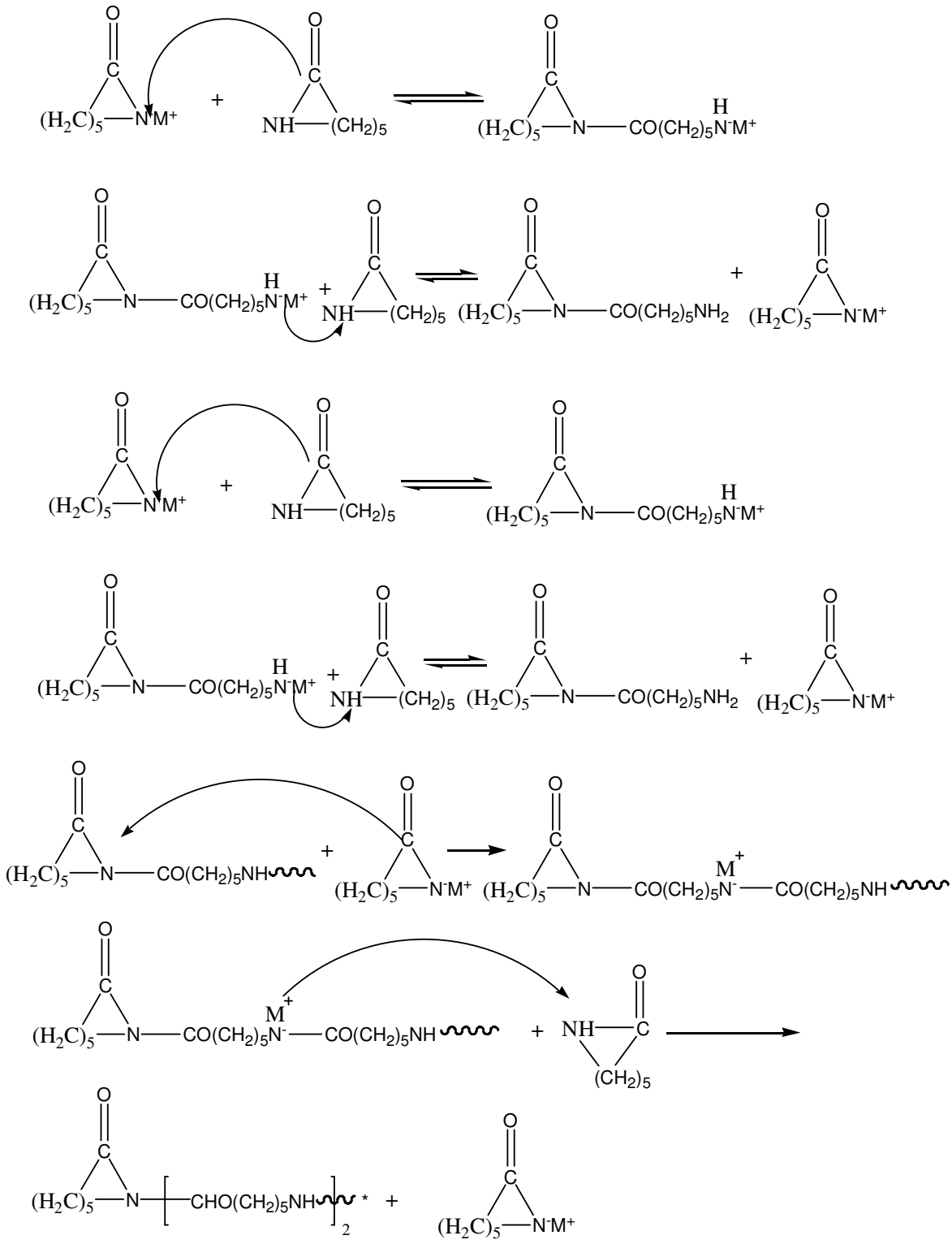

Scheme 2. 6 Mechanism of anionic ring-opening polymerization of epsilon caprolactam

CHAPTER 3

Experimental Details

3.1 Chemicals and Materials

The following chemicals were commercially available and used as received: Pluronic 123(Aldrich), Hydrochloric acid (VWR international), Anhydrous ether(Aldrich), Tetraethyl orthosilicate (Aldrich), anhydrous Tetrahydrofuran(Aldrich), 3-aminopropyltrimethoxysilane (Aldrich), 1,1,1,3,3,3-hexamethyldisilazane (Aldrich), anhydrous toluene (Aldrich), Hexane (VWR international), DI water (Georgia Tech chemistry department), Sodium silicate (Aldrich), hexane (VWR international), ethanol (VWR international), Hexadecyltrimethylammonium bromide (CTAB) (Aldrich), anhydrous dichloromethane (Aldrich), Phosphorous pentachloride (Aldrich), 4, 4'-Azobis(4-cyanopentanoic acid) (ABCA) (Aldrich), Methyl methacrylate (Aldrich) was distilled to get rid of inhibitor, Magnesium bromide ethyl etherate (Aldrich), poly(acrylic acid) average M_w ~5,100 (Aldrich), Poly(4-styrenesulfonic acid) average M_w ~200,000 (Aldrich)

3.2 Measurements and Instrumentation

H^1 NMR (300MHz) spectra were recorded on a Varian Gemini 300 Spectrometer in Georgia Tech NMR center.

The Differential Scanning Calorimetry (DSC), performed on a Model of Q200 from TA instrument in Polymer, Textile and Fiber Engineering department and Dr

Beckham's Lab in Polymer, Textile and Fiber Engineering department, was used to determine the melting temperature and glass transition temperature of polymer. Samples were heated at a rate of 10 °C/min.

Thermogravimetic analysis (TGA) was performed on a Model of Q5000 from TA instrument in Polymer, Textile and Fiber Engineering department. Samples were heated under a nitrogen and air stream from 30 to 750 °C at a rate of 10 °C/min. The organic loading was measured from the weight loss from 200 to 650 °C. The organic loading was determined by assuming two methoxy linkages to the surface before hydrolysis and three methoxy linkages after hydrolysis. For the traditional amine-functionalized SBA-15 and BMS, two methoxy linkages were assumed.

Relative Molecular weights of polymers were measured by gel permeation chromatography(GPC) with waters 2690 separations module with HR 4, 3 and 1 THF columns equipped with water 910 refractive index detector. Polystyrene standards was used for the calibration plot and tetrahydrofuran was used as solvent.

Scanning electron microscope was performed on LEO 1530 and Hitachi 800 from Georgia Tech Electron Microscope Center.

Surface area and pore size distribution data were obtained from Surface Area and Porosity Analyzer (ASAP 2020) from Micromeritics by Sudhakar. The sample was degassed for 16 h at 90 °C in degas port to remove moisture and gaseous impurities present. The isothermal N_2 gas adsorption and desorption were carried out in analysis port at 77 K using liquid nitrogen enclosure. The sample weight was carefully weighed before degassing, after degassing and after surface area analysis to determine the accuracy of measurement. The specific surface area, pore size and pore size distribution

were determined using Brunauer, Emmet, Teller (BET) method and density functional theory (DFT) methods.

FT-IR spectra were obtained on a model of Vector 22 from Brunker. Most silica samples and composites samples based on silica were prepared as KBR pellets. Other chemicals can be dissolved in a good solvent is mounted as a film on KBR standard sample.

Wide angle X-ray scattering was done on the Rigaku Micro Max 002 X-ray generator operated at 45 kV and 0.66 mA and equipped with R-axis VICC detector. For X-ray studies, single filaments were mounted on the tip of a 0.3 mm diameter glass fibers (Hamilton Research Cat. no. HR8-030) or powder silica were placed in the glass tubes. Crystallinity and orientation from wide angle X-ray diffraction were determined using the software MDI Jade 6.1. AreaMax software was used for background subtraction and integration. The area due to the crystalline and amorphous contribution of the polymer was determined by peak fitting analysis. Prior to executing the auto-fit program, the height and breadths of each peak were adjusted manually in order to provide a reasonable starting point for the curve fitting algorithm to begin. Each peak was modeled using a Gaussian-Lorentzian peak shape. In general, agreement between model predictions and the data were exceptional, yielding coefficients of determination, such as residual error of fit which is very small, usually around 3%. Despite the good agreement, the degree of crystallinity obtained via this analysis still can only be treated as approximate because the initial guess for each peak will influence these results.

FT-IR was trained and most silica samples were prepared as KBR pellets.

3.3 Syntheses

3.3. 1 Mesoporous Silica/PMMA Nanocomposites

3.3.1.1 The preparation of mesoporous silica

3.3.1.1.1 The preparation of mesoporous silica SBA-15

Synthesis of SBA-15: 18.0 g pluronic 123 (EO-PO-EO block copolymer) and 99.5 g 37 wt% HCl were added to 561 g of DI water, and the mixture was stirred under room temperature until a clear solution was obtained. 39.8 g of tetraethyl orthosilicate (TEOS) was added to the clear solution and the mixture was stirred for 20 hours at 35°C. To swell the pores, a temperature treatment of 80°C for 24h was applied. The resulted white solids were filtrated from the solution and copious amount of DI water was used to wash them until there is no bubble from the washed water. The white solids were dried under 80°C. To get rid of all surfactants, the white solids were calcinated using the following temperature program: (1) increasing the temperature (1.2 °C/min) to 200 °C, (2) heating at 200 °C for 1 h, (3) increasing at 1.2 °C/min to 550 °C, and (4) holding at 550 °C for 6 h. Approximately 11.5 g of SBA-15 was collected with this method. Prior to use, the SBA-15 was dried under vacuum at 150 °C for 12 h to remove physisorbed surface water and stored in a vacuo.

3.3.1.1.2 The preparation of mesoporous silica-Bimodal Mesoporous Silica (BMS)

A total of 3.92 g of CTAB followed by 2 g of Na_2SiO_3 were dissolved in 70 ml distilled water with mechanically stirring in an autoclavable polypropylene bottle at room temperature. Then 7 ml of ethyl acetate were quickly added under stirring. After 1min

the stirring was stopped and the mixture was allowed at room temperature for 5 h, then the mixture was placed under 90°C for aging another 50 h. The resulted white solids were washed with copious distilled water and dried in oven. To get rid of the surfactants, the white solids were calcinated using the following temperature program: (1) increasing the temperature (1.2 °C/min) to 600 °C, (2) heating at 600 °C for 20 h. Prior to use, the SBA-15 was dried under vacuum at 120°C for 12 h to remove physisorbed surface water and stored in a vacuo.

3.3.1.2 APTMS grafted onto the surface of mesoporous silica

Mesoporous silica (SBA-15 or BMS) was suspended in anhydrous toluene in a flask under nitrogen atmosphere. After addition of excess APTMS, the mixture was stirred for 24 h. After filtration, the solids were washed with anhydrous toluene three times, once with hexane and were dried overnight at ll0°C under vacuum. The dried white solids were stored in a vacuo.

3.3.1.3 Preparation of 4'-azobis(4-cyanopentanoyl chloride)(ABCC)

Separately a slurry of 40g PCl_5 (190mmol) in 100ml CH_2C1_2 was added to a suspension of 5g ABCA (18mmol) in 50ml CH_2Cl_2 at 0°C (ice water bath). The mixture was stirred overnight under nitrogen while it warmed up to room temperature. The yellow solid was filtered off the mixture, 300 ml dry hexane was added to the filtered colorless solution and ABCC crystallized at 0°C as a white powder. ABCC was washed with dry and cold hexane and dried in vacuum oven at room temperature and stored in a closed plastic bottle in a refrigerator, giving 85% yield.

3.3.1.4 ABCC grafted to the surface of mesoporous silica

A solution of 1.0 g ABCC in 50 ml CH_2C1_2 was added dropwise to a suspension of 2.0g APTMS functionalized silica in CH_2C1_2 with 0.5 ml triethylamine over 1 h while the silica was stirred mechanically. After stirring for an additional 24 h the silica was filtered, washed twice with an acidified water/alcohol (1/1 v/v) mixture, twice with water/alcohol (1/1 v/v), DMSO stirred for 4 hours, then washed twice with alcohol and twice with ether. The initiator immobilized silica was dried overnight in vacuum oven under room temperature. The dried solids were stored in a vacuo.

3.3.1.5 ABCC initiated polymerization of MMA

3.3.1.5.1 ABCC initiated polymerization of MMA in toluene solution

In a typical reaction, solution of methyl methacrylate monomer (20g) in anhydrous toluene (30g) was added to a three-necked round flask under Argon with above synthesized ABCC-functionalized-BMS (or SBA-15, 0.55g) with mechanically stirring. The flask was stirred for additional 2 hours to allow the solution diffused into the nano-channels of BMS. Afterwards, the flask was heated in an oil bath at 80°C for 20 hours. The white solids obtained were dissolved in plenty of THF and refluxed with THF, and centrifugation was used to separate solids from the solution. The above step was repeated until no free polymer could be extracted from the mesoporous silica. The white solids were precipitated from the solution after PMMA-BMS/THF was poured into a beaker with plenty of ether. Afterwards the white solids were stored after being dried in a vacuum oven under room temperature.

3.3.1.5.2 ABCC initiated bulk polymerization of MMA

Firstly 0.55g mesoporous silica with immobilized initiator ABCC was added to the three-necked flask which was evacuated shortly until 0.05 mmHg reached, the white solids were kept under 0.05mmHg for another 20mins. Pure distilled MMA monomer without inhibitor was injected into the vacuumed flask using a syringe. The mixture was still kept under vacuum until no bubbles rise from the mesoporous silica. The flask was heated in an oil bath at 80°C under argon for at least 24 hours. THF was injected into the flask to dissolve the free PMMA synthesized during the polymerization but weren't attached to the surface of mesoporous silica. White solids were separated from the solution using centrifuger at 7000 rpm for 10 mins. The white solids collected were repeated above steps of dissolve and centrifugation until no free polymer can be found in solvent. The mixture of white solids with a little THF was poured into a beak with sufficient of ether and separated with centrifuger. Drying the white solids under room temperature and stored in a plastic bottle.

3.3.2 Preparation of mesoporous silica/nylon 6 nanocomposites

3.3.2.1 Method 1 to prepare mesoporous silica/nylon nanocomposites

3.3.2.1.1 The preparation of Chloro-isophthaloyl-N-ε-caprolactam

Isophthaloyl dichloride(6mmol) was dissolved in anhydrous toluene(30ml) at the presence of triethylamine(4mmol) in a three necked flask under argon protection. Solution of ε-caprolactam(4mmol) dissolved in anhydrous toluene(15ml) was added to flask drop by drop at room temperature. The reaction was stopped when ε-caprolactam

was disappeared in the mixture through monitoring with thin layer chromatography. The mixture of triethylamine hydrochloride and isophthaloyl bis-ε-caprolactam were removed through filtration. The solution after filtration was evaporated using a rotary evaporator until white crystals begin to precipitate at the temperature of 40° C. N-(3-chloroformylbenzoyl)-ε-caprolactam with form of white crystals was precipitated after very little anhydrous diethyl ether was added to the residue solution. Around 8g pure chloro-isophthaloyl-N-caprolactam crystals were obtained after repeatedly washing of the white crystals with using diethyl ether.

3.3.2.1.2 Graft N-acyllactam on the surface of mesoporous silica

Typically 3.09g chloro-isophthaloyl-N-caprolactam was added to 2.43g of amine functionalized SBA-15 (BMS) in 30ml anhydrous methane dichloride with 0.7 ml triethylamine. This mixture was stirred for 30h at room temperature. The resulting solids was filtered, washed with water, DMSO, methanol, methane dichloride and hexane, dried under vacuum at 90°C for 24 h, and then stored in a vacuo.

3.3.2.1.3 Silanol Capping on N-acyllactam Functionalized SBA-15.

Typically, 1 g of HMDS was added to a slurry of 1.0 g of N-acyllactam-SBA 15 in 20 ml of anhydrous toluene in a two necked 100 mL round-bottom flask. The mixture was then stirred at room temperature under an Argon atmosphere for 24 h. The product was recovered and washed with copious amounts of toluene and THF. The solid product was then dried in vacuo at 100 °C for 40 h before being stored in a vacuo.

3.3.2.1.5 Anionic polymerization to synthesize BMS silica/nylon-6 nanocomposites

Typically, 10 g of epsilon-caprolactam was placed in a 100ml round bottom flask and heated to 140°C with vacuum until 5% of monomer was pulled out. While temperature of the flask was slowly decreased to room temperature, 1ml anhydrous DMAC was injected into the flask and mixed with monomer of epsilon-caprolactam. 1 g of N-acyllactam functionalized mesoporous silica (SBA-15 or BMS) was added to the flask and they were placed on the surface of solid epsilon-caprolactam/DMAC mixture, temperature was slowly increased to 100°C under 1mm Hg to let the monomer/solvent diffuse into the nano-channels of mesoporous silica. Temperature was decreased again to allow all monomer to become solids while high vacuum was kept at least 20 mins to let the anhydrous DMAC was extracted as much as possible. The temperature of flask was increased to 140°C with normal pressure and stirring, 1ml of 1M MgBrEt solution was injected into the flask with stable temperature of 140°C. Reaction continued until it was stopped after 24 h. Suitable formic acid was added to the flask and stirring for a long time until a homogeneous solution was obtained, the mesoporous silica were separated from formic acid using centrifuger running 15 minutes at a rate of 7000 rpm. Formic acid was repeatedly used to wash the white solids until no nylon 6 can be found in formic acid. The white solids were washed with ether and dried under room temperature in a vacuum oven after most ether evaporated in open hood.

3.3.2.2 Method 2 to synthesize mesoporous silica/nylon nanocomposites

3.3.2.2.1 Preparation of N-3-((N-3-(trimethoxysilanyl)n-propyl)benzamidyl)-benzoyl-epsilon-caprolactam

Separately 3.52g 3-aminopropyltrimethoxysilane and 30ml anhydrous THF were added to a three-necked flask under argon. The solution of 5.58g Chloro-isophthaloyl-N-ε-caprolactam dissolved in solution of 20ml THF and 2.02g triethylamine was dropwise added to the flask with mechanically stirring at 0°C (ice water bath). The mixture was stirred overnight under nitrogen while it warmed up to room temperature. After filtration, white solids were separated from the mixture. The solution after filtration was place in a one-necked flask, which was rotated from a rotated evaporator to get rid of all solvent. Finally colorless viscous liquid were obtained and stored in a closed plastic bottle.

3.3.2.2.2 Grafting N-3-((N-3-(trimethoxysilanyl)n-propyl)benzamidyl)-benzoyl-epsilon-caprolactam onto the surface of mesoporous silica.

Excess N-3-((N-3-(trimethoxysilanyl)n-propyl)benzamidyl)-benzoyl-epsilon-caprolactam was added to 1g of mesoporous silica(SBA-15 or BMS) in anhydrous toluene. The mixture was allowed to stir for 24 h at room temperature under argon. The resulting solids were filtered, washed with anhydrous toluene twice, dried under vacuum at 80°C overnight and then stored in a vacuo.

3.3.2.2.3 Silanol-Capping N-acyllactam immobilized mesoporous silica.

The capping synthesis was carried out by stirring a large excess of hexamethyldisilazane (HMDS) with N-acyllactam functionalized mesoporous silica obtained from the previous step in anhydrous toluene at room temperature under argon for 24h. The resulting solid was filtered and washed with toluene and hexane repeatedly, dried under vacuum at 80°C overnight and then stored in a vacuo.

3.3.2.2.4 Anionic polymerization to synthesize mesoporous silica/nylon-6 nanocomposite

Similar to previous step of 3.3.2.1.5, anionic polymerization was initiated for mixture of silanol-capping N-acyllactam immobilized mesoporous silica and epsilon-caprolactam. Mesoporous silica/nylon nanocomposites without free nylon were obtained after the resulted white solids were repeated washed with fomic acid and finally washed with ether. The synthesized mesoporous silica/nylon 6 composites were dried in a vacuum oven at 50°C and stored in a vacuo.

3.3.3 Mesoporous silica/polystyrenesulfonic acid or polyacrylic acid nanocomoposites

3.3.3.1 Preparation of mesoporous silica

A total of 3.92 g of CTAB followed by 2 g of Na_2SiO_3 were dissolved in 70 ml distilled water with mechanically stirring in an autoclavable polypropylene bottle. The sodium polyacrylate solution was dropped to the PP bottle with stirring. Then 3, 5 or 7 ml of ethyl acetate were quickly added under stirring, the amount of ethyl acetate corresponds to samples MS-1, MS-2 and MS-3 respectively. After 30s the stirring was stopped and the mixture was allowed at room temperature for 5 h, then the mixture was placed under 90°C for aging another 50 h. The resulting white solids were washed with copious distilled water.

3.3.3.2 Preparation of mesoporous silica/polyacrylic acid nanocomposite with morphology of round particle.

A total of 3.92 g of CTAB followed by 2 g of Na2SiO3 were dissolved in 60 ml distilled water with mechanically stirring in an autoclavable polypropylene bottle. Afterwards 0.3 g sodium polyacrylate (Mw 5100) was dissolved in 10g distilled water. The sodium polyacrylate solution was dropped to the PP bottle with stirring until homogenous mixture. Then 3, 5 or 7 ml of ethyl acetate were quickly added under stirring, the amounts of ethyl acetate corresponding to samples 1, 2 and 3. After 30s the stirring was stopped and the mixture was allowed at room temperature for 5 h, then the mixture was placed under 90°C for aging another 50 h. The resulted white solids were washed with copious distilled water and were refluxed with a large amount of 1M H_2SO_4/methonal to get rid of the surfactants. After reflux with methanol, the solids was filtered and dried in a vacuum oven.

3.3.3.3 Preparation of BMS/poly(styrene sulfonic acid) nanocomposite

A total of 3.92 g of CTAB were dissolved in 58 ml distilled water with mechanically stirring in an autoclavable polypropylene bottle. Afterwards 1g poly(sodium 4-styrene sulfonate) (M_w 200,000) followed by 2 g of Na_2SiO_3 was dissolved in 12g distilled water in a beaker. The solution in the beaker was dropped to the PP bottle with stirring until homogenous mixture. Then 3, 5 or 7 ml of ethyl acetate were quickly added under stirring, the amounts of ethyl acetate corresponding to samples 1, 2 and 3. After 30s the stirring was stopped and the mixture was allowed at room temperature for 5 h, then the mixture was placed under 90°C for aging another 50 h. The resulted white solids were washed with copious distilled water and were refluxed with a

large amount of 1M H_2SO_4/methonal to get rid of the surfactants. After reflux with a lot of methanol, the solids was filtered and dried in a vacuum oven.

3.3.3.4 The preparation of SBA-5/PSSA nanocomposites

Synthesis of mesoporous silica/PSSA nanocomposites: 6.05 g pluronic 123 (EO-PO-EO block copolymer), 3.73g 30 wt% of poly(4-styrene sulfonate acid)(M_w 200,000) and 34.7 g 37 wt% HCl were added to 160.1 g of DI water, and the mixture was stirred under room temperature until a clear solution was obtained. 12.65 g of tetraethyl orthosilicate (TEOS) was added to the clear solution and the mixture was stirred for 20 hours at 35°C. To swell the pores, a temperature treatment of 80°C for 24h was applied. The resulted white solids were filtrated from the solution and copious amount of DI water was used to wash them until there is no bubble from the washed water. The white solids were dried at 80°C. To get rid of all surfactants, the white solids were refluxed with a large amount of 1M H_2SO_4/methonal. After reflux with excess methonal, the solids was filtered and dried in a vacuum oven.

3.3.3.5 Preparation of mesoporous silica/poly(styrene sulfonic acid) nanocomposite using TEOS

Method 1 under base condition: A total of 1.582 g of CTAB, 0.799 g of NaOH was dissolved in 100 ml distilled water with mechanically stirring in an autoclavable polypropylene bottle. Afterwards sodium polyacrylate (M_w 5100) was dissolved in the solution with stirring until homogeneous solution. Afterwards 8.403 g of TEOS was added to the homogeneous solution and the mixture was stirred for 20 hours at 35°C. To

swell the pores, a temperature treatment of 80°C for 24h was applied. The resulting white solids were filtrated from the solution and copious amount of DI water was used to wash them until there is no bubble from the washed water. The white solids were dried at 80°C. To get rid of all surfactants, the white solids were refluxed with a large amount of 1M H_2SO_4/methonal. After reflux with excess methanol, the solids was filtered and dried in a vacuum oven.

Method 2 under acid condition: A total of 1.582 g of CTAB, 10 g 37% of HCl was dissolved in 90 ml distilled water with mechanically stirring in an autoclavable polypropylene bottle. Afterwards 0.412g poly(sodium 4-styrene sulfonate)(M_w 200,000) was dissolved in 10 ml water. The above two solution was mixed with stirring until homogeneous solution. Afterwards 8.403 g of TEOS was added to the homogeneous solution and the mixture was stirred for two days at 35°C. To swell the pores, a temperature treatment of 80°C for 24h was applied. Other steps are the same as method 1. Finally 4.2 g white solids were obtained after drying.

3.3.3.6 Polymerization of epsilon-caprolactone with supported catalysts of mesoporous silica/PSSA nanocomposites.

In a typical reaction, 20ml anhydrous toluene was combined with 1 g of dodecane in a three necked flask fitted with rubber septum. 0.1 ml benzyl alcohol and 6 g epsilon-caprolactone are added to the flask. And 0.3 g supported catalysts of mesoporous silica/PSSA nanocomposites are added to the flask. The flask was placed to an oil bath with temperature of 52°C for three days with GC monitored the conversion. The solution was centrifuged to separate the solid catalysts of mesoporous silica/PSSA

nanocomposites, the separated solution was placed in equipment of rotating evaporator to get rid of toluene. Afterwards, a yellow oily liquid are obtained and placed into cold hexanes to get white polymer. The synthesized polymer was characterized with H^1 NMR and GPC.

CHAPTER 4

MESOPOROUS SILICA/PMMA NANOCOMPOSITES

To initiate the free radical polymerization inside the nano-channels of mesoporous silica, one simple way is to evaporate the mixture of monomer with initiator inside the nano-channels and initiate the polymerization. This method can synthesize polymer inside the nano-channels while the synthesized polymer has no covalent bonds with the surface of mesoporous silica, and synthesized polymer can't grow out of the nano-channels and cover the mesoporous silica because there is no free monomer outside the nano-channels. To overcome this disadvantages, the better way is to graft the initiator onto the surface of mesoporous silica through covalent bonds.

Scheme 4.1 provides the procedures of grafting a kind of initiator ABCA for free radical polymerization onto the surface of mesoporous silica and polymerization can be initiated inside the nano-channels through surface initiated free radical polymerization. The synthesized polymer can grow from the initiator center on silica surface and out of nano-channels if there is enough MMA monomer while all surface initiated polymer are still covalent bonded with the surface of mesoporous silica.

This proposed synthesis scheme grafts initiator on the surface of silica through amine groups which are commonly grafted onto silica surface through APTMS in literatures. Chosen initiator of ABCA can be used to initiate free radical polymerization of most monomer with vinyl group. MMA monomer is chosen to finish the polymerization with this method while other monomer can also be polymerized through free radical polymerization.

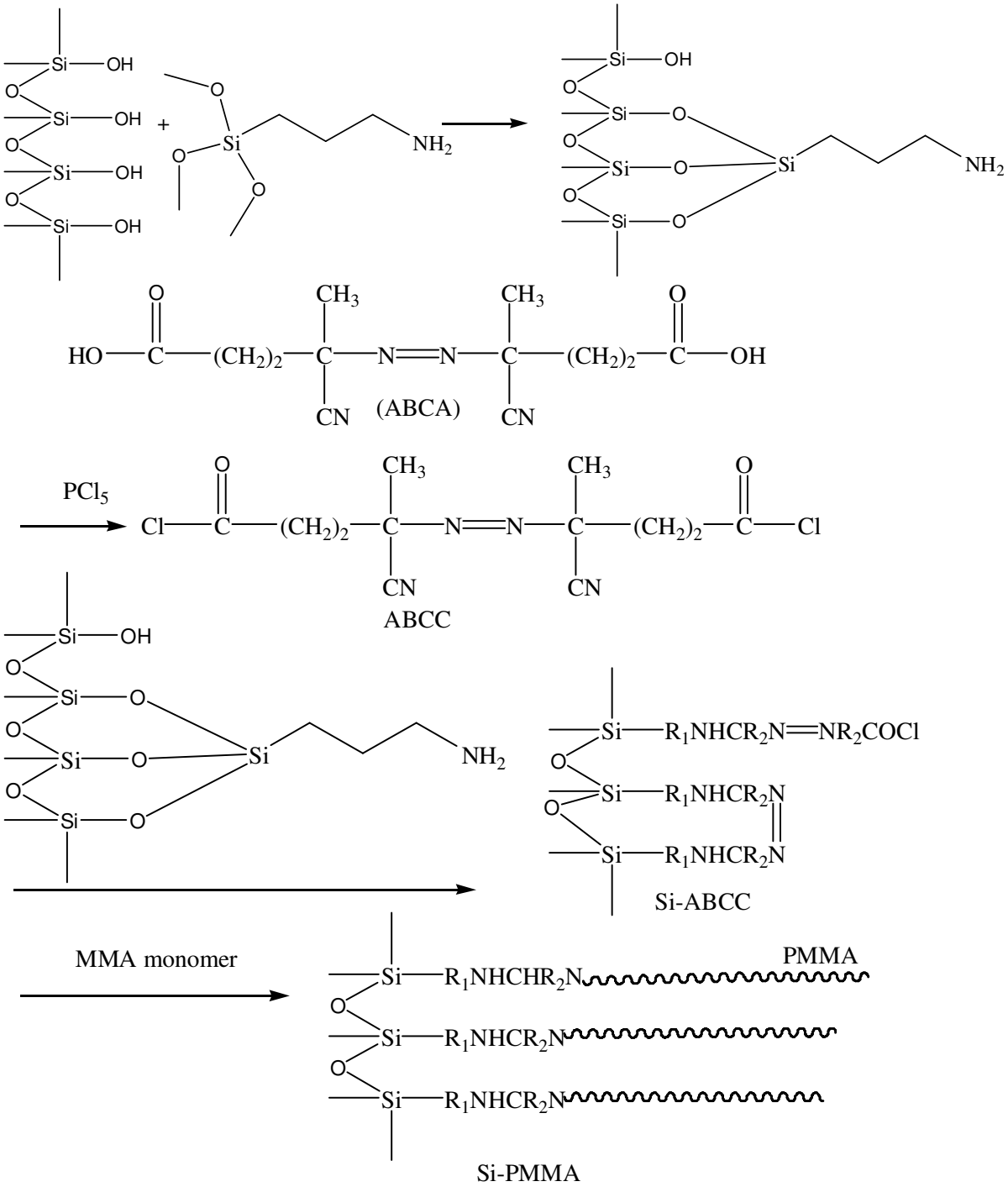

Scheme 4. 1 Procedures to synthesize mesoporous silica/PMMA nanocomposites

4.1 Synthesis of SBA-15/PMMA composites

4.1.1 The initiator ABCC immobilized mesoporous silica SBA-15

Scheme 4.1 shows the procedures to synthesize mesoporous silica/PMMA nanocomposites. ABCA is a kind of azo-initiator and it can be used to initiate free radical polymerization for many monomers with vinyl group. In this research, ABCA should be transferred to ABCC so that carboxylic acid can be transferred to acid chloride which can react with amine groups. Synthesis of ABCC using ABCA, the PCl_5 and ABCA was stirred overnight to make all carboxylic acid groups to be transferred to acid chloride because less reaction time will produce incomplete conversion. There is a carboxylic acid peak at position of 12.2 from H^1 NMR spectra of ABCA (Figure 4.1), however there isn't carboxylic acid peak from H^1 NMR spectra of ABCC (Figure 4.2). The comparison of these two NMR spectra tells us that all carboxylic acid groups are successfully transferred to acid chloride after the reaction. And all other peaks also just verify the structure of ABCA and ABCC. Because the acid chloride is very active and to be easily transferred back to carboxylic acid, some acid chloride groups of the ABCC will be transferred to carboxylic acid after ABCC was stored over some time, which is verified from the phenomena that very few solids can not be dissolved in methylene dichloride. Ideally, both acid chloride groups of ABCC can react with amine groups on the surface of mesoporous silica if there is no impurity. Because of the existence of impurity from ABCC, not all the initiator molecules are linked to the mesoporous silica surface with two ends of initiator of ABCC. To get rid of unreacted ABCA or other impurities, the immobilized radical initiator was repeatedly washed with DMSO and washed with alcohol and ether.

Figure 4.3 shows the FT-IR spectra of dried SBA-15, amine immobilized SBA-15 and initiator immobilized SBA-15. As amine groups are grafted onto the surface of BMS, FT-IR spectra of amine-functionalized-BMS shows the amine absorptions peaks at 1550 and 695 cm^{-1}, proving the amine functional groups are grafted onto BMS. When the second grafting step of ABCC reacted with amine groups from the silica surface was finished, FT-IR spectra of ABCA-functionalized-BMS shows the amide absorptions peaks at 1640 and 1450 cm^{-1}, proving that new functional group of amide bonds have been formed. FT-IR spectrum of radical initiator ABCC immobilized SBA-15 also shows a small peak at 1720(cm^{-1}), proving the existence of carbonyl bonds.

DSC thermograms also verify that initiator ABCC was mounted onto the surface of mesoporous silica through amine group, which was immobilized onto the surface of mesoporous silica SBA-15 to form ABCC immobilized SBA-15. DSC thermograms of ABCC (Figure 4.4) showed endotherm at 81°C and exotherm at 115°C. The endotherm is its melting peak because its melting temperature is 80°C. The exotherm is the decomposed peak because the initiator only decomposes above its melting point in the dry solid state. DSC thermograms of ABCC (Figure 4.5) immobilized silica showed endotherm at 42 °C and exotherm at 119°C. The endotherm at 42°C is the solvent of ether peak. It is very difficult to get rid of all solvent for ABCC immobilized mesoporous silica at room temperature because of the large surface area and structure of ultra-small nano-channels. And the solids were repeatedly washed with organic solvent which is diffused into the nano-channels, and it is difficult to evaporate all nano-channels entrapped solvent at room temperature even under very high vacuum. High temperature drying will produce the decomposition of initiator of ABCC. The exotherm at 119°C is

the initiator decomposition peak and 119°C is 4 degree C higher than 115°C which is the decomposition temperature of pure ABCC. The decomposition temperature of ABCC immobilized SBA-15 is 4°C higher than that of ABCC, the reason is probably that the solid support SBA-15 limit the moving activity of initiator and higher energy barrier are needed to overcome. The similarity of DSC curve of immobilized ABCA and ABCC verifies the initiator of ABCC is successfully grafted onto the surface of mesoporous silica SBA-15.

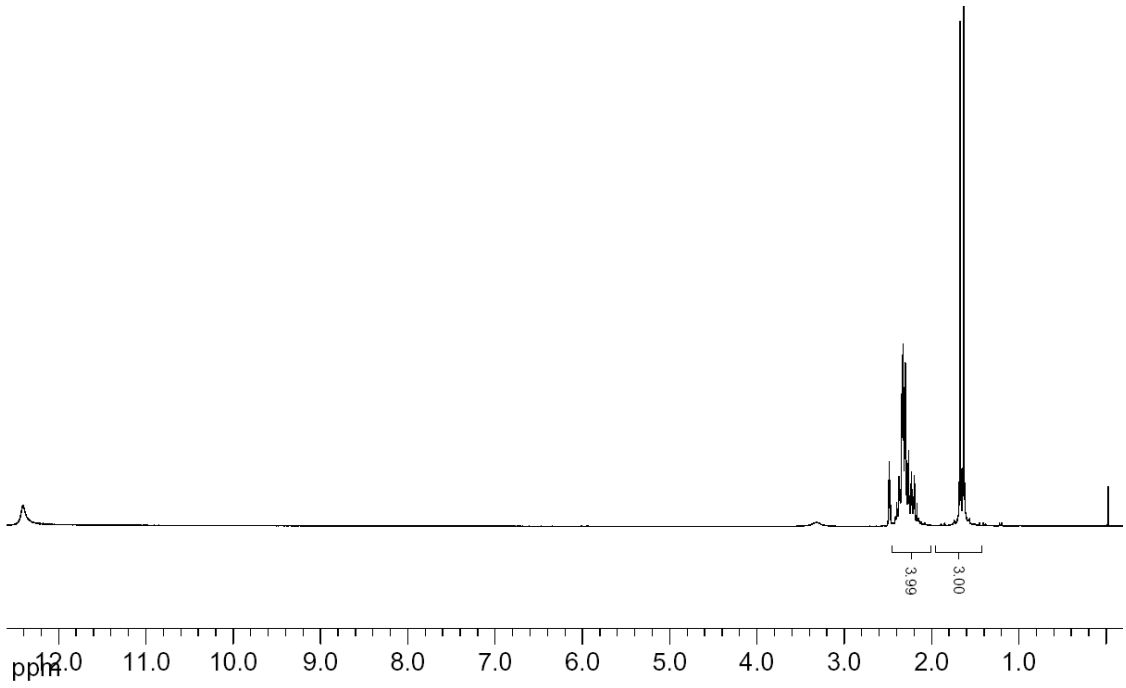

Figure 4. 1 H^1 NMR of ABCA

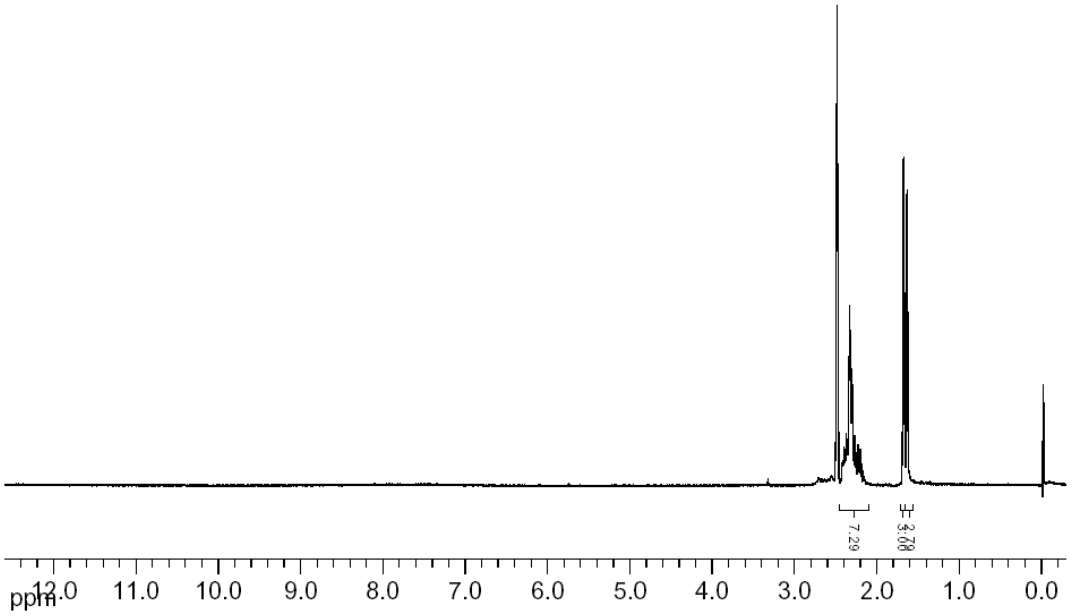

Figure 4. 2 H^1 NMR of ABCC

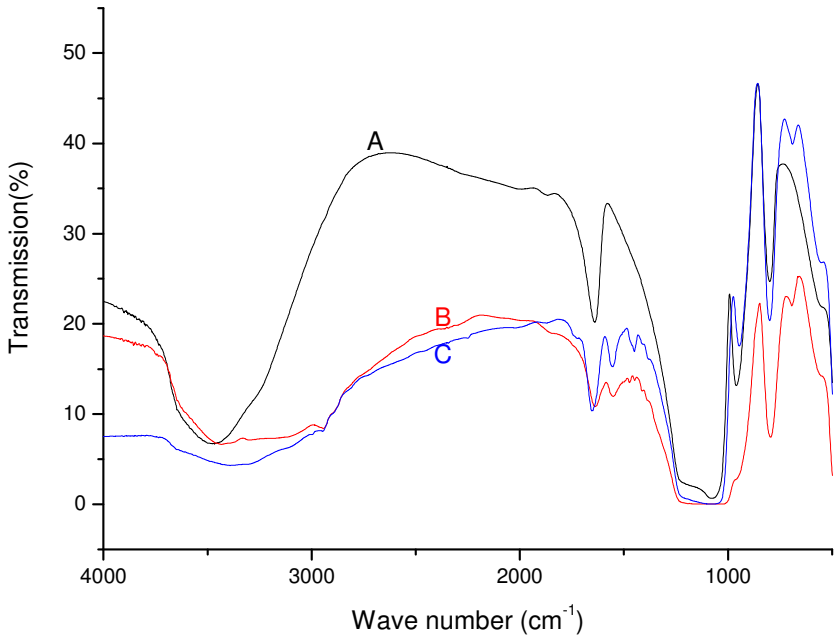

Figure 4. 3 Spectra of (A) SBA-15, (B) immobilized amine and (C) immobilized ABCA

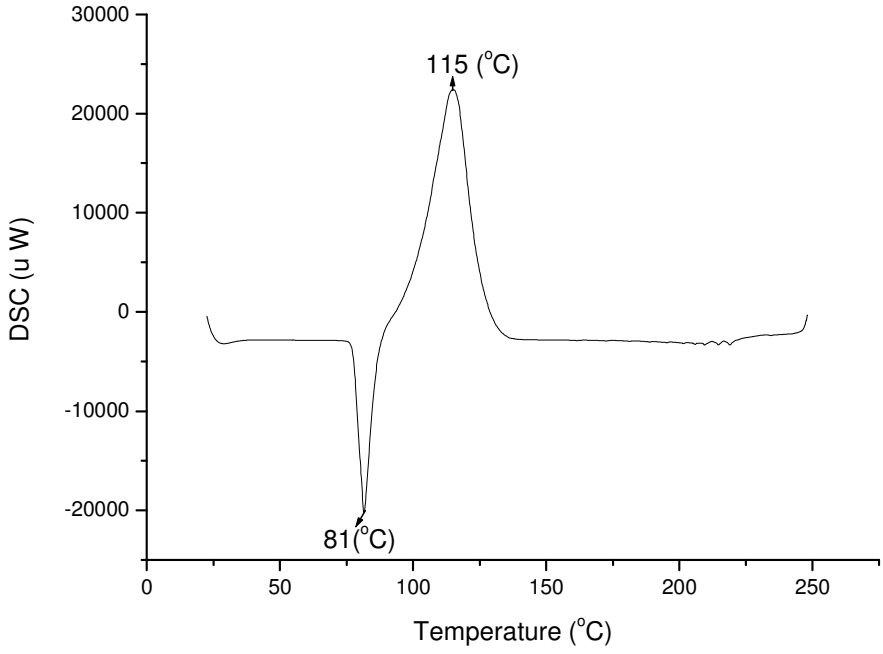

Figure 4. 4. D. s. c thermograms of ABCC

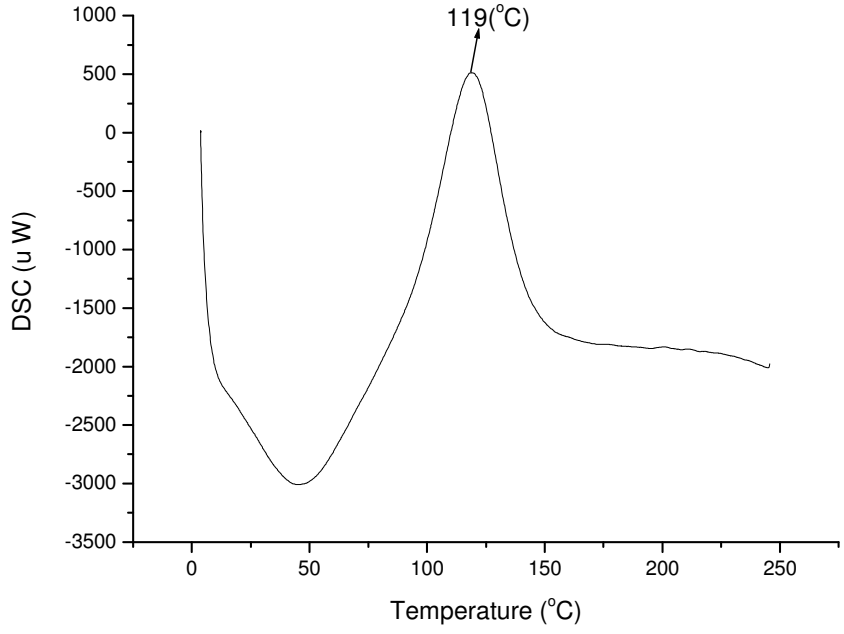

Figure 4. 5 D. s. c thermograms of ABCC immobilized SBA-15

4.1.2 Synthesized SBA-15/PMMA nanocomposites

PMMA was synthesized when MMA monomer, radical initiator immobilized SBA-15 and toluene were stirred for 36 h at 80 °C. All radical initiators were grafted onto the surface of SBA-15, but some initiator molecules only had one end linked to the surface of SBA-15. When the initiator molecules were decomposed, one radical would be free from the surface of SBA-15 and initiated the polymerization and formed a PMMA chain without covalent bond from the surface of solid support SBA-15. Another radical with one end covalent bonded with silica surface would also initiate the polymerization and formed a PMMA chain. These PMMA without covalent bond with silica surface would be dissolved in THF and was separated from silica SBA-15-supported-PMMA using method of centrifugation. SBA-15/PMMA composites were collected after repeatedly washing and drying. These PMMA without bonds with silica surface could also be precipitated from PMMA/THF solution when the solution was added to petroleum ether. The synthesized pure PMMA and SBA-15/PMMA composites were characterized with DSC, TGA and GPC.

DSC thermograms of synthesized PMMA (Figure 4.6) showed the glass transition temperature at 110°C and the synthesized PMMA was amorphous PMMA because there was no melting peak. From DSC thermograms of SBA-15/PMMA nanocomposite(Figure 4.7), there was a nonobvious glass transition point which was 8°C higher than that of pure PMMA, the reason was probably that the solid support SBA-15 limited the flexibility of the PMMA molecular chain. From the comparison, the glass transition temperature of pure PMMA was more obvious and lower than that of SBA-15/PMMA composites.

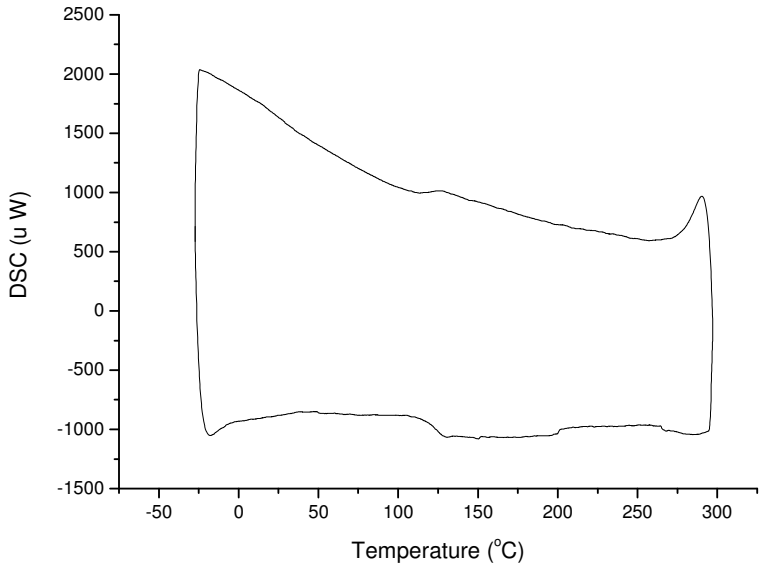

Figure 4. 6 D. s. c thermograms of synthesized PMMA without covalent bonds with mesoporous silica

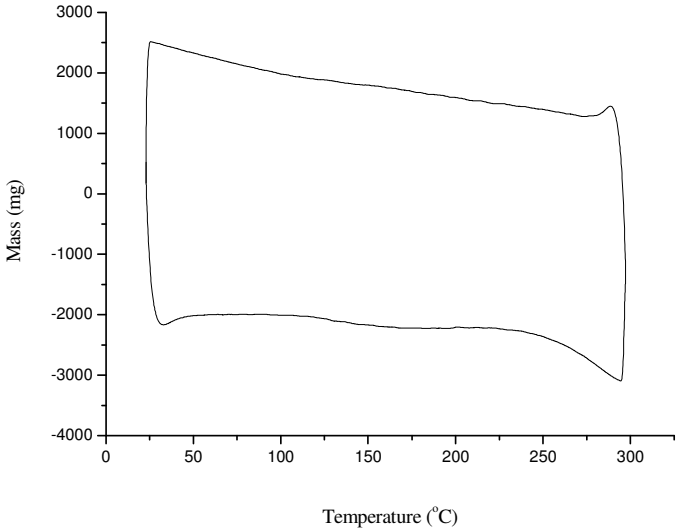

Figure 4. 7 D. s. c thermograms of SBA-15/PMMA composites

TGA of synthesized pure PMMA without covalent bonds with silica surface (Figure 4.8) showed PMMA began to decompose at 300°C and its mass decreased to zero

at 400°C, the decomposition temperature(using the largest decomposition rate as decomposition temperature) of PMMA was at 350°C. TGA of PMMA/SBA-15 nanocomposites (Figure 4.9) showed the composite began to decompose at 300°C and its remaining mass decreased to 50% of the original mass at 600°C and then a stably flat curve was obtained which told us that 50 wt% of the composites was PMMA and 50 wt% of the composites was mesoporous silica SBA-15. The decomposition temperature was 370°C which was 20°C higher than that of pure PMMA. Both TGA curves showed a similarity of decomposition which also verified the existence of PMMA in SBA-15/PMMA composites.

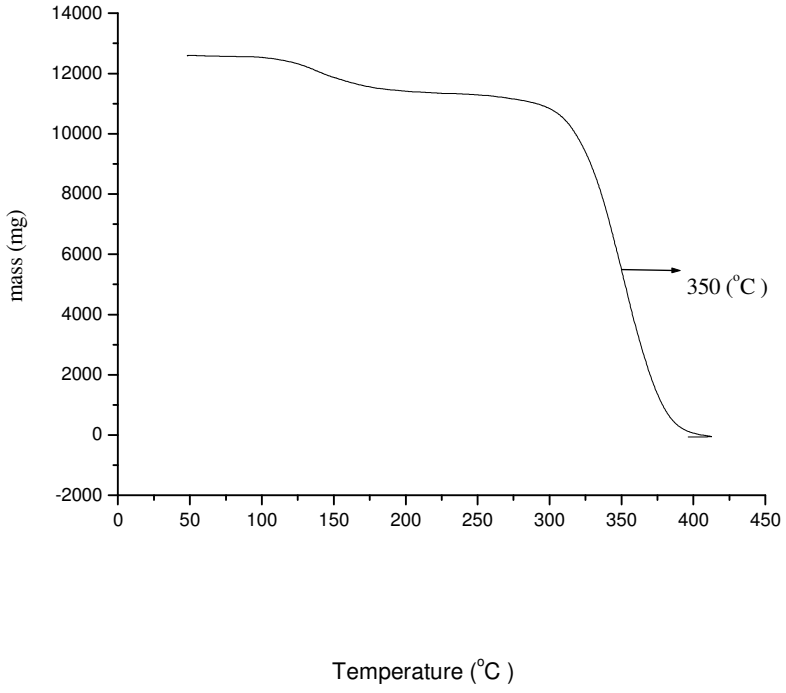

Figure 4. 8 TGA graph of PMMA free of mesoporous SBA-15

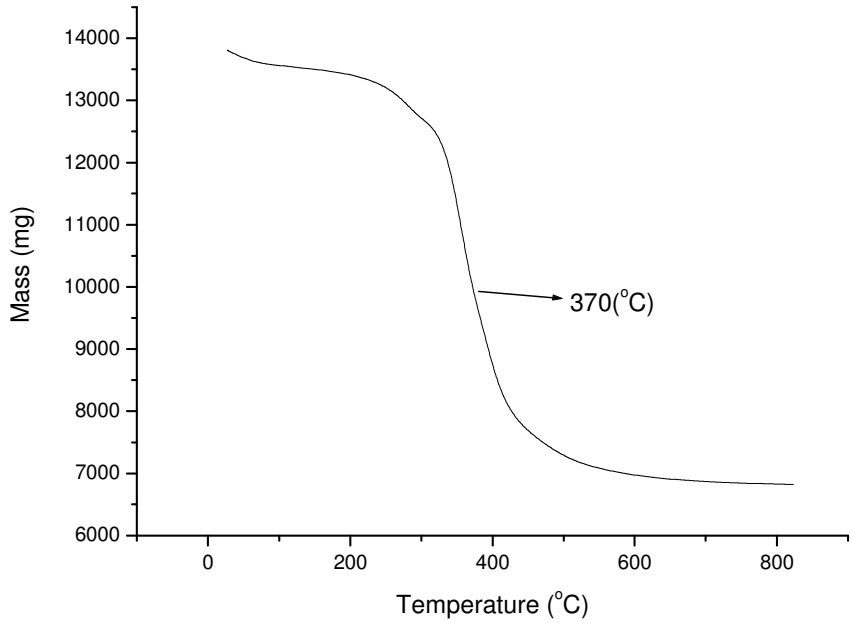

Figure 4. 9 TGA graph of PMMA/SBA-15 nanocomposite

The synthesized PMMA without covalent bonds with silica surface was also characterized with GPC, the result showed that the M_n was 121263 g/mol, the M_w was 211845 g/mol and its polydispersity index was 1.75. Because morphology of SBA-15 was irregular, it was very difficult to investigate the change of morphology. We planned to use another mesoporous silica materials BMS (bimodal mesoporous silica) to do further research.

4.2 Synthesis of BMS/PMMA nanocomposites

The bimodal mesoporous Silica (BMS) was synthesized according to steps from the literature. Figure 4.10 showed the synthesized BMS with spherical morphology, and

the diameter of the sphere was around 2.5 μm. The pore distribution of BMS was shown in Figure 4.12 which showed two different range of pore distribution, most pore sizes were between 10 and 30nm, and a few pores were between 2 and 5nm. This was the reason why this mesoporous silica was called bimodal mesoporous silica.

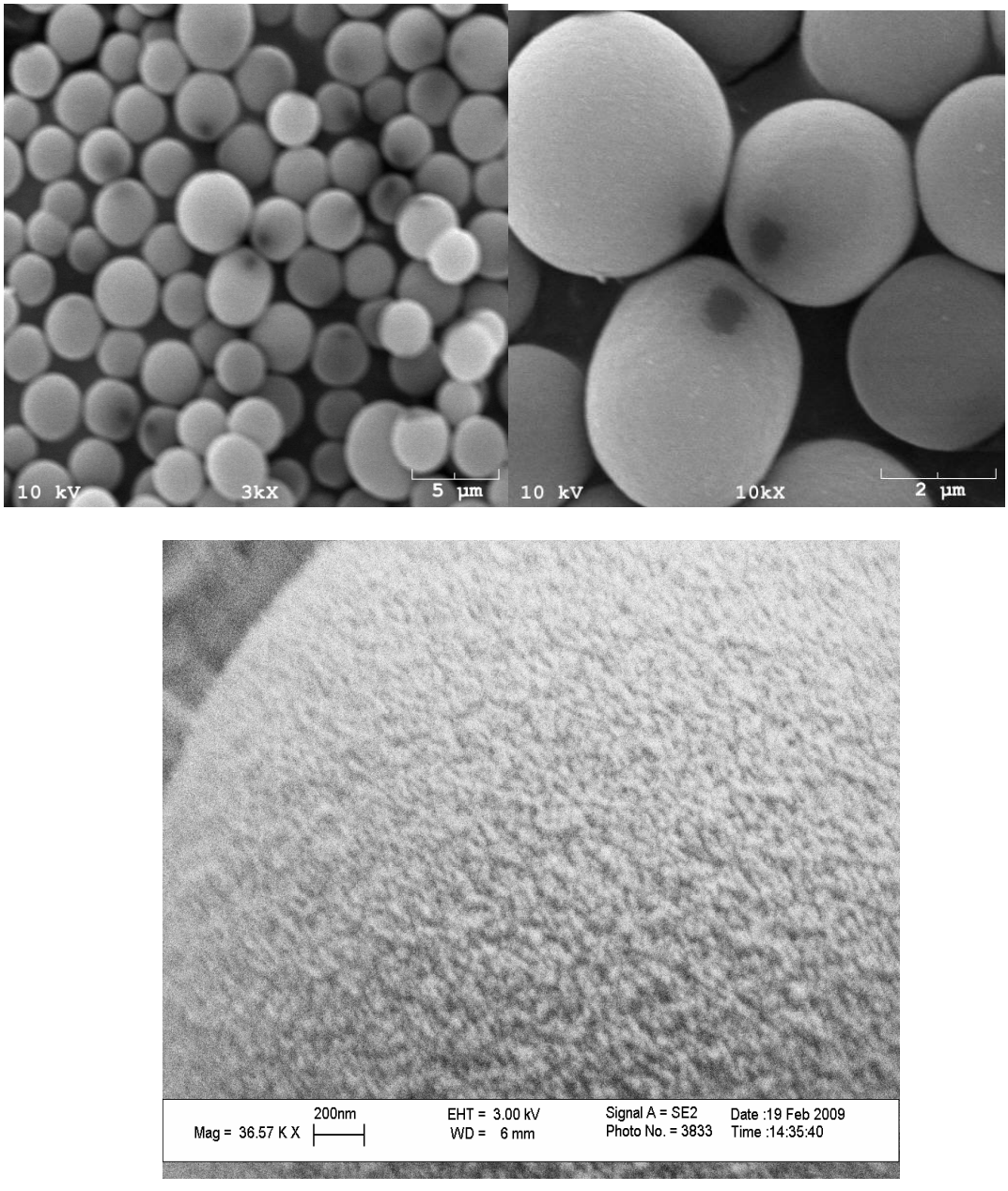

Figure 4. 10 Scanning electron microscopy(SEM) images of BMS with different magnifications.

4.2.1 Surface analysis of BMS and its derivatives

Because SBA-15 doesn't posses regular morphology, it was very difficult to tell the difference of pure SBA-15 surface with SBA-15/PMMA composites. With the similar steps to graft ABCC onto the surface of mesoporous SBA-15, ABCC-immobilized-BMS was synthesized. Adsorption isotherms of nitrogen graph of BMS, amine immobilized BMS and ABCA immobilized BMS (Figure 4.11) and shows that all three curves were pronounced hysteresis loop, which revealed the presence of mesopores. From pure BMS, amine-immobilized-BMS to ABCC-immobilized-BMS, the pore width didn't change a lot, but the pore volume decreased significantly (Figure 4.12). Both pore volume and surface area of these three mesoporous materials are shown in Table 4.1 characterized from nitrogen adsorption/desorption isotherm, which shows that both pore volume and surface area were decreased as more chemicals were grafted onto the surface of BMS. From pure BMS, amine immobilized BMS to ABCC immobilized BMS, the surface area was decreased from 606.8, 362.0 to 246.3 m^2/g, and the pore volume was decreased from 1.775, 1.314 to 0.956 cm^3/g. The reason was that the diameters of the nano-channels decreased as organic chemicals grafted onto silica surface, therefore, the surface area and pore volume would also decrease accordingly. We see that the pore volume decreased almost 45% when initiator molecule was grafted on silica surface. These BET data also verified that the amine and ABCC molecules were successfully grafted onto the surface of inner wall of mesoporous silica BMS. Compared with the surface area of the inner walls of nano-channels, the surface outside the nano-channels could be neglected. Scanning electron microscopy (SEM) images of ABCC immobilized BMS (Figure 4.13)

also showed spherical BMS although there were very few impurities between the spheres. The diameters of sphere were the same as the pure BMS.

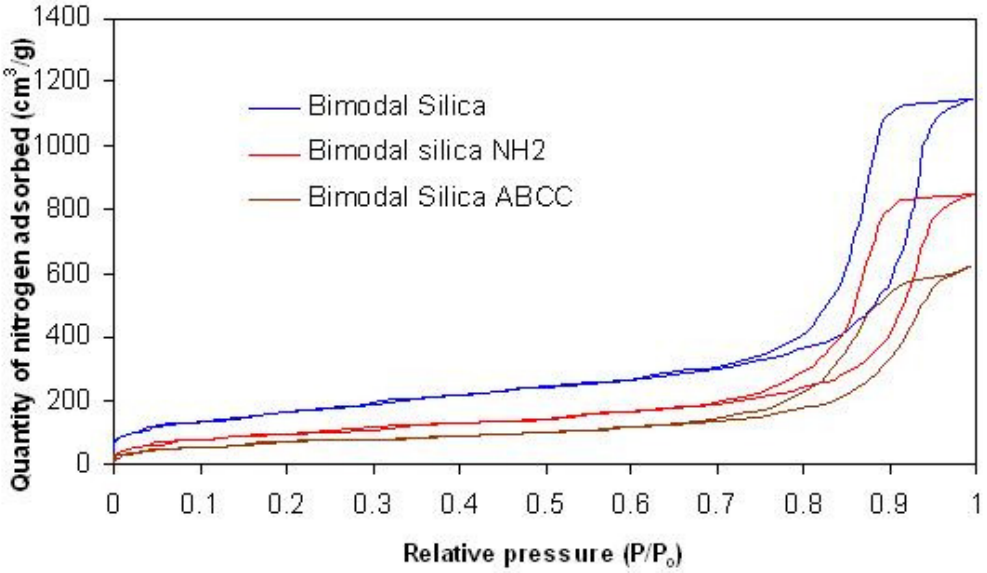

Figure 4. 11 Adsorption isotherms of nitrogen at 77K on BMS, amine immobilized BMS and ABCA immobilized BMS

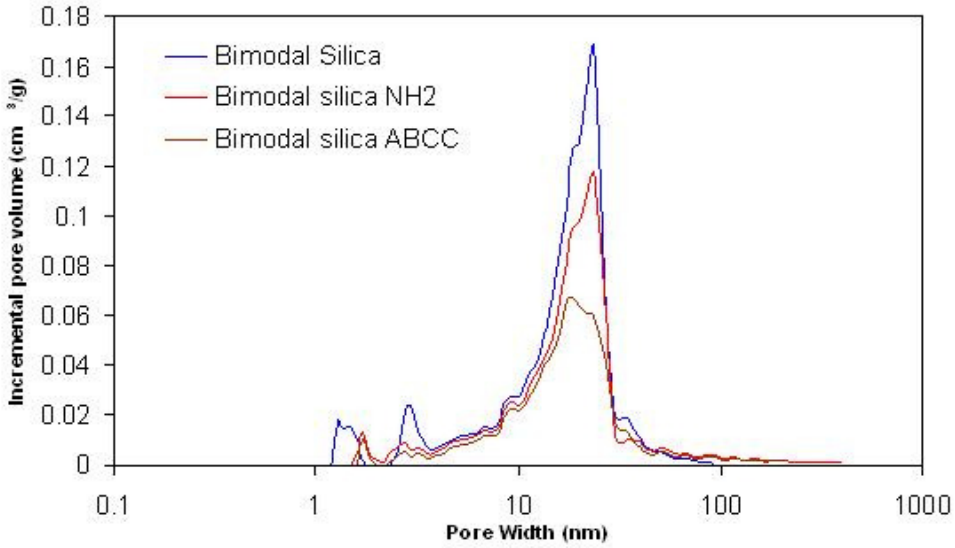

Figure 4. 12 Pore size distribution of BMS, amine immobilized BMS and ABCA immobilized BMS

Table 4. 1 Adsorption isotherms of nitrogen data for BMS, amine immobilized BMS and ABCC immobilized BMS

Sample name	Surface area(m^2/g)	Pore Volume(cm^3/g)
BMS	606.8	1.775
NH2 immobilized BMS	362.0	1.314
ABCC immobilized BMS	246.3	0.956

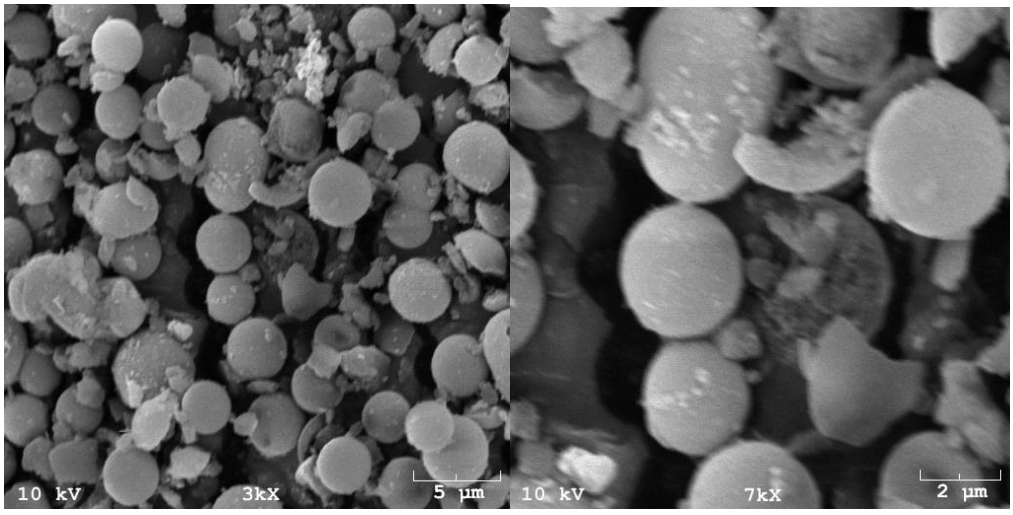

Figure 4. 13 Scanning electron microscopy(SEM) images of ABCC immobilized BMS with different magnifications.

4.2.2 Thermal analysis of BMS/PMMA nanocomposites

The organic loading was measured by determining the weight loss between 200°C to 600°C through TGA. Figure 4.14 show the thermogravimetic analysis (TGA) graph of amine immobilized BMS (left) and ABCC immobilized BMS (right). For amine immobilized BMS, the weight loss between 200°C and 600°C is 7.52% which

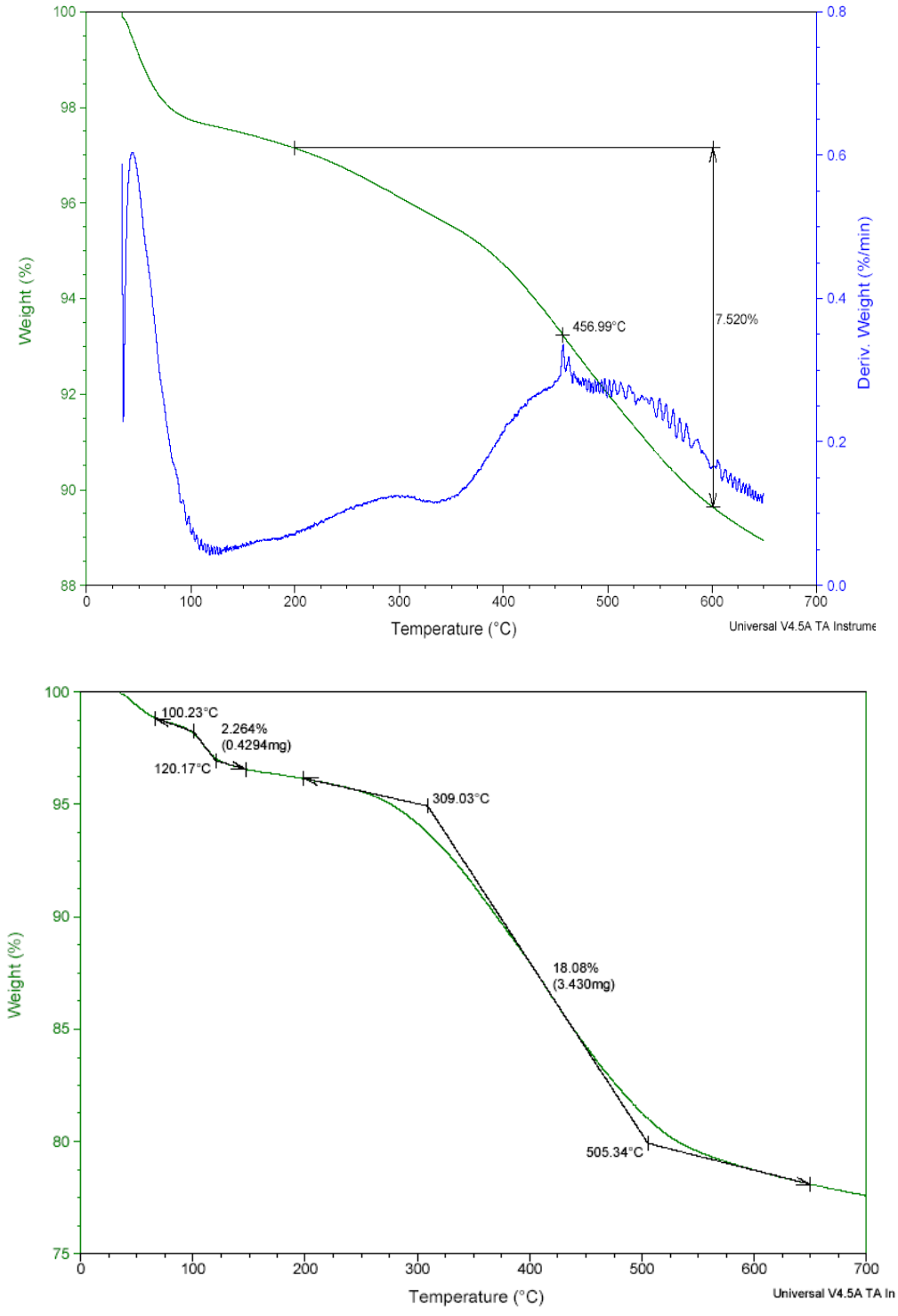

Figure 4. 14 Thermogravimetic analysis (TGA) graph of amine immobilized BMS (upper) and ABCA immobilized BMS (lower)

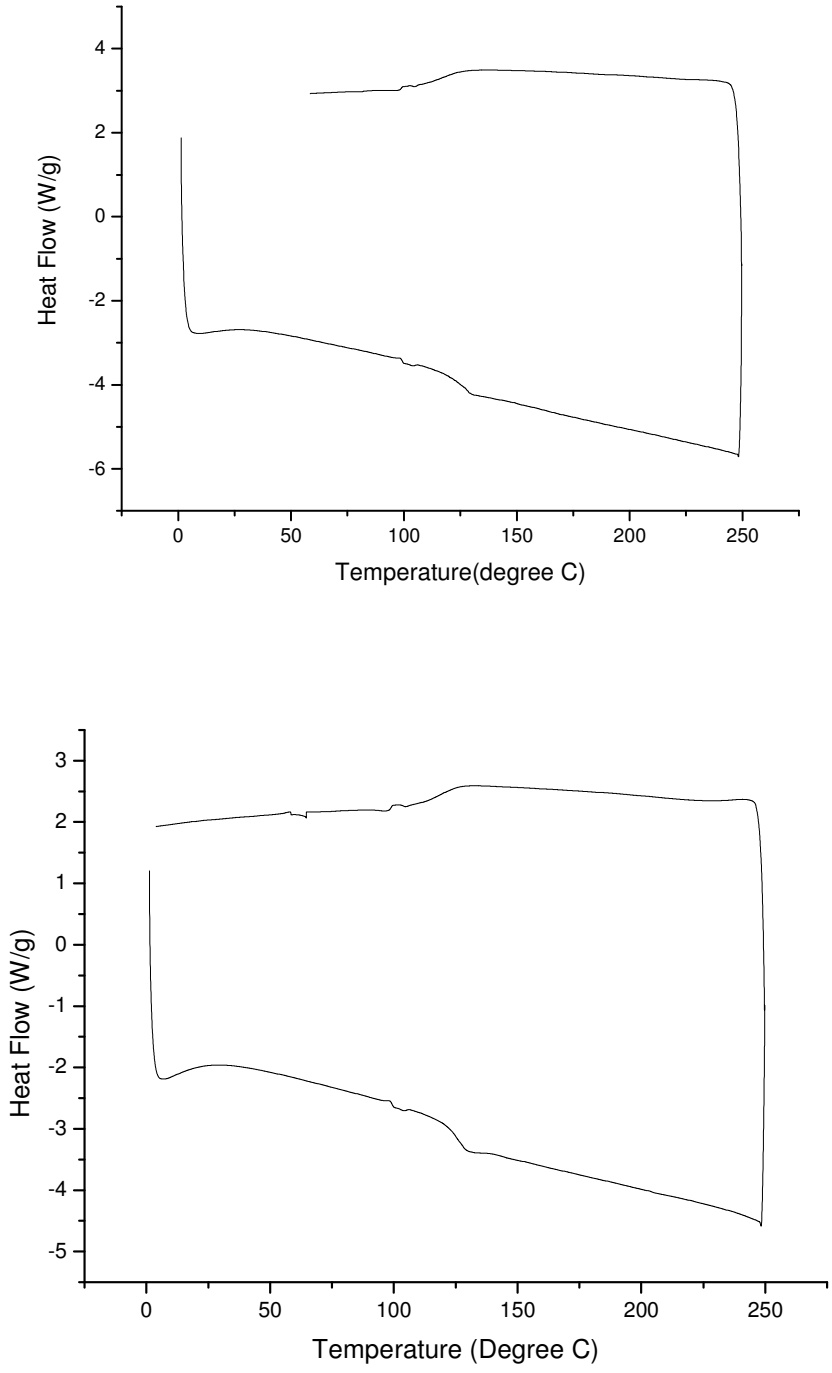

Figure 4. 15 D.S.C thermograms of BMS/PMMA (upper) and pure commercial PMMA (lower)

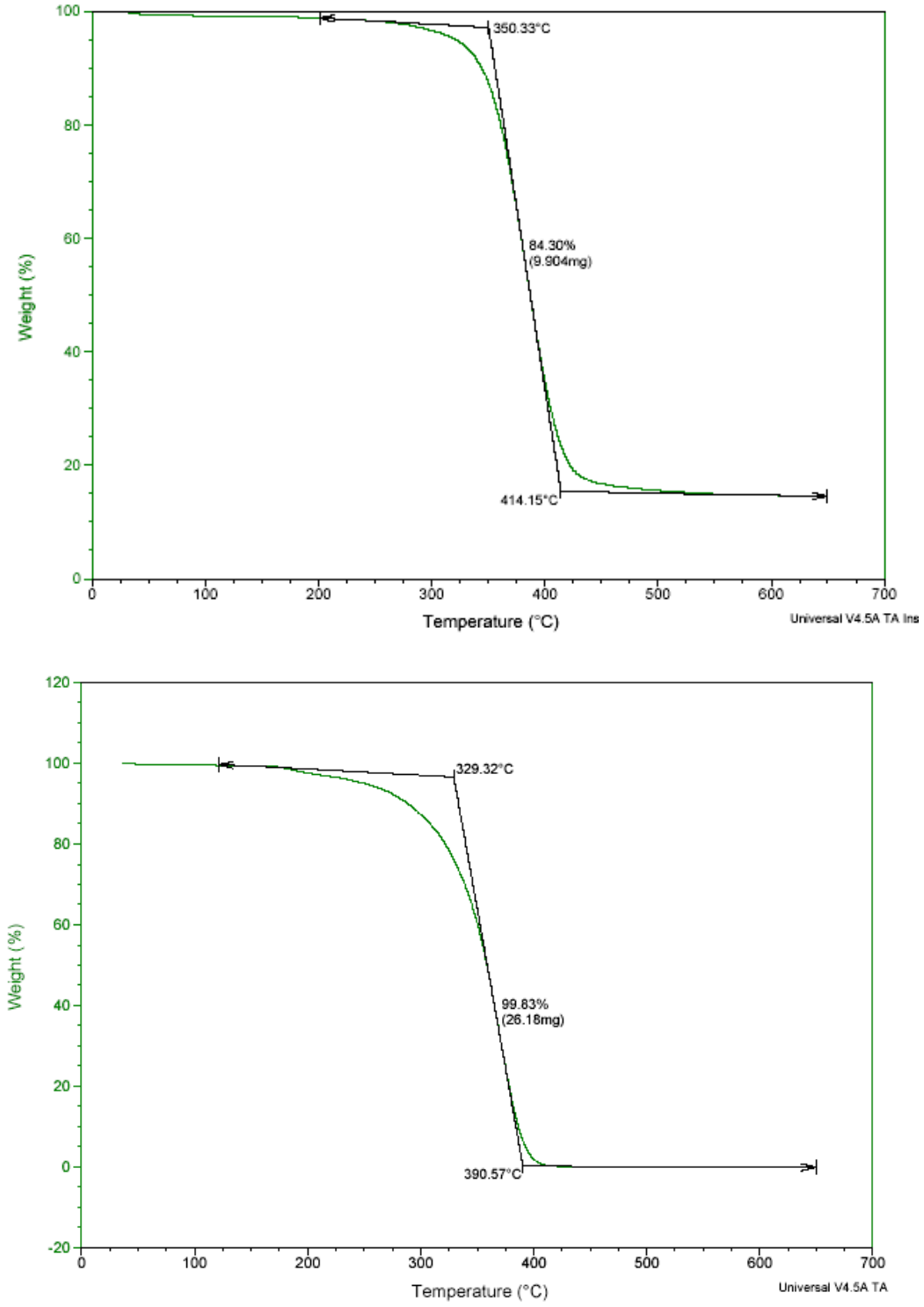

Figure 4. 16 Thermogravimetic analysis (TGA) graph of BMS/PMMA spheres (upper) and pure commercial PMMA (lower)

corresponded to 1.4 mmol NH_2 /g materials. For ABCC immobilized BMS, the weight loss between 200°C and 600°C is 18.08% which corresponds to 0.37 mmol ABCC /g materials. This calculation showed less than 30 mol% of amine reacted with ABCC and formed ABCC immobilized BMS. Most of amine on silica surface was still kept as amine groups, it was very difficult to control the density of amine sites on silica surface. Jones'[53] did some progress on how to control the density of amine sites on mesoporous silica surface using multiple grafting steps through grafting large benzyl spacers on the molecule chain of APTMS.

Glass transition temperature of BMS/PMMA was 127.3°C which was 2.3°C higher than that of pure PMMA (125°C) from DSC (Figure 4.15). Using the fast decomposition point as decomposition temperature, the decomposition temperature of BMS/PMMA was 386°C which was 17°C higher than that of pure PMMA (359°C) from TGA (Figure 4.18). Using the beginning decomposition point as decomposition temperature, the decomposition temperature of BMS/PMMA was 350°C which was 21°C higher than that of pure PMMA (329°C). Figure 4.16 showed that BMS/PMMA composites began to decompose at 350°C and finished decomposition at 414°C, the range from the decomposition beginning to decomposition finishing was 64°C. For pure commercially available PMMA from Aldrich, PMMA began to decompose at 329°C and finished decomposition at 391°C, and the decomposition temperature range was 62°C. Compared with the pure commercially available PMMA, the BMS/PMMA composites began to decompose at a higher temperature (21°C higher), finished decomposition at a higher temperature (23°C higher), but the range of decomposition was almost the same (around 60°C). For mesoporous BMS/PMMA composites, covalent bonds between

PMMA and mesoporous silica decreased the mobility of PMMA chains, thus both glass transition temperature and decomposition temperature were enhanced for the BMS/PMMA composites when it was compared with pure PMMA.

4.3.3 SEM analysis of BMS/PMMA nanocomposites

A direct SEM imaging of the BMS/PMMA showed a spherical PMMA surface with diameter of 5μm (Figure 4.17), and all BMS were covered with PMMA. However, after the removal of PMMA via thermal defunctionalization under nitrogen at 700°C, the diameter of sphere become 2.5μm again because all PMMA were calcinated at high temperature (Figure 4.18). There were some ashes for PMMA with BMS after high temperature thermal defunctionalization. So the removal of PMMA from the surface of mesoporous silica via thermal defunctionalization obviously made the SEM analysis more straightforward. The SEM analysis comparison also verified that the mesoporous silica were covered with polymer, which had almost the same thickness as the diameter of pure spherical BMS because both mesoporous silica and BMS/PMMA composites were well spherical morphologies with just different diameters. The spherical morphology of BMS/PMMA composites also indicated that the synthesized PMMA grew out of the nano-channels and covered the silica surface with the same thickness, most of the polymer chains should had very close molecular weight so that the thickness covered on silica surface could be the same. After repeatedly washed with organic solvent, all PMMA without covalent bonds with silica surface were washed. We could assume that all PMMA covered on silica surface grew from the nano-channels by the surface initiated free radical polymerization.

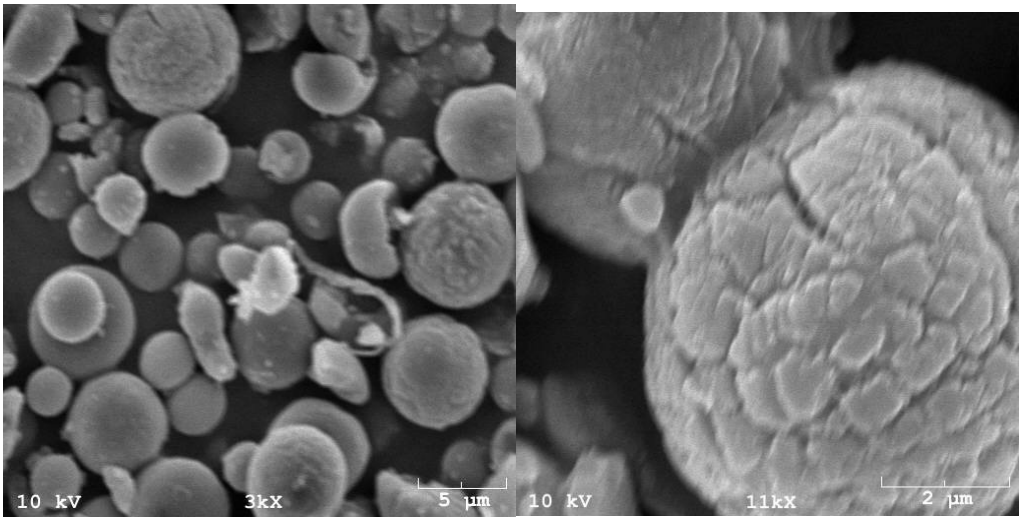

Figure 4. 17 Scanning electron microscopy(SEM) images of BMS/PMMA spherical composites with different magnifications.

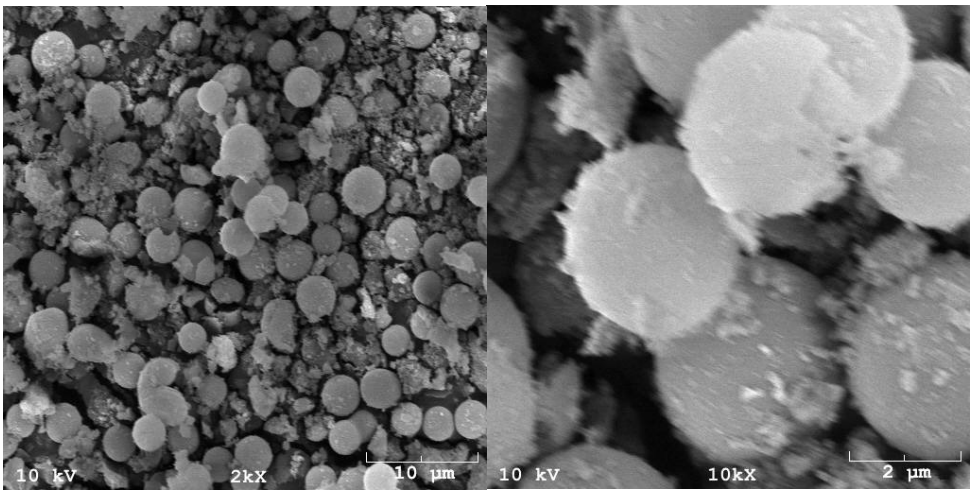

Figure 4. 18 Scanning electron microscopy (SEM) images of BMS/PMMA sphere after thermal defunctionalization (700°C) with different magnifications.

Because we used spherical BMS as supported materials, we could directly find the morphology changing between the pure BMS and BMS/PMMA composites. However, SBA-15 with irregular morphology couldn't show us the direct image changing.

We could also easily tell whether the free polymers were totally washed out, and the direct image also give a direct proof that synthesized PMMA had covalent bonds with silica surface. If there was no covalent bond between the polymer and silica, the polymers should be washed out with solvent.

Well spherical BMS/PMMA composites with diameter around 5μm were shown from a direct SEM imaging of BMS/PMMA (Figure 4.17). After polymerization, the spherical diameter of BMS/PMMA was increased from 2.5μm, the spherical size of BMS, to 5μm. When the spherical diameter increased by one time, the volume of the sphere would increase by 7 times because the volume of a sphere was proportional to cube of radius.

Assuming the density of silica was 2.2g/cm^3, and the density of PMMA was 1.16g/cm^3, and assuming all pores were filled with PMMA after PMMA were initiated from the nano-channels. Then 1g of BMS has a volume of 0.455 (1/2.2) cm^3. From the nitrogen adsorption isotherms, 1g BMS would contain 0.956 cm^3 pore volume. So for 1 g BMS, the total volume of PMMA bonding to BMS was 4.14 cm^3 (7×0.455+0.956) which corresponded to 4.80g (4.14×1.16) PMMA. So the weight percentage of PMMA in BMS/PMMA composites was 83% (4.8/5.8). Thermogravimetic analysis (TGA) showed weight loss between 200°C and 600°C was 85%. Considering the volume of initiator of ABCA grafted onto the surface of BMS, the TGA weight loss (Figure 4.16) showed that the weight percentage of PMMA in BMS/PMMA composites was 84.5% which was very close to 83% obtained from theoretical calculation of volume, density data from SEM and nitrogen adsorption/desorption isotherms. In real case, there would be some difference because not all organic solvent inside the nano-channels of ABCC immobilized BMS

would be evaporated before the ABCC immobilized BMS was placed to reaction system. The pore volume of nano-channels of ABCC immobilized BMS was much smaller than the volume increase produced from thickness increase outside of the nano-channels when more PMMA grew out of the nano-channels and covered on silica surface.

4.2.4 XRD analysis of BMS/PMMA nanocomposites

To better characterize the BMS/PMMA composites, X-ray diffraction was used. BMS/PMMA sphere composites (Figure 4.19) showed 4 peaks of 2-theta at 14.016, 21.06, 30.973 and 42.947. BMS sphere (Figure 4.20) showed one peak of 2-theta at 21.833. Using the BMS sphere as background, the X-ray diffraction of BMS/PMMA subtracted that of BMS, Figure 4.21 showed three 2-theta peak at 14.12, 30.97 and 42.06 which corresponded to 6.26A, 2.89A and 2.15A which was very close to the XRD peak of pure PMMA which showed three 2-theta peaks at 13.622, 30.678 and 41.65 corresponding to 6.5A, 2.91A and 2.17A separately. The peak around 14 for PMMA was considered as the amorphous peak. Another two common peaks were considered to result from local order region. From the comparison data between BMS/PMMA composites and pure PMMA, the BMS/PMMA composites XRD showed that PMMA segment distance was smaller than that of pure PMMA which meant the PMMA segments were more compact when grafting from the surface of mesoporous silica inside the nano-channels. And the area of another two 2-theta peaks at 31 and 42 for PMMA bonding BMS was larger than that of pure PMMA which meant PMMA chain on the surface of mesoporous silica were locally more ordered than pure PMMA segment.

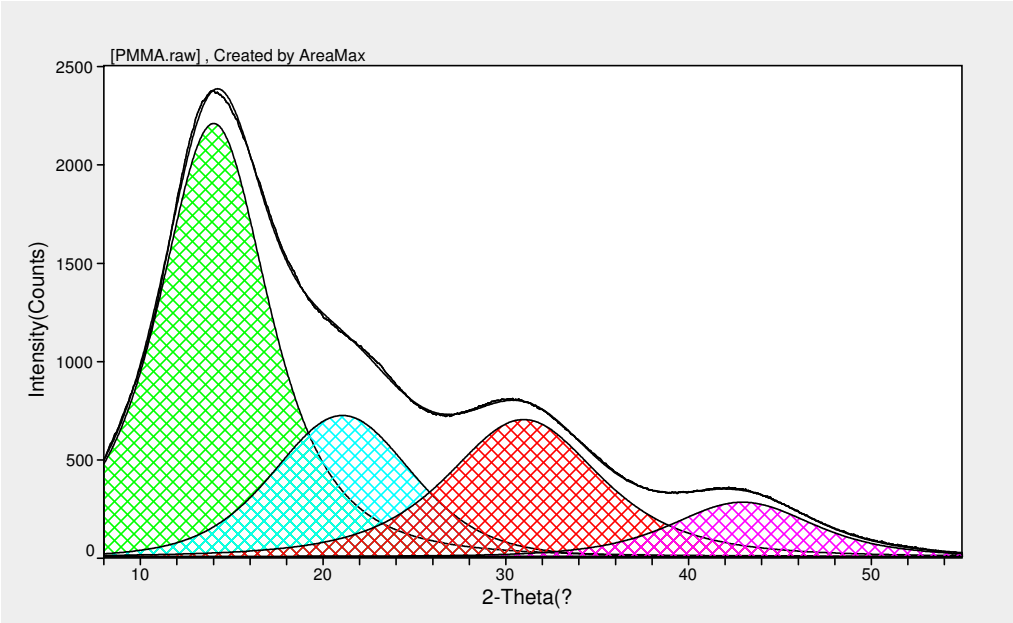

Figure 4. 19 X-ray diffraction pattern of BMS/PMMA sphere composites

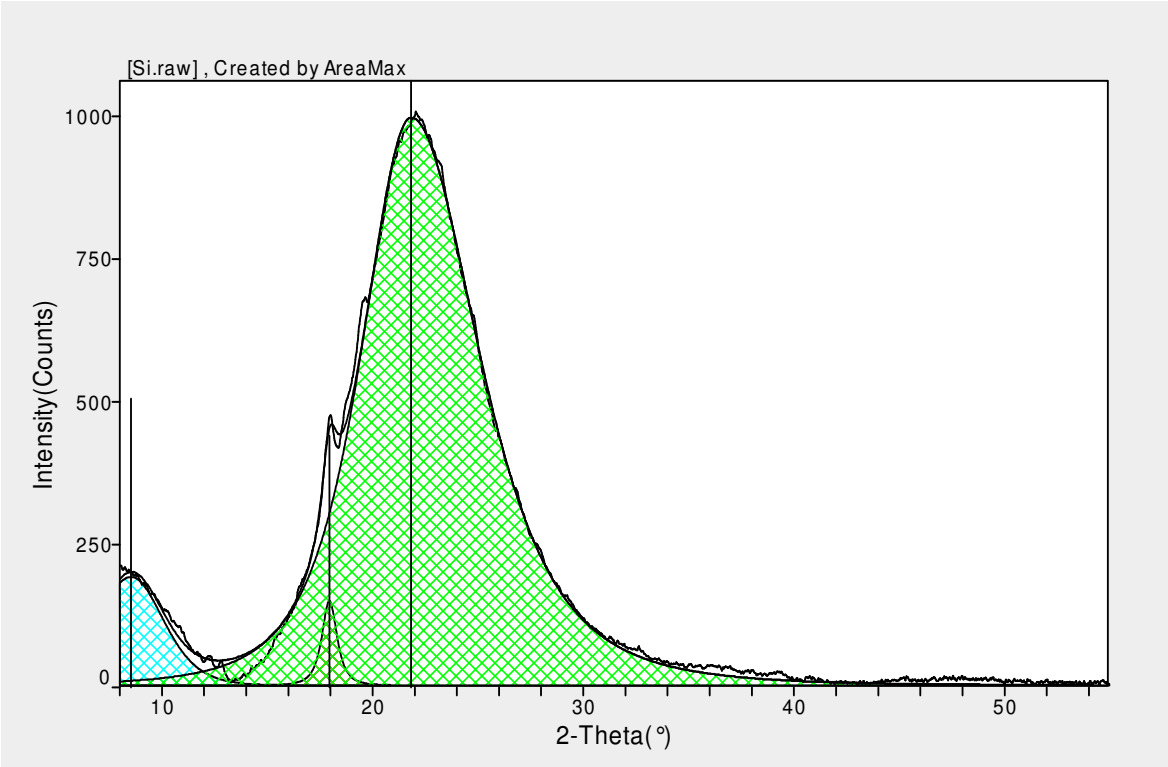

Figure 4. 20. X-ray diffraction pattern of BMS sphere

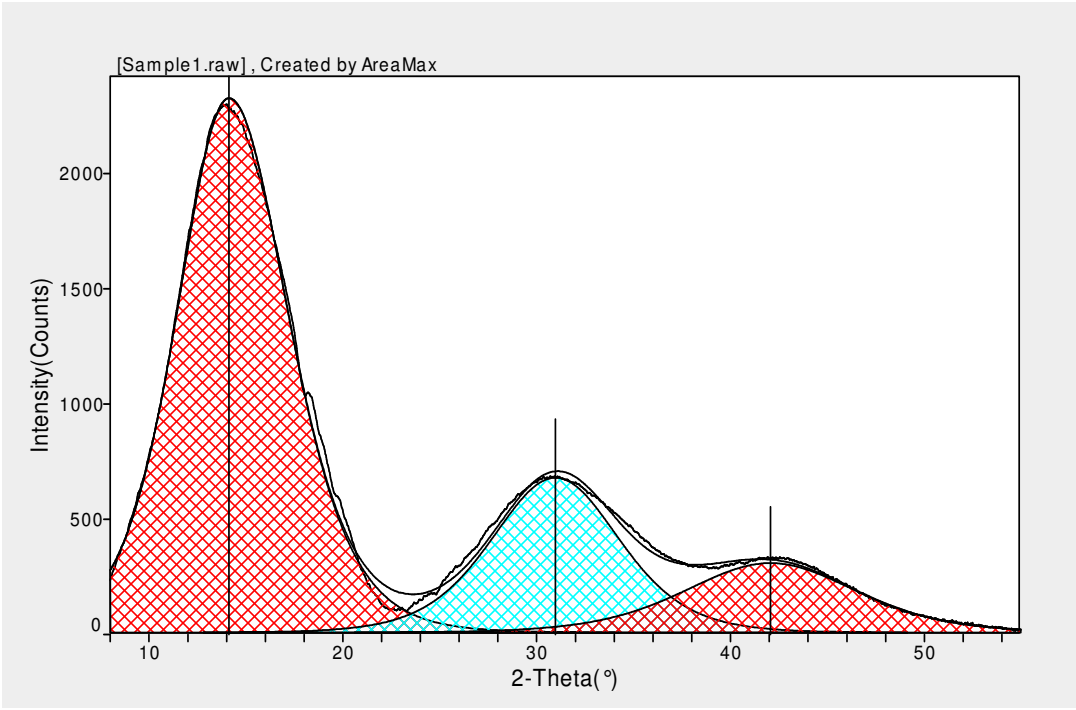

Figure 4. 21 X-ray diffraction pattern of BMS/PMMA sphere using BMS as background

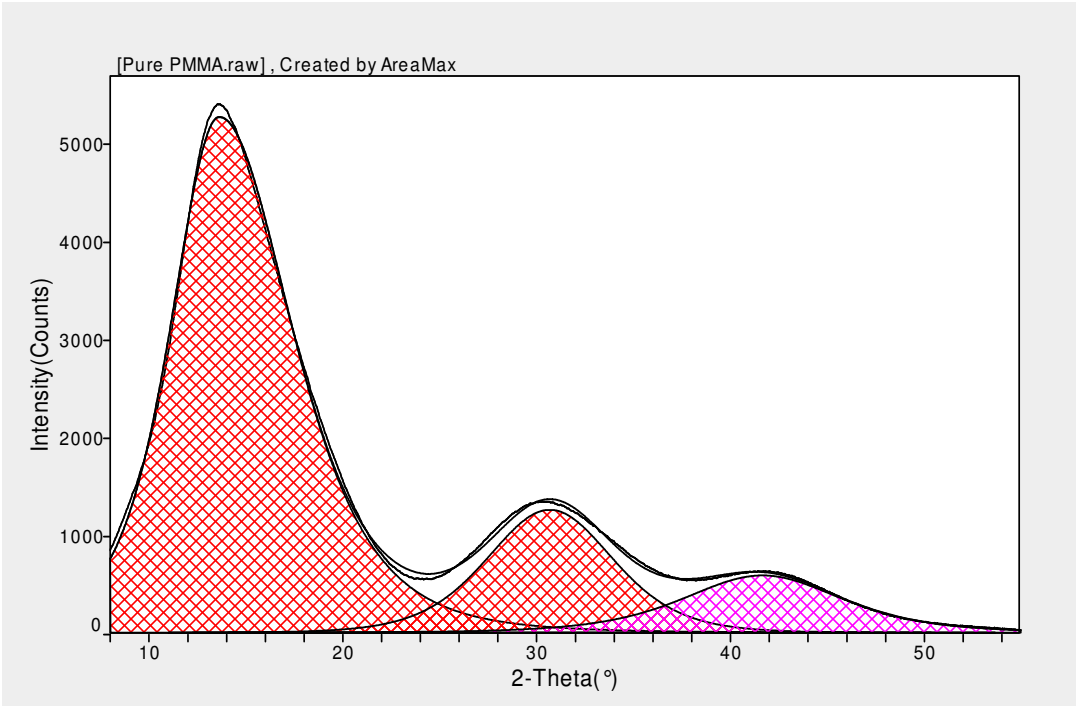

Figure 4. 22 X-ray diffraction pattern of commercial pure PMMA

4.3 Spherical PMMA capsule after Silica removed with hydrofluoric acid

Silica (SiO_2) can react with hydrofluoric acid (HF) to produce silicon tetrafluoride and water. Thus, silica network can be removed with hydrofluoric acid with the following reaction formula.

$$SiO_2 + HF \rightarrow SiF_4 + H_2O$$

The BMS/PMMA spherical nanocomposites were placed in 30wt% hydrofluoric acid for two days and thereafter washed repeatedly with pure water, thus the silica inside the composites would be removed totally. Because all silica surfaces were covered with polymer chain, a long time of silica in solution of hydrofluoric acid was necessary to remove all silica networks because it needed time for hydrofluoric acid to diffuse through polymer. Figure 4.27 showed TGA graph of PMMA after silica was removed, this figure showed that the PMMA sphere began to decompose at 351°C, and finished decomposition at 405°C. The range of decomposition was 55°C. The remaining weight was 0 wt% after 450°C which meant all calcinated material was PMMA sphere, so all silica was removed with hydrofluoric acid.

4.3.1 Thermal behavior of spherical PMMA capsule after Silica removed

Pure PMMA was purchased from Sigma-Aldrich with molar mass of 300,000g/mol which began to decompose at 329°C and finished decomposition at 391°C, and the decomposition temperature range was 62°C (Figure 4.28). The TGA graph of spherical pure PMMA derived from PMMA/silica composites with silica removed with hydrofluoric acid showed that PMMA began to decompose at 350°C and the decomposition finished at 401°C (Figure 4.25), and the range of decomposition was 50°C.

From the comparison of these two curves, the PMMA spheres derived from silica removing from PMMA/silica composites had much higher decomposition temperature and much narrower range of decomposition temperature than pure PMMA. The decomposition temperature of spherical PMMA capsule was the same as that of BMS/PMMA nanocomposites (Figure 4.26) and 21°C higher than that of pure purchased PMMA obtained from Sigma-Aldrich.

TGA was also used to compare the thermal behavior of PMMA/silica composites and PMMA spheres derived from PMMA/silica composites with silica removed with hydrofluoric acid. Figure 4.26 showed PMMA/silica composites began to decompose at 350°C and decomposition finished at 414°C. And Figure 4.27 showed PMMA spheres from PMMA/silica composites with silica removed with hydrofluoric acid (HF) began to decompose at 350°C and finish decomposition at 401°C. Figures showed pure spherical PMMA with silica removed began to decompose at the same temperature as PMMA/silica composites at 350°C. However, pure commercial PMMA finished decomposition at 391°C which was 23°C lower than that of PMMA/silica composites. And the range of decomposition of pure commercial PMMA was also 18°C larger than that of PMMA/silica composites. The TGA graph showed the PMMA spheres from the BMS/PMMA composites with silica removed with hydrofluoric acid had the same decomposition temperature and range of decomposition as the BMS/PMMA composites. The remove of silica network from BMS/PMMA nanocomposites wouldn't change the thermal behavior of PMMA. Both the BMS/PMMA composites and PMMA obtained from the composites had higher decomposition temperature and narrower decomposition temperature range than that of pure commercially available PMMA. Hydrofluoric acid

couldn't dissolve PMMA, the PMMA structure would not be destroyed after silica was dissolved in hydrofluoric acid. The TGA showed the same shape of curve for both mesoporous silica/PMMA composites and spherical PMMA spheres obtained from BMS/PMMA composites because both materials had the same structure and removal of silica with hydrofluoric acid wouldn't change the structure of spherical PMMA. TGA of spherical PMMA obtained from BMS/PMMA composites also verified that all silica networks were removed with hydrofluoric acid because the weight is decreased to 0 wt% after PMMA finished decomposition.

DSC graph of pure commercial PMMA (Figure 4.23) showed a glass transition temperature of 125°C. DSC graph of PMMA spherical capsules (Figure 4.24) showed a glass transition temperature of 124°C. So there was no difference for glass transition temperature between pure commercially available PMMA and PMMA spherical capsules obtained from BMS/PMMA composites. Previous chapter showed T_g of SBA-15/PMMA was a little higher than that of pure commercially available pure PMMA. This was because SBA-15 had a much smaller diameter than BMS. Most BMS nano-channels had a pore distribution between 10-30 nm while most SBA-15 nano-channels had a pore distribution between 2-8nm. PMMA synthesized from large pores showed the same T_g as commercially available PMMA, while PMMA synthesized from smaller pores showed a higher T_g than commercially available PMMA. The reason was probably that small pores had small space which limited the mobility of polymer chain segment. When the pore size was increased to a certain value, the pore would not affect the mobility of polymer

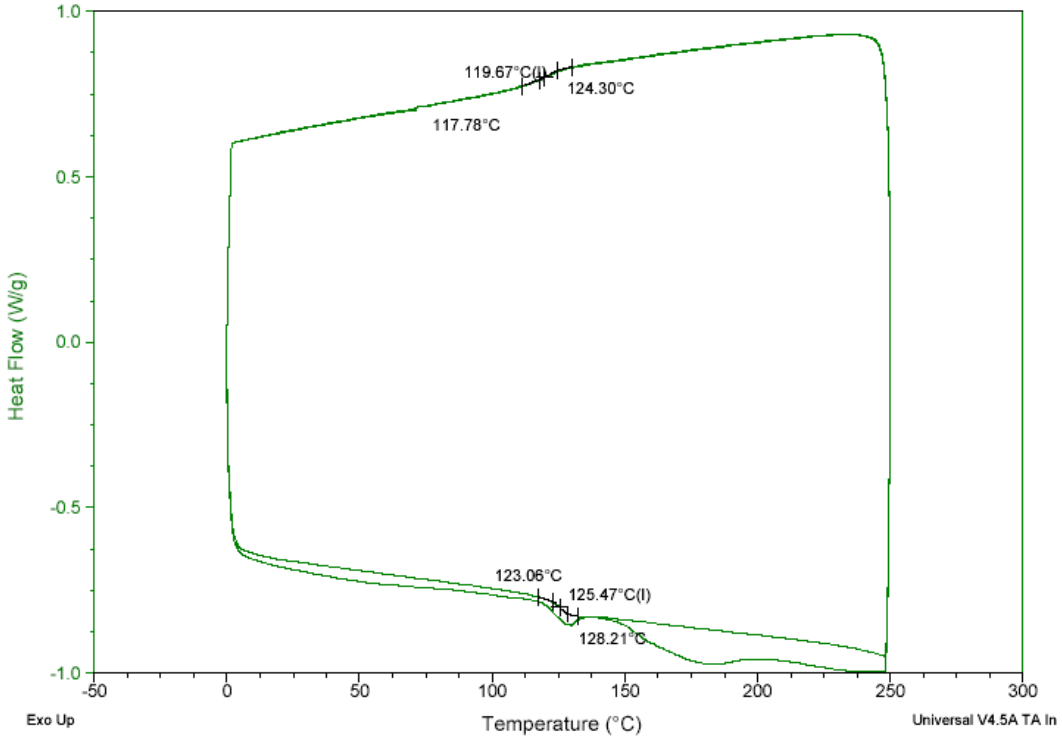

Figure 4. 23. D.S.C thermograms pure commercial PMMA

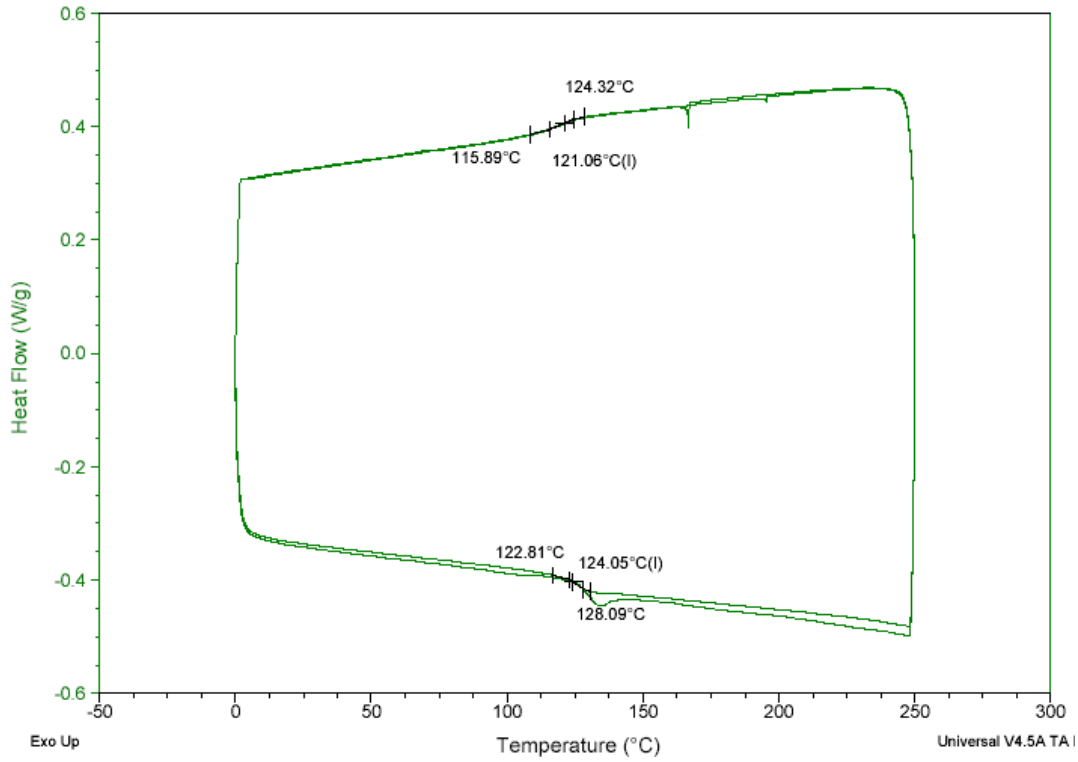

Figure 4. 24 D.S.C thermograms of silica free spherical PMMA

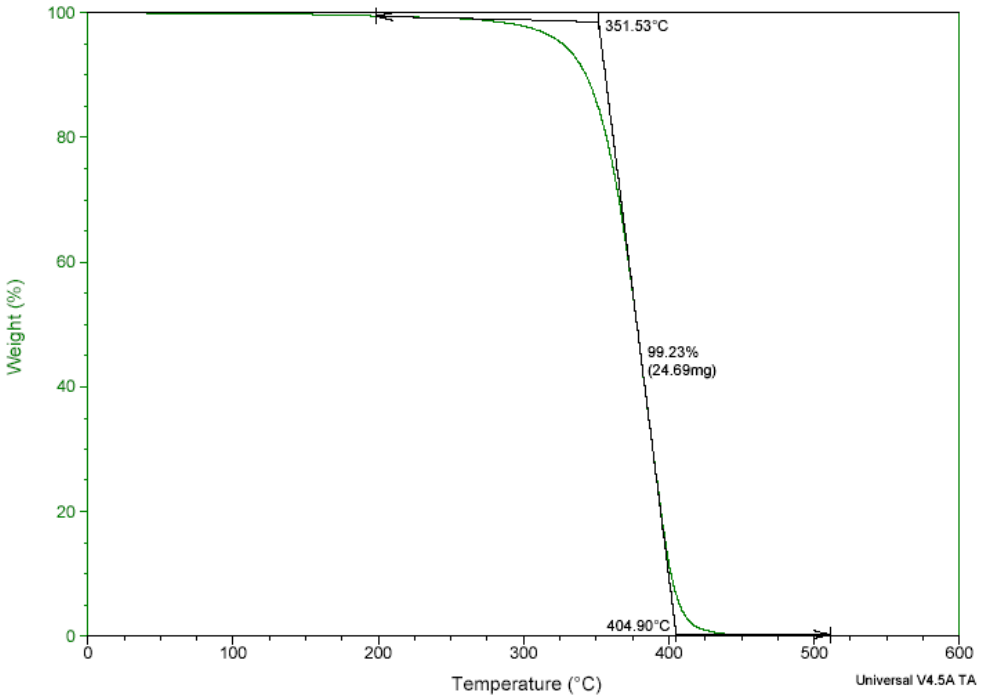

Figure 4. 25 Thermogravimetic analysis (TGA) graph of spherical PMMA derived from BMS/PMMA composites

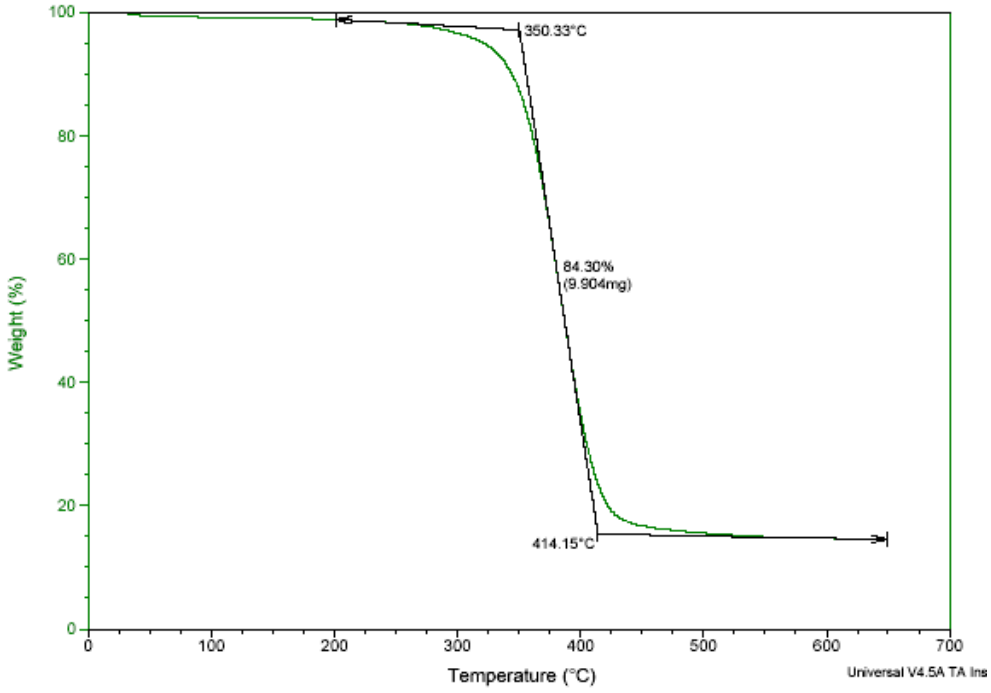

Figure 4. 26 Thermogravimetic analysis (TGA) graph of PMMA/BMS composites

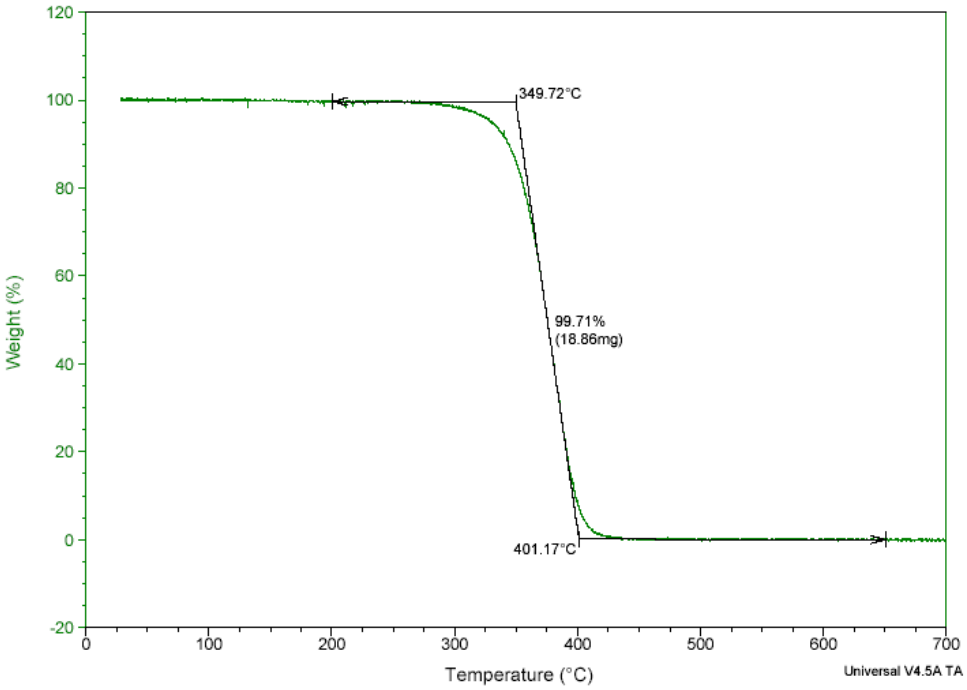

Figure 4. 27 Thermogravimetic analysis (TGA) graph of synthesized free PMMA

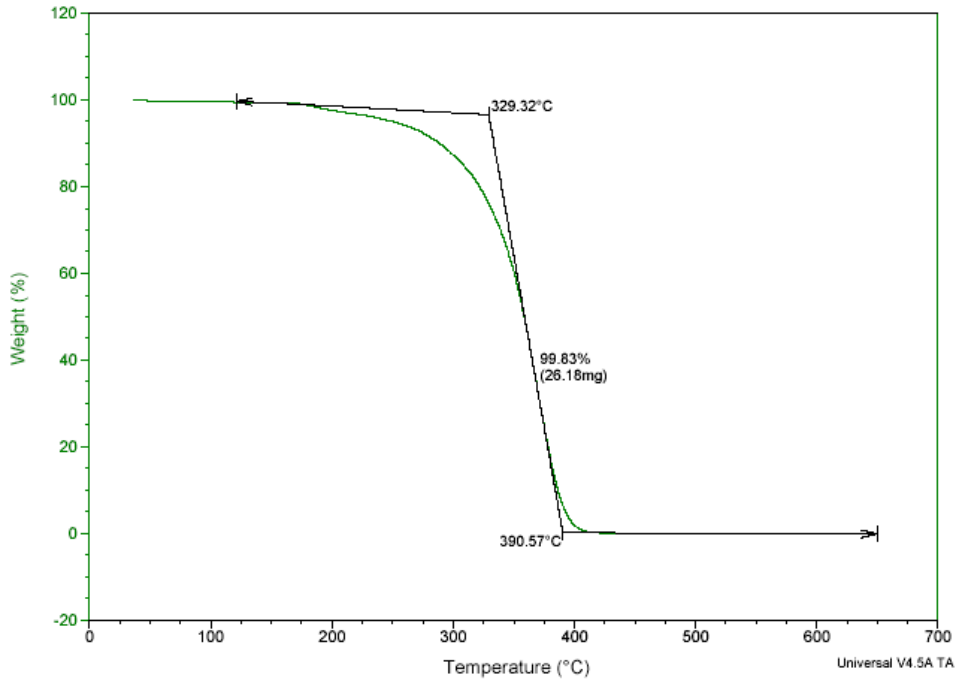

Figure 4. 28 Thermogravimetic analysis (TGA) graph of pure commercial PMMA

segment any more. Thus, the T_g of synthesized PMMA from a large pore would be the same as the commercially available PMMA.

From the above analysis, the removal of silica network using hydrofluoric acid wouldn't change the thermal behavior of PMMA. Spherical PMMA obtained from BMS/PMMA composites showed the same glass transition temperature, decomposition temperature and decomposition range as BMS/PMMA nanocomposites. PMMA obtained from BMS/PMMA nanocomposites had a higher decomposition temperature and a narrower decomposition range than that of pure commercially available PMMA. And a smaller size of nano-channels would increase T_g of synthesized PMMA while larger nano-channels wouldn't.

4.3.2 SEM characterization of spherical PMMA capsule after Silica removed

When the PMMA/silica composites were synthesized, THF was used to wash the composites over ten times. Therefore, all free PMMA without connection with supported materials of mesoporous silica would be dissolved in THF and washed out, and only the PMMA with covalent bond with silica surface couldn't be washed out and still covered the silica surface. The SEM pictures (Figure 4.29) showed the regular well spherical morphology of PMMA/Silica composites and PMMA spherical capsules. From these figures, it was very clear that all silica surfaces were covered with polymer even after composites were repeatedly washed with THF. PMMA couldn't be dissolved in hydrofluoric acid, so the structure of PMMA couldn't be destroyed when BMS/PMMA composites were placed in 30% hydrofluoric acid solution. After mesoporous silica was removed with hydrofluoric acid, the morphology of PMMA was unchanged. Figure 4.30

show SEM of PMMA spherical capsules after silica was removed with hydrofluoric acid at different magnifications. These figures show uniformly spherical morphologies which didn't change after silica were removed. The PMMA spheres even didn't collapse after silica was removed. The direct SEM image gave a direct proof that removal of silica network wouldn't change the morphology of PMMA spheres. The hydrofluoric acid will only dissolve silica network and thus the thermal behavior of polymer wouldn't be changed ether.

Unlike the morphology obtained from Figure 4.17 which showed a rough surface, Figure 4.30 showed spherical PMMA with smooth surface and narrow distributed spherical diameter. These direct SEM images also verified that all BMS were covered with PMMA. If some BMS were not covered polymer, there would be some holes among spherical PMMA capsule after silica network was removed with hydrofluoric acid. Although the diameters of spherical PMMA capsule were not the same, we could tell that the diameters had a narrow distribution.

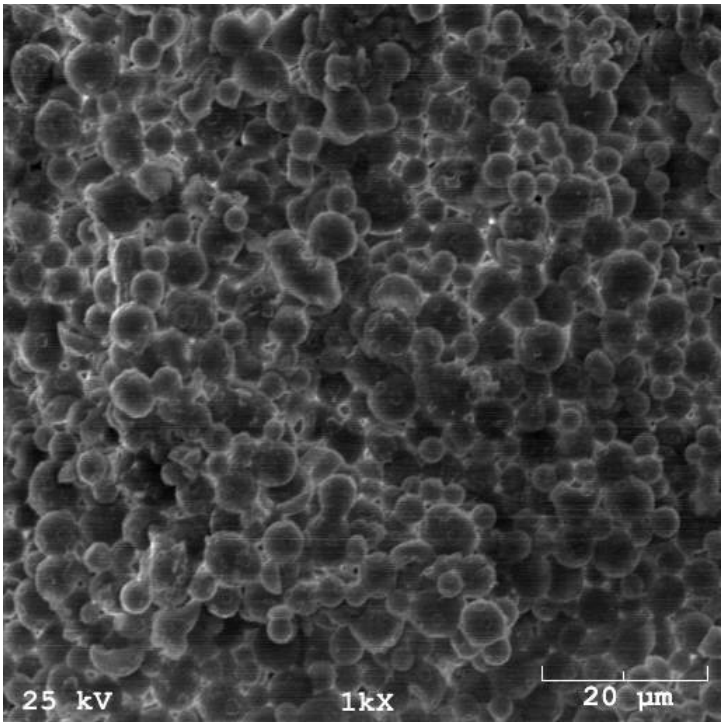

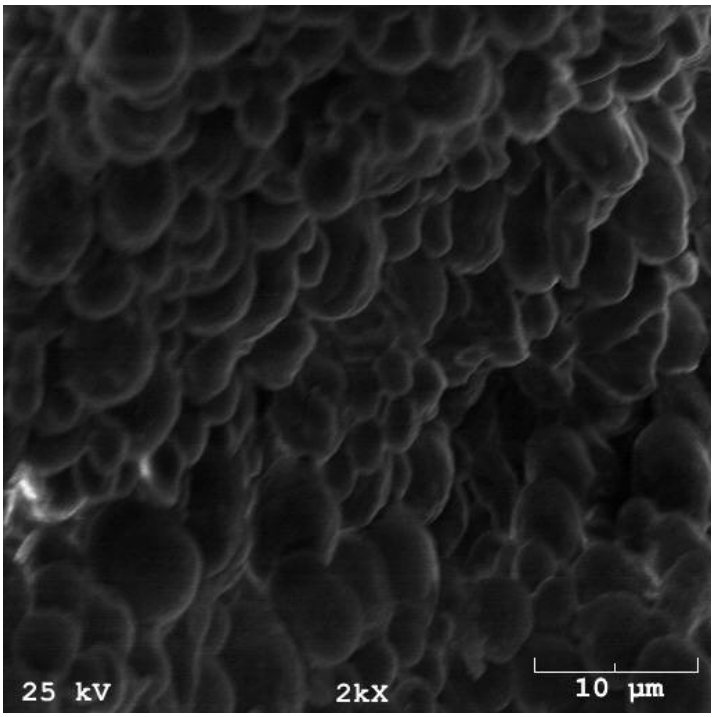

Figure 4. 29 Scanning electron microscopy (SEM) of BMS/PMMA composites synthesized with bulk polymerization (upper graph), PMMA spherical capsules produce from bulk polymerization after silica were removed with hydrofluoric acid (lower graph).

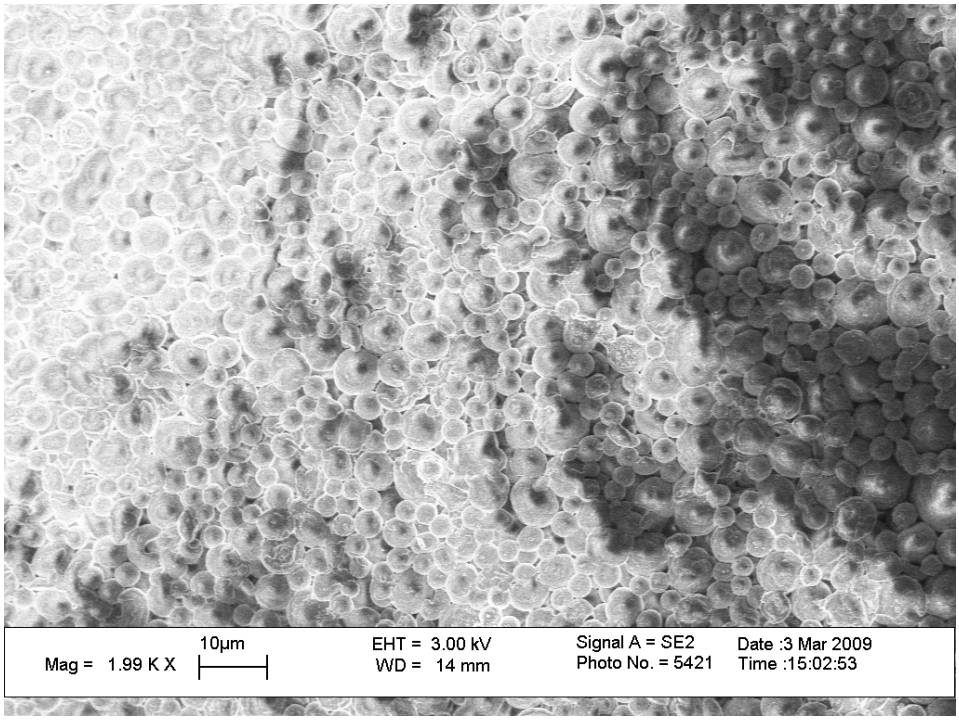

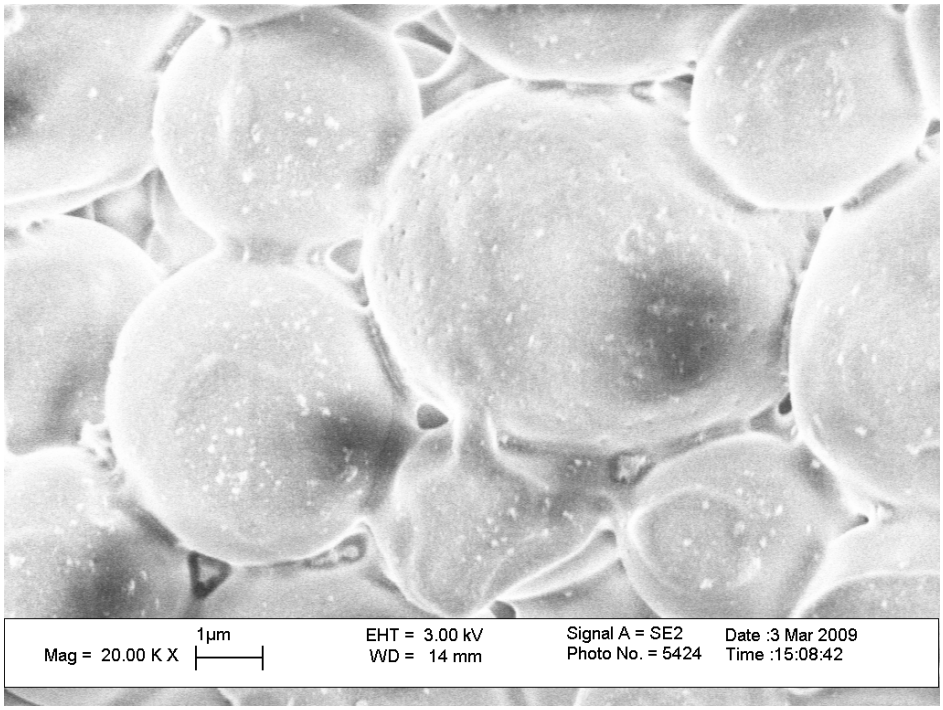

Figure 4. 30 Scanning electron microscopy(SEM) of spherical PMMA capsules with different magnifications produced with solution polymerization after silica were removed with hydrofluoric acid

4.4.3 GPC analysis of spherical PMMA capsule after Silica was removed

The PMMA spherical capsules with mesoporous silica removed with hydrofluoric acid could be dissolved in THF and GPC could be used to characterize the molecular weight and polydispersity index. The spherical PMMA dissolved in THF also verified that all silica networks were removed with hydrofluoric acid. And the synthesized PMMA were linear polymers without crosslinks between the polymer chains. Table 4.2 showed the GPC result of three different PMMA with label sample 1, sample 2 and sample 3. Sample 1 was PMMA spherical capsules after Silica was removed with HF solution. Sample 2 was synthesized PMMA mixture of free PMMA without bond with silica surface and PMMA spherical capsules with bonds with silica surface after silica was removed. Sample 3 was commercially available PMMA with number average molar mass of 300,000g/mol from Aldrich. The GPC results showed that sample 1 of PMMA spherical capsules had the highest number average molar mass of 800,000g/mol and very lower polydispersity index of only 1.09. The mixture of free PMMA and PMMA spherical capsules have M_n of 660,000g/mol and PDI of 1.17, which showed the molecular weight was lower and PDI was higher than those of PMMA spherical capsules. The results showed that there was a molecular weight difference between free PMMA and PMMA spherical capsules produced during the polymerization. And the number average molar mass of free PMMA produced during in the procedures was less than that of PMMA with covalent bonds with the surface of mesoporous silica. The commercially available PMMA with designed M_n of 300,000g/mol showed tested M_n of 270,000g/mol and PDI of 1.81. GPC result of sample 3 showed there was a difference between our GPC results and prescribed data because prescribed 300,000g/mol showed 270,000g/mol with

our GPC. For free radical polymerization, the polydispersity index will usually well larger than 1, and the living polymerization will produce polydispersity index a little higher but very close to 1. The polydispersity was smaller, which meant the polymers had the similar molecular weight and polymer chain had the same length. For PMMA initiated inside the nano-channels of mesoporous silica, the polydispersity index was only a little higher than 1 which meant the free radical polymerization inside the nano-channels was different with the normal free radical polymerization. The reason suggests that the probability of chain termination was decreased due to the sterical constraints inside the nano-channels of mesoporous silica. The mobility of polymer chain was also limited inside the nano-reactors, so the free radical polymerization initiated and propagated inside the nano-reactor was different with other bulk polymerization or solution polymerization initiated and propagated without sterical constraints. For emulsion polymerization, a free radical could initiate the polymerization and polymer propagated inside each micelle like bulk polymerization until another free radical entered the micelle and terminated the polymerization. So the principle of emulsion polymerization was different with bulk polymerization. Rate of bulk polymerization was controlled through rate of initiation and propagation, however, emulsion polymerization is controlled through particle number N_c(initiator and surfactant concentration control the reaction rate and degree of polymerization). So even emulsion polymerization is also free radical polymerization, it can produce polymers with ultra-high molecular weight and ultra-low polydispersity index. Like emulsion polymerization, each nano-channel of mesoporous silica could be considered as a micelle. There were more than one initiator grafted on the surface of inner walls of nano-channels. Because the initiators were

covalent bonded with silica surface, the free radical couldn't freely move inside the nano-channels after initiators decomposed and polymerization was initiated. The initiator on silica surface would initiate the polymerization at a certain condition and the polymer grew inside the nano-channels until the radical was terminated with another free radical. The probability of polymer chain termination was thus decreased compared with bulk polymerization. Thus polymers with ultra-high molecular weight and very low polydispersity index were synthesized inside the nano-channels.

The GPC data showed the free radical polymerization initiated inside the nano-channel was a 'living polymerization' which had a ultra-high molecular weight and ultra-low polydispersity index. And this result also gave a good explanation to the phenomena of BMS was covered with PMMA with the same thickness and uniformly spherical morphology.

Table 4. 2 GPC data for PMMA spherical capsule

Sample	Mn	Mw	PDI
1(PMMA spherical capsule)	792253	863713	1.09
2(Overall synthesized PMMA)	656567	768876	1.17
3(purchased from Aldrich)	270840	491571	1.81

4.4 Comparison of bulk polymerization and solution polymerization with and without vacuum steps

MMA monomer was dissolved in anhydrous toluene which was easy to diffuse into the nano-channels. MMA monomer could diffuse into the inside of the nano-channels with the help of anhydrous toluene and polymerization could be initiated with initiator on the surface of the wall of the inner channels. However, it was not easy for MMA monomer to diffuse into the nano-channels of mesoporous silica without the help of toluene because of the surface tension, and air inside the nano-channels would also not allow MMA monomer to fill the nano-channels. Vacuum condition with special steps was used to help to push pure MMA monomer into the nano-channels. Two different polymerization methods of solution polymerization and bulk polymerization would probably produce composites with different morphologies and properties.

The experiments with four samples are compared. Sample 1 was 0.5g ABCC-immobilized-BMS initiating 20ml MMA within 20ml toluene without vacuum steps, where MMA/toluene solution was allowed to diffuse into the nano-channels and polymerization was initiated. All samples 2, 3 and 4 finished polymerization after vacuum steps, where MMA monomer was injected into vacuumed flask with ABCC-immobilized-BMS. Sample 2 was 0.5g ABCC-immobilized-BMS initiating polymerization of 5ml MMA monomer without solvent, sample 3 was 0.5g ABCC-immobilized-BMS initiating polymerization of 5ml MMA with 5ml anhydrous toluene, and sample 4 was 0.2g ABCC-immobilized-BMS initiating polymerization of 10ml MMA with 10ml anhydrous toluene. The detailed steps to produce mesoporous silica/PMMA using bulk polymerization and solution polymerization were shown in

chapter 3. TGA was used to test the decomposition temperature and mass percentage of PMMA of the composites.

Table 4.3 showed TGA data for BMS/PMMA composites. For sample 1, the mass percentage loss of PMMA in the composites between 200°C and 600°C was 84%, which meant around 5.2g synthesized PMMA were covalent bonded onto the surface of 1g BMS. There was 20g MMA monomer for 0.5g ABCC-immobilized-BMS, 17.4g free PMMA were synthesized and could be washed with THF because they weren't covalent bonded onto the surface of BMS. For sample 4 with vacuum steps, and all other polymerization condition was the same as the condition of sample 1. And the mass percentage of PMMA in composites was 93% which was almost 10 percent higher than sample 1 without vacuum steps. Both sample 1 and sample 4 with surplus MMA monomer for ABCC-immobilized-BMS. From the comparison results of sample 1 and sample 4, vacuum steps could increase the amount of polymer covalent bonded on the surface of mesoporous silica. Sample 2 showed almost the same percentage of mass as sample 3, which meant there was no big difference for mass percentage of PMMA in BMS/PMMA composites for bulk polymerization and solution polymerization with vacuum steps. But the decomposition temperature of composites produced with bulk polymerization was almost 10°C higher than that of composites produced with solution polymerization. Table 4.3 showed that vacuum steps could increase the mass percentage of polymer in composites, bulk polymerization could increase the decomposition temperature of the composites, and solution polymerization and bulk polymerization couldn't change the mass percentage of polymer in composites when both polymerizations were finished with vacuum steps.

Table 4.3 TGA data for BMS/PMMA composites

Sample	Temperature of decompose (°C)	End temperature of decomposition (°C)	Decomposition temperature range (°C)	Mass percentage of PMMA (%)
1	350	414	64	84%
2	356	411	55	89%
3	346	413	67	88%
4	342	400	58	93%

1 is for 0.5gSi/20ml MMA+20ml toluene without vacuum steps, 2 is for 0.5g Si/5ml MMA with vacuum steps, 3 was for 0.5g Si/5ml MMA+5ml toluene with vacuum steps, 4 was for 0.2g Si/10ml MMA+10ml toluene with vacuum steps.

SEM graph showed both bulk polymerization and solution polymerization could synthesize BMS/PMMA composites with spherical morphologies. The diameters of the spherical balls produced from both methods were also in the same range.

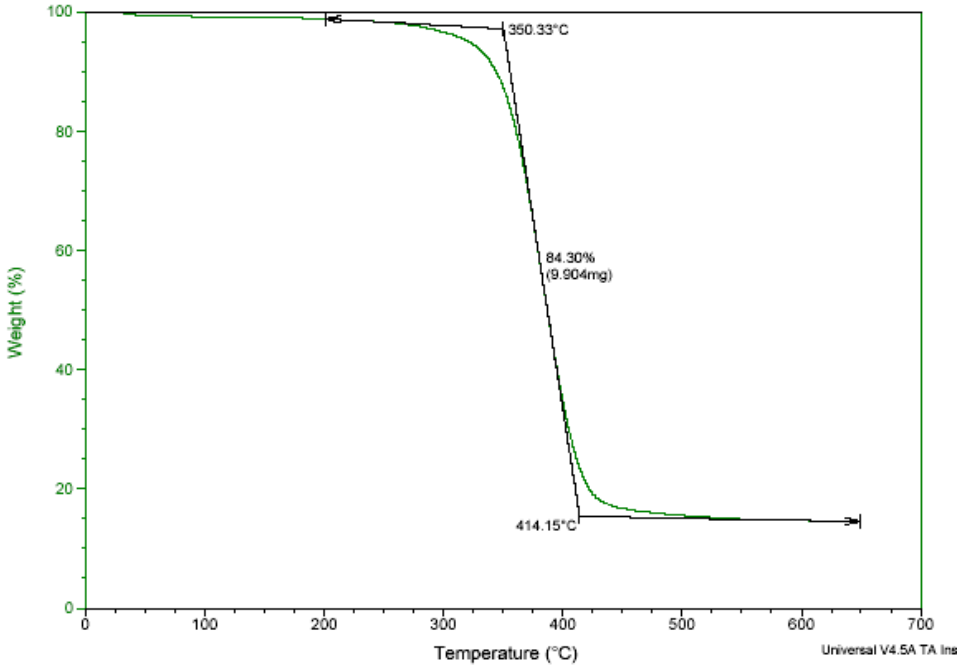

Figure 4. 31 Thermogravimetic analysis (TGA) graph of BMS/PMMA composites (sample 1) synthesized with solution polymerization without vacuum steps.

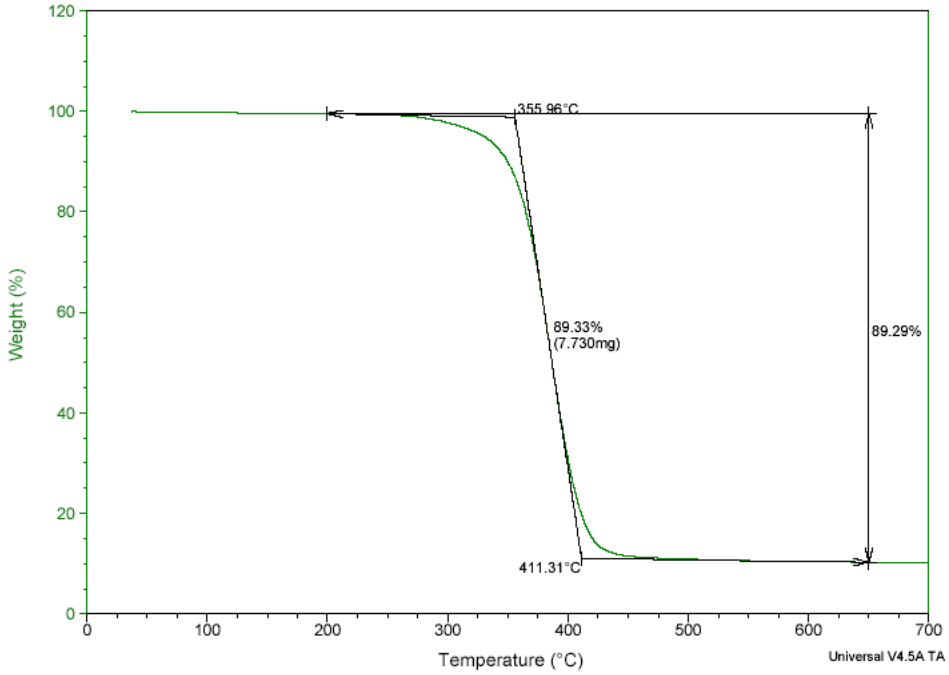

Figure 4. 32 Thermogravimetic analysis (TGA) graph of BMS/PMMA composites (sample 2) synthesized with bulk polymerization with vacuum steps.

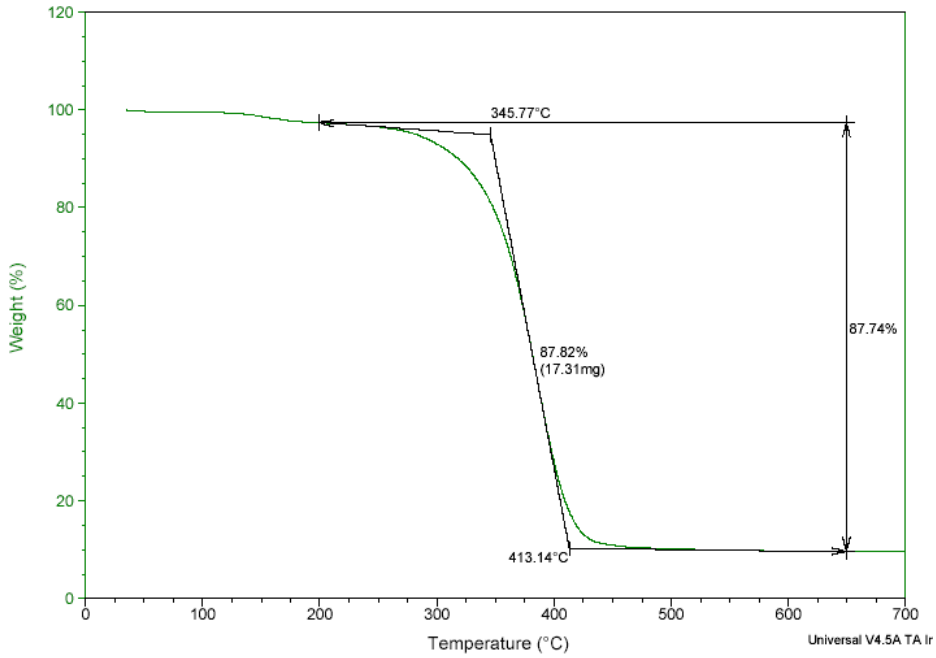

Figure 4. 33 Thermogravimetic analysis (TGA) graph of BMS/PMMA composites (sample 3) synthesized with solution polymerization with vacuum steps.

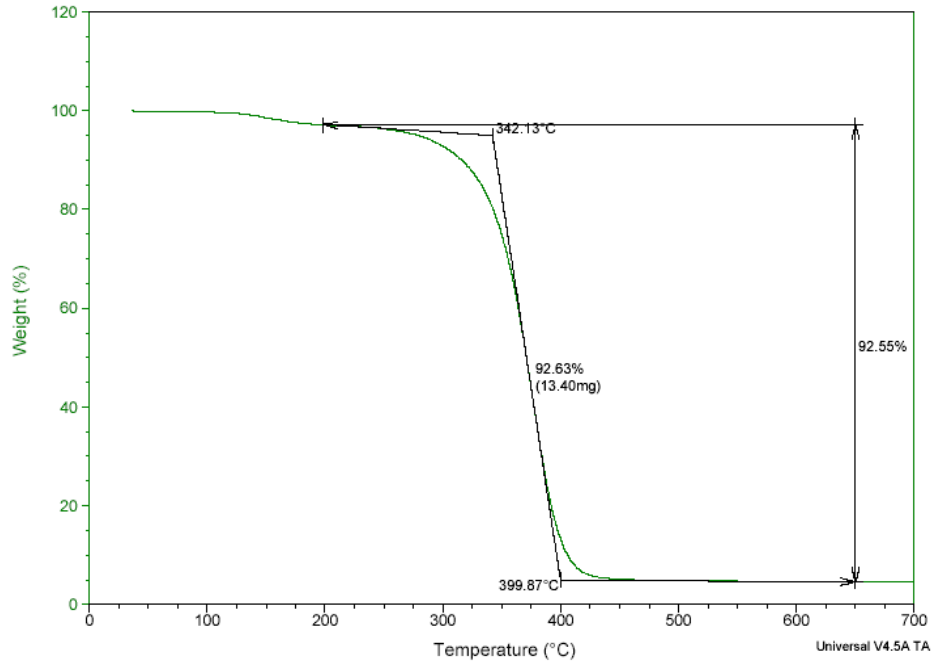

Figure 4. 34 Thermogravimetic analysis (TGA) graph of BMS/PMMA composites (sample 4) synthesized with solution polymerization with vacuum steps.

4.5 Conclusion

In this part of the research, a kind of azo-initiator of ABCC was successfully grafted onto the surface of mesoporous silica through a two steps surface grafting, in which amine groups were grafted on silica surface in the first step and ABCC grafted on silica surface in the second step. The initiator-immobilized mesoporous silica initiated the free radical polymerization inside the nano-channels of mesoporous silica using both solution polymerization and bulk polymerization.

BET adsorption/desorption isotherms showed that values of all surface area, average pore size and pore volume of mesoporous silica decreased as one more post-grafting step was finished on the surface of mesoporous silica. DSC and TGA helped to verify the successful grafting of initiator of ABCC on the surface of mesoporous silica. The ABCC-immobilized mesoporous silica initiated the free radical polymerization of MMA monomer inside the nano-channels and new polymerized PMMA grew out of the nano-channels and covered the surface of BMS spheres. The PMMA/BMS composites synthesized by this procedure showed spherical morphology with narrow distribution of diameters around 5μm which was almost double of the diameter of pure BMS. The synthesized BMS/PMMA showed a higher glass transition temperature, higher decomposition temperature and narrower decomposition range than those of pure commercial PMMA.

PMMA was separated from the surface of mesoporous silica after hydrofluoric acid dissolving silica networks. The pure PMMA particles had a spherical morphology which was the same as spherical BMS/PMMA composites, which also showed that the polymer didn't collapse after supported silica was removed. The spherical PMMA

capsule obtained from BMS/PMMA composites was shown to have special properties, such as ultra-high molecular weight around 800,000 g/mol, very low polydispersity index of 1.1, higher glass transition temperature and higher decomposition temperature than that of pure commercial available PMMA.

The weight percentage of polymer in BMS/PMMA composites wouldn't change with vacuum steps for both solution polymerization and bulk polymerization, while vacuum step would increase the weight percentage of polymer in composites.

Methods were developed to graft initiator onto the surface of mesoporous silica and to synthesize PMMA spherical particles with narrow distribution of spherical diameter. The same procedure could also be used to synthesize other monomer with vinyl functional groups. The surface initiated free radical polymerization was close to a living polymerization which could produce polymers with ultra-high molecular weight and ultra-low polydispersity index. The spherical PMMA capsule obtained from BMS/PMMA nanocomposites showed the same thermal behavior as them in composites, which showed a higher decomposition temperature and narrower decomposition range than commercial available PMMA.

CHAPTER 5

MESOPOROUS SILICA/NYLON 6 NANOCOMPOSITES

From the literature, method used previous to produce silica/nylon composites were simple physical blending of silica and nylon 6 above the melting temperature of nylon 6. In the previous chapter a new method to graft a kind of azo-initiator on the surface of mesoporous silica, and synthesizing spherical BMS/PMMA composites and spherical PMMA capsules with excellent properties. Therefore, we also plan to investigate a method to initiate a kind of surface initiated ring-opening polymerization.

The next step is to use the silanol groups on the surface of mesoporous silica and synthesize nylon 6 with covalent bond with the surface of mesoporous silica. In previous chapter, ABCC was grafted onto silica surface through two steps of surface grafting. Similar to the previous method, we also have to graft initiator onto the surface of mesoporous silica through silanol groups in the first step, and the initiator initiate the anionic ring-opening polymerization of epsilon-caprolactam in the second step. When polymerization is finished, the nylon 6 is expected to grow from the surface of mesoporous silica and out of the nano-channels.

5.1 Designed procedure 1 to synthesize mesoporous silica/nylon 6 nanocomposites

Scheme 5.1 shows a designed procedure to synthesize mesoporous silica/nylon 6 nanocomposites. According to this designed procedure, N-acyllactam, which is a necessary initiator for anionic ring-opening polymerization to synthesize nylon 6, with an

active functional group of acid chloride to be used to be grafted onto the surface of silica through silanol group is synthesized in the first step. Then APTMS is grafted onto the surface of mesoporous silica in step 2, which will introduce amine groups on the surface of mesoporous silica. In the third step, acid chloride group can react with amine group which is grafted on the surface of mesoporous silica in the second step, through which N-acyllactam is successfully grafted onto the surface of mesoporous silica. The left unreacted silanol groups on the surface of mesoporous silica can be removed through HMDS according to reaction condition. The last step is to initiate the anionic ring-opening polymerization of epsilon-caprolactam to synthesize nylon-6 from the surface of mesoporous silica. Using this new method to produce mesoporous silica/nylon 6 nanocomposites, a step by step and characterization of the chemicals synthesizing and grafted must be done to verify the check the feasibility of designed procedure.

Similar to previous ABCC grafting steps, amine group is used to build the bridge between silica surface and initiator center of N-acyllactam. The different part is that the reaction condition of anionic polymerization is much tougher than free radical polymerization. Solid state NMR was used to characterize mesoporous silica based derivatives.

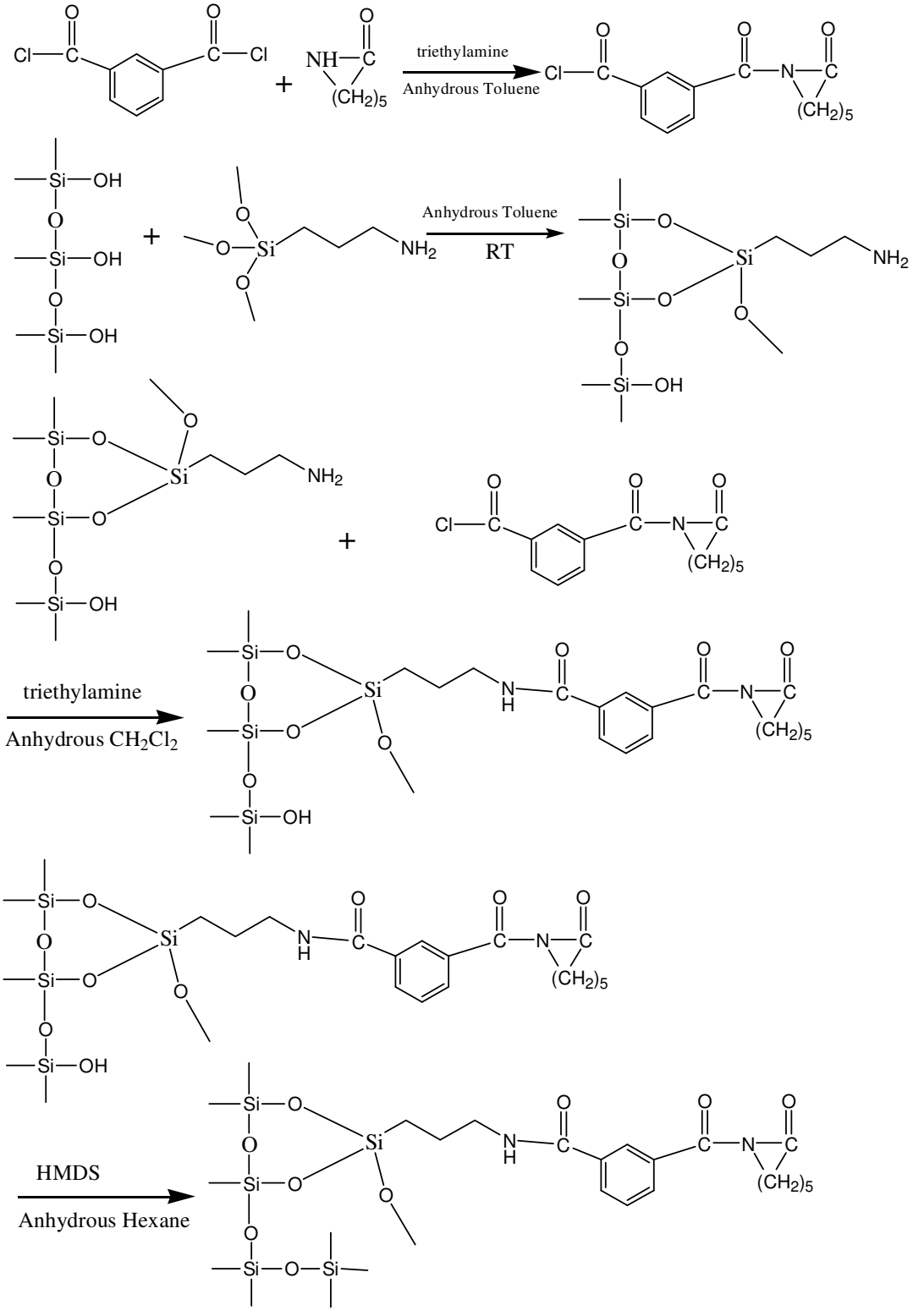

Scheme 5. 1 designed procedure 1 to synthesize N-Acyllactam grafted mesoporous silica

5.1.1 Synthesis and characterization of of Chloro-isophthaloyl-N-ε-caprolactam

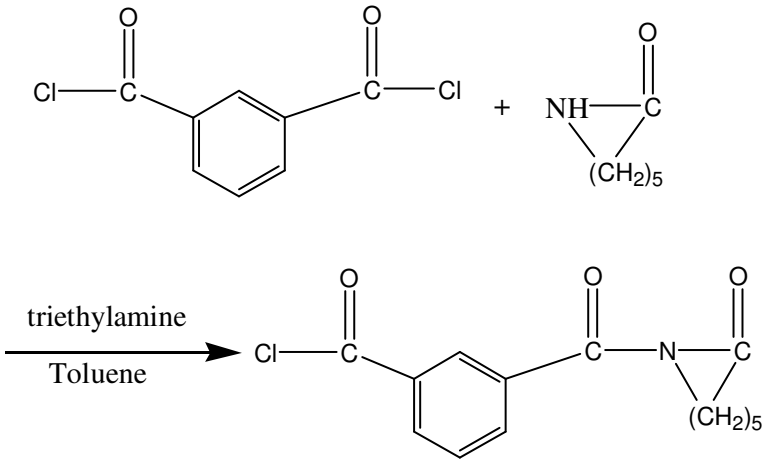

Scheme 5.2 Synthesis of Chloro-isophthaloyl-N-ε-caprolactam

According to mechanism of anionic ring-opening polymerization of epsilon-caprolactam, N-acyllactam is a necessary initiator. However, in the current literature it is very difficult to find N-acyllactam with reactive functional group which can be used to graft it onto the surface of mesoporous silica. A new N-acyllactam with reactive functional group needs to be synthesized. Scheme 5.2 showed the synthesis formula of Chloro-isophthaloyl-N-ε-caprolactam which was a kind of N-acyllatam with functional group of acid chloride. With the detailed synthesis step in chapter 3, it was found that plenty of isophthaloyl dichloride easily reacted with epsilon caprolactam. When one acid chloride group reacted with the amide group of epsilon caprolactam, the reactivity of another acid chloride would be decreased due to steric effect and electron effect, so it was possible to keep one acid chloride group unreacted while another acid chloride group reacted with epsilon caprolactam to form the designed N-acyllactam. After recrystallization, the white crystals were characterized with ^{1}H-NMR, FT-IR, Mass-spectrometry and DSC.

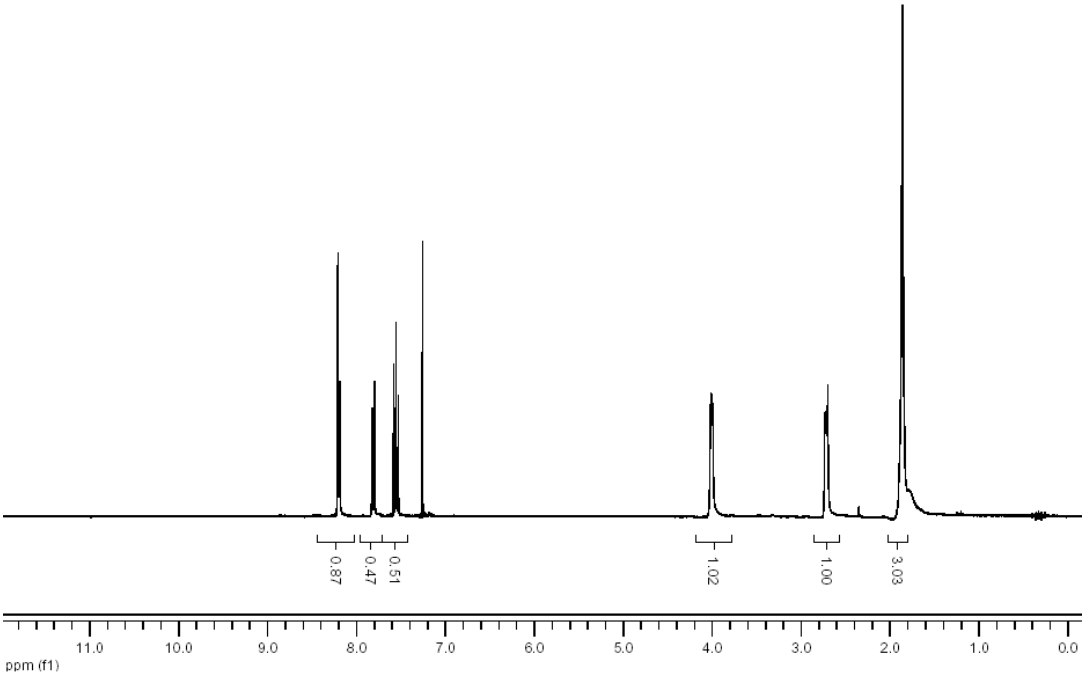

Figure 5. 1 ^{1}H NMR spectrum of Chloro-isophthaloyl-N-ε-caprolactam

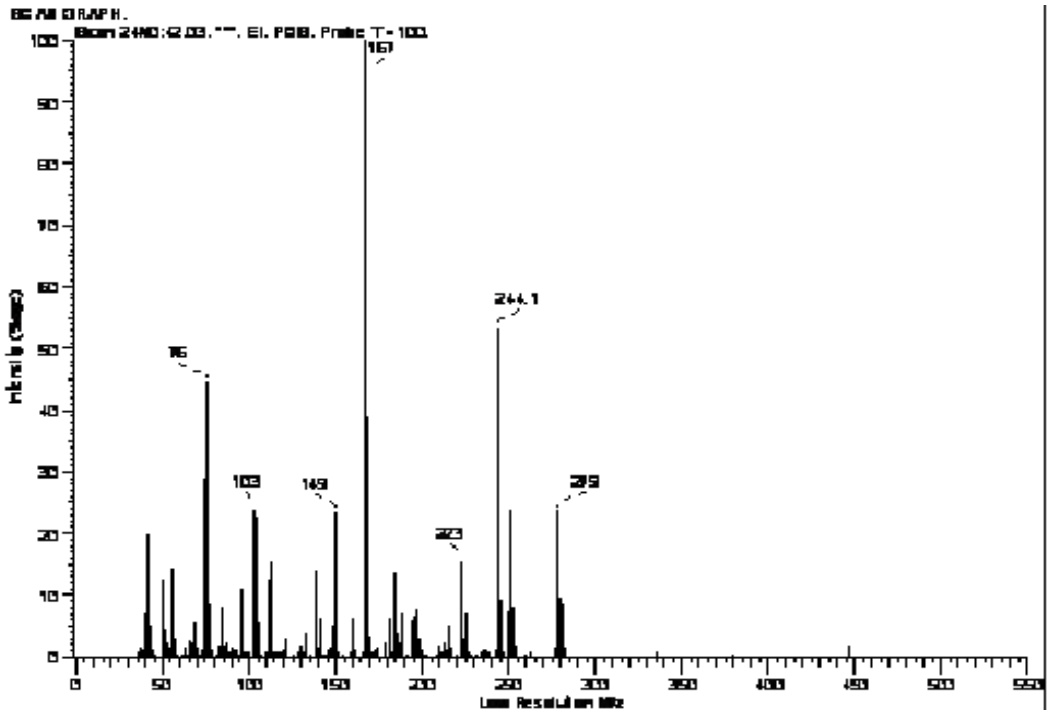

Figure 5. 2 Mass spectrometry spectrum of Chloro-isophthaloyl-N-ε-caprolactam

Table 5. 1 Possible molecular formula corresponding to molecular weight obtained from mass spectrometry.

Observed Mass	Int.	Calculated	ppm	mmu	Formula
		279.06220	-17.6	-4.9	C9.H14.N3.O5.35Cl
		279.06403	-11.0	-3.1	C8.H19.N.O5.35Cl2
		279.06439	-9.7	-2.7	C15.H9.N3.O3
		279.06566	-5.2	-1.4	C4.H138.N2.O4
		279.06573	-4.9	-1.4	C17.H11.O4
		279.06615	-3.4	-1.0	C.H141.N3.O3.35Cl
		279.06622	**-3.2**	**-0.9**	**C14.H14.N.O3.35Cl**
		279.06671	-1.4	-0.4	C11.H17.N2.O2.35Cl2
		279.06749	1.4	0.4	3.H143.O4.35Cl
		279.06798	3.1	0.9	H146.N.O3.35Cl2
		279.06834	4.4	1.2	C7.H136.N3.O
		279.06841	4.7	1.3	C20.H9.N.O

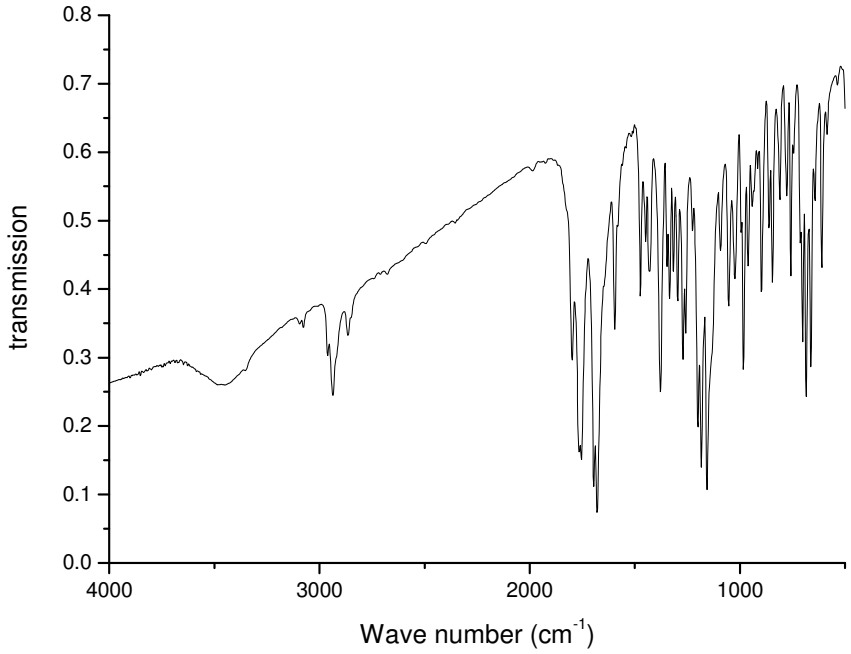

Figure 5. 3 FT-IR spectra of Chloro-isophthaloyl-N-ε-caprolactam

From the ^{1}H NMR spectra (300MHz, $CDCl_3$): six peaks and their structure can be found with δ 8.21 (d, 2H), 7.81 (s, 1H), 7.56 (t, 1H), 3.94-4.04 (m, 2H) ,2.68-2.76 (m, 2H) , 1.80-1.92 (m, 6H). Mass spectrometry showed the observed mass was 279.06749 which corresponded to the possible molecular formula in table 4.1. IR spectra showed there was carbonyl group, benzyl group. All NMR, MS and FT-IR showed that the structure was just the designed structure of Chloro-isophthaloyl-N-ε-caprolactam. And the DSC spectra showed m.p. 95.3°C. d.p. 149.0°C. This newly synthesized chloro-isophthaloyl-N-ε-caprolactam had two functional groups on both sides, one is N-acyllactam group which could initiate the anionic ring-opening polymerization of ε-caprolactam to produce nylon 6, another functional group was very reactive group of acid chloride which could react with all chemicals with active hydrogen. It was also easy to graft chemicals with reactive hydrogen, such as amine groups, onto the surface of mesoporous silica. Then the newly synthesized chloro-isophthaloyl-N-ε-caprolactam builded a connection between nylon 6 and supported materials with silanol groups on their surface.

5.1.2 Immobilizing N-acyllactam onto the surface of SBA-15

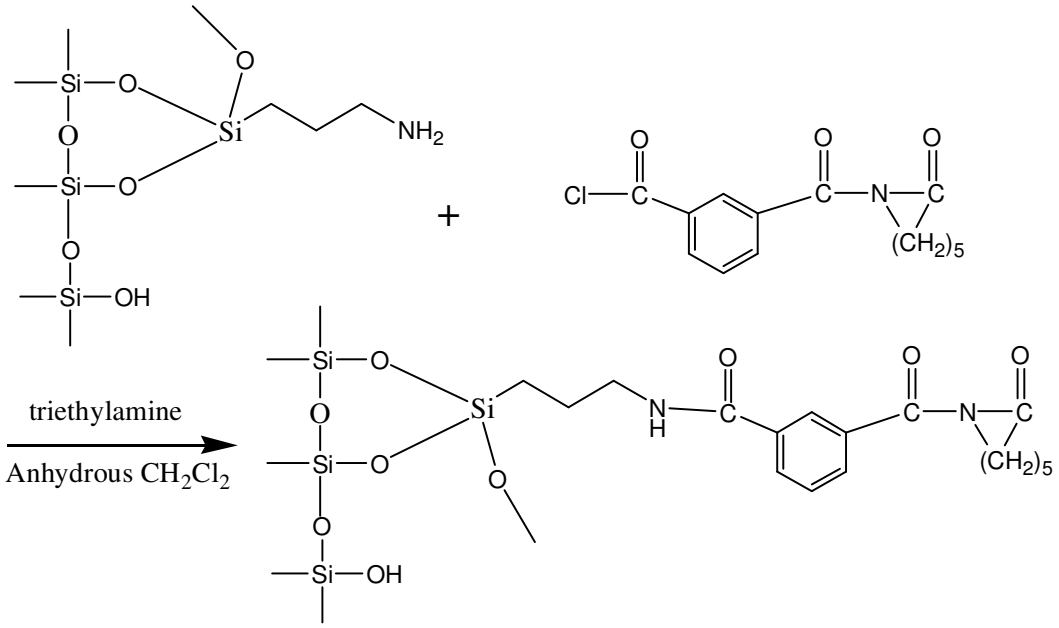

Scheme 5. 2 grafting of N-acyllactam on the surface of mesoporous silica

Scheme 5.2 outlines the synthesis steps of grafting N-acyllactam onto the surface of mesoporous silica through the reaction between amine group and acid chloride group. To modify mesoporous silica surface, R-Si(OR')$_3$ is a common formula used to react with the silanol groups on silica surface. 3-aminopropyltrimethoxysilane (APTMS) was used to react with silanol group, through which amine groups were grafted onto silica surface which was detailed characterized in previous chapter. The grafted amine groups reacted with acid chloride group and built covalent bond between mesoporous silica and chloro-isophthaloyl-N-ε-caprolactam. Silica surface with plenty of silanol groups are highly hydrophilic which will play two roles during the reaction procedures. On the one side, highly hydrophilic surface will help the diffusion of polar monomer into the nano-channels of mesoporous silica. On the other side, the existence of silanol groups on silica surface will probably produce side reaction during anionic ring-opening polymerization because anionic polymerization is very sensitive to hydroxyl groups. With silanol

capping step, HMDS will consume all silanol groups on the surface of mesoporous silica to produce a highly hydrophobic surface. Whether the capping step is necessary or not for polymerization depends on the type of further reaction. If the further reaction is very sensitive to silanol groups, the silanol capping step is necessary. Otherwise, there is no need to finish this silanol capping step.

To examine whether all designed steps are finished, solid NMR and N_2 desorption/adsorption isotherms are used for characterization. ^{29}Si CP-MAS NMR spetra can show the resonance change of silicon because mesoporous silica network is composed of silicon and oxygen. And ^{13}C CP-MAS NMR spectra can verify whether organic functional groups are successfully grafted onto the surface of mesoporous silica. There is no organic functional group between the silica networks for pure mesoporous silica, ^{13}C CP-MAS NMR spectra can show the change when organic functional groups are grafted onto the surface of silica through silanol groups. And the spectra can also characterize the detailed structure of organic groups on the surface of mesoporous silica. Mesoporous silica is composed of nano-channels which give mesoporous silica an extra large surface area. Nitrogen desorption/adsorption isotherm is an excellent technique to test the surface area, channels size and pore volume, through which we can tell whether the grafting steps are finished successfully or not. If the average size of nano-channel is becoming smaller, or the surface area is becoming smaller, it means more organic groups are grafted on the inner walls of mesoporous silica. TGA is used to test the amount of organic loading on the surface of mesoporous silica through collecting the mass loss between 200°C and 650°C. With the calculation of collected mass loss and basic assumption, the amount of organic functional groups can also be obtained.

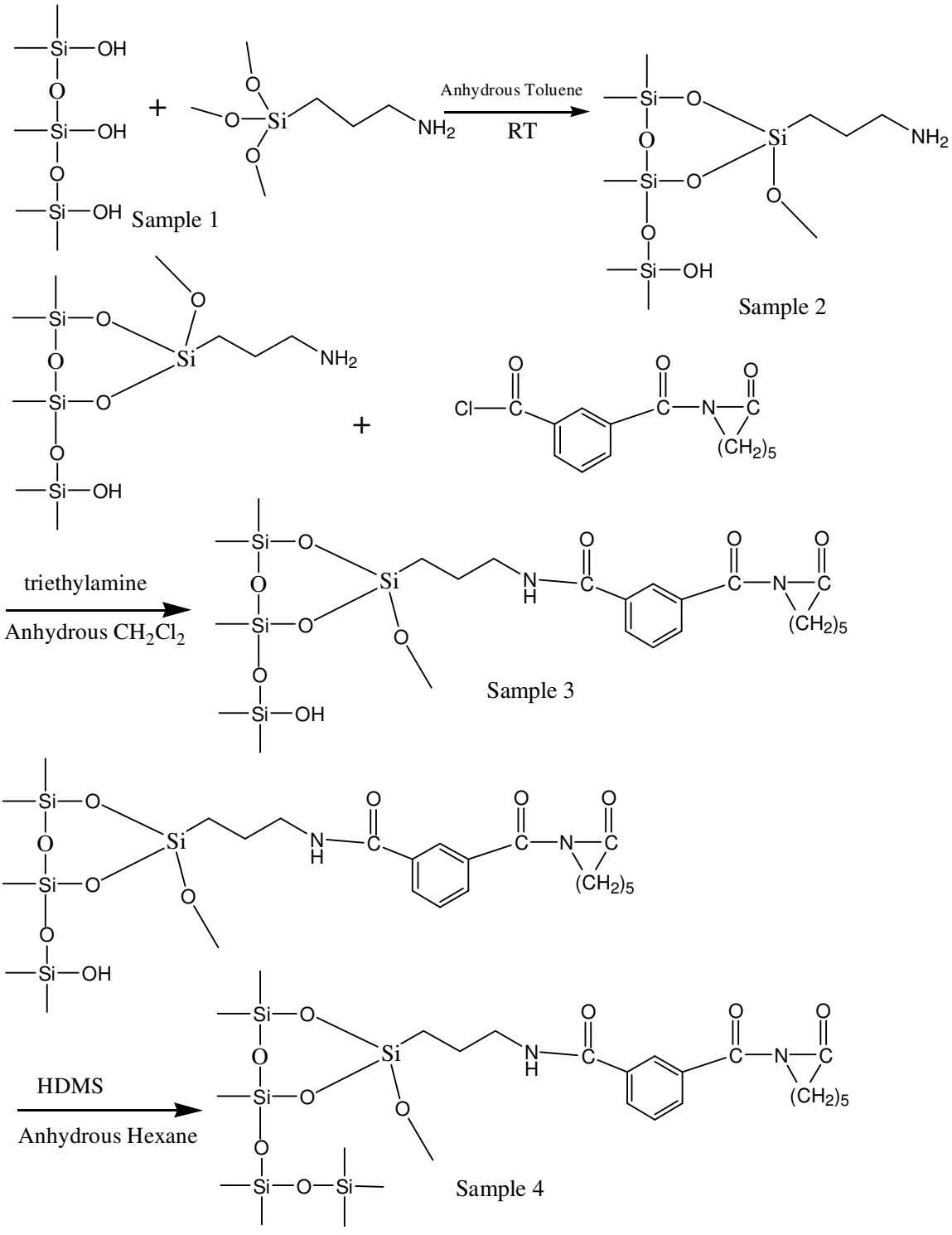

Scheme 5. 3 designed procedure of making N-acyllactam immobilized SBA-15

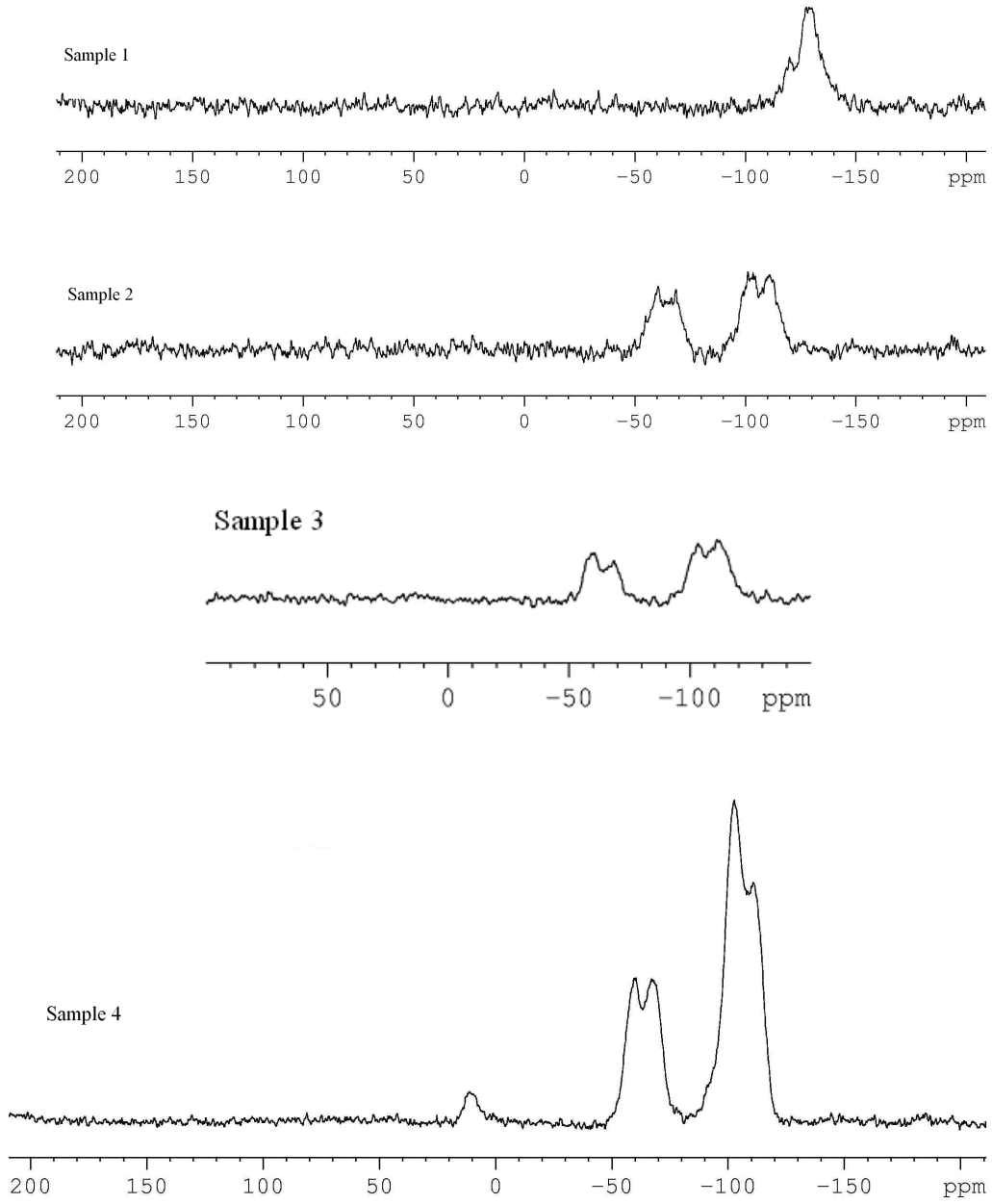

Figure 5. 4 ^{29}Si CP-MAS NMR spectra for sample (1): dried SBA-15; sample (2): amine immobilized SBA-15; sample (3): N-acyllactam immobilized SBA-15; sample (4): capping N-acyllactam SBA-15

5.1.3 Solid NMR characterization of mesoporous silica derivatives

^{29}Si CP-MAS NMR spectra are shown in Figure 5.4 for sample (1) dried pure SBA-15; sample (2) amine immobilized SBA-15; sample (3): N-acyllactam immobilized SBA-15 and sample (4) capping N-acyllactam SBA-15. The spectra of dried SBA-15 showed only one peak between -120 and -140 ppm which was the structure of silica network. The spectra of amine immobilized SBA-15 showed two peaks, one of which was between -90 and -110, another was between -50 and -70. The peak between -50 and -70 showed the existence of extra silicon which was grafted onto the surface of mesoporous silica through APTMS. And the peak between -90 and -110 showed the Q^2, Q^3 and Q^4 silicon resonances[54] which meant the peak was shifted because some organic groups were grafted onto the surface of silica network. The N-acyllactam immobilized SBA-15 (sample 3) had the same spectra as amine immobilized SBA-15(sample 2), the reason was extra organic groups on the surface of silica would not changed the silicon resonance. Compared with the N-acyllactam immobilized SBA-15 (sample 3), capping N-acyllactam immobilized SBA-15 (sample 4) had one more peak between 15 and 5. The existence of this peak between 15 and 5 told the finish of capping step where HMDS reacted with silanol group to import extra silicon atom on silica network.

^{13}C CP-MAS NMR spectra are shown in Figure 5.5 for sample (2) amine immobilized SBA-15; sample (3): N-acyllactam immobilized SBA-15 and sample (4) capping N-acyllactam SBA-15. The peaks read from the ^{13}C CP-MAS NMR spectra was shown in Table 5.2 which also gave the corresponding functional groups. Table 5.2 told that more carbon peaks could be found after more organic groups were grafted onto the surface of silica. Table 5.2 showed aromatic carbons peak was located at 129ppm for N-

acyllactam immobilized SBA-15 while there was no aromatic carbons peak for amine immobilized SBA 15. The new peaks and their corresponded functional groups verified the successful finish of designed organic grafting steps.

Table 5. 2 ^{13}C CP-MAS NMR Chemical Shifts for amine immobilized SBA-15, N-acyllactam immobilized SBA-15 and capping N-acyllactam immobilized SBA-15

Sample 2		Sample 3		Sample 4	
-Si-CH_2-	9	-Si-CH_2-	9	-Si-CH_2-	9
-Si-CH_2-CH_2-	24	-Si-CH_2-CH_2-	24	-Si-CH_2-CH_2-	24
-CH_2-CH_2-NH_2	43	-CH_2-CH_2-NH_2	43	-CH_2-CH_2-NH_2	43
		Aromatic carbons	129	Aromatic carbons	129
		-CO-N=	160	-CO-N=	160
		-CO-NH-	200	-CO-NH-	200
				-Si-CH_3	0

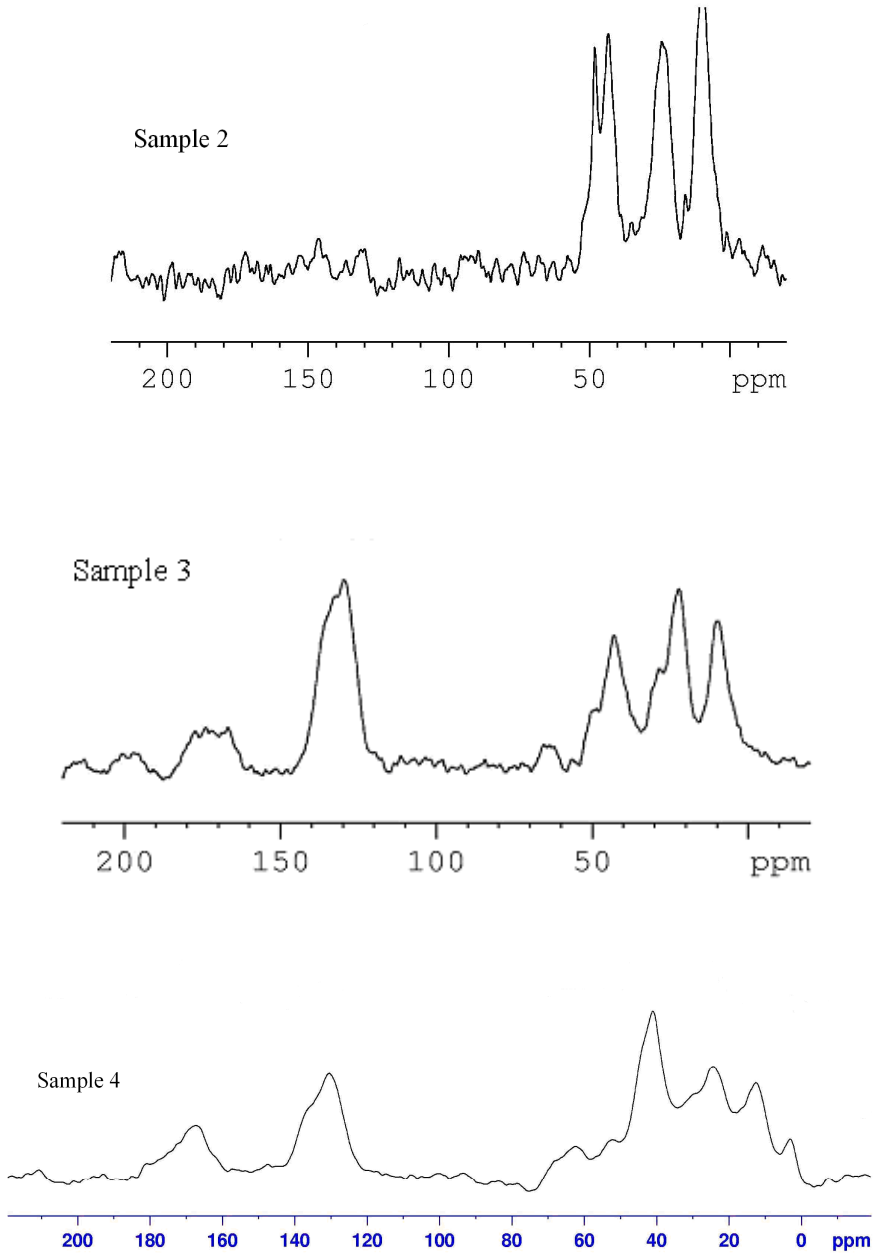

Figure 5. 5 ^{13}C CP-MAS NMR spectra for sample 2: amine immobilized SBA-15; sample 3: N-acyllactam immobilized SBA-15; sample 4: capping N-acyllactam SBA-15

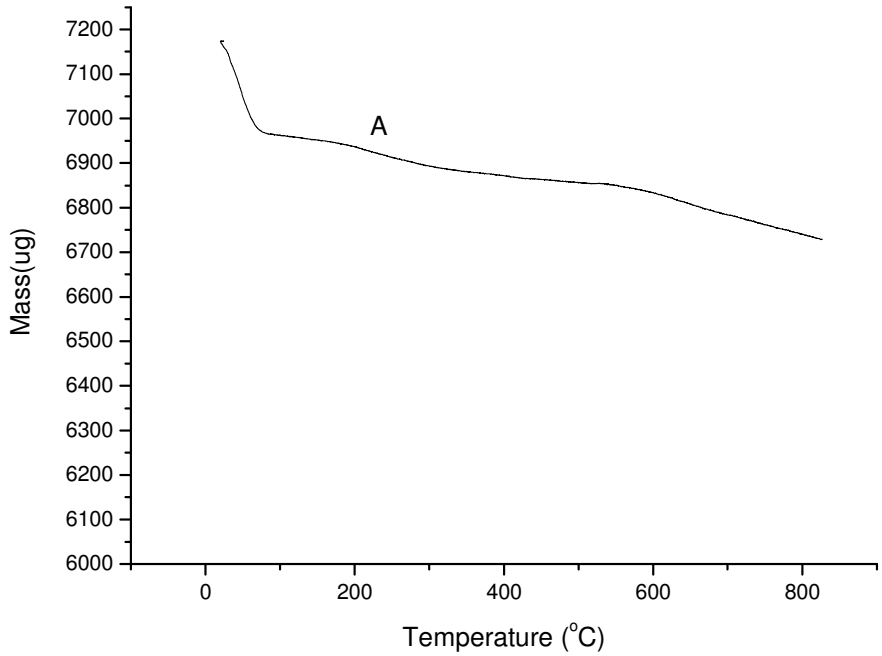
7200
7100
7000
6900
6800
6700
6600
6500
6400
6300
6200
6100
6000
Mass(ug)
A
0
200
400
600
800
Temperature (°C)

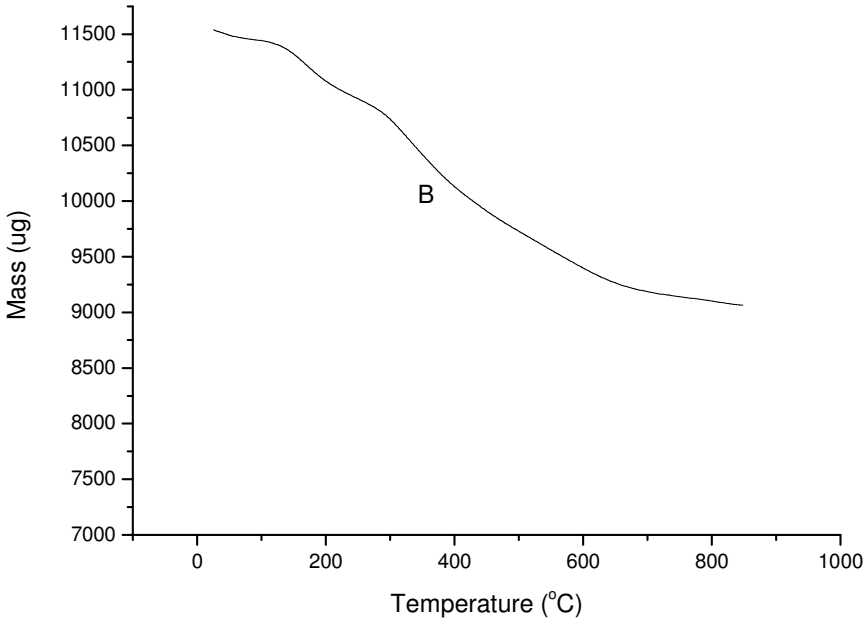
11500
11000
10500
10000
9500
9000
8500
8000
7500
7000
Mass (ug)
B
0
200
400
600
800
1000
Temperature (°C)

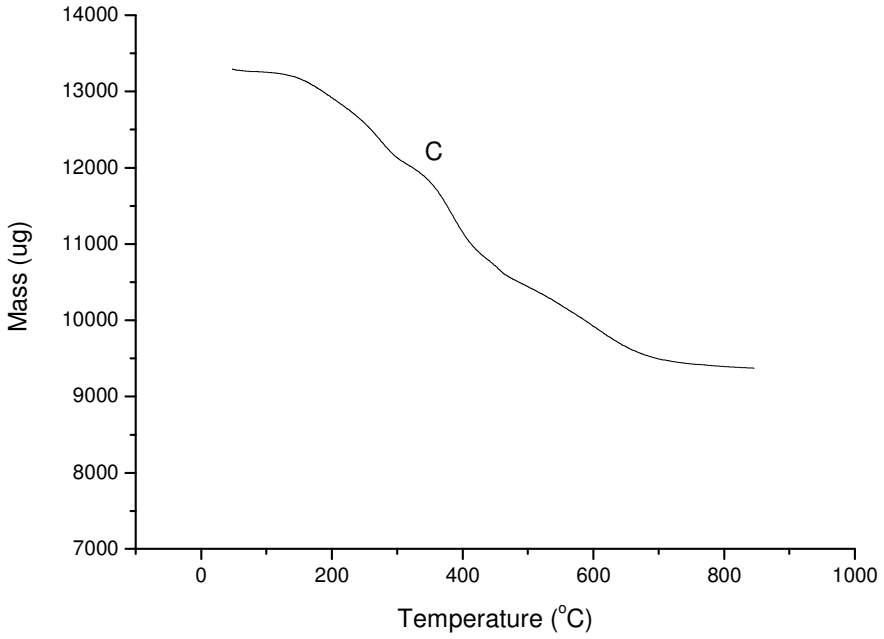

Figure 5. 6 TGA graph of (A) SBA-15; (B) amine immobilized SBA-15; (C) N-acyllactam immobilized SBA-15;

5.1.4 Thermal analysis and BET analysis of BMS derivatives

Thermogravimetic analysis (TGA) was performed to calculate the amount of organic loading on the surface of mesoporous silica SBA-15. Samples were heated under nitrogen from 30 to 700 °C at a rate of 10 °C/min. The organic loading was measured by measuring the weight loss between 200 and 650 °C. For the traditional amine-functionalized SBA-15, the organic loading was determined by assuming two methoxy linkages to the surface. The weight loss was calculated with the mass loss of calcinated organic loading over the mass of silica/organic composites. Figure 5.6 showed TGA graphs of (A) SBA-15; (B) amine immobilized SBA-15; (C) N-acyllactam immobilized

SBA-15. For dried silica SBA-15, the weight loss was only 3% which meant only few silanol groups loss at high temperature. For amine immobilized SBA-15, the weight loss was 16.4%. Assuming two methoxy linkages to the silica surface, the immobilized amine should be 2.3 mmol of NH_2/g material. For N-acyllactam immobilized SBA-15, the weight loss was 27.2% which meant immobilized N-acyllactam should be 0.56mmol N-acyllactam/g materials. So there were still approximately 75% amine groups of the surface of mesoporous silica SBA-15 which didn't reacted with the acid chloride groups The left amine groups would probably terminate the anionic polymerization to synthesize nylon-6.

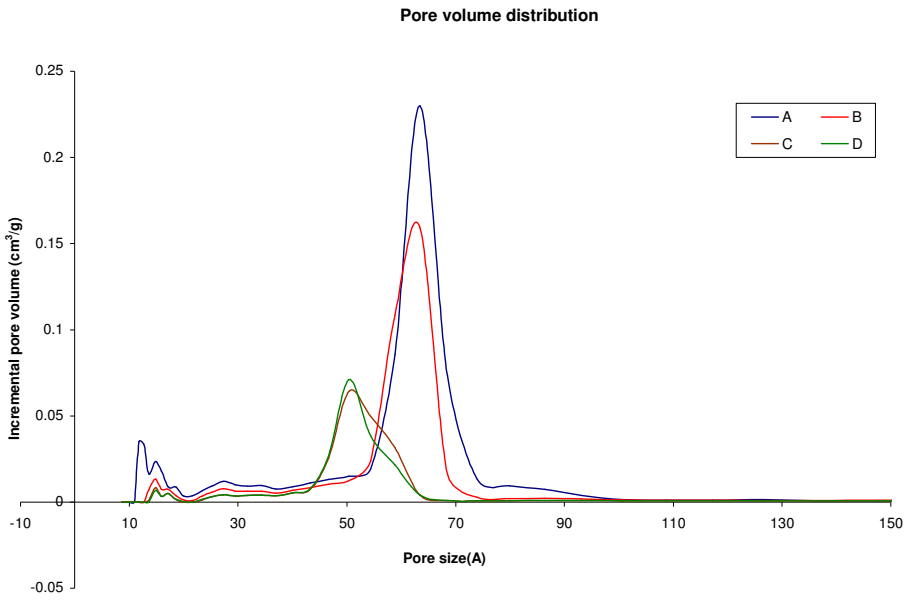

Figure 5. 7 Pore volume distribution with pore size of (A) SBA-15; (B) amine immobilized SBA-15; (C) N-acyllactam immobilized SBA-15; (D) capping N-acyllactam immobilized SBA-15

For characterization of mesoporous materials, nitrogen physisorption isotherm was used. Figure 5.7 showed pore volume distribution with pore size of SBA-15, amine immobilized SBA-15, N-acyllactam immobilized SBA-15 and capping N-acyllactam immobilized SBA-15. Figure 5.7 showed that pore volume peaks became smaller as the peaks shifted toward smaller pore size. The parameters of surface area, pore volume and pore size were shown in Table 5.3. The listed data showed that all surface area, pore volume and pore size were decreased from sample A to sample D. Although the pore size only decreased from 4.6 to 3.8nm, while the surface area sharply decreased from 785 to 183 m^2/g and the pore volume sharply decreased from 0.86 to 0.26 cm^3/g.

Table 5. 3 Materials parameters get from nitrogen isotherms

Sample number	Surface area(m^2/g)	Pore Volume(cm^3/g)	Pore size (nm)
A	784.8936	0.855886	4.6020
B	342.7454	0.494370	4.5248
C	193.9172	0.272534	3.8298
D	183.0104	0.255362	3.7851

All solid ^{29}Si NMR, ^{13}C NMR, TGA and nitrogen physisorption isotherm results showed that N-acyllactam were successfully grafted onto the surface of the inner wall of mesoporous silica SBA-15 after multiple functional grafting.

5.1.5 Synthesized nylon/SBA-15 nanocomposites

Monomer of epsilon-caprolactam was allowed to be pushed into the nano-channels of mesoporous silica under the vacuum condition with detailed steps given in chapter 3. Under a certain reaction condition, the monomer will be initiated with the initiator of N-acyllactam on the surface of mesoporous silica under the injected catalyst of magnesium bromide ethyl etherate.

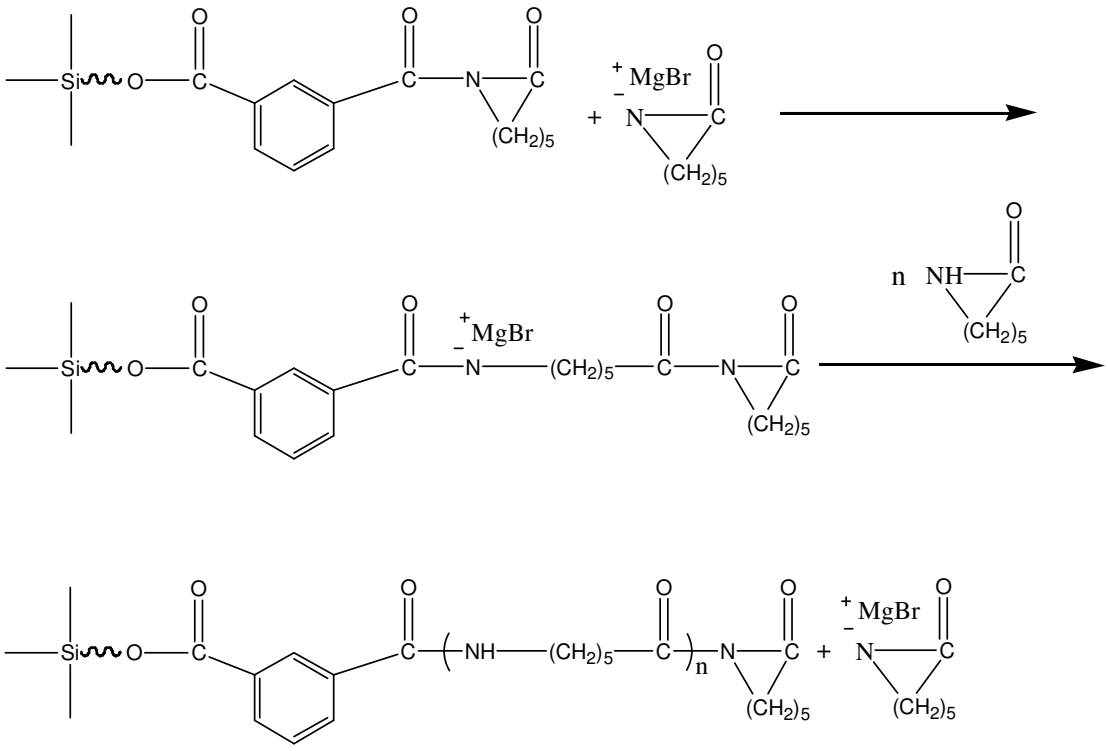

Scheme 5. 4 designed procedure of anionic ring-opening polymerization of epsilon-caprolactam to produce mesoporous/silica nanocomposites.

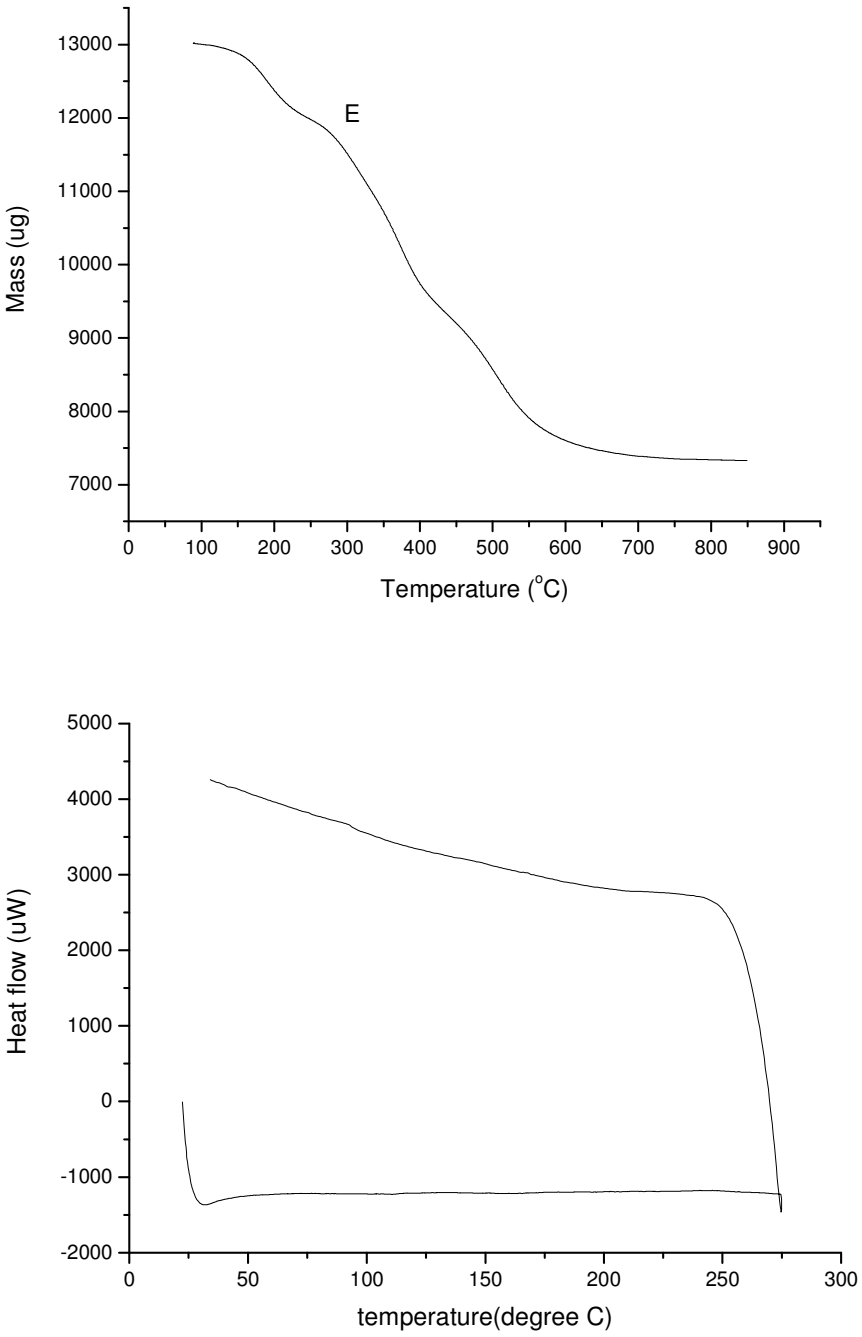

Figure 5. 8 TGA graph of synthesized nylon/SBA-15 nanocomposites (upper), D.S.C graph of nylon/SBA-15 nanocomposites(lower)

The melting temperature of ε-caprolactam is 70°C, and its boiling point is 140°C/10 mmHg. Anionic ring-opening polymerization is very sensitive to moisture or other chemicals with active hydrogen. Because of ultra small pore size of nano-channels and low pore volume, it is very hard for ε-caprolactam monomer to fill the nano-channels. Monomer of epsilon caprolactam contains water which forms hydrogen bond with epsilon-caprolactam monomer. Caprolactam monomer is dried by distilling off about 5% by weight of caprolactam under vacuum at 140°C. Here we use freeze-thaw procedures under vacuum condition and ultrasonic equipment to help the monomer fill nano-channels. Flask with dried caprolactam monomer was kept at 140°C under high vacuum, afterwards, the temperature of flask was allowed to decrease until the caprolactam monomer froze as solids. N-acyllactam immobilized mesoporous silica was placed on the surface of MMA monomer, and temperature of flask was slowly increased to 140°C to allow monomer of epsilon caprolactam diffuse into the nano-channels with high vacuum. The temperature was sharply decreased and increased again to repeat the above steps. After 3 cycles of freeze-thaw procedures, the melting mixture was placed under ultrasonic for 30 mins. Then the mixture was allowed to be initiated with injection of catalyst of 1.0M MgBrEt into the flask at 140°C. Monomer of epsilon caprolactam formed white solid as reaction went on. The reaction was stopped after 12 hours. Formic acid was poured into flask with stirring, white solids were obtained after filtering. The step of washing with formic acid and filtration was repeated 4 times, and the resulted nanocomposite was characterized with TGA, DSC.

TGA data of dried obtained white solids showed weight loss of 40.3% which was a little higher than weight loss of N-acyllactam immobilized SBA-15 (27.2%) (Figure

5.8). The TGA data showed 0.3g extra weight loss per g SBA-15. Assuming the density of nylon 6 was 1.23g/cm^3, and all pore volume was filled with nylon 6. Then the amount of nylon 6 per g SBA 15 would be 0.32g (0.26×1.23) which was very close to the TGA data. The TGA data showed that all pores were filled with new synthesized chemicals. DSC thermograms (Figure 5.8) couldn't show the glass transition temperature and melting temperature of the synthesized chemicals. Monomer of epsilon-caprolactam would form caprolactam bromide salt after catalysts were added to reaction system, the nano-channels filled chemicals could also be caprolactam salt.

Surplus left amine groups on the surface of mesoporous silica which didn't react with acid chloride groups from chloro-isophthaloyl-N-ε-caprolactam because of steric effects in the second organic grafting step. The amine groups could terminate the anionic ring-opening polymerization and epsilon-caprolactam monomer would only form salt with catalysts of magnesium bromide ethyl etherate. With this procedures, no synthesized nylon 6 was proved to fill with nano-channels although each step was proved to be successful using characterization method of solid NMR and nitrogen desorption/adsorption isotherms, and the chemicals which filled with the nano-channels could be caprolactam salt.

5.1.4 Nylon-6/BMS nanocomposites

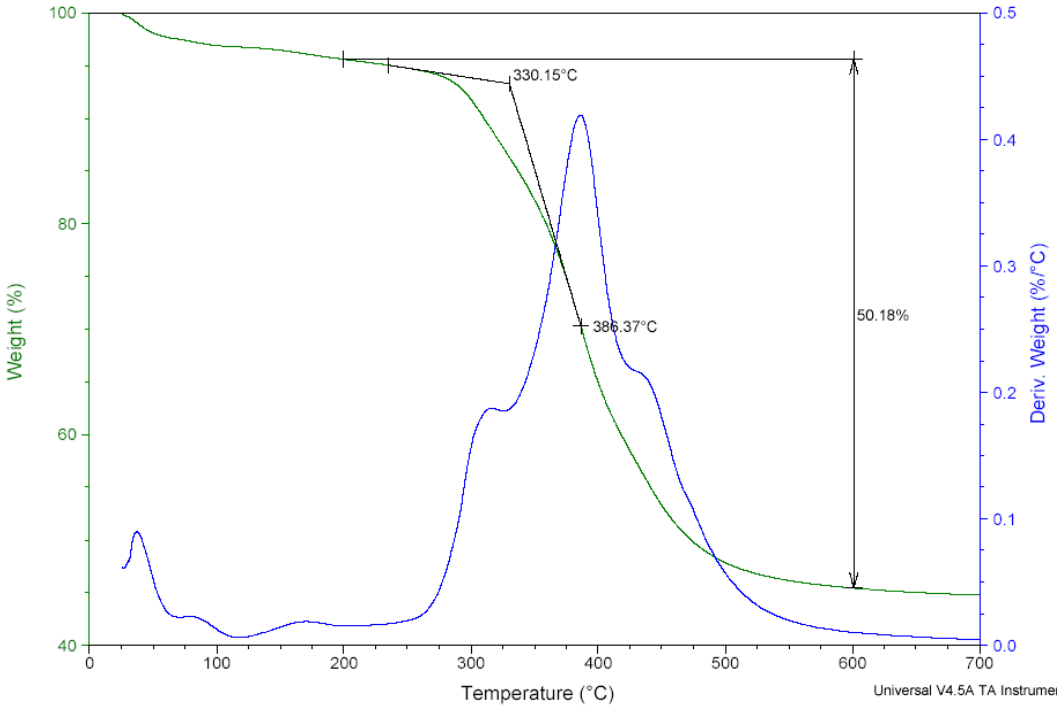

Figure 5. 9 TGA of BMS/nylon 6 composites

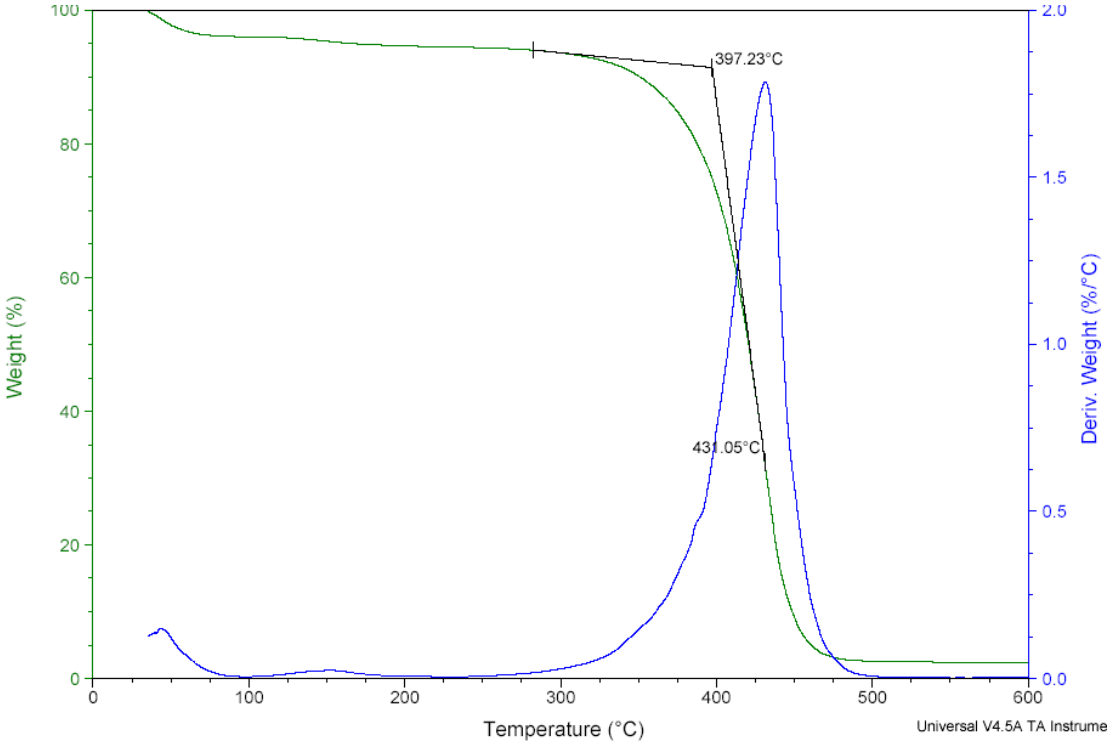

Figure 5. 10 TGA of pure nylon 6

With the steps to produce Nylon 6/SBA-15 composites, similar steps were used to produce nylon-6/BMS nanocomposites. We failed to obtain nylon 6 from the previous step of synthesis when we use SBA-15 as the supported materials. Considering the size of nano-channels of SBA-15 was only several nanometers which were too small, we used BMS to replace SBA-15 and repeated steps of the previous designed procedures. The newly synthesized BMS/nylon 6 composites were characterized with TGA and DSC.

The TGA of pure nylon 6 (Figure 5.10) showed a single step of decomposition in the range of 397-480°C. And the beginning decomposition temperature was 397°C which was much higher than that of synthesized composites. And TGA of BMS/nylon 6 composites showed a broader decomposition range. It began decomposition at 330°C, finished decomposition until 500°C. And there was 50.2% weight loss between 200°C and 600°C. DSC thermograms couldn't show glass transition temperature and melting point of nylon 6 for BMS/nylon 6 composites.

For BMS/PMMA composites, 1 g BMS could produce 5.45g PMMA on the surface of BMS. Both SBA-15/nylon 6 and BMS/nylon 6 could only produce less than 1 g of nylon 6 on the surface of mesoporous silica. To avoid the effect of extra large amount of left amine groups on silica surface during anionic ring-opening polymerization, a new synthesis procedure was designed to synthesize mesoporous silica/nylon 6 composites.

5.2 New designed approach to synthesize mesoporous silica/nylon-6 nanocomposites

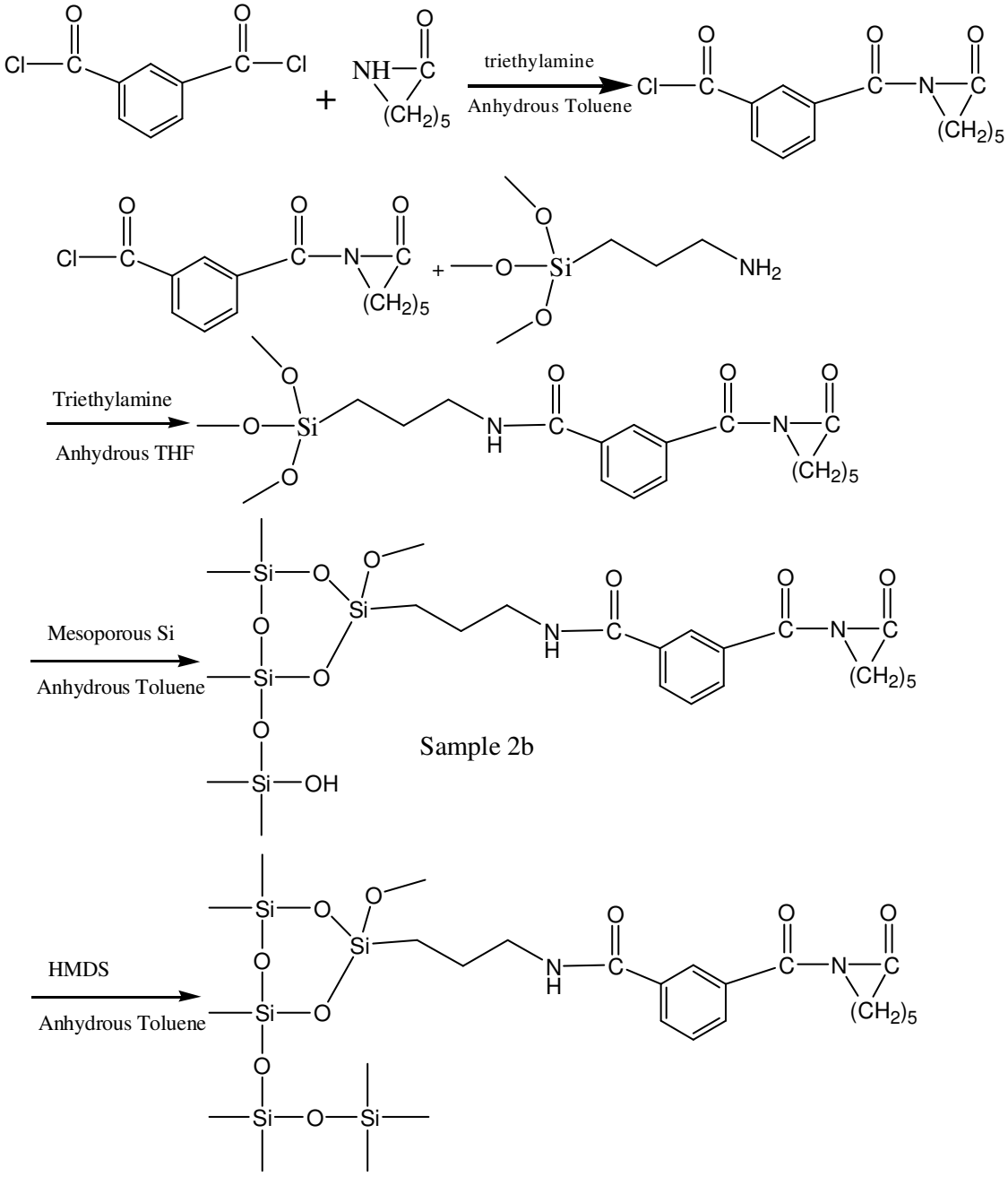

Sample 2b

Sample 3b

Scheme 5. 5 New designed procedures to synthesize N-acyllactam immobilized mesoporous silica

The proposed procedure in 5.1 could successfully graft N-acyllactam onto the surface of mesoporous silica, however, it couldn't solve the problem of surplus left amine groups on the surface of mesoporous silica. The large amount of left amine groups would terminate the anionic ring-opening polymerization of epsilon-caprolactam, which was the main reason that high molecular weight nylon 6 couldn't be produced in the nano-channels and only caprolactam salt formed during the reaction. After careful review, this new proposed procedure was designed to use 3-aminopropyl-trimethoxysilane and N-(3-chloroformylbenzyl)-epsilon-caprolactam to synthesize N-3-((N-3-(trimethoxysilanyl)n-propyl)benzamidyl)-benzoyl-epsilon-caprolactam which contained both trimethoxysilanyl group and N-acyllactam group. The trimethoxylsilanyl group could react with the silanol group on the surface of mesoporous silica, through this way the whole molecule could be covalent bonded onto the surface of mesoporous silica. The grafted N-acyllactam was used as initiator to initiate the anionic ring-opening polymerization of epsilon-caprolactam to form nylon 6.

After the molecule was connected onto the surface of mesoporous silica, there were no left amine groups on silica surface. The proposed procedure would not introduce any surplus amine groups onto silica surface. Therefore, it could exclude the side reaction produced from amine. The more detailed procedure and analysis would be covered in the following chapters.

5.2.1 Synthesis of N-3-((N-3-(trimethoxysilanyl)n-propyl)benzamidyl)-benzoyl-epsilon-caprolactam

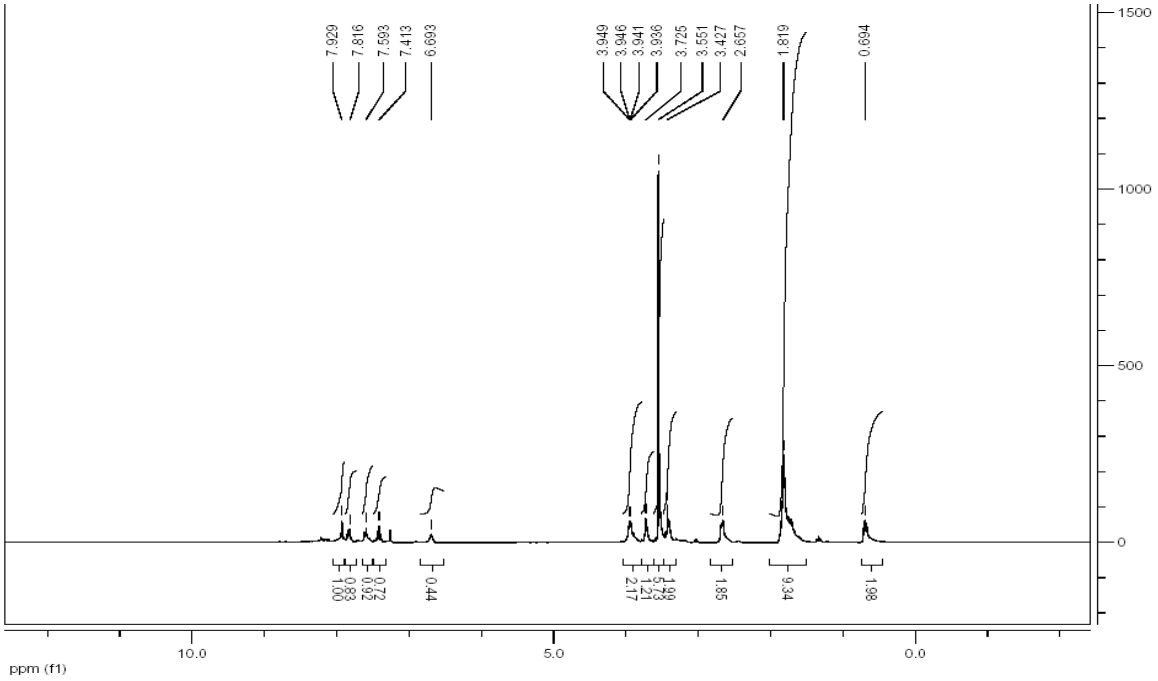

Figure 5. 11 NMR spectrum of N-acyllactam bonding APTMS

In the new proposed procedure, pure N-3-((N-3-(trimethoxysilanyl)n-propyl)benzamidyl)-benzoyl-epsilon-caprolactam was the most important substance. Pure N-(3-chloroformylbenzoyl)-epsilon-caprolactam was used to react with the same molar of 3-aminopropyl-trimethoxysilane in anhydrous THF with the existence of triethylamine. After careful separation and purification, colorless oil with high viscosity was derived. Deutrated chloroform was used as solvent for the new synthesized chemical characterized with ^{1}H NMR. Figure 5.11 showed the ^{1}H NMR spectra of newly synthesized substance.

Figure 5.11 showed NMR spectra of N-3-((N-3-(trimethoxysilanyl)n-propyl)benzamidyl)-benzoyl-epsilon-caprolactam. From the spectra, twelve peaks and their structure could be found with δ 8.21 (d, 2H), 7.81 (s, 1H), 7.56 (t, 1H), 3.94-4.04 (m, 2H) ,2.68-2.76 (m, 2H) , 1.80-1.92 (m, 6H). The NMR spectra verified the structure

of designed N-3-((N-3-(trimethoxysilanyl)n-propyl)benzamidyl)-benzoyl-epsilon-caprolactam.

5.2.2 Immobilizing the synthesized long chain N-acyllactam onto the surface of bi-modal mesoporous Silica

Scheme 5.5 showed the new designed approach to synthesize mesoporous silica/nylon 6. According to scheme 5.3, the first step was grafting APTMS onto the surface of mesoporous silica. The second step was that the amine group from APTMS reacted with chloro-isophthaloyl-N-ε-caprolactam. With this method, some amine groups wouldn't be reacted and remained on the silica surface. According to the calculation from TGA results, only 0.56mmol of 2.3mmol amine/g would react with N-(3-chloroformylbenzoyl)-epsilon-caprolactam to form amide functional group, and 1.74 mmol amine/g materials weren't reacted. Approximately 75% of amine groups weren't reacted from the calculation. To avoid a large amount of left amine groups onto the surface of mesoporous silica, APTMS reacted with the same molar chloro-isophthaloyl-N-ε-caprolactam with the existence of triethylamine. After purification, pure APTMS-N-acyllactam was obtained with the form of colorless viscous oil. Pure APTMS-N-acyllactam was dissolved in anhydrous toluene and the solution diffused into the nano-channels of mesoporous silica. The trimethoxysilanyl group reacted with silanol group and N-acyllactam-APTMS was successfully grafted onto the surface of inner walls of nano-channels. This new method was compared with the old designed procedure, APTMS grafting step was missing. Through one direct grafting step, synthesized N-acyllactam-APTMS was grafted onto the surface of mesoporous silica and there was no

extra left amine groups were remained on silica surface. Final step of silanol capping step was used to get rid of all silanol groups on silica surface. Solid NMR of ^{29}Si CP-MAS NMR and ^{13}C CP-MAS NMR were used to characterize the synthesized solids to verify the reaction of grafting steps.

^{29}Si CP-MAS NMR spectra were shown in Figure 5.12 for sample (1b) dried bimodal silica; sample (2b) N-acyllactam immobilized bimodal silica and sample(3b): capping N-acyllactam BMS; (4): capping N-acyllactam SBA-15. The spectra of sample 1b showed only one peak between -120 and -140 ppm for BMS, which verified the structure of pure silica network(-Si-O-Si-). The spectra of N-3-((N-3-(trimethoxysilanyl)n-propyl)benzamidyl)-benzoyl-epsilon-caprolactam immobilized BMS (sample 2b) showed two peaks, one of which was between -90ppm and -110ppm, another was between -50ppm and -70ppm. The peak between -50ppm and -70ppm showed extra silicon which was connected with organic functional groups. This peak came from the trimethoxylsilanyl groups which were grafted onto the surface of mesoporous silica through the silanol groups. And the peak between -90ppm and -110ppm showed the Q^2, Q^3 and Q^4 silicon resonances[54] which meant the peak was shifted because some organic groups were grafted onto the surface of silica network.

The capping N-3-((N-3-(trimethoxysilanyl)n-propyl)benzamidyl)-benzoyl-epsilon-caprolactam immobilized BMS (sample 3b) had three peaks, two (-90 and -110ppm, -50 and -70ppm) of which were the same as the spectra of uncapping N-3-((N-3-(trimethoxysilanyl)n-propyl)benzamidyl)-benzoyl-epsilon-caprolactam immobilized mesoporous BMS. One more peak which was located between 5ppm and 15ppm was derived from the group of $–Si(CH_2)_3$ which came from the capping reaction of HMDS

with the silanol group. The ^{29}Si CP-MAS NMR spectra of samples 1b, 2b and 3b were compared with ^{29}Si CP-MAS NMR spectra (Figure 5.5) of samples 1, 2 and 3 in the previous designed procedure, the position of all peaks were very similar, but the intensity of these peaks were quite different. The spectra of sample 3b showed almost the same intensity for two peaks of (-Si$(CH_2)_3$) and (=Si(OCH_3)-), however, the spectra of sample 4 showed a relatively small peak of (-Si$(CH_2)_3$) compared with another peak of (=Si(OCH_3)-). The spectra proved that there were more groups of (=Si(OCH_3)-) than groups of (-Si$(CH_2)_3$).

Most of silanol groups on the silica surface reacted with APTMS to form group of (=Si(OCH_3)-), only very few silanol groups were left to react with HMDS to form the group of (-Si$(CH_2)_3$). That was the reason why the intensity of (=Si(OCH_3)-) was much higher than that of (-Si$(CH_2)_3$). However, it was different for sample 3b. The size of N-3-((N-3-(trimethoxysilanyl)n-propyl)benzamidyl)-benzoyl-epsilon-caprolactam was much larger than that of APTMS, a lot of silanol groups on the silica surface would not react with trimethoxylsilanyl group to form (=Si(OCH_3)-) due to the steric effect. This left silanol groups could react with HDMS to form (-Si$(CH_2)_3$) because of the small size of HDMS. That was the reason why the relative intensities of peak from (-Si$(CH_2)_3$) to (=Si(OCH_3)-) was much higher for sample 3b than sample 4.

.

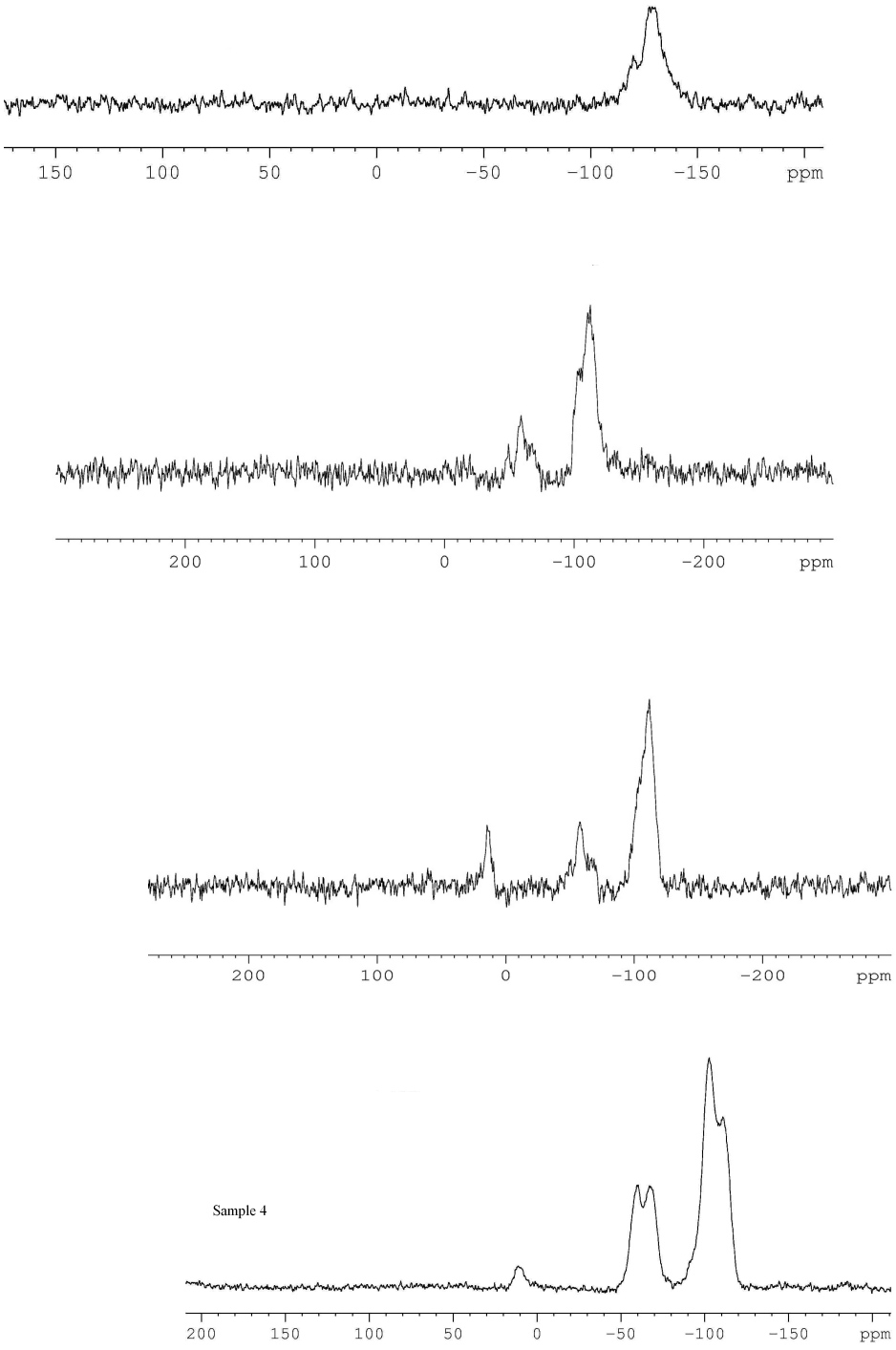

Figure 5. 12 ^{29}Si CP-MAS NMR spectra for sample (1b): dried bimodal Si; sample (2b): N-acyllactam immobilized bimodal Si; sample (3b): capping N-acyllactam BMS; (4): capping N-acyllactam SBA-15

Table 5. 4 ^{13}C CP-MAS NMR chemical shifts for amine immobilized BMS, N-acyllactam immobilized BMS and capping N-acyllactam immobilized BMS

Sample 2		Sample 3		Sample 4	
-Si-CH_2-	9	-Si-CH_2-	9	-Si-CH_2-	9
-Si-CH_2-CH_2-	24	-Si-CH_2-CH_2-	24	-Si-CH_2-CH_2-	24
-CH_2-CH_2-NH_2	43	-CH_2-CH_2-NH_2	43	-CH_2-CH_2-NH_2	43
Aromatic carbons	129	Aromatic carbons	129	Aromatic carbons	129
-CO-N=	160	-CO-N=	160	-CO-N=	160
-CO-NH-	200	-CO-NH-	200	-CO-NH-	200
		-Si-CH_3	0	-Si-CH_3	0

^{13}C CP-MAS NMR spectra were shown in Figure 5.13 for sample (2) amine immobilized BMS; sample (3): N-acyllactam immobilized BMS and sample (4) capping N-acyllactam BMS. The peaks read from the ^{13}C CP-MAS NMR spectra was shown in Table 5.4 which also corresponded to their functional groups. Table 5.4 told that more carbon peaks could be found after more organic groups were grafted onto the surface of silica. Aromatic carbons peak was located at 129 ppm for N-acyllactam immobilized BMS while there was no aromatic carbons peak for amine immobilized BMS.

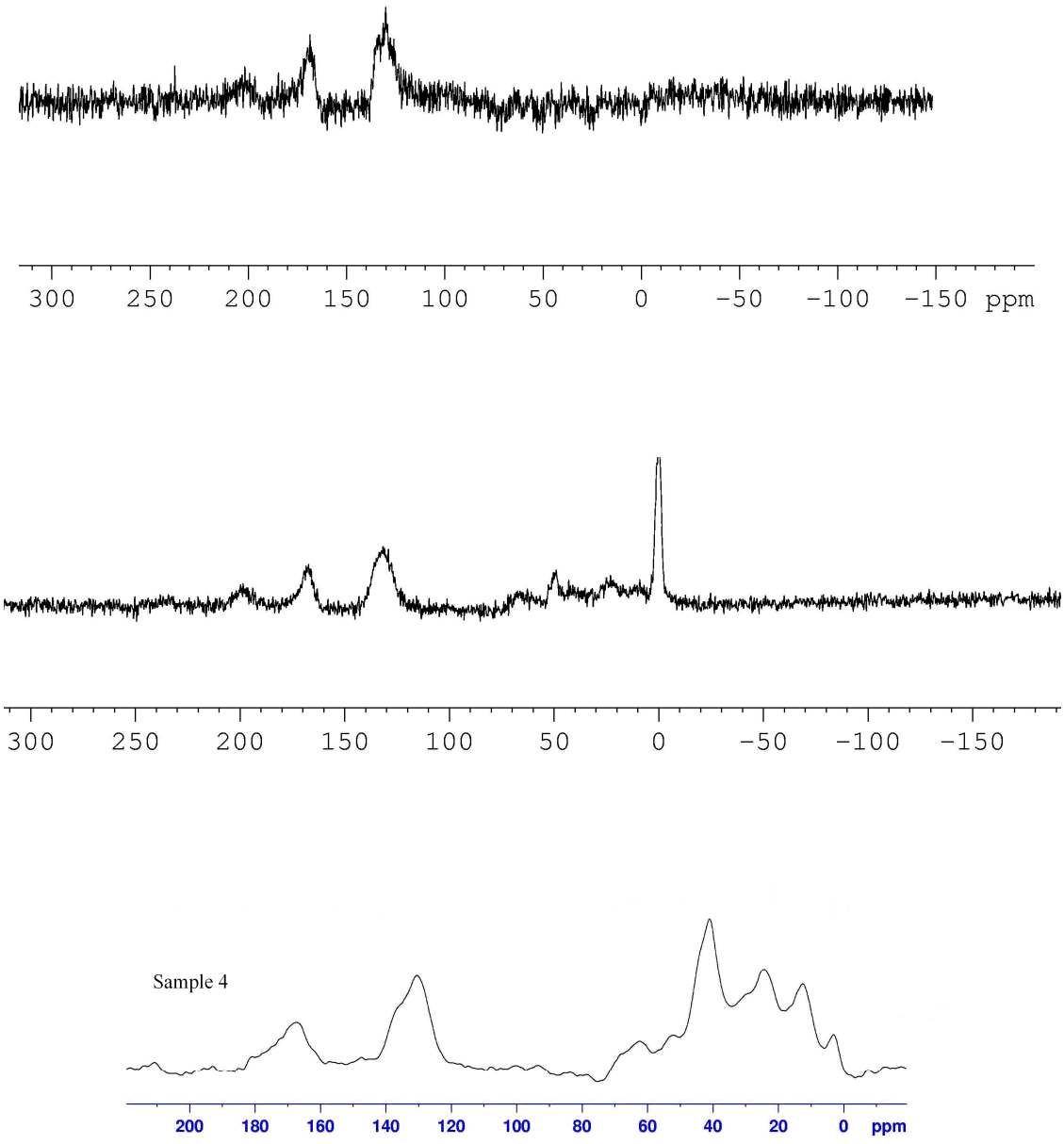

Figure 5. 13 ^{13}C CP-MAS NMR spectra for sample (2b): N-acyllactam immobilized BMS; sample (3b): capping N-acyllactam BMS; (4): capping N-acyllactam SBA-15

5.2.3 Initiating anionic ring-opening polymerization inside the nano-channels and obtained mesoporous silica/nylon-6 nanocomposites

To overcome the difficulties of pushing epsilon-caprolactam into the nano-channels of mesoporous silica, a vacuum step with special controls was used. With the special control steps, 5 mass% of epsilon-caprolactam monomer was distilled under vacuum condition in flask. When the flask was cooled down, a small quantity of anhydrous DMAC was injected into flask with melted epsilon caprolactam monomer. The mixture of DMAC and caprolactam monomer would form solids when flask cooled down to room temperature. N-acyllactam immobilized bimodal mesoporous silica was placed onto the surface of mixture of DMAC and epsilon caprolactam. Flask under vacuum condition of 1 mm Hg was slowly heated until the mixture of DMAC and caprolactam melted. The flask was cooled down and heated for three times under vacuum condition. Finally the cooled mixture was kept under vacuum for 20 mins to get rid of all DMAC. For these special steps, DMAC was added to caprolactam monomer to decrease the viscosity and surface tension of monomer, which would help the monomer to be pushed into nano-channels of mesoporous silica. While the existence of polar organic solvent with monomer would also affect the anionic ring-opening polymerization, the final step of vacuum at room temperature was to get rid of DMAC and avoid the possible side reaction produced from DMAC. This method was verified as a good method to push caprolactam monomer into the nano-channels of mesoporous silica. The mesoporous silica with filled monomer in nano-channels was kept at 140°C, catalyst of magnesium bromide ethyl etherate was injected into the flask and reaction was kept enough time until white solids were obtained. Formic acid was poured into flask and centrifugation was

used to separate nylon 6/BMS nanocomposites from nylon 6/formic solution. FT-IR, SEM and solid NMR were used to characterize synthesized BMS based derivatives and composites.

5.2.3.1 Solid NMR characterization of synthesized BMS and its derivatives

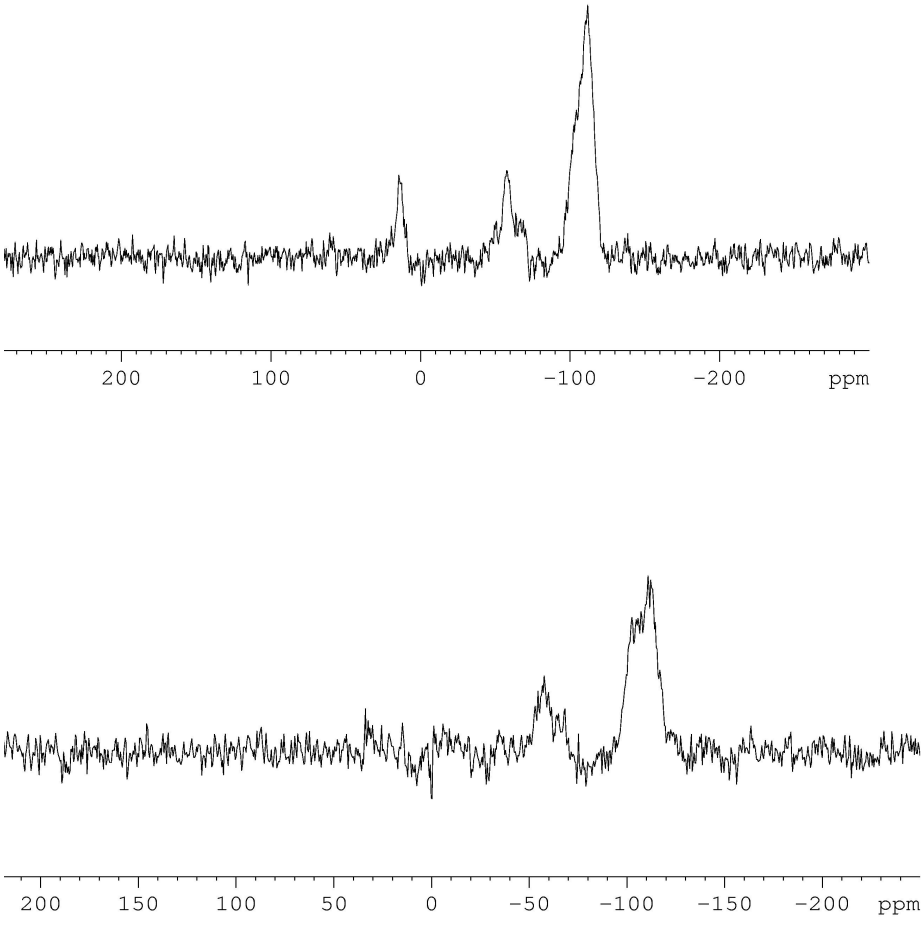

Figure 5. 14 ^{29}Si CP-MAS NMR spectra for sample (3b) capping N-acyllactam BMS; sample (5) synthesized BMS/nylon 6 nanocomposites

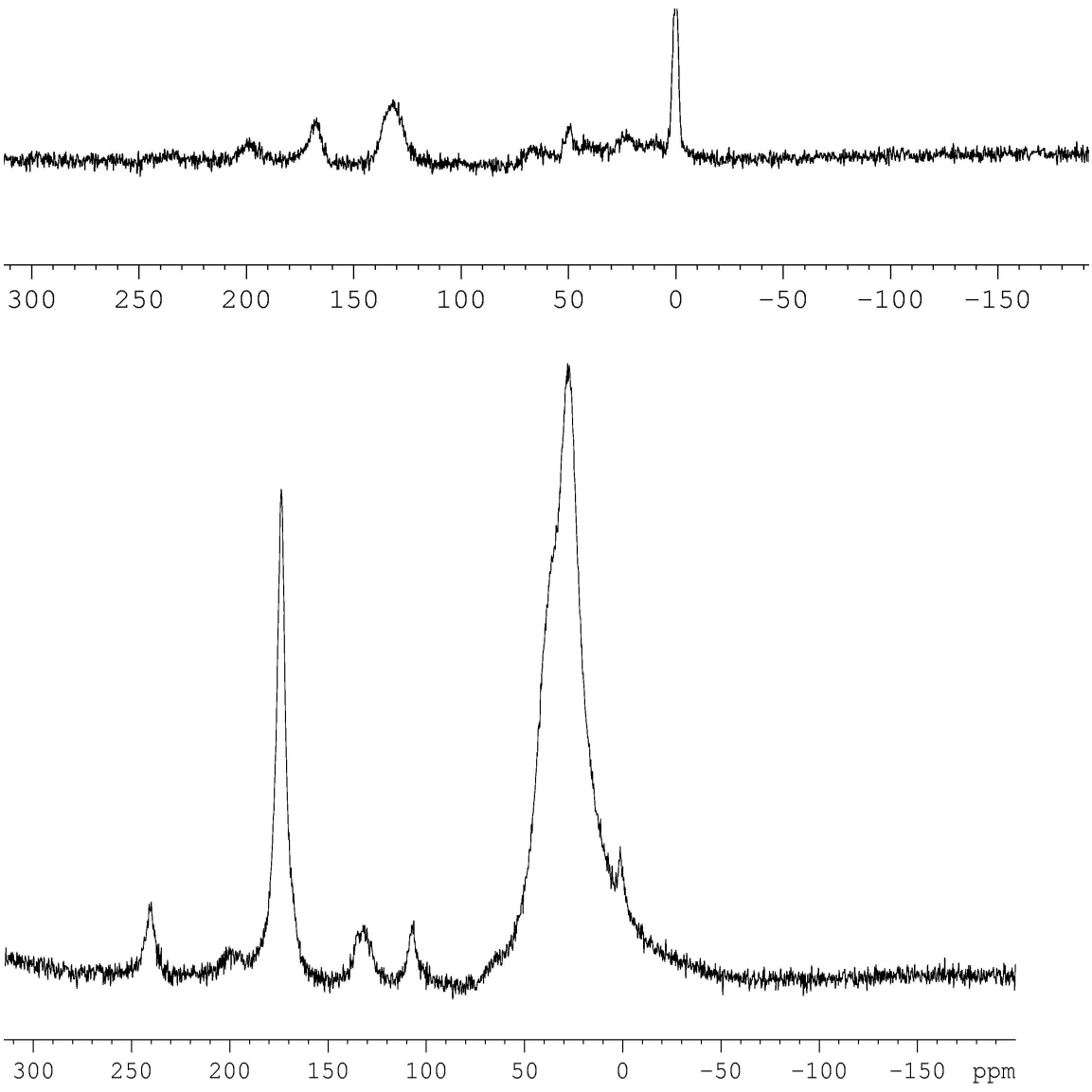

Figure 5. 15 ^{13}C CP-MAS NMR spectra for sample (3b) capping N-acyllactam BMS; sample (5)nylon 6/BMS nanocomposites.

Figure 5.14 showed ^{29}Si CP-MAS NMR spectra for sample (3b) capping N-acyllactam-functionalized-BMS and sample (5) synthesized BMS/nylon 6 nanocomposites. Both ^{29}Si CP-MAS NMR spectra didn't show big difference of peak

position between capping N-acyllactam immobilized BMS and nylon 6/BMS nanocomposites. The nano-channels of mesoporous silica were filled with synthesized nylon which didn't import extra silicon into the synthesized composites after polymerization.

Figure 5.15 showed ^{13}C CP-MAS NMR spectra for for sample (3b) capping N-acyllactam BMS and sample (5)nylon 6/BMS nanocomposites. These two spectra of nylon 6/BMS nanocomposites and capping N-acyllactam immobilized BMS were obviously different. The spectra of nylon 6/BMS nanocomposites showed broad peak with high intensity, and spectra of capping N-acyllactam immobilized BMS showed narrow peak with weak intensity. The nano-channels of mesoporous silica were filled with nylon 6, which were long carbon chains that were characterized with ^{13}C CP-MAS NMR spectra. Peaks from BMS/nylon 6 nanocomposites were shown in ^{13}C NMR (solid state): 6 15.7 (-CH3); 25.7 (-CHzCH3); 27.3 (-COCHZCH2-); 33.8-34.1 (-CH2-); 35.6 (-COCH,-); 41.7 (-$NHCH_2$-); 129 (Aromatic carbons); 172.7 (-CO-); 200 (-CO-NH-). Most of carbon from CH had peak in the range of 0-50ppm. For nylon 6, there was a very broad peak between 0 and 50ppm which meant a large amount of peaks of CH overriding each other. And the peak from carbonyl group (-CO-) was also much stronger than that of capping N-acyllactam immobilized BMS. The comparison of solid ^{13}C NMR spectra showed new synthesized nylon 6 was with supported materials of BMS after anionic ring-opening polymerization.

5.2.3.2 FT-IR characterization of synthesized BMS and its derivatives

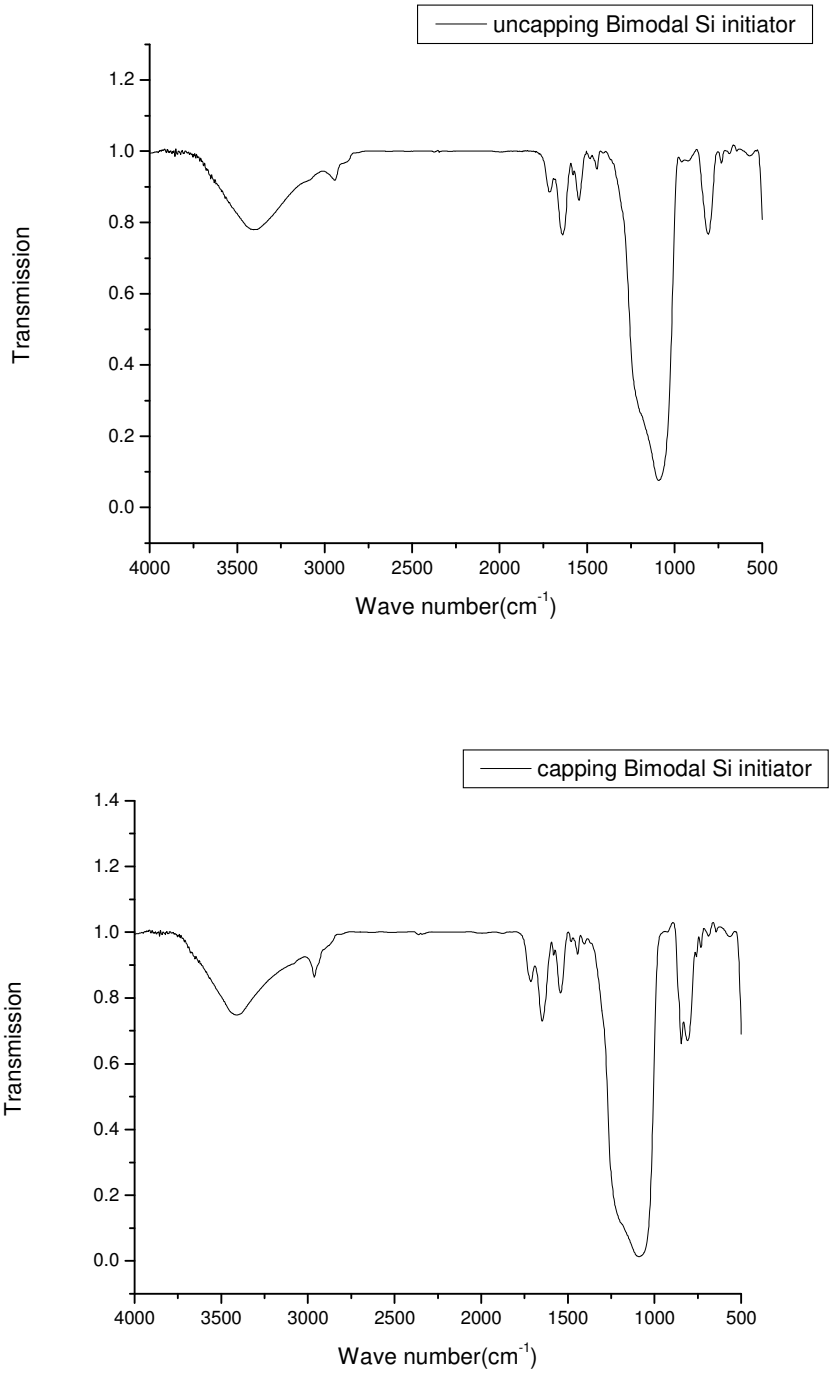

Figure 5. 16 FT-IR spectra of sample (2b): N-acyllactam immobilized BMS; sample (3b): capping N-acyllactam-immobilized-BMS;

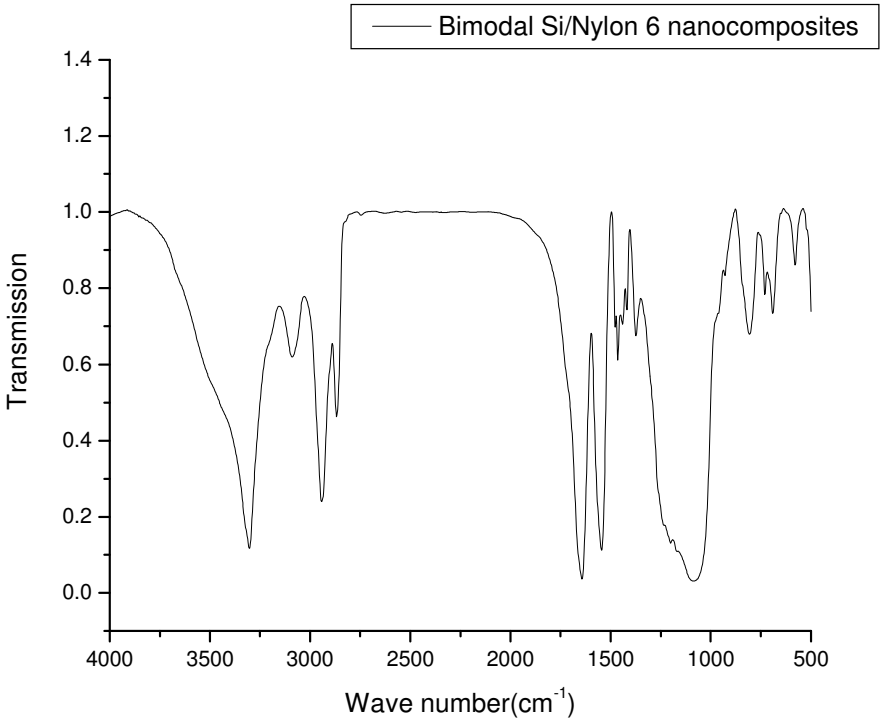

Figure 5. 17 FT-IR spectra of sample sample (5) BMS/nylon 6 nanocomposites.

FT-IR spectra were collected for materials after various steps of N-acyllactam grafting step, silanol capping step and anionic ring-opening polymerization step. Synthesized N-acyllactam-immobilized-BMS was shown in Figure 5.16, characteristic peak of aliphatic CH (2870 cm^{-1}), carbonyl group (1540 cm^{-1}, 1670 cm^{-1}). During silanol capping step, silanol group (-Si-OH) was consumed and trimethylsilazane (-Si-O-$Si(CH_3)_3$) formed. There was no big difference between N-acyllactam-immobilized-BMS and silanol capping N-acyllactam-immobilized-BMS. Figure 5.17 showed FT-IR spectra of nylon 6/BMS nanocomposites which was very similar to the FT-IR spectra of pure

nylon 6. All characteristic peaks of nylon 6 could also be found in Figure 5.17. FT-IR verified nylon 6 was synthesized after polymerization.

5.2.3.3 SEM characterization of synthesized BMS and its derivatives

Scanning electron microscopy (SEM) was a direct method to display the morphologies of mesoporous BMS and its derivatives. Figure 5.18 showed scanning electron microscopy (SEM) images of BMS with different magnifications. Different silica spheres were shown with diameters around 2.5 μ m. Figure 5.19 showed scanning electron microscopy (SEM) images of synthesize BMS/nylon 6 nanocomposites with different magnifications.

From the SEM images, BMS/nylon 6 composites had a different surface with pure BMS. And BMS/nylon 6 spherical particles were highly charged in Figure 5.19. The spherical composites were charged, and it was very difficult to see the detailed surface very clearly with high magnification. And it was also very difficult see the details inside the nano-channels of mesoporous silica. The surface image shown in Figure 5.19 told that the surface of mesoporous silica spheres were covered with a slice of polymer, the diameter of spherical BMS/nylon 6 composites was very close to that of pure spherical BMS. Different surface of spheres with the same diameter told the existence of newly synthesized nylon 6 but the amount of newly synthesized nylon 6 covered on silica surface could be neglected. The SEM image couldn't show the percentage of nylon 6 in BMS/nylon 6 composites. The detailed percentage of nylon 6 synthesized in the nano-channels should be calculated according to TGA experimental data.

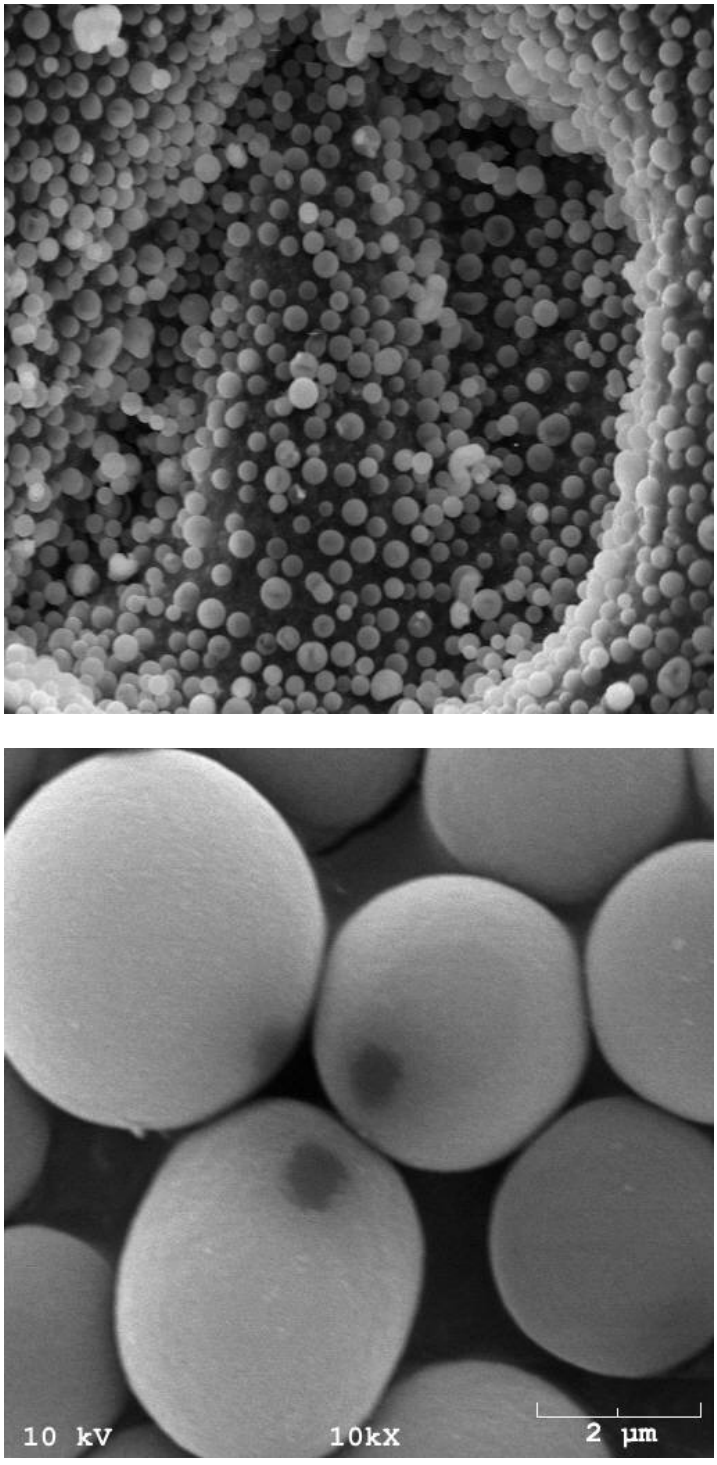

Figure 5. 18 Scanning electron microscopy(SEM) images of BMS with different magnifications.

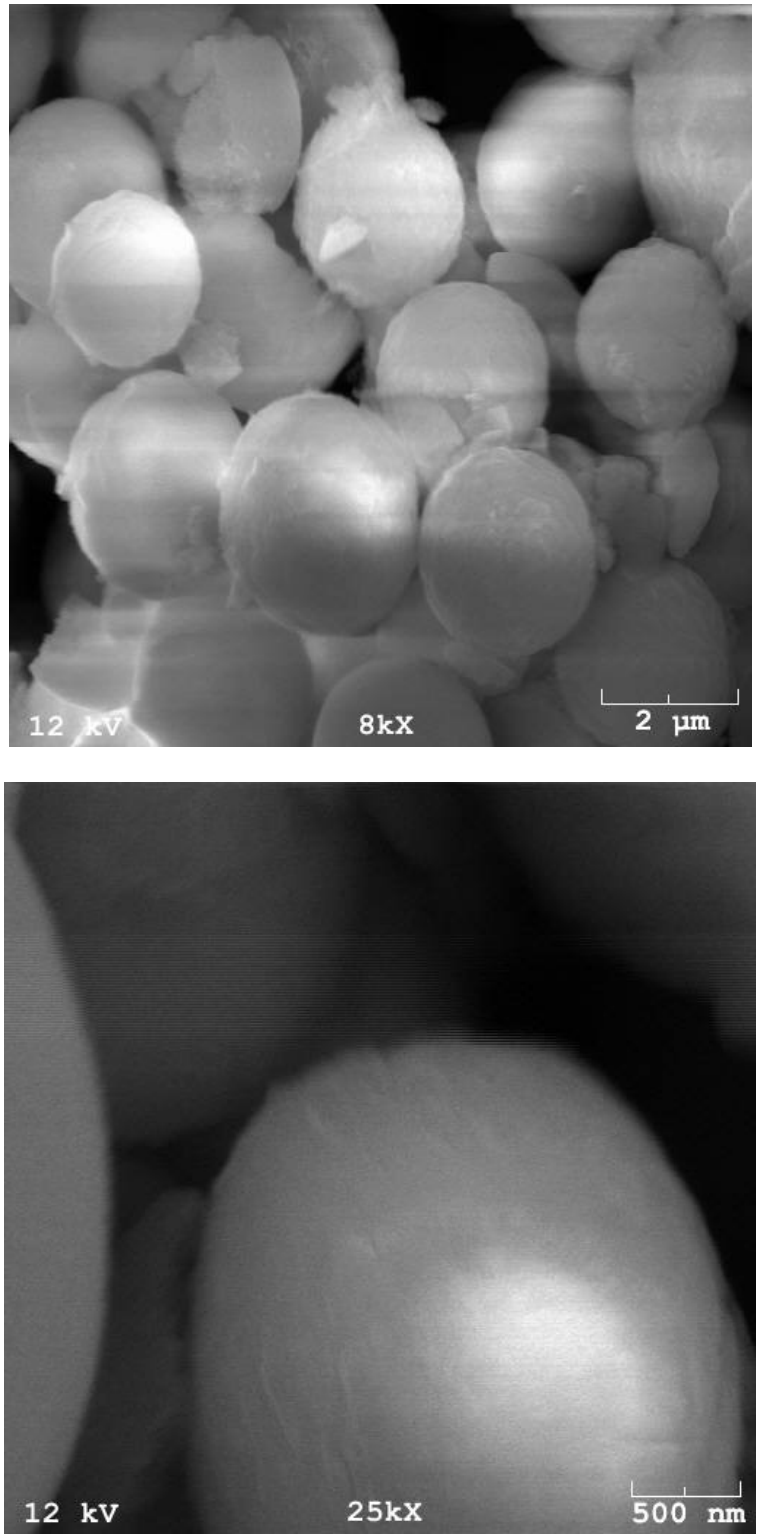

Figure 5. 19 Scanning electron microscopy(SEM) images of synthesize nylon 6/BMS nanocomposites after repeatedly washed with formic acid with different magnifications.

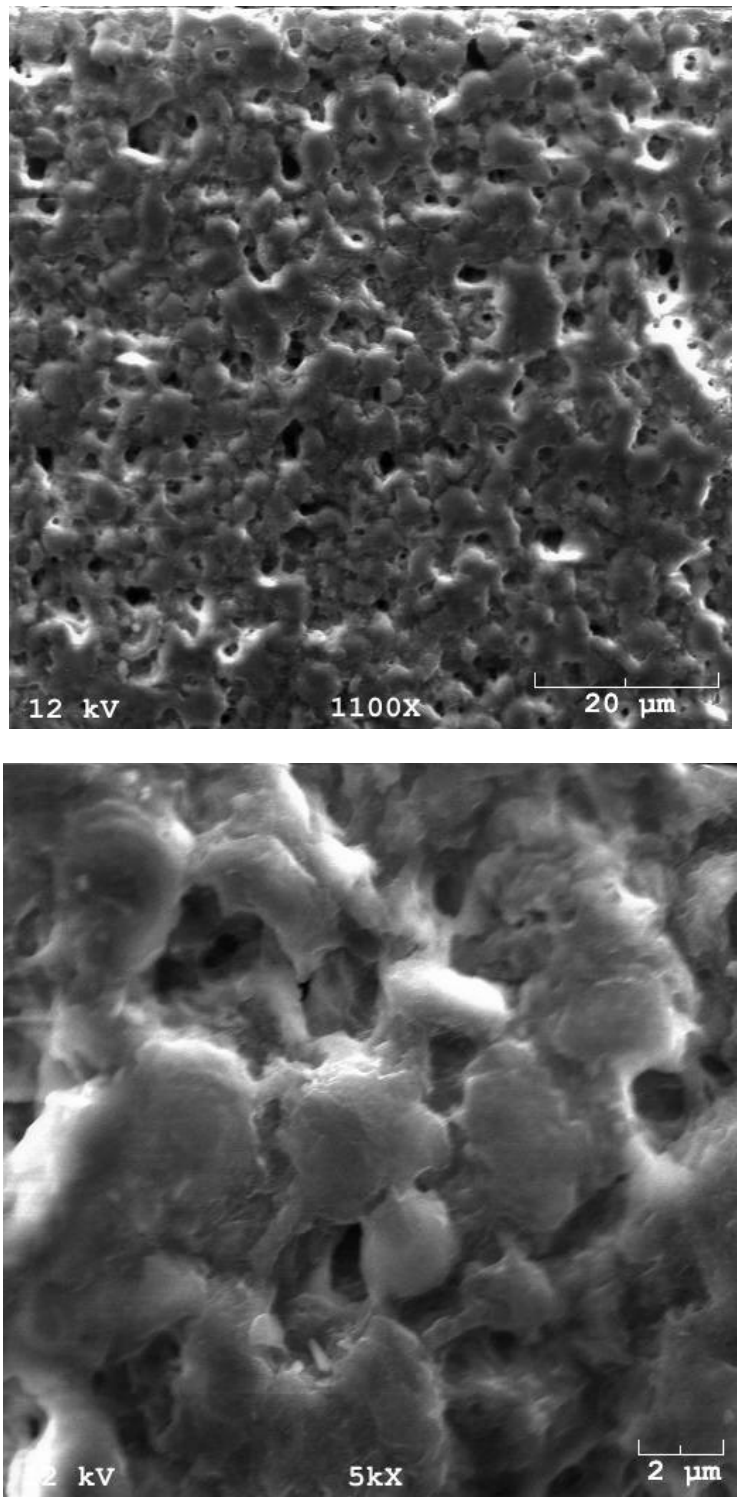

Figure 5. 20 Scanning electron microscopy(SEM) images of synthesize nylon 6/BMS nanocomposites film before free nylon was washed out with different magnifications.

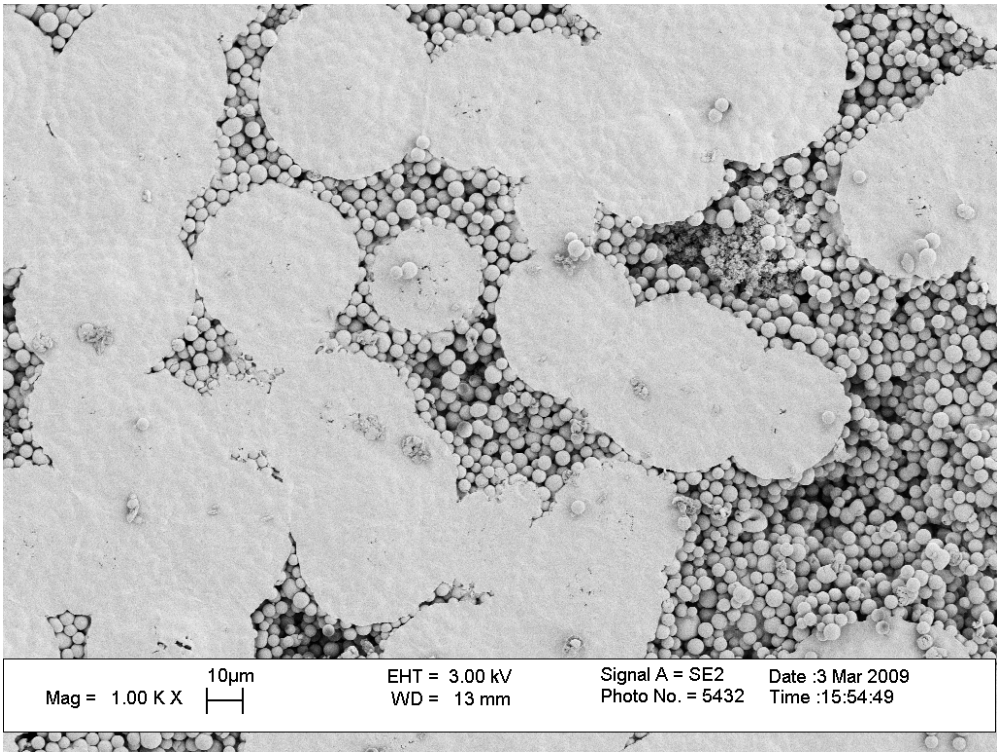

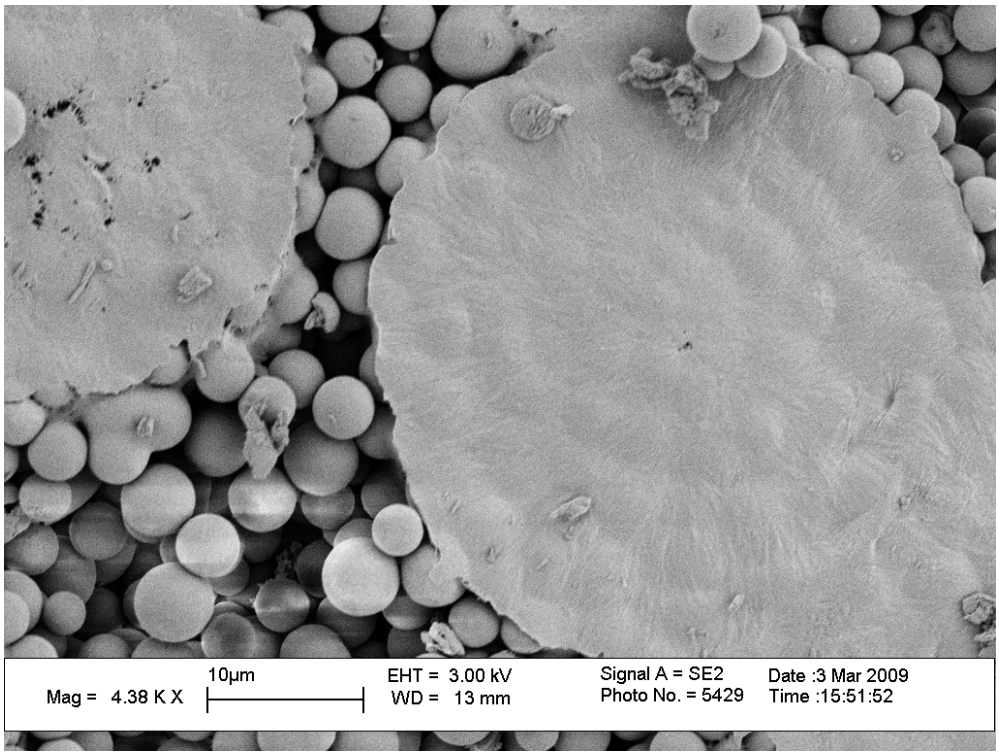

Figure 5. 21 Scanning electron microscopy (SEM) images of physical blending of nylon 6/BMS composites film

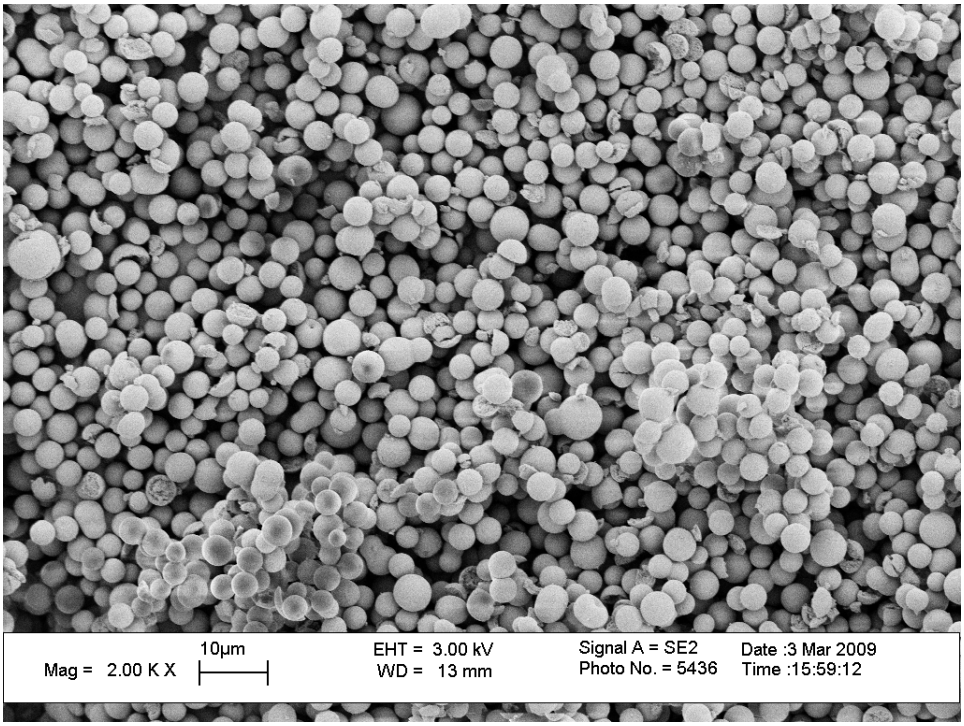

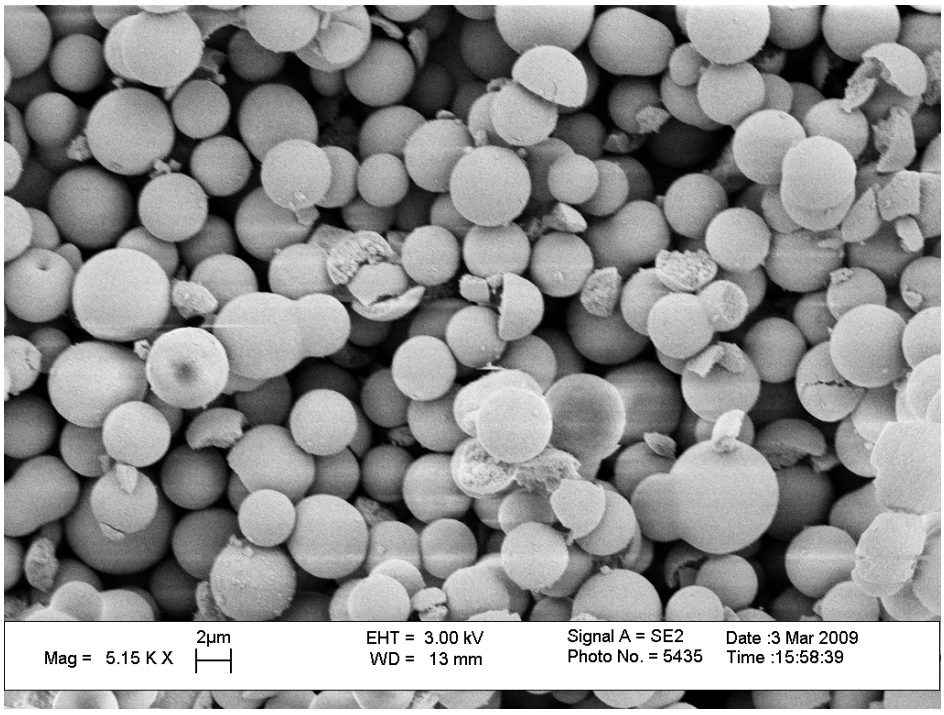

Figure 5. 22 Scanning electron microscopy (SEM) images BMS obtained from physical blending of nylon 6/BMS nanocomposites repeatedly washed with formic acid

When anionic ring-opening polymerization was completed, some synthesizing nylon 6 had no covalent bonds with surface of mesoporous silica. The mixture of composites and free polymer were dissolved in formic acid to form a homogeneous solution. It was easy to make a thin film of synthesized BMS/nylon 6 composites using a knife on the surface of glass.

Figure 5.20 showed scanning electron microscopy (SEM) images of synthesize BMS/nylon 6 nanocomposites film before free nylon 6 was washed out using formic acid. All three SEM pictures clearly showed polymers covered on the surface of BMS and polymers filled the gaps between the silica spheres. SEM image also showed some holes inside the films. The SEM pictures showed a significant amount of nylon 6 was synthesized outside of the nano-channels, and this newly synthesized nylon 6 could be washed out using formic acid. We could conclude that these synthesized nylon 6 on silica surface and between silica spheres had no covalent bonds with silica surface. The reason was probably that initiator of N-acyllactam initiated the ring-opening polymerization inside the nano-channels, but living chains propagated and grew out of the channels and formed new living chains after chain transferring. All epsilon-caprolactam monomer were polymerized to nylon 6 inside the nano-channels and outside of nano-channels.

Figure 5.20 also showed that BMS were well distributed in synthesized nylon 6 for the thin film. To get direct comparison of synthesized BMS/nylon 6 and physical blending of BMS/nylon 6, we made thin films of physical blending of BMS and commercial available nylon 6. We mixed BMS and commercial nylon 6 in formic acid with stirring over 12 hours, and thin film was made with the same method as the previous synthesized BMS/nylon 6 composites films. Scanning electron microscopy (SEM) image

of physical blending of nylon 6/BMS composites film (Figure 5.21) showed nylon 6 was phase separated with BMS. There was a very poor connection between BMS and nylon 6, and nylon 6 covered on a lot of silica spheres while the gaps between BMS couldn't be filled with nylon 6. We could conclude that our method could produce homogeneous BMS/nylon 6 composites, while physical blending of BMS and nylon 6 could only produce a phase separated BMS/nylon 6 composites.

The physical blending of BMS/nylon 6 composites was repeated washed with formic acid and centrifugation was used to separate BMS from the solution. The scanning electron microscopy (SEM) images (Figure 5.22) of obtained BMS showed only BMS spheres and all nylon 6 was washed out. There was no nylon 6 covering on BMS surface or filling the gaps between BMS. And shown silica surface was the same as pure BMS, which told us free nylon 6 couldn't be totally washed out using formic acid. Figure 5.22 could also verify that BMS were covered with a thin film of nylon 6 after polymerization shown in Figure 5.19.

5.2.3.4 Thermal analysis of BMS based derivatives

Thermogravimetric analysis (TGA) was used to test the thermal decomposition point of BMS/nylon 6 nanocompoistes, and the amount of organic loading could also be calculated through collecting the mass loss between 200°C and 650°C. Figure 5.21 showed TGA graph of dried bimodal mesoporous silica. The sample of bimodal mesoporous silica was placed in vacuum oven at 150°C overnight before it was run on TGA experiments. The mass loss between 200°C and 650°C was only 0.267% which meant the mass loss could be neglected. For pure BMS, the mass loss at high temperature

was considered from the loss of silanol groups. When pure BMS was placed in vacuum oven over 12 hours, all moisture inside the nano-channels could be removed from the TGA calculation. When the further organic loading was calculated, we assumed there was no mass loss for pure dried bimodal mesoporous silica.

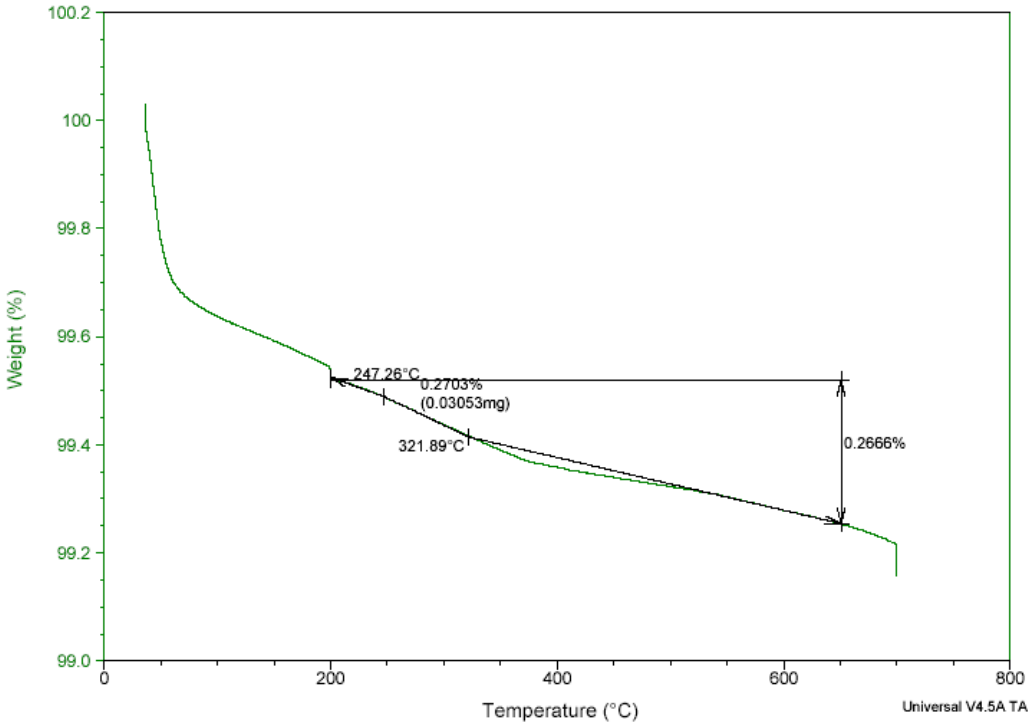

Figure 5. 23 TGA graph of dried bimodal mesoporous silica

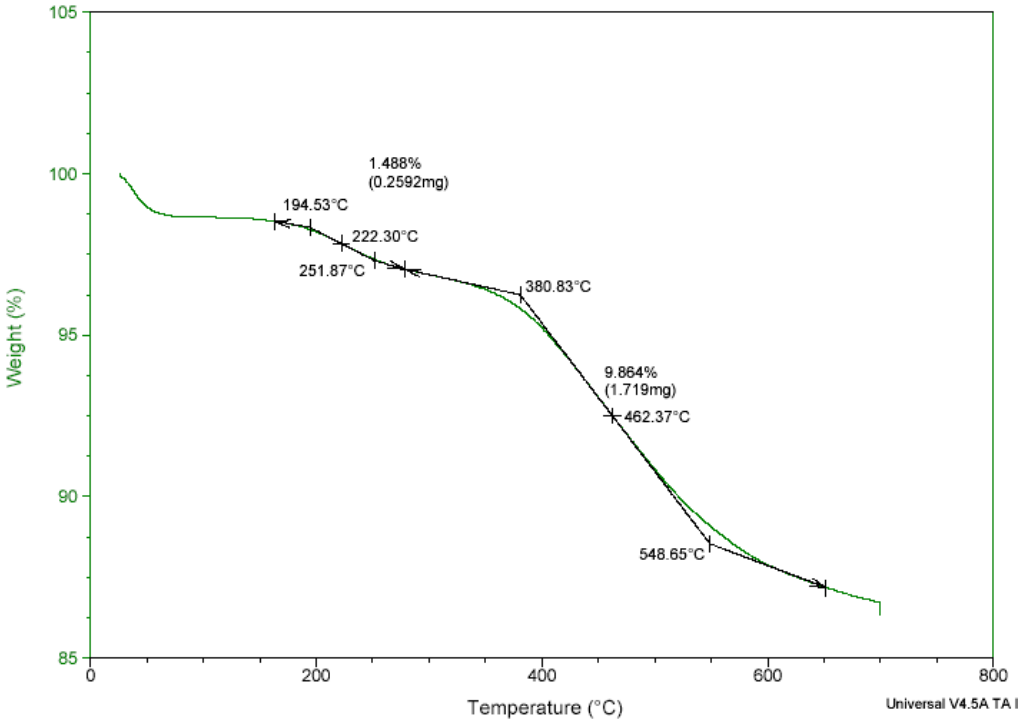

Figure 5. 24 TGA graph of uncapping N-Acyllactam immobilized BMS

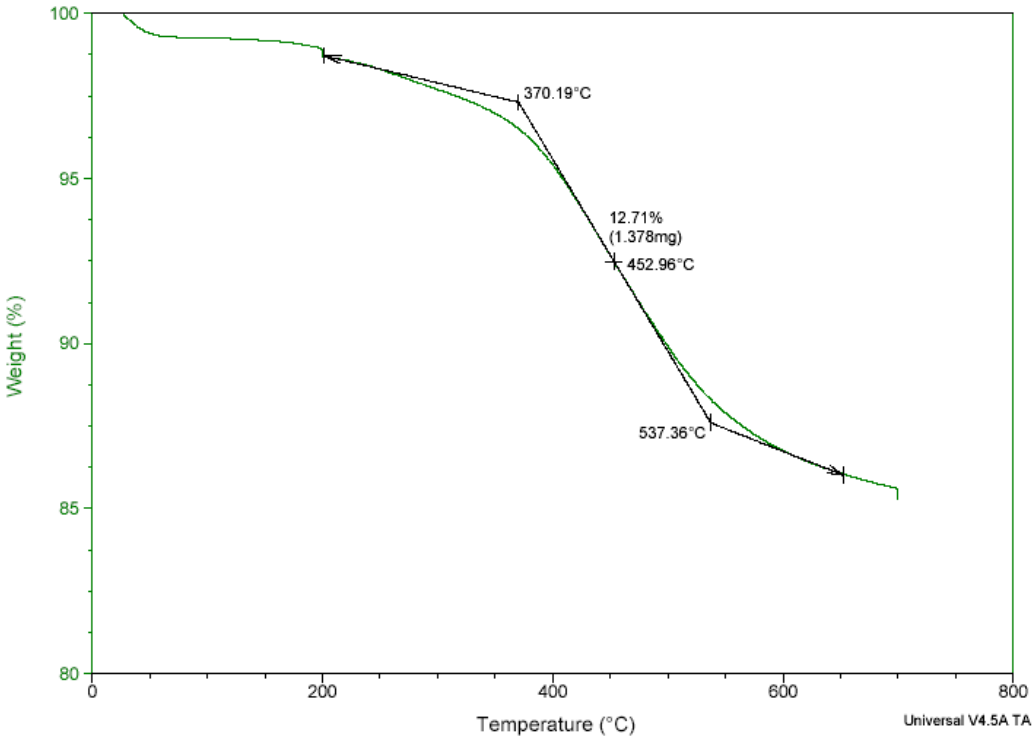

Figure 5. 25 TGA graph of capping N-acyllactam immobilized BMS

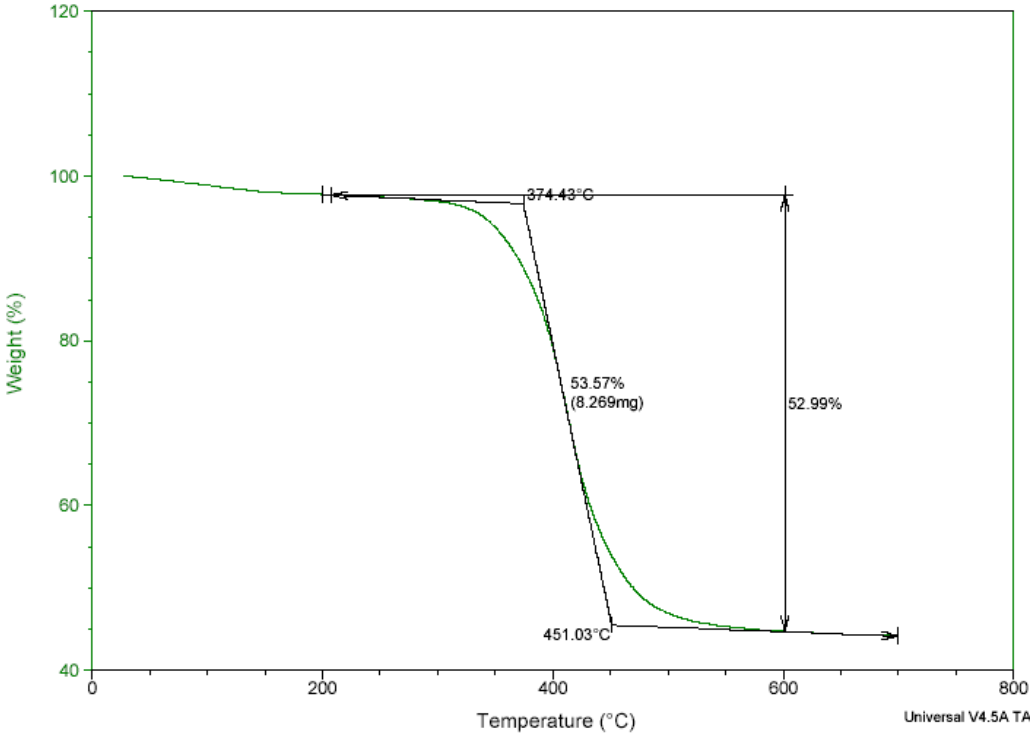

Figure 5. 26 TGA graph of synthesized nylon 6/BMS nanocomposites

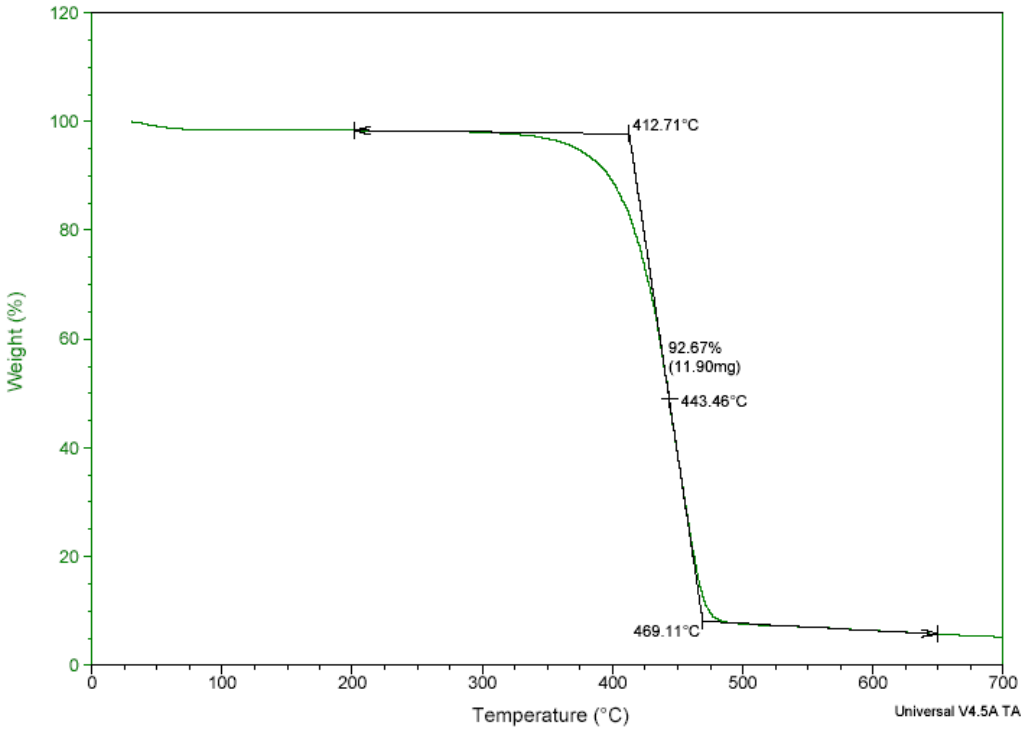

Figure 5. 27 TGA graph of synthesized free nylon 6 without covalent bond with BMS

Figure 5.24 showed TGA graph of uncapping N-Acyllactam immobilized BMS which showed two stages of decomposition. The first stage of decomposition began at 195°C and ended at 252°C, and the second stage of decomposition began at 381°C and ended at 549°C. The total mass loss was 16.91%. The organic loading was determined by assuming two methoxyl linkages to silica surface after N-acyllactam was grafting onto the suface of BMS. The organic loading of the initiator group of N-acyllactam was 0.65 mmol N-acyllactam/g uncapping N-acyllactam immobilized BMS. In other words, 1 gram of pure dried BMS could load 0.78 mmol of N-acyllactam group on the surface of BMS. With the previous experiments which showed 1 gram of pure dried BMS could load as much as 2.1 mmol of amine groups. Because of the steric effects of long chain initiator molecule, only very few amount of silanol groups could be loaded with initiator molecule. And a large amount of silanol groups should be removed with a step of capping procedure with HMDS.

Figure 5.25 showed TGA of capping N-acyllactam immobilized BMS which showed only one stage of decomposition, which was different from the decomposition of uncapping N-acyllactam immobilized BMS which showed two stages of decomposition. The stage of decomposition began at 370°C and ended at 537°C. The whole mass loss was 12.71%. It was a little confusing that capping N-acyllactam immobilized BMS had a less mass loss than uncapping N-acyllactam although more organic groups were grafted on silica surface during silanol capping step. The reason was explained as following: silanol groups were transferred to trimethylsilazane groups during capping step, and trimethylsilazane groups would be transferred back to new silanol groups when the capping composites was calcinated at high temperature. This meant one more silicon

atom (Si) with three silanol groups (OH) replaced a silanol group (OH). Through the capping step, more mass which couldn't be calcinated was grafted on the surface of silica which would decrease the calcinated mass during TGA experiments. Assuming all silanol groups were replaced with trimethylsilazane groups ($-Si(CH)_3$) which would be calcinated to silanol groups($-Si(OH)_3$) at high temperature. With the calculation (0.1691/0.1271-1), 1 gram of uncapping N-acyllactam immobilized BMS had approximately 4.5mmol unreacted silanol groups which reacted with HMDS during the capping step. With the assumption, one gram of BMS had 6.02 mmol silanol groups, of which only 12.6% was grafted with initiator functional groups of N-acyllactam. While 87.4% of silanol groups should be transferred to trimethylsilazane groups during the capping step. Even surplus APTMS was used to graft amine on surface of BMS, only about one third of silanol groups could be transferred to amine groups. With the calculation, the capping step was very necessary to get rid of silanol groups which would terminate the anionic ring-opening polymerization of epsilon-caprolactam. There was only one stage of decomposition for capping N-acyllactam immobilized BMS after all silanol groups were transferred to trimethylsilazane groups, we could tell the reason of the first stage of decomposition of uncapping N-acyllactam immobilized BMS was produce by left silanol groups on silica surface.

TGA graph of synthesized nylon 6/BMS nanocomposites (Figure 5.26) showed 53 wt% of the composites was calcinated between 200 and 650°C. The composites began to decompose at 374°C and finished decomposition at 451°C. From the SEM pictures, the diameters of spherical BMS didn't change before and after polymerization, we could assume that all nylon 6 formed inside the nano-channels and the amount of nylon 6

covered on BMS surface was neglected. With the previous weight loss of 12.71% organic loading and assuming the extra mass loss from the newly synthesized nylon 6, the calculation showed that one gram of capping N-acyllactam immobilized BMS was filled with approximately 0.873g of new synthesized nylon 6. The synthesized nylon 6 was crystalline nylon 6 which was shown in Figure 5.29. Assuming the density of crystalline nylon was 1.23g/cm^3, the volume of 0.873g of nylon 6 would be 0.71 cm^3. Assuming all the initiator functional groups grafted on the surface of BMS initiated polymerization and formed polymer chain, the calculated molecular weight of synthesized nylon 6 should be 1340g/mol. In real case, only few amount of initiator could initiate the polymerization, so the calculated molecular weight should be much less than the real molecular weight.

When the synthesized BMS/nylon6 composites were placed in the solution of hydrofluoric acid, the silica network was dissolved in the solution, and the synthesized nylon 6 inside the nano-channels was also dissolved in hydrofluoric acid. The hydrogen bond of nylon 6 was destroyed by hydrofluoric acid, and nylon 6 inside nano-channels couldn't form large spheres like PMMA spheres in previous chapter because nylon 6 covered on BMS was neglected. At current moment, we couldn't find a good method to directly characterize the molecular weight of synthesized nylon 6. So 1 gram of capping N-Acyllactam immobilized BMS could produce 0.873g nylon 6 which filled 0.71 cm^3 nano-channels according to the calculation based on assumptions.

For comparison, we also collected the nylon 6 which was synthesized during the polymerization but without covalent bond with the surface of mesoporous silica. TGA graph of those nylon 6 (Figure 5.27) showed that the free nylon 6 began decomposition at 412°C and finished decomposition at 469°C. We found that the decomposition

temperature of free nylon 6 was almost 40°C higher than the synthesized BMS/nylon 6 composites. For nylon6/BMS composites, the decomposition temperature was 374°C which was very close to the decomposition temperature of capping N-acyllactam immobilized BMS. The reason was that the calcinated organic loadings of composites included both synthesized nylon 6 and other organic functional groups which were grafted on silica surface during initiator grafting step and silanol capping step.

For the effect of hydrogen bonding, the decomposition temperature of nylon 6 was much higher that those organics with short carbon chain like methyl groups. Therefore, the decomposition temperature of collected nylon 6 without covalent bonds with silica surface was much higher than that of nylon 6/BMS composites. And the total weight of collected free nylon between 200°C and 650°C was about 93 wt% which was 7 percent smaller than 100%. There was 2 wt% loss before 200°C, and 5 wt% residues after 650°C which came from the catalysts of magnesium and very few amount of broken BMS which couldn't be separated.

The same procedures of synthesizing nylon 6/BMS nanocomposites was taken at different time, the experimental result would also be a little different. Figure 5.28 showed TGA graph of different synthesized nylon 6/BMS nanocomposites. This figure showed a different decomposition temperature and mass loss with the previous composites (Figure 5.26). But the difference was very small.

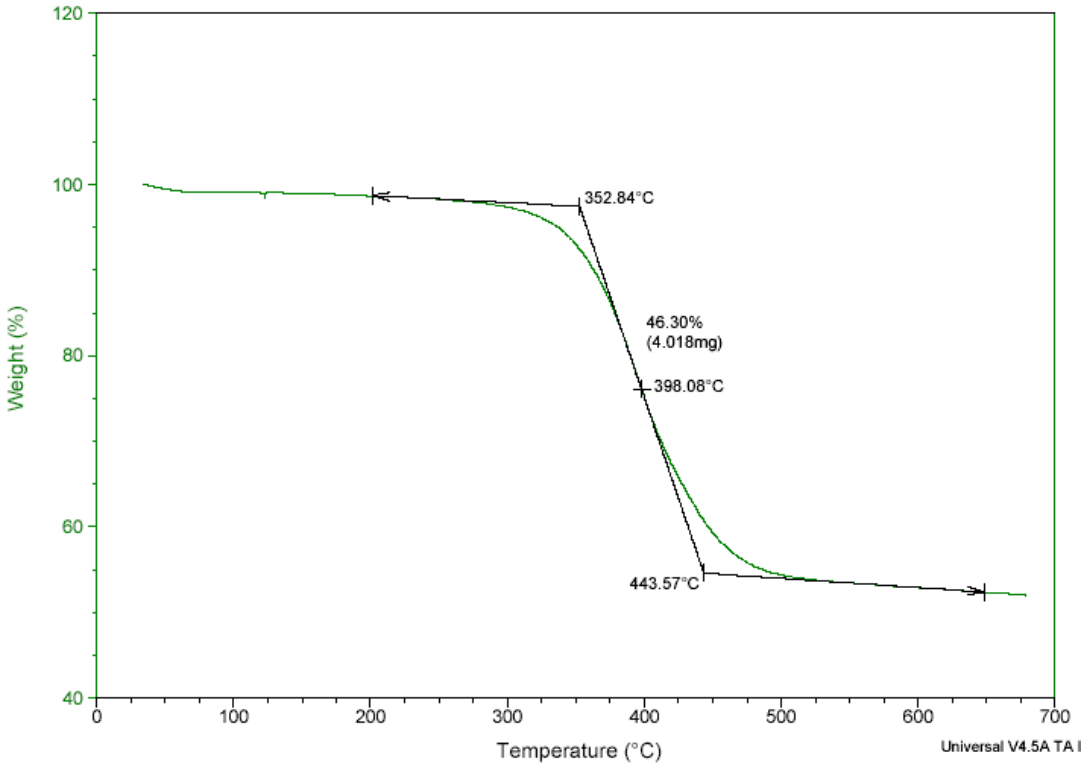

Figure 5. 28 TGA graph of synthesized nylon 6/BMS nanocomposites

Differential Scanning Calorimetry (DSC) was used to characterize the crystal behavior of synthesized nylon 6. Figure 5.29 showed DSC of synthesized nylon 6/BMS nanocomposites. This figure showed the glass transition temperature of the composites was 46°C, and melting temperature was 213°C. The enthalpy during the melting region is 20.31 J/g composites. Only 46.6 mass% of the composites was nylon 6 which produced the crystal enthalpy, the transferred enthalpy for nylon 6 inside the nano-channels was 43.58 J/g nano-channels filled nylon 6. We also collected the synthesized nylon 6 without covalent bond with the surface of mesoporous silica which was run on DSC for comparison. DSC of obtained nylon 6 without covalent bonds with silica surface (Figure

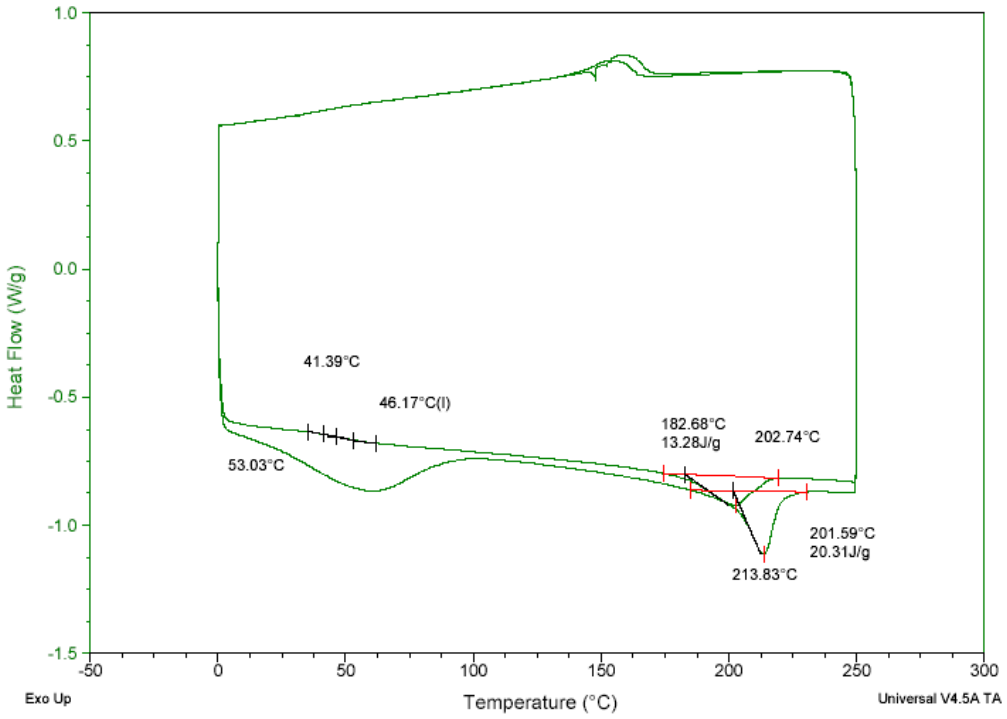

Figure 5. 29 DSC of synthesized nylon 6/BMS nanocomposites

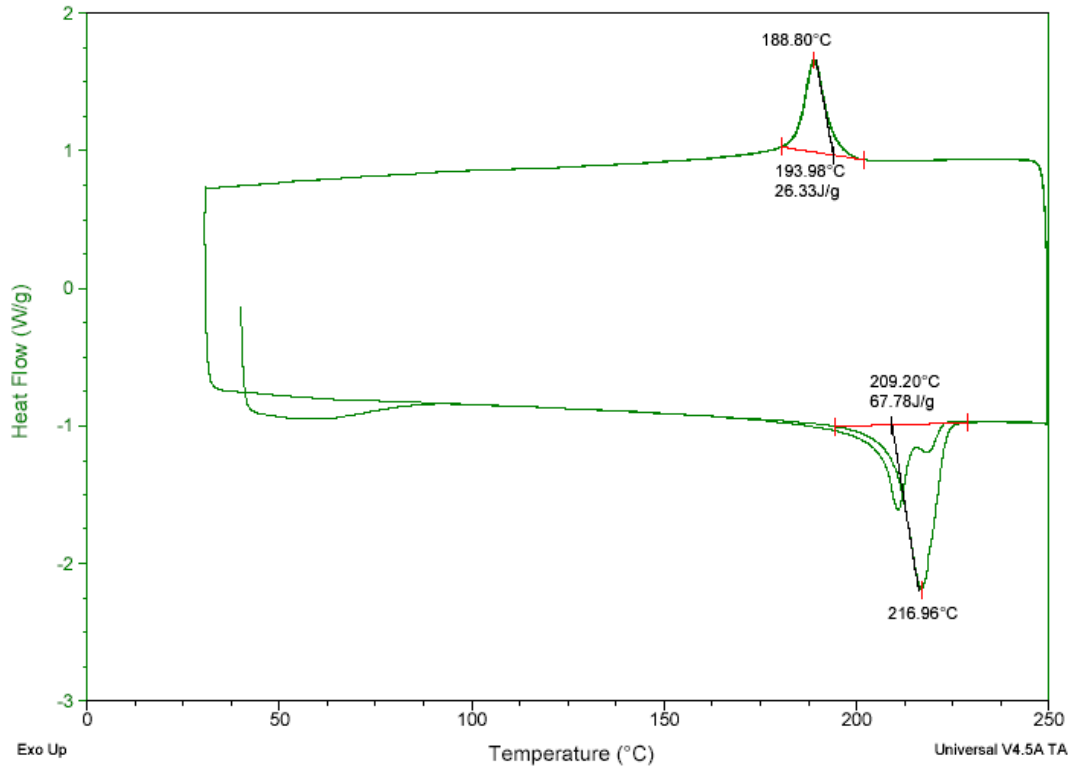

Figure 5. 30 DSC of synthesized nylon 6 without covalent bonds with BMS

5.30) showed melting temperature of 217 °C and enthalpy of 67.8 J/g nylon 6. Both two values were higher than previous data of nano-channel filled nylon 6. The properties of nylon 6 in literature showed a glass temperature of 47°C and a melting temperature of 220°C which were the same as the data we obtained in our test. This result told us the synthesized nylon 6 inside the nano-channels showed the same thermal behavior as those synthesized nylon 6 outside of the nano-channels and commercial nylon 6. And the data also helped to prove that the materials inside the nano-channels were synthesized nylon 6 which was not epsilon-caprolactam salt which was produced with our first designed procedures.

5.2.3.4 XRD characterization of synthesized BMS and its derivatives

To better characterize the BMS/nylon 6 composites, wide angle X-ray diffraction (WXRD) was further used to characterize the polymer crystals. Literature shows[55,56,57,58] crystallization temperature and time could change the crystal formation of the α-form versus γ-form. Three investigations showed that crystallization for extend periods of time below 130°C leaded only γ-form crystallites while above 190°C leaded only α-form crystallites, and mixture of the two form crystallites would be formed if temperature was between 130°C and 190°C. These two form crystallites were widely studied using WXRD. α-form crystallite was monoclinic crystal structure[59,60,61,62,63,64] with lattice constants of a=0.956nm, b=1.724nm, c=0.801nm, β=67.5º and characteristic d-spacings of d_{200}≈0.370nm, $d_{002+202}$≈0.44nm. γ-form crystallite was hexagonal/pseudohexagonal crystal structure with lattice constants of a=0.472nm, b=1.688nm, γ=120º.

Wide angle X-ray diffraction pattern of nylon 6 outside nano-channels we synthesized (Figure 5.31) showed three 2θ locations occurring at approximately 2θ=20.08 º, 20.4 º and 24.2 º. The 2θ locations of 2θ=20.08 ºand 24.2 º corresponding to α-form crystallite and location of 20.4 º corresponding to amorphous peak. The 2θ locations of 20.08 had characteristic d-spacing of $d_{002+202}$≈0.44nm, and angle of 24.2 º was corresponding to d_{200}≈0.370nm. The crystallinity was approximately 53.9% according to the calculation of area. This nylon 6 had no covalent bond with the surface of mesoporous silica, it crystallized when its formic acid solution was poured into water.

Wide angle X-ray diffraction pattern of synthesized nylon 6/BMS composites (Figure 5.32) showed four 2θ locations occurring at approximately 2θ=20.0 º, 20.5 º, 21.7 º and 24.0 º. Compared with Figure 5.31, Figure 5.32 had one more peak occurring at 2θ=21.7 º which had a d-spacing of d_{001}≈0.41nm, which represented the characteristic d-spacing of γ-form crystallites. For the nylon 6/BMS composites, there were two different crystallites of α-form crystallite and γ-form crystallite inside the nano-channels of mesoporous silica. According to the calculation of ratio of area of peak, the total crystallinity was 19.5%, of which there was 16.2% α-form crystallites and 3.3% γ-form crystallites. But we have some problems in the calculation based on the characterization. Nylon 6 inside the nano-channels couldn't be separated from mesoporous silica, and XRD result was based on the composites. Whether the new peak of γ-form crystallite coming from silica was not proved here. But we couldn't obtain this new peak when we tried to add data of pure silica with data of pure nylon 6. And this crystallinity didn't reflect the real case because of the existence of silica. The real crystallinity should be larger than this calculation.

The BMS/nylon 6 composites we synthesized were poured to formic acid with other synthesized nylon 6 without covalent bonds with silica surface. Nylon 6 inside the nano-channels of mesoporous silica couldn't be dissolved in formic acid because of the covalent bond connection between the polymer and the surface of inner-wall. The nylon 6 inside the nano-channels included two different crystallites of α-form crystallite and γ-form crystallite at the synthesized temperature of 140°C. The existence of mesoporous silica which had a characteristic peak at 2θ=22 °, which affected on the shape and strength of the peaks of crystallites. Here, the peak of α-form crystallite inside the nano-channels was slightly lower than that of pure nylon 6 while the amorphous peak was slightly higher. To get rid of the influence of mesoporous silica, the strength of pure BMS was used as background which was subtracted with the intensity of BMS/nylon 6 composites through AreaMax software. The derived XRD figure was shown in Figure 5.33. Figure 5.33 couldn't be simulated using software MDI like other XRD spectra. And the background signal of silica wouldn't be the same as this in composites, this Figure 5.33 only showed us a direct image and we couldn't obtain correct crystallinity.

We also obtained the X-ray diffraction pattern of commercial nylon 6 from Aldrich (Figure 5.34) which showed a very similar pattern with nylon 6(Figure 5.31) we synthesized. There were three peaks occurring at 2θ=20.02 °, 20.04 ° and 24.2 ° which represented the positions of α-form crystallite nylon 6 and amorphous nylon 6. The overall crystallinity was approximately 47%, and the residual error of fit was 2.54%. This meant the commercial nylon 6 from Sigma-Aldrich contained only α-form crystallites. This XRD results verified the existence of crystalline nylon 6, and it also characterized

the crystallinity of polymers and characterized the form of crystal for synthesized nylon 6 inside the nano-channels of mesoporous silica.

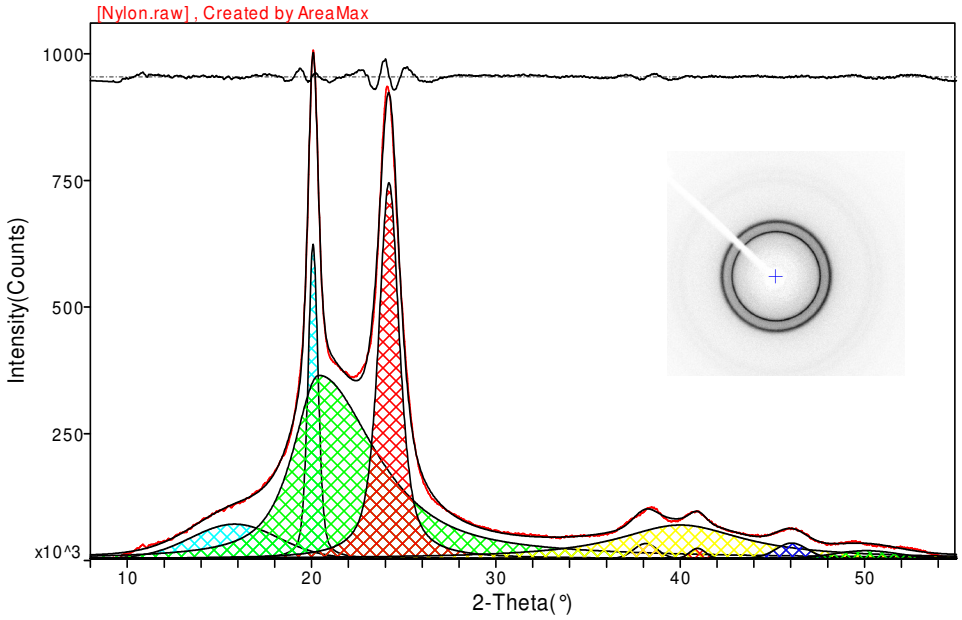

Figure 5. 31 X-ray diffraction pattern of synthesized nylon 6 separated from solution

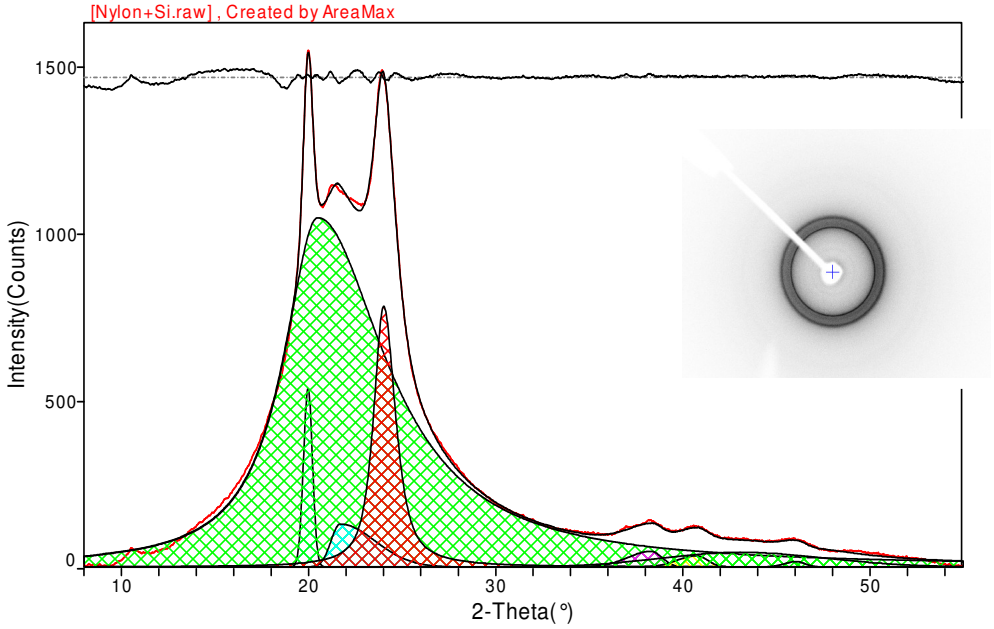

Figure 5. 32 X-ray diffraction pattern of synthesized nylon 6/BMS composites

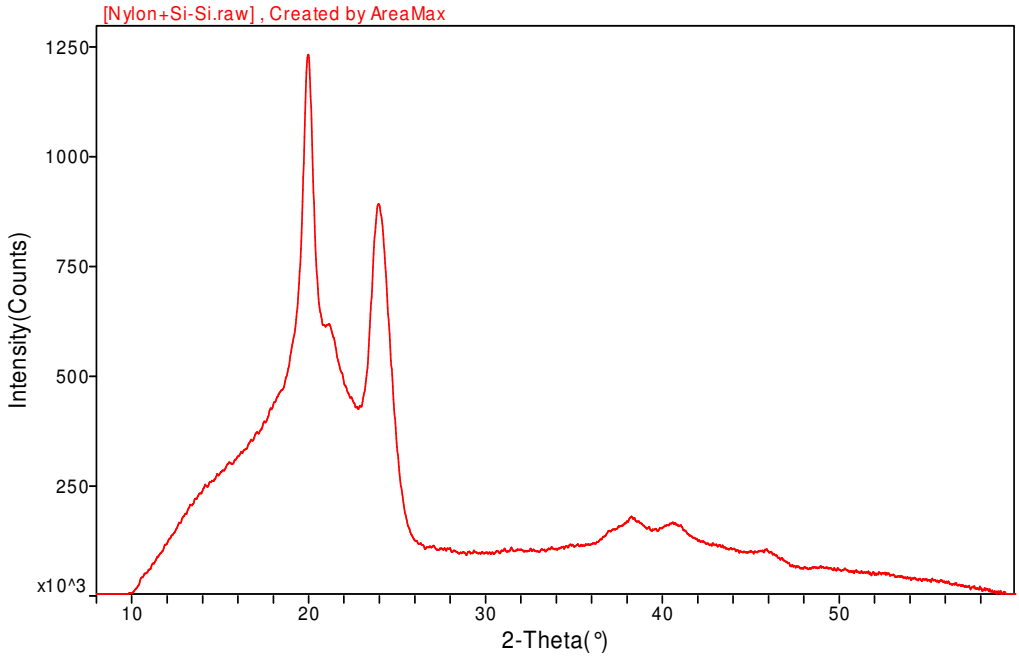

Figure 5. 33 X-ray diffraction pattern of nylon 6/BMS composites after spectra subtracted spectra of pure BMS

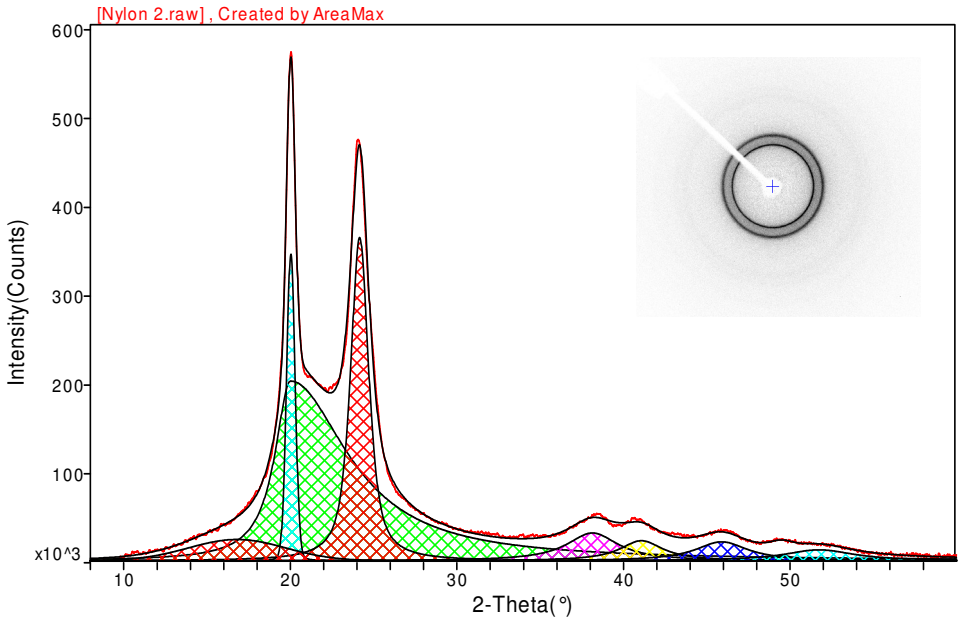

Figure 5. 34 X-ray diffraction pattern of commercial nylon 6 from Aldrich

5.3 Conclusion

In this chapter, two different procedures were designed to initiate the anionic ring-opening polymerization inside the nano-channels of mesoporous silica BMS to synthesize nylon 6/BMS nanocomposites. For procedure 1, initiator of N-acyllactam was attached on the surface of mesoporous silica through the amine group which was grafted on the surface of inner wall of mesoporous silica through APTMS grafting step. Experimental data showed this designed procedure could only produce epsilon-caprolactam salt and nylon 6 couldn't be synthesized inside the nano-channels of mesoporous silica. The reason came from APTMS grafting step which grafted plenty of amine groups on surface of mesoporous silica. Only 25% of grafted amine groups were connected with initiator center of N-acyllactam while other 75% of amine groups were left on silica surface. The anionic ring-opening polymerization was terminated by left amine groups and epsilon-caprolactam salt formed from catalysts of Magnesium bromide ethyl etherate reacted with monomer of epsilon caprolactam.

For procedure 2, newly synthesized chemical of N-3-((N-3-(trimethoxysilanyl)n-propyl)benzamidyl)-benzoyl-epsilon-caprolactam was synthesized and grafted onto the surface of inner-walls of mesoporous silica at one step which would not attach amine groups on silica surface. And silanol capping step consumed the left silanol groups on silica surface. This procedure successfully initiated the anionic ring-opening polymerization inside the nano-channels of mesoporous silica and BMS/nylon 6 composites were obtained with the designed procedure 2. The nano-channels filled synthesized nylon 6 contained α-form crystallite and γ-form crystallite. And the synthesized nylon 6 was expected with covalent bonds with the surface of silica inside

the nano-channels. Synthesized nylon 6 outside the nano-channels was separated from composites and it contained 53.9% α-form crystallite. TGA data showed around 50 wt% loss for synthesized nylon 6/BMS composites, while SEM showed BMS/nylon 6 had the same diameter as pure BMS sphere. SEM showed that all the nylon 6 we synthesized was inside the nano-channels. DSC also showed glass transition temperature of 46°C and melting temperature of 214°C for nylon 6/BMS nanocomposites. TGA showed decomposition temperature of 374°C which was the same as that of initiator immobilized mesoporous silica while 40°C lower than that of pure nylon 6 because of organics grafted onto the surface of inner-walls of mesoporous silica.

In order to graft initiator of N-acyllactam onto the surface of mesoporous silica, two new chemicals were synthesized. The first new chemical was chloro-isophthaloyl-N-ε-caprolactam, which had one acid chloride group to provide the potential future grafting reactions with active hydrogen. The second new chemical is N-3-((N-3-(trimethoxysilanyl)n-propyl)benzamidyl)-benzoyl-epsilon-caprolactam which could react with the silanol groups on the surface of mesoporous silica. Both new chemicals provided the further potential grafting of initiator with group of N-acyllactam with other solid surface.

According to the assumptions and TGA data, there was 6.02 mmol silanol groups on the surface of 1g BMS. There would be 2.1 mmol amine groups to be grafted onto the surface of BMS if surplus APTMS was used. With synthesized procedure 1, 0.56 mmol N-acyllactam was grafted on the surface of mesoporous silica while 1.54 mmol amine group was left on silica surface. For designed synthesized procedure 2, 0.78 mmol N-acyllactam could be grafted on the surface of mesoporous silica while other 5.24 mmol

silanol groups could be consumed with hexamethyldisilazane (HMDS) in silanol capping step.

Through our designed procedure 2, nylon 6 was synthesized through in situ anionic ring-opening polymerization inside the nano-channels and the synthesized nylon 6 was expected to have covalent bonds with silica surface. The synthesized BMS/nylon 6 spherical composites we synthesized could be well distributed in nylon 6, while physical blending of BMS and nylon 6 could only produce phase separated BMS/nylon 6 mixture.

CHAPTER 6

MESOPOROUS SILICA/POLYELECTROLYTE NANOCOMPOSITE

Polyelectrolyte, such as polyacrylic acid (PAA), poly(4-styrenesulfonic acid) and Nafion, was embedded into the framework of mesoporous silica through sol-gel method was reported[65,66]. The mesoporous silica-polyelectrolyte hybrid frameworks provide materials various properties of structure rigidity, functionalities and they can be widely used in the fields of catalysis, separation and fuel cell. However, the reported synthesis steps of mesoporous silica-polyelectrolyte frameworks are much more complex than amorphous silica-polyelectrolyte nanocomposites, and the frameworks obtained from our synthesis have no regular morphologies. It is very important to find a simple direct synthesis method of mesoporous silica-polyelectrolyte frameworks with regular morphologies. In this chapter, a simple direct method to synthesize silica-polyelectrolyte frameworks is described.

Jones CW et al reported a recoverable metal-free catalyst for the green polymerization of epsilon-caprolactone using sulfonic acid functionalized mesoporous silica[67] which was synthesized through post-synthesis procedures. To get the sulfonic acid functionalized mesoporous silica, Jones CW used multiple grafting steps and functionalizing steps after mesoporous silica was synthesized using sol-gel method. With this method, the resulting poly-caprolactone was found to have ultra-low polydispersity index. To check the acid catalysis of synthesized silica-polyelectrolyte frameworks, we use them as catalysts to initiate the polymerization of epsilon-caprolactone to find whether polycaprolactone can be synthesized with this method.

To make a simple direct synthesis method of mesoporous silica-polyelectrolyte frameworks with regular morphologies, a number of mesoporous silica with regular morphologies according to the literature method[68] were synthesized first. Then we improved the synthesis steps and changed the reaction conditions. The mesoporous silica-polyelectrolyte frameworks we synthesized were characterized with SEM, BET and FT-IR. We also characterized the newly synthesized poly-epsilon-caprolactone with mesoporous silica-polyelectrolyte frameworks as catalysts.

6.1 Synthesis of mesoporous silica with different ethyl acetate

With the same ratio of CTAB/Na_2SiO_3, the amount of added ethyl acetate was increased from 15ml, 25ml and 35ml. Three silica structures were named as MS-1, MS-2 and MS-3 were synthesized according to the increasing sequence of ethyl acetate. Figure 6.1 showed the SEM image of MS-1 which was fiber structure with fiber diameter of about 1.7 μm, the length of the fiber was up to 40 μm. Figure 6.2 showed the SEM image of MS-2 which was also fiber structure with fiber diameter of around 2.2μm which was a little larger than that of MS-1. Figure 6.3 showed the SEM image of MS-3 which was spherical in structure with a sphere diameter between 4 and 6μm. Zukal A and his group[68] explained this phenomenon of morphology difference with increasing concentration of ethyl acetate. At low concentration of ethyl acetate which will hydrolyze in water and decrease the PH value of the mixture, the CTAB is structure directing agent which will form cylindrical micelles in water according to the mechanism of “end effect”. The surfactant micelles run continuous throughout the body of the micrometer dimension mesoporous silica fiber. As higher concentration of ethyl acetate which produces lower

PH value and disturb the gradual arrangement of micelles into a hexagonal array. Therefore, when the ratio of ethyl acetate increases to a certain value, the mesoporous silica structure will change from fibers to spheres.

The MS-3 was named as bimodal mesoporous silica (BMS) and it was mentioned the previous two chapters to synthesize BMS/PMMA and BMS/nylon 6 nanocomposites. In the previous two chapters, we successfully initiated the free radical polymerization to synthesize PMMA and anionic ring-opening polymerization to synthesize nylon-6 inside the nano-channels of BMS. Unlike most mesoporous silica, BMS have two advantages in relation to BMS/polymer composites. First, they have two different pore distributions. Most of the pore size has a distribution between 10 and 30nm, and fewer pores size distribute from 2 to 6 nm. The second advantage is that BMS has well defined spherical morphology. We can do some calculations based on the diameter changes and TGA weight loss. If we chose a kind of mesoporous silica without regular morphology, it will be difficult for us to do these kinds of calculations.

MS-1 and MS-2 show morphology of long fiber. And the diameters of the fibers are also very close to each other shown from Figure 6.1 and Figure 6.2. These two kinds of mesoporous silica provide a good method to synthesize long fiber with mesoporous structure.

The synthesis procedures of using ethyl acetate to control the PH value of reaction system to synthesize MS-1, MS-2 and MS-3 provide us a very simple direct method to synthesize mesoporous silica with regular morphologies, which also inspires us to find an improved procedure of synthesizing mesoporous silica-polyelectrolyte framework with regular morphologies.

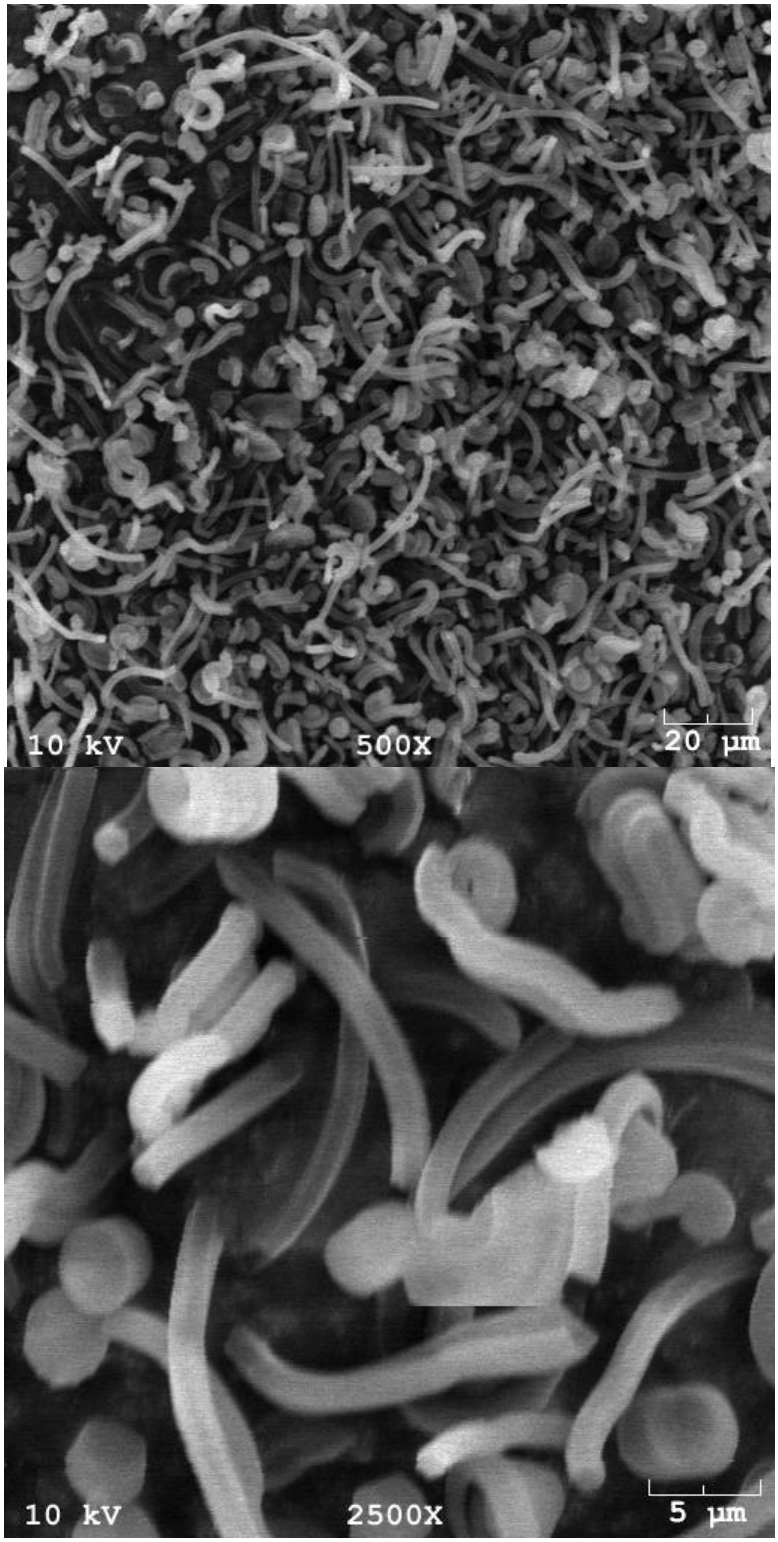

Figure 6. 1 SEM image of MS-1 with different magnifications

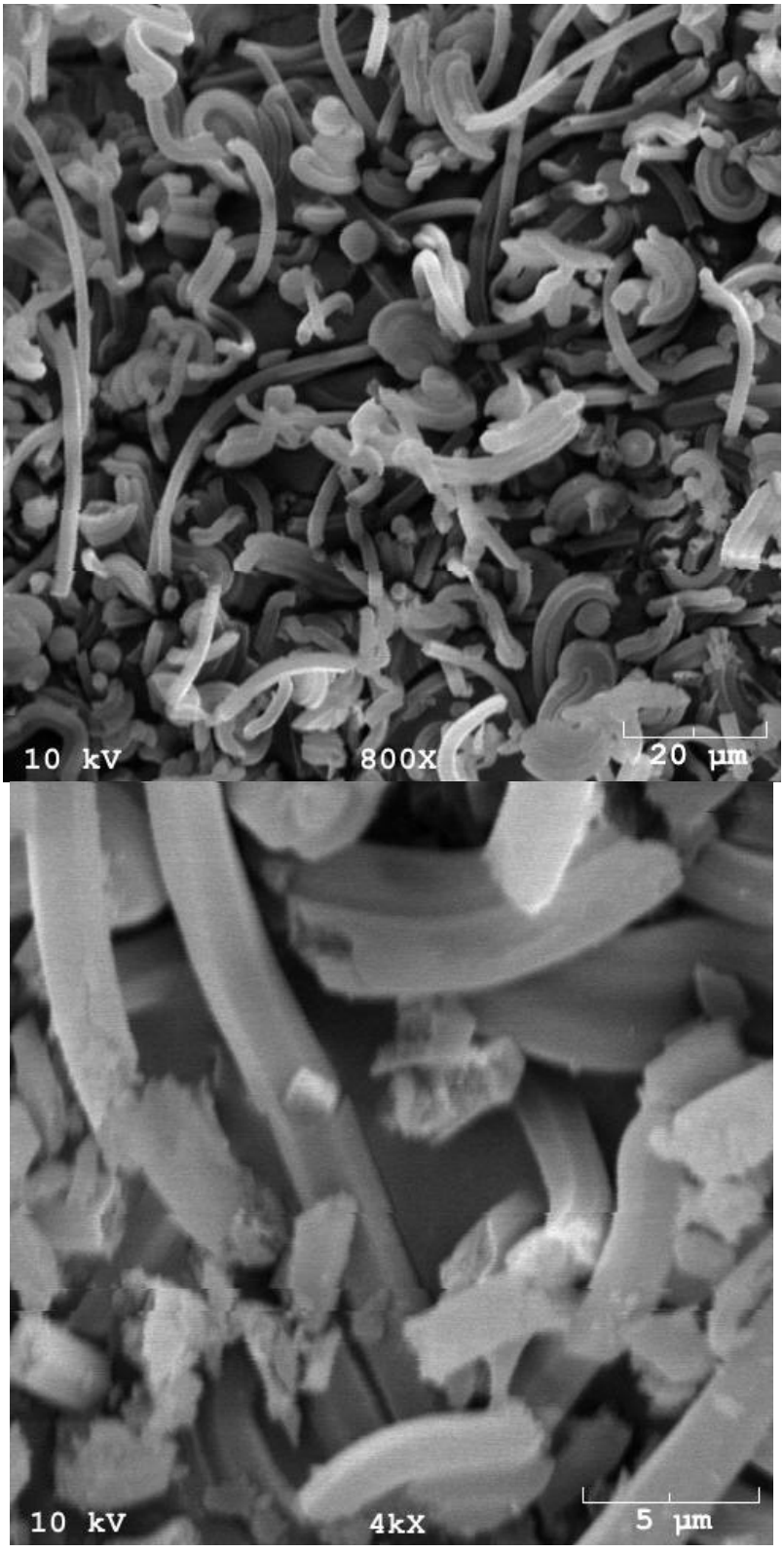

Figure 6. 2 SEM image of MS-2 with different magnifications

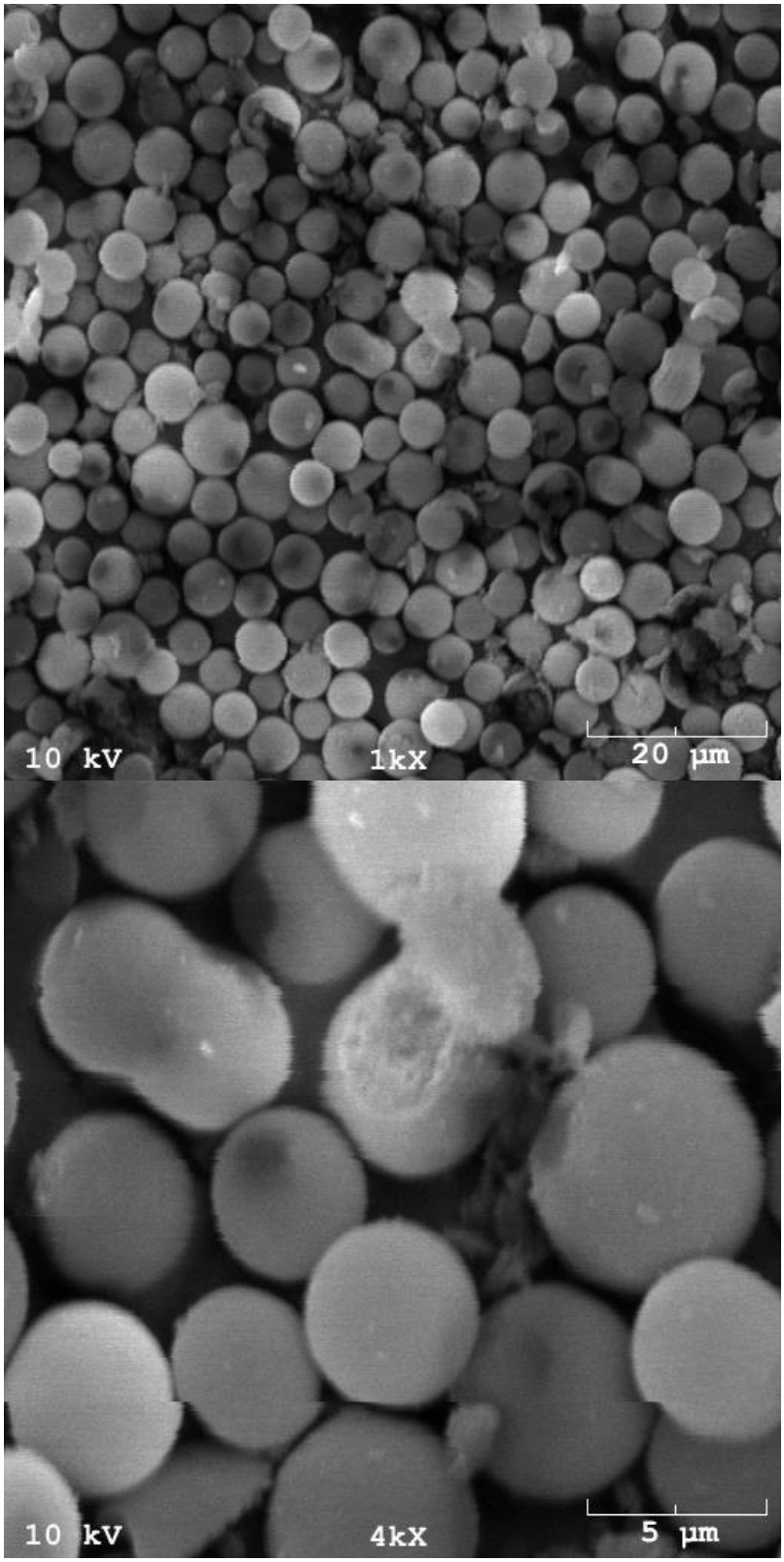

Figure 6. 3 SEM image of MS-3 with different magnifications

6.2 Synthesis of mesoporous silica/PAA or PSSA nanocomposites with different conditions

With the same ratio of CTAB/Na_2SiO_4/PAA**,** the amount of added ethyl acetate was increased and the resulting three silica/PAA nanocomposites were named as AA-MS-1, AA-MS-2 and AA-MS-3 according to the increasing amount of ethyl acetate. With the similar method to synthesize mesoporous silica/PAA nanocomposites, PAA was replaced with PSSA, and three silica/PSSA nanocomposites were named as SSA-MS-1, SSA-MS-2 and SSA-MS-3 with the increasing ethyl acetate. All resulted silica/polyelectrolyte nanocomposites were refluxed with 1M H_2SO_4/MeOH and MeOH.

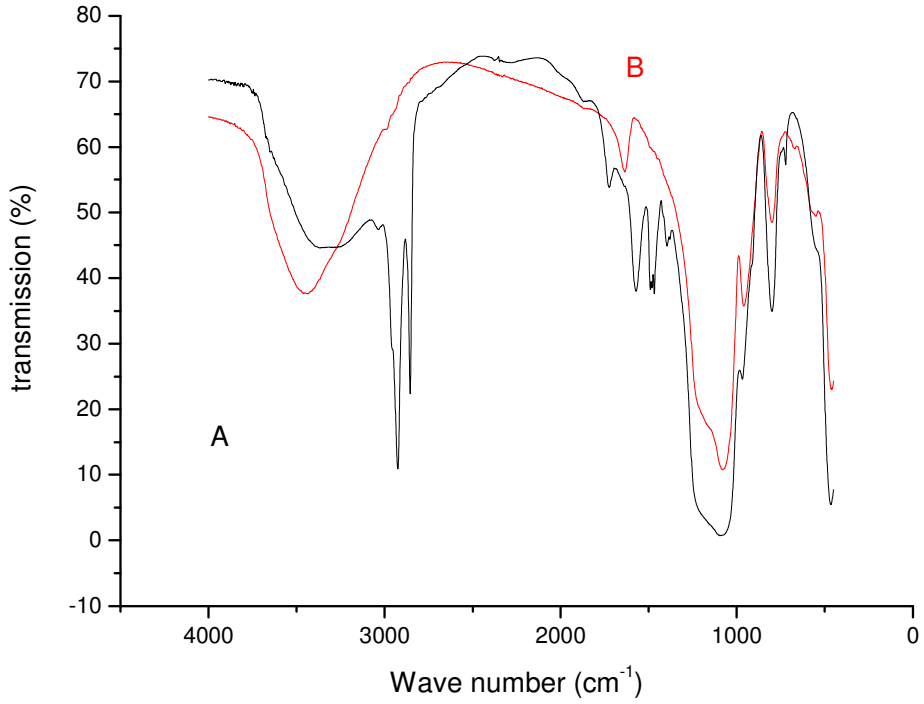

Figure 6. 4 FT-IR spectra of (A) as-synthesized and (B) template free silica/PAA nanocomposite

Infrared spectra of as-synthesized and template-free (extracted) samples were shown in Fig 6.4. In the as-synthesized sample, strong absorptions of the surfactant were observed approximately at 2929 and 2850 cm−1 (Fig. 6.4A). These absorptions were disappeared after the treatment with H_2SO_4 (Fig. 6.4B), which indicated all surfactants were removed. The methods to synthesize different kinds of mesoporous silica from the literature use high temperature calcination to get rid of all surfactants. However, we couldn't get rid of the surfactants using high temperature calcination because high temperature calcination would also calcinate the polyelectrolyte chain across the silica network. The mixture of sulfonic acid and methanol could get rid of all surfactants of CTAB while the polyelectrolyte was still remained across the framework of mesoporous silica. And sulfonic acid could also transfer the polyelectrolyte salt on silica surface to polyelectrolyte acid.

SEM image of AA-MS-1, AA-MS-2, AA-MS-3 SSA-MS-1, SSA-MS-2 and SSA-MS-3 were shown in Figure 6.5, Figure 6.6 and Figure 6.7. These figures didn't show structure of fiber like pure MS in Figure 6.1 and Figure 6.2. SEM of AA-MS-1 didn't show any regular morphology, and SEM of AA-MS-2 showed co-existence of three morphologies of spheres, mushroom heads and fibers. But SEM of AA-MS-3 showed a regular spherical structure. The phenomena of co-existence of three different morphologies of sphere, mushroom head and fiber in SEM image of AA-MS-2 indicated that morphology changed from fiber to mushroom head and sphere with increasing concentration of ethyl acetate. For cylindrical micelles, the surfactant molecules were forced to pack into hemispherical caps at each end of cylindrical micelles. With a certain

concentration of ethyl acetate which just disturbed the cylindrical micelles structure, three morphologies like fibers, mushroom heads and spheres were co-existed.

For SSA-MS-1, SSA-MS-2 and SSA-MS-3, the change of morphology was not the same as the change of AA-MS-1, AA-MS-1 and AA-MS-3. For SSA-MS-1, there were some spheres and some irregular structure. For SSA-MS-2, three structures were alo co-existed. However, for SSA-MS-3, we couldn't find regular spherical structure and only disturbed irregular sphere structure was shown. The reason was probably coming from the influence of added polyelectrolyte salt.

CTAB was a kind of cationic surfactants, which would form salt with organic acid and precipitated from the solution. To avoid the precipitation during the synthesis, the sodium salt of organic acid such as PAA and PSSA was used. As ethyl acetate hydrolyzed to acid in water, the acid would transfer part of polyelectrolyte salt to polyelectrolyte acid which would react with CTAB to form precipitation and destroyed the regular morphologies of surfactant micelles. The PH value of reaction system also decreased faster than without polyelectrolyte salt during reaction system. Because hydrolyzed organic acetic acid could evaporate out of the autoclavable PP bottle when there was no polyelectrolyte sodium in the reaction system. When polyelectrolyte sodium was used in reaction system, the part of hydrolyzed acid would be transferred to polyelectrolyte sodium and the acetic couldn't evaporate out of the PP bottle.

The mechanism became much more complex with polyelectrolyte sodium than without polyelectrolyte sodium resulted from the potential reaction between the polyelectrolyte acid and surfactant of CTAB. The reaction time, stirring time, ratio of

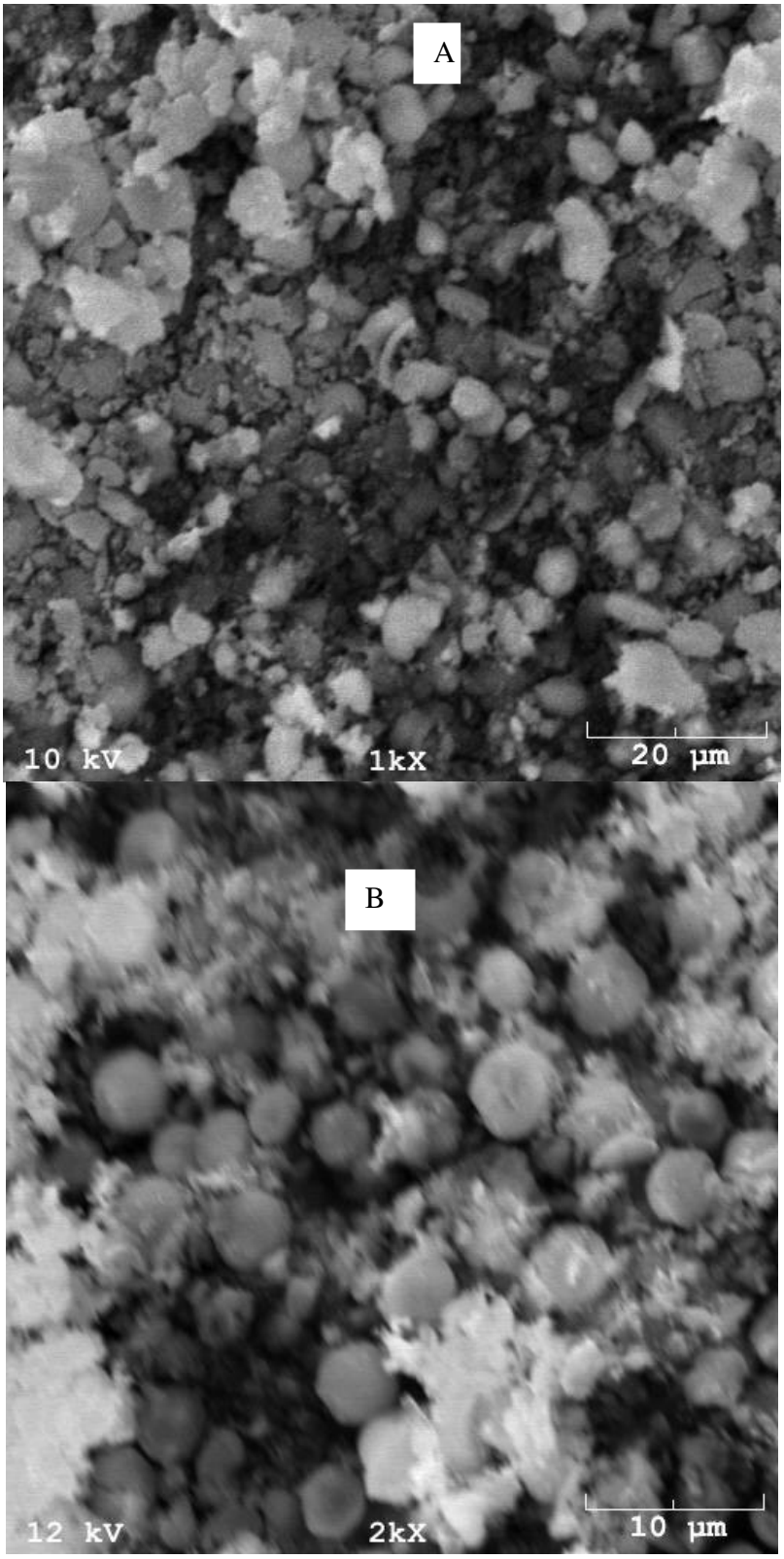

Figure 6. 5 SEM image of (A) AA-MS-1; (B) SSA-MS-1

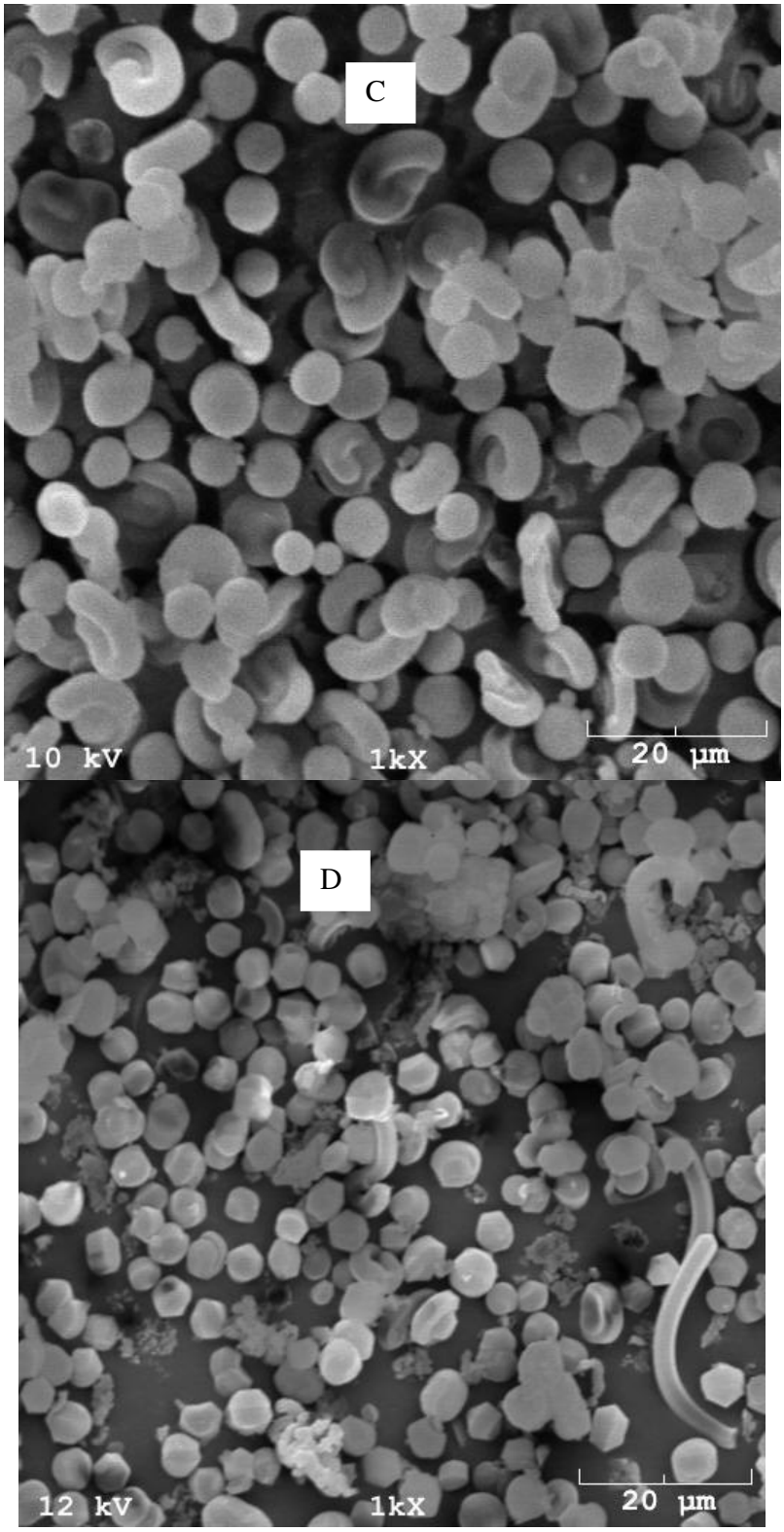

Figure 6. 6 SEM image of (C) AA-MS-2; (D) SSA-MS-2.

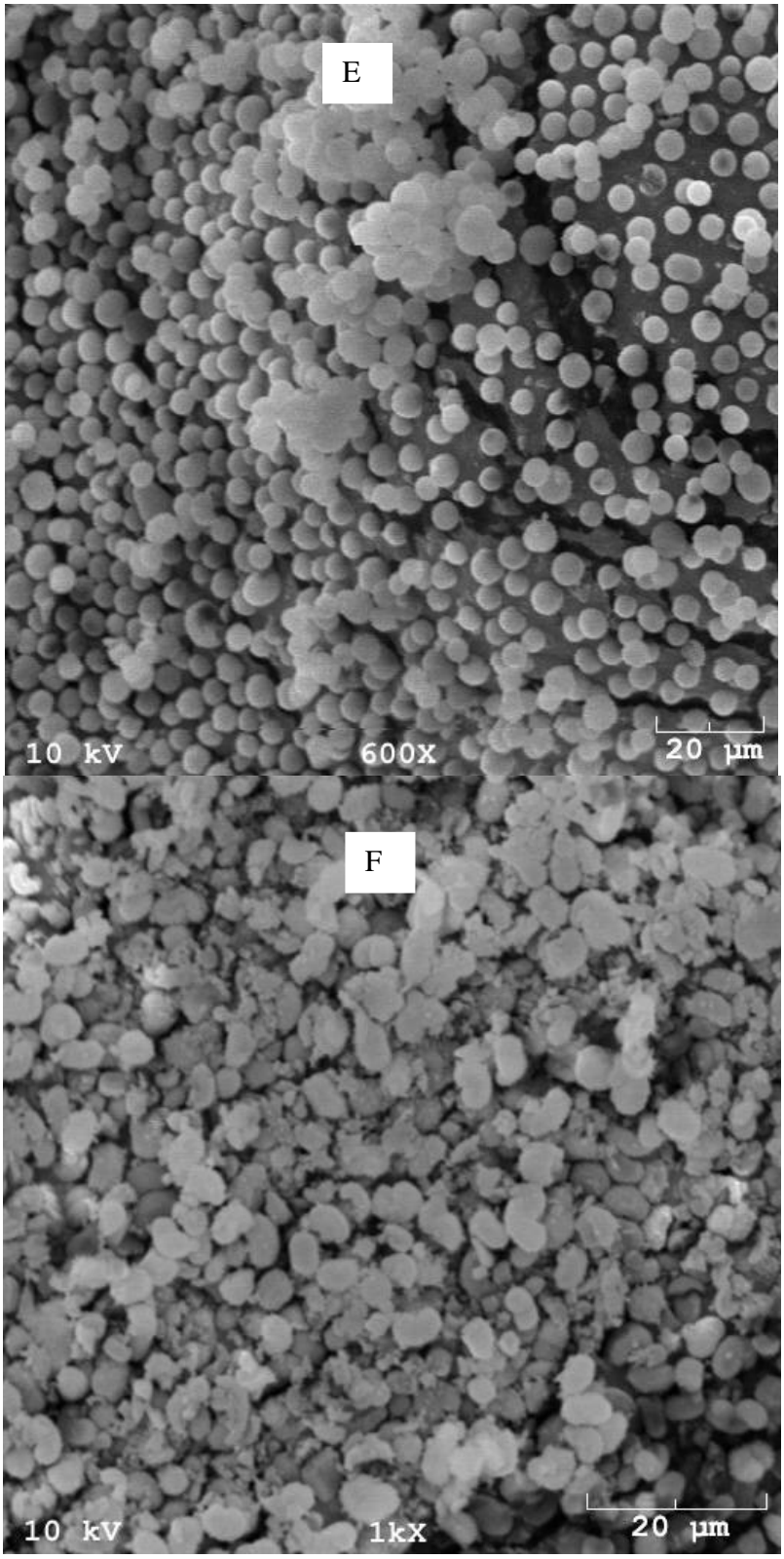

Figure 6. 7 SEM image of (E) AA-MS-3; (F) SSA-MS-3

different components, reaction temperature would be very important to this reaction system to synthesize mesporous silica/polyelectrolyte acid nanocomposites with regular morphologies.

6.3 Synthesis of other mesoporous silica/ polyelectrolyte nanocomposite

In previous method to synthesize mesoporous silica/ polyelectrolyte nanocomposite, sodium silicate was used as silica sources. Tetraethyl orthosilicate (TEOS) was used replace sodium silicate as silica sources under acid reaction system and base reaction system. The detailed synthesis procedures were described previously in chapter 3. The sample synthesized under base condition was named as sample 4, and sample synthesized under acid condition was named as sample 6.

To overcome the disadvantages of surfactants of CTAB which would form salt with polyelectrolyte acid and precipitate from the solution, pluronic 123 (EO-PO-EO block copolymer) rather than CTAB was used to synthesize SBA 15/PSSA nanocomposites under acid environment. The detailed procedures were described in chapter 3.

SEM image of mesoporous silica/PAA composites under base environment (Figure 6.8) and acid environment(Figure 6.9) showed morphology of particles without regular morphology. The particle size was up to 10μm, and a lot of particles congregated together to form big particles. The particles with regular morphologies shown in Figure 6.6 and Figure 6.7 could be separated from each other, but it was difficult to separate these particles from each other shown in Figure 6.8 and Figure 6.9. This synthesis method was obtained from the method to synthesize SBA-15 from literature.

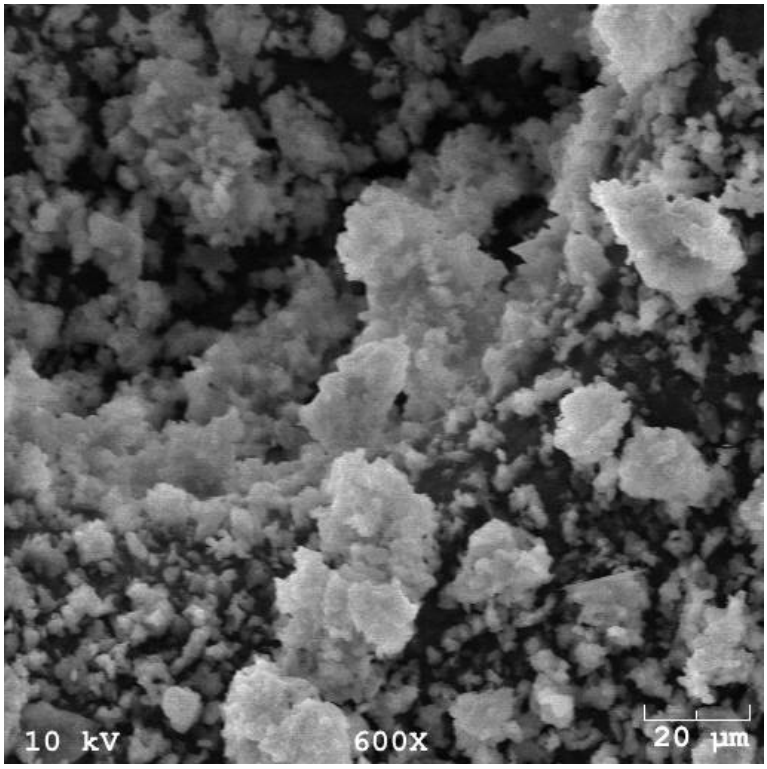

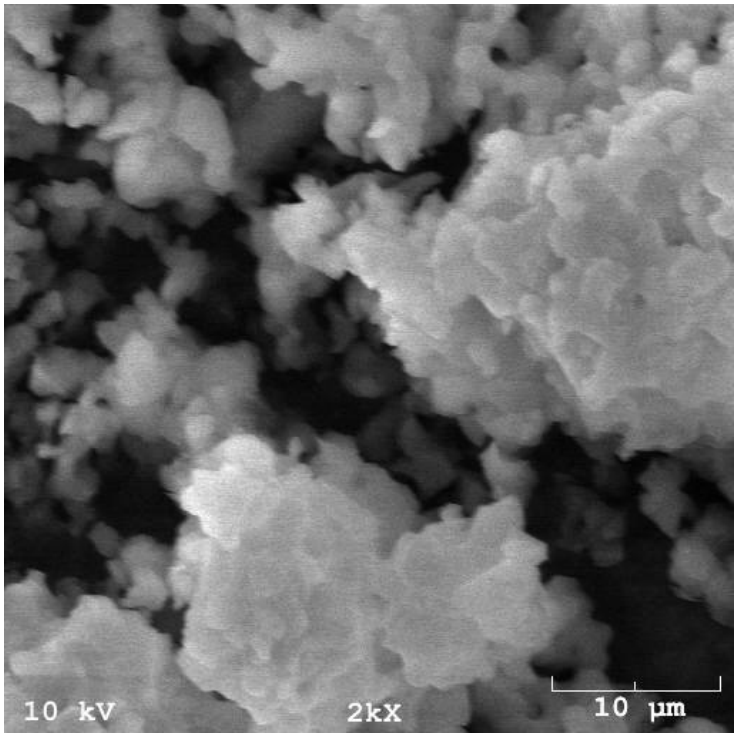

Figure 6. 8 SEM image of sample 4: mesoporous silica/PAA composites under base environment with different magnification.

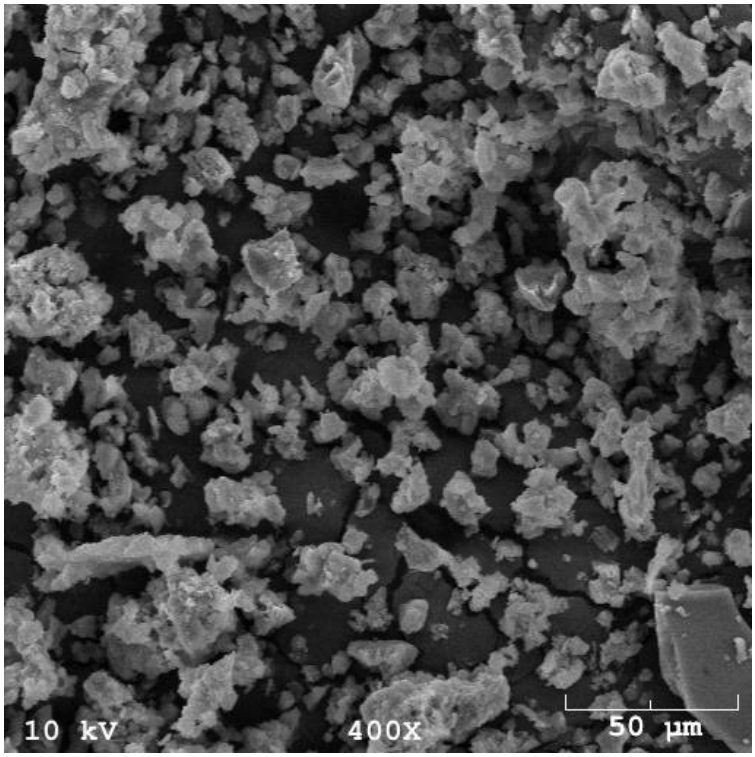

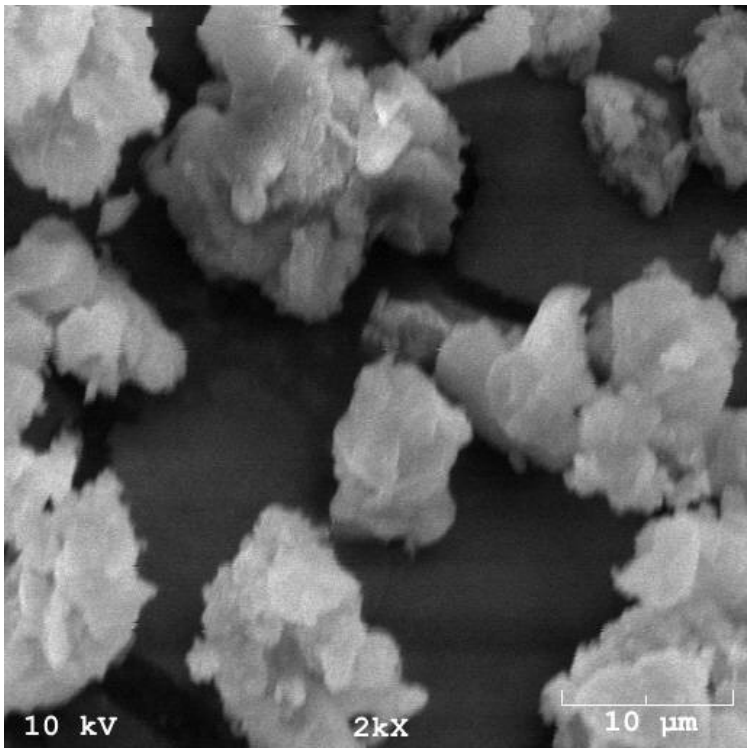

Figure 6. 9 SEM image of sample 6: mesoporous silica/PSAA composites under acid environment with different magnification.

Nitrogen adsorption/desorption isotherms was used to characterize the surface area, average pore size and pore volume for different AA-MS-nanocomposites. The detailed data were shown in table 6.1. As more ethyl acetate was added to the same system at different time shown in sample 1, sample 2 and sample 3 separately, BET surface area decreased, but both BJH average pore size and pore volume increased. When TEOS was used to replace silicate salt as silica resources (sample 4 and sample 6), BET surface area increased significantly, and both BJH average pore size and pore volume decreased a lot. Figure 6.10 showed N_2 adsorption/desorption isotherms and their corresponding BJH pore size distribution curves for all samples. The N_2 isotherms showed typical curves for mesoporous materials from the loop which formed between adsorption curve and desorption curve. All silica materials synthesized were mesoporous silica/polyelectrolyte composites, but their surface area, pore size, pore volume and morphologies were different.

Table 1 Adsorption isotherms of nitrogen data for different AA-MS nanocomposites

Sample No	BET Surface Area (m^2/g)	BJH average pore size (nm)	BJH adsorption pore volume (cm^3/g)
1 AA-MS-1	748 ± 7	6.26	1.17
2 AA-MS-2	559 ± 10	10.87	1.35
3 AA-MS-3	512 ± 3	16.18	1.88
4 AA-MS-4	1100 ± 3	3.11	0.94
5 AA-SBA-5	579 ± 5	14.22	1.92
6 SSA-MS-6	896 ± 33	2.38	0.37

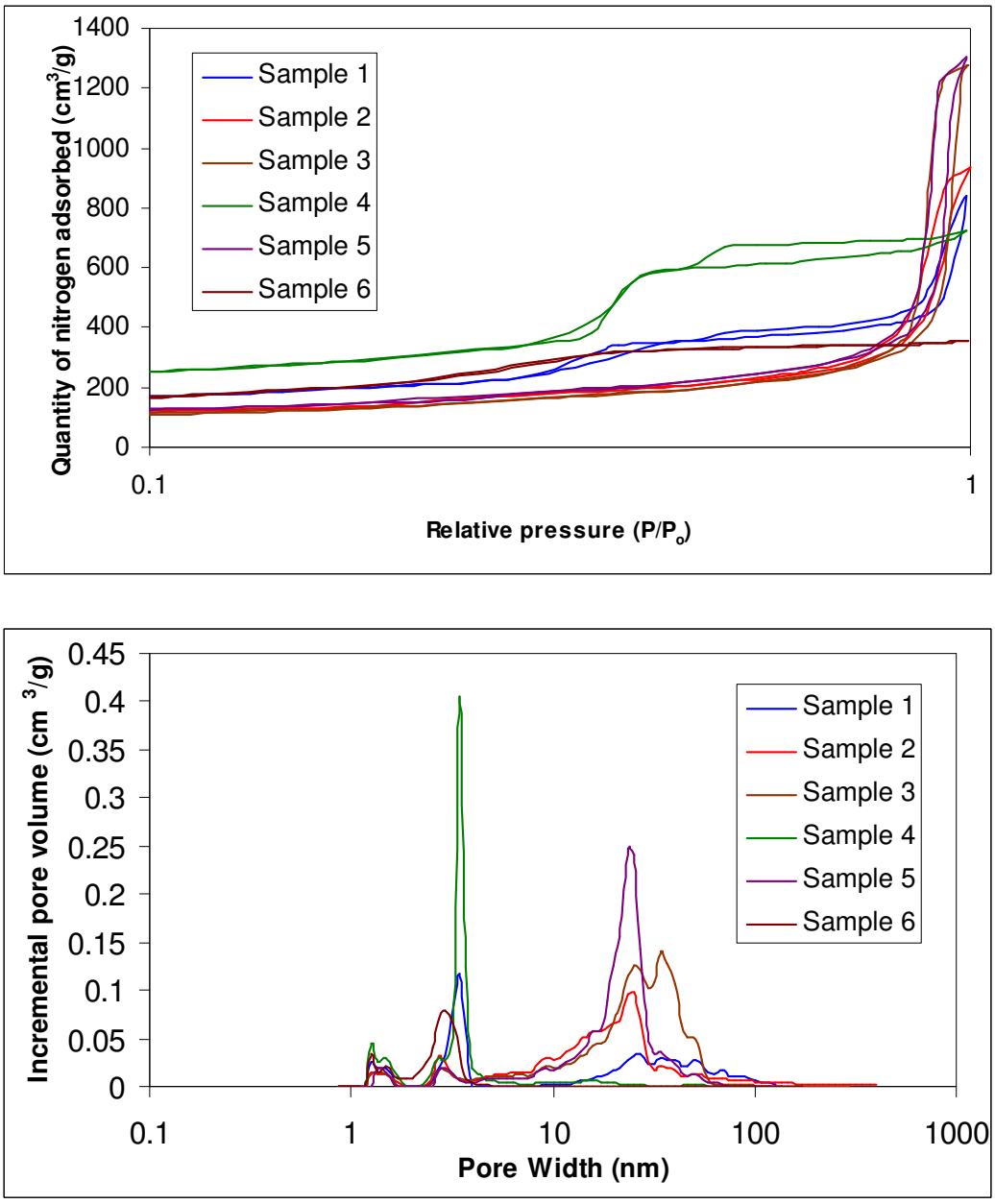

Figure 6. 10 N2 sorption isotherms(upper) and the corresponding BJH pore size distribution curves(lower) for sample 1: AA-MS-1; sample 2: AA-MS-2; sample 3: AA-MS-3; sample 4: AA-MS-4; sample 6: SSA-MS-6

6.4 Poly-epsilon-caprolatone synthesized with derived mesoporous silica/PSSA nanocomposites

In previous chapter, a description was given to synthesize mesoporous silica/polyelectrolyte nanocomposites with different morphologies, surface area, average pore size and pore volume. To check the acid catalysis of the synthesized nanocomposites, monomer of epsilon-caprolcatone was used to polymerize with synthesized nanocomposites as catalyst to check whether designed polymer could be obtained. A detailed synthesis procedure was shown in chapter 3. Here we use two different solid of mesoporous silica/PSSA nanocomposites as catalysts. The first one is PSSA-MS-03, and the second is PSSA-SBA.

The poly-epsilon-caprolactone synthesized was characterized with ^{1}H NMR and GPC. ^{1}H NMR spectra of poly-epsilon-caprolactone which was polymerized with catalysts of mesoporous silica/PSSA nanocomposites is shown in Figure 6.11, and ^{1}H NMR spectra of synthesized poly-epsilon-caprolactone polymerized with catalysts of PSSA-MS-03 is shown in Figure 6.12. From the ^{1}H NMR spectra (300MHz, $CDCl_3$) from Figure 6.11, five peaks could be found and their structure was characterized as δ 4.03 (2H), 3.61 (1H), 2.28 (2H), 1.62 (4H), 1.35 (2H). From the ^{1}H NMR spectra (300MHz, $CDCl_3$) from Figure 6.12, five peaks and their structure was characterized as δ 4.04 (2H), 3.63 (1H), 2.29 (2H), 1.63 (4H), 1.36 (2H). Both ^{1}H NMR spectra showed exactly the same peak position with different area at position of 3.61 which is the end group of hydrogen. Figure 6.11 showed the area at δ 3.61 was 0.26, whereas Figure 6.12 showed the area at 3.63 was 0.33. All other peak had the same area. For the peak at δ of

3.61, a smaller area meant a larger molecular weight from the ratio of end group to the repeating units for hydrogen was smaller.

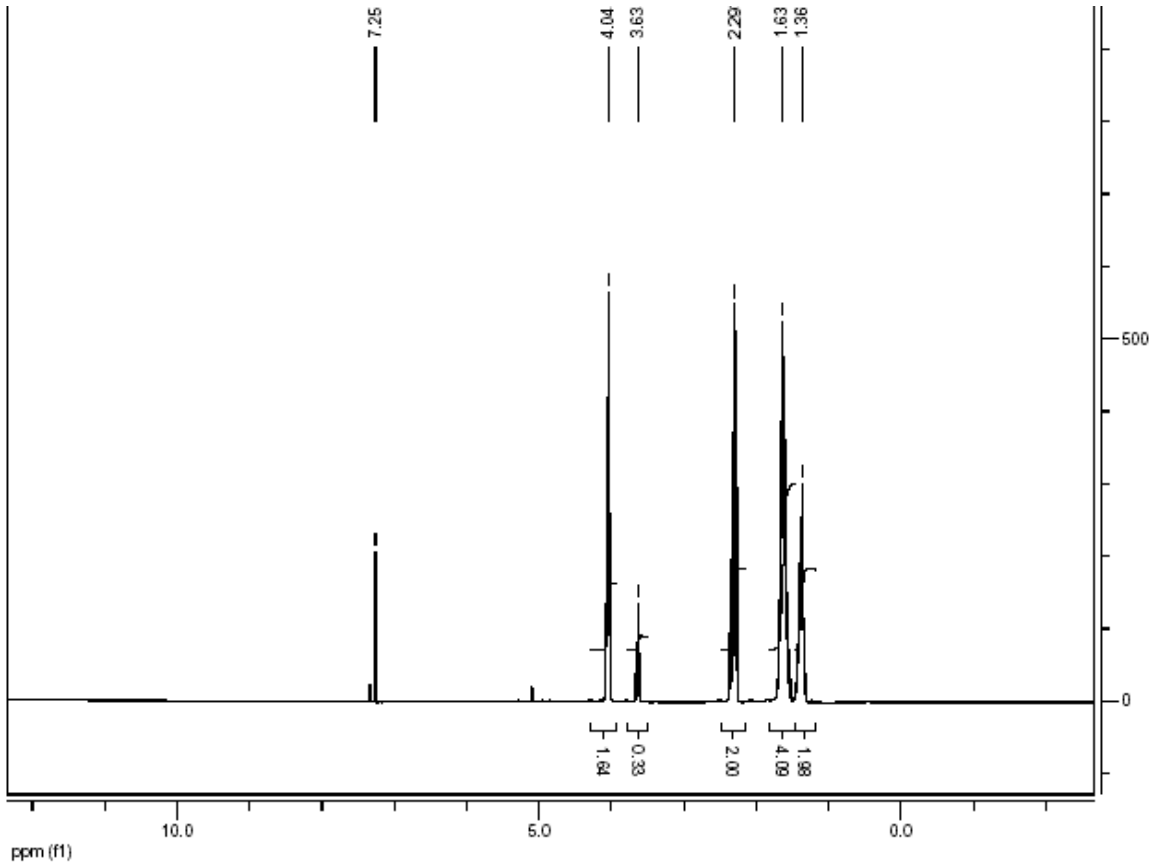

Figure 6. 11 ^{1}H NMR spectrum of synthesized poly-epsilon-caprolactone with catalysts of mesoporous silica/PSSA nanocomposites

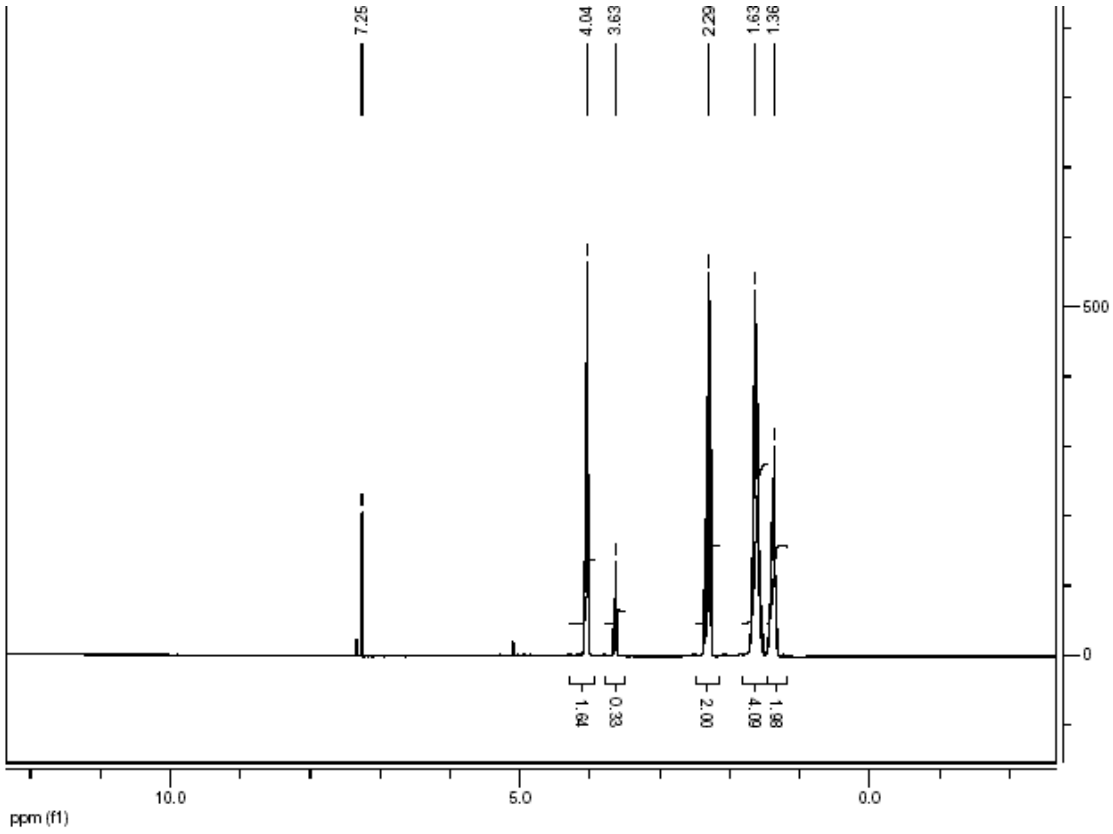

Figure 6. 12 ^{1}H NMR spectrum of synthesized poly-epsilon-caprolactone with catalysts of PSSA-MS-03

GPC was used to characterize the molecular weight and polydispersity index. For polymer synthesized using catalysts of mesoporous silica/PSSA nanocomposites, we found that M_n was 2463, M_w was 3060 and PDI was 1.24. For polymer synthesized using catalysts of PSSA-MS-03s, the M_n was 2318, M_w was 2765 and PDI was 1.19. Both GPC data showed similar molecular weight and low polydispersity index. The polydispersity was obtained around 1.2 which was much smaller than 2.0 when TsOH was used as catalysts to synthesize caprolactone. Jone CW's group also obtained PDI between 1.1 and

1.2 for poly-epsilon-caprolactone with using catalysts of SBA-SO_3H which was obtained through post-synthesis steps.

Poly-epsilon-caprolactone with mean molecular weight around 2400 g/mol was synthesized using mesoporous silica/PSSA nanocomposites synthesized. The polymer synthesized had ultra-low polydispersity index. This result also verified that the mesoporous silica/PSSA nanocomposites had very well acid catalysis.

6.5 Conclusion

In this chapter, different mesoporous silica/polyelectrolyte nanocomposites were synthesized using silica sources of sodium silicate or TEOS under different condition. When sodium silica was used as silica sources and other conditions were kept the same with increasing ethyl acetate, mesoporous silica/polyelectrolyte nanocomposites synthesized had decreasing surface area, increasing average pore size and decreasing pore volume. The experiments also showed nanocomposites synthesized with silica sources of TEOS had a higher surface area, lower average pore size and lower pore volume than those composites synthesized with silica sources of sodium silicate.

Experiments also showed that it was difficult to obtain mesoporous silica/polyelectrolyte nanocomposites with regular morphologies when sodium silicate was used as silica sources and polyelectrolyte was strong acid such as poly (styrene sulfonic acid) to use. Mesoporous silica/polyelectrolyte nanocomposites with regular morphologies could be obtained if polyelectrolyte was weak acid such as poly (acrylic acid). When TEOS was used as silica sources, nanocomposites without regular

morphologies were obtained no matter polyelectrolyte with strong acid or weak acid was used.

Both mesoporous silica/PSSA nanocomposites synthesized from silica sources of sodium silicate or TEOS could be used as acid catalysts to initiate the polymerization of epsilon caprolactone. The poly(epsilon caprolactone) had ultra-low polydispersity of around 1.2 which was very close to PDI obtained by living polymerization. The mesoporous silica/PSSA nanocomposites could be used to synthesize poly (epsilon caprolactone) with PDI close to those synthesized with catalyst of SBA-SO_3H in literature.

CHAPTER 7

CONCLUSIONS AND RECOMMENDATIONS

In this work, two approaches were developed to graft initiators on the surface of mesoporous silica to initiate the free radical polymerization and anionic ring-opening polymerization inside the nano-channels of mesoporous silica to synthesize mesoporous silica/polymer nanocomposites. This work also addressed a simple direct method to synthesize mesoporous silica/polyelectrolyte nanocomposites through sol-gel method.

7.1 conclusions

The key conclusions are:

a) mesoporous silica/PMMA nanocomposites

A kind of azo-initiator ABCC was successfully grafted on the surface of mesoporous silica to form ABCC-immobilized mesoporous silica which successfully initiated the free radical polymerization of MMA inside the nano-channels of mesoporous silica through both solution polymerization and bulk polymerization.

The PMMA/BMS composites we synthesized showed spherical morphologies with narrow distribution of diameters around 5μm, which was almost double of the diameter of pure spherical BMS. The PMMA/BMS showed a higher glass transition temperature and higher decomposition temperature than pure commercial PMMA. Around 90 wt% of the PMMA/BMS composites were newly polymerized PMMA.

PMMA was separated from the surface of mesoporous silica when supported material of silica networks was dissolved by hydrofluoric acid. The pure PMMA obtained from BMS/PMMA composites showed a spherical morphology and some special properties over commercial PMMA, such as ultra-high molecular weight around 800,000 g/mol, very low polydispersity index of 1.1 and higher decomposition temperature. The spherical PMMA capsules obtained from BMS/PMMA nanocomposites didn't collapse after silica was removed, and they showed the same thermal behavior as BMS/PMMA composites with higher decomposition temperature and narrow temperature range of decomposition.

b) Mesoporous silica/nylon 6 nanocomposites

The existence of amine groups on the surface of mesoporous silica would terminate the anionic ring-opening polymerization of epsilon caprolactam and produced caprolactactam salt with catalysts of magnesium bromide ethyl etherate. One new chemicals of N-3-((N-3-(trimethoxysilanyl)n-propyl)benzamidyl)-benzoyl-epsilon-caprolactam was synthesized and grafted onto the surface of inner-walls of mesoporous silica, by which no extra amine groups were grafted on silica surface and nylon 6/BMS nanocomposites were synthesized.

Characterization of ^{29}Si CP-MAS NMR, ^{13}C CP-MAS NMR, BET adsorption/desorption isotherm and TGA proved the successful finish of all post grafting steps on the surface of mesoporous silica.

The nylon 6/BMS nanocomposites we synthesized were spheres with the same diameter as pure BMS. About 50 wt% of the composites was newly synthesized nylon 6

and almost all nano-channels of mesoporous silica were filled with the nylon 6. The nylon 6 was proven to contain α-form crystallites and γ-form crystallites with covalent bonds with the surface of silica inside the nano-channels. The spherical composites had the same glass transition temperature and melting temperature as pure commercial nylon 6, having the same decomposition temperature as N-acyllactam-immobilized BMS but lower than commercial pure nylon 6.

Based on the assumptions and TGA tested data, one gram of BMS had 6.02 mmol silanol groups on its surface. There would be 2.1 mmol amine groups to be grafted onto the surface of BMS if only excess APTMS was used to graft onto the surface of mesoporous silica. And 0.56 mmol N-acyllactam could be grafted on the surface of mesoporous silica through amine groups. But 0.78 mmol N-acyllactam could be directly grafted on the surface of mesoporous silica through newly synthesized initiator of N-3-((N-3-(trimethoxysilanyl)n-propyl)benzamidyl)-benzoyl-epsilon-caprolactam.

Result also showed that the BMS/nylon 6 spherical composites could be well distributed in nylon 6, while physical blending of BMS and nylon 6 could only produce phase separated BMS/nylon 6 mixture.

c) Mesoporous silica/polyelectrolyte nanocomposites

Different mesoporous silica/polyelectrolyte nanocomposites were synthesized using silica sources of sodium silicate and TEOS under different conditions. When sodium silica was used as silica sources and other conditions were kept unchanged but with increasing ethyl acetate, mesoporous silica/polyelectrolyte nanocomposites had decreasing surface area, increasing average pore size and pore volume. The experiments

also showed nanocomposites synthesized using silica sources of TEOS had a higher surface area, lower average pore size and lower pore volume than those composites synthesized by using silica sources of sodium silicate.

When sodium silicate was used as silica sources, it was difficult to get mesoporous silica/polyelectrolyte nanocomposites with regular morphologies if polyelectrolyte was strong acid such as poly (styrene sulfonic acid), however, mesoporous silica/polyelectrolyte nanocomposites with regular morphologies was possible if polyelectrolyte was weak acid such as poly (acrylic acid). When TEOS was used as silica sources, nanocomposites without regular morphologies would be obtained when both strong acid and weak acid was used as polyelectrolyte.

Mesoporous silica/PSSA nanocomposites synthesized with sodium silicate or TEOS as silica sources could be used as acid catalysts to initiate the polymerization of epsilon caprolactone, the obtained poly (epsilon caprolactone) had ultra-low polydispersity index of around 1.2 which was very close to PDI obtained by living polymerization. The mesoporous silica/PSSA nanocomposites were proven a good acid catalyst.

7.2 recommendations

a) Mesoporous silica/PMMA composites

The mesoporous silica/PMMA spherical composites were synthesized through free radical polymerization with excess monomer and long enough reaction time. Although we obtained spherical composites with double diameter of that of pure BMS, we didn't study the kinetics of chain growing on the surface of silica surface.

Experiments showed the newly synthesized PMMA wasn't cross-linked polymer because they could be dissolved in solvent and GPC showed a very high molecular weight. We didn't solve the problem why PMMA covered on the surface of BMS had thickness up to μm. To understand the phenomena, a series of experiments with different reaction time should be designed to study the mechanism of chain growing on the surface of silica.

Spherical silica was not a good filler to enhance the mechanical properties of composites because its morphology couldn't produce enough friction. We didn't investigate their application to be used as filler. But it was possible for us to choose other mesoporous silica with irregular morphology and rough surface to initiate polymerization with the initiator grafting method because the covalent bonds between silica surface and polymer build a very strong connection between the filler and matrix. This method also provided a good method to produce a core-shell structure which had a wide application in biomaterials. Its application could be further investigated in the future.

b) Mesoporous silica/nylon 6 nanocomposites

Previously synthesized PMMA/BMS composites could contain PMMA up to 90 wt%, synthesized nylon 6/BMS could only contain nylon 6 around 50 wt%. And newly synthesized nylon 6 couldn't cover the silica surface with high thickness just like PMMA.

The nylon 6/BMS synthesized didn't show special properties over commercial nylon 6, such as glass transition temperature and melting temperature. This was because the chosen BMS had diameter of nano-channels between 10 nm and 30 nm which was larger than the thickness of fold chain crystal lamellar. To obtain extended chain crystal inside the nano-channels, mesoporous silica with smaller nano-channels of less than 3nm should be used. But smaller pore size would increase the difficulties to push monomer of

epsilon caprolactam inside the nano-channels. Further experiments were suggested to focus on the synthesis of nylon 6/mesoporous silica with smaller pore size.

c) Mesoporous silica/polyelectrolyte nanocomposites

Although different mesoporous silica/PAA naocomposites and mesoporous silica/PSSA nanocomposites were synthesized under different conditions, it was very hard to obtain mesoporous silica/PSSA nanocomposites with regular morphology. It was suggested to design experiments with different reaction condition to study the tendency of morphologies changing.

We used mesoporous silica/PSSA nanocomposites as acid catalysts to initiate the polymerization of epsilon caprolactone and obtained poly(epsilon caprolactone) with very low polydispersity index. It was suggested to synthesize a series of poly(epsilon caprolactone) with different molecular weight and compare the properties of synthesized polycaprolactone.

REFERENCES

[1] C. T. Kresge, M. E. Leonowicz, W. J. Roth, J. C.Vartuli, J. S. Beck. *Ibid*, 1992, 359, 710

[2] J. S. Beck *et al.*, *J. Am. Chem. Soc.* 1992, 114, 10834

[3] C. T. Kresge, M. E. Leonowicz, W. J. Roth, J. C. Vartuli and J. S. Beck. *Nature.* 1992, 359, 710

[4] D. Y. Zhao, J. Feng, Q. Huo, N. Melosh, G. H. Fredrickson, B. Chmelka and G. D. Stucky. *Science*. 1998, 279, 548

[5] D. Zhao, Q. Huo, J. Feng, B. F. Chemlka and G. D. Stucky *J. AM. Chem. Soc.* 1998, 120, 6024

[6] Y. Lu. *Angew. Chem., Int. Ed. Engl*. 2006, 45, 7664

[7] H. Yang, N. Goombs and G. A. Ozin. *Nature* 1997, 386, 692

[8] Q. S. Huo; D. Y. Zhao, J. L. Feng; Weston Kenneth; S. K. Buratto, G. D. Stucky, S. Schacht, F. Schuth. *Adv. Mater*. 1997, 9, 974

[9] J. F, Wang, J. P. Zhao, B. Y. Asoo, G. D. Stucky. *J. AM. Chem. Soc.* 2003, 125, 13966

[10] A. Sellinger, P. M. Weiss, A. Nguyen, Y. Lu, R. A. Assink, W Gong and C. J. Brinker. *Nature*. 1998, 394, 256

[11] M. Fujiwara, K. Shiokawa and Y. Zhu. *J. Mol. Catal. A. Chem.* 2007, 264, 153

[12] J. H. Clark, D. J. Macquarrie. *Chem. Commu*n. 1998, 8, 853.

[13] R. Anwander, I. Nagl, M. Widenmeyer, G. Engelhardt, O. Groeger, C. Palm, T. Roser. *J. Phys. Chem. B* 2000, 104, 3532.

[14] A. Stein, B. J. Melde, R. C. Schroden. *Adv. Mater*. 2000, 12, 1403

[15] E. Cano-Serrano, G. Blanco-Brieva, J. M. Campos-Martin, J. L. G. Fierro, *Langmuir* 2003, *19*, 7621-7627.

[16] J. Wen, G. L. Wilkes, *Chem. Mater.* 1996, 8, 1667

[17] A. Sayari, S. Hamoudi, *Chem. Mater*. 2001, 13, 3151.

[18] S. L. Burkett, S. D. Sims, S. Mann, *Chem. Commun*. 1996, 1367

[19] D. J. Macquarrie, *Chem. Commun.* 1996, 1961

[20] M. H. Lim, A. Stein, *Chem. Mater.* 1999, 11, 3285

[21] X. L. Ji, E. Hampsey, Q. Y. Hu, J. B. He, Z. H. Yang, Y. F. Lu. *Chem. Mater*. 2003, 15, 3656

[22] J. Brown, L. Mercier, T. J. Pinnavaia. *Chem Commun.* 1999, 69

[23] D. J. Macquarrie, D. B. Jackson. *Chem. Commun*. 1997, 1781

[24] S. R. Hall, C. E. Flower, B. Lebeau, S. Mann. *Chem. Commun.* 1999, 201

[25] T. Asefa, N. Coombs, G. A. Ozin. *Nature* 1999, 402

[26] H. Fan, Y. Lu, A. Stump, S. T. Reed, T. Baer, R. Schunk, V. Perez-Luna, G. P. Lopes, C. J. Brinker. *Nature* 2000, 405, 56

[27] K. J. Shea, D. A. Loy, Webster

[28] S. Guan, S. Inagaki, T. Ohsuna. O. Terasaki. *J. Am. Chem. Soc*. 2000, 122, 5660

[29] A. Sayari, S. Hamoudi, Y. Yang, I. L. Moudrakovski, J. R. Ripmeester. *Chem. Mater.* 2000, 12, 3857

[30] B. J. Melde, B. T. Holland, C. F. Blanford, A. Stein. *Chem. Mater*. 1999, 11, 3308

[31] Y. F. Lu, H. Fan, N. Doke, D. A. Loy, R. A. Assink, D. A. Lavan, C. J. Brinker. *J. Am. Chem. Soc.* 2000, 122, 5258

[32] K. Landskron, B. D. Hatton, D. D. Perovic, G. A. Ozin. *Science*. 2003. 302, 267

[33] H. Pei, J. Tang, J. Pang, H. S. Ashbaugh, C. J. Brinker, Z. Yang, Y. F. Lu. *J. AM. Chem. Soc.* 2006, 128, 5304

[34] K. Kageyama, J. Tamazawa, T. Aida. *Science* 1999, 285, 2113

[35] Y. J. Han, J. Kim, G. D. Stucky, *Chem. Mater*. 2000 12, 2068

[36] H. J. Shin, R. Ryoo, Z. Liu, O. Terasaki. *J. Am. Chem. Soc*. 2001, 123, 1246.

[37] C. G. WU, T. Bein. *Science* 1994, 266, 1013

[38] S. M. Ng, S. Ogino, T. Aida. *Macromol. Rapid Commun.* 1997, 18, 991

[39] S. A. Johnson, D. Khushalani, N. Coombs, T. E. Mallouk, G. A. Ozin. *J. Mater. Chem.* 1998, 8, 13

[40] H. L. Frisch, J. E. Mark, *Chem. Mater.* 1996, 8, 1735.

[41] C. G. WU, T. Bein. *Science* 1994, 266, 1757

[42] T. Ogoshi, K.M. Kim and Y. Chujo, *J. Mater. Chem.* 2003, 13, 2202

[43] O. Yu, Posudievsky, G. M. Telbiz, V. K. Rossokhaty. *J. Mater. Chem*. 2006, 16, 2485

[44] Y. Wei, D. Jin, D. J. Brennan, D. N. Rivera, Q. Zhuang, N. J. DiNardo and K. Qiu, *Chem. Mater,* 1998. 10, 769

[45] T. H. Mourrey, S. M. Miller, J. A. Wesson, T. E. Long and L. W. Kelts, *Macromolecules* 1992, 25, 45

[46] S. Wang, Z. Ahmad and J. E. Mark, *Chem. Mater.*1994. 6, 943

[47] Y. Wei, D. C. Yang and L. G. Tang, *Makromol. Chem. Rapid Commun.* 1993. 14, 273.

[48] Y. Lu, Y. Yang, A. Sellinger, M. Lu, J. Huang, H. Fan, G. Lopez, A. R. Burns, J. Shelnutt, C. J. Brinker. *Nature* 2001, 410, 913

[49] H. Y. Fan, Y. F. Lu, A. Stump, S. T. Reed, T. Baer, R. Schunk, V. Perez-Luna, G. P. Lopez, C. J. Brinker. *Nature* 2000, 405, 6782

[50] C. J. Brinker, Y. Lu, A. Sellinger, H. Fan. *Adv. Mater*. 1999, 11, 579

[51] H. S. Peng, J. Tang, L. Yang, J. B. Pang, H. S. Ashbaugh, C. J. Brinker, Z. Z. Yang, Y. F. Lu. *J. AM. Chem Soc* 2006, 128, 5304

[52] Odeon. *The principle of Polymerization.*

[53] J. C. Hicks, C. W. Jones. *Langmuir.* 2006, 2676

[54] D. W. Sindorf, G. E. Maciel. *J. Phys. Chem.* 1982, *86*, 5208

[55] K. H. Illers, H. Haberkorn,. *Makromol Chem.* 1971;142, 31–67

[56] G. Gurato, A. Fichera, F. Z. Grandi, R. Zannetti, P. Canal. *Makromol Chem* 1974;175(3):953–75.

[57] M. Kyotani, S. Mitsuhashi. *J Polym Sci*, Part A-2 1972;10(8):1497–508.

[58] T. D. Fornes, D. R. Paul. *Polymer*, 2003, 44, 3945-361

[59] S. M. Aharoni. *Nylons,Their synthesis, Structure, and Properties*. Chichester; New York: Wiley; 1997.

[60] H. Arimoto, M. Ishibashi, M. Hirai, Y. Chatani. *J Polymer Sci Pt A* 1965, 3(1):317–26.

[61] D. R. Holmes, C. W. Bunn, D. J. Smith. *J Polymer Sci* 1955, 17:159–77.

[62] M. I. Kohen, editor. *Nylon plastics handbook*. New York: Hanser; 1995.

[63] F. Rybnikar, J. Burda. *Textiltech* 1961;12:324–31.

[64] L. G. Roldan, H. S. Kaufman. *Polym Lett* 1960;1:603–8.

[65] Y. S. Kang, H. I. Lee, Y. Zhang, Y. J. Han, J. E. Yie, G. D. Stucky, J. M. Kim. *Chem. Commun*. 2004, 1524-1525

[66] C. W. Jones, K. Tsuji and M. E. Davis, *Nature*,1998, 393, 52.

[67] B. C. Wilson, C. W. Jones. *Macromolecules*, 2004, 37, 9709-9714

[68] G. S. Ekloff, J. Rathousky, A. Zukal. *Int. J. Inorg.Mater.* 1999, 1, 97